

Development and Application of Bioorthogonal Palladium-Labile Derivatives of Cytotoxic Pyrimidine Analogues

Jason T. Weiss

PhD in Molecular Medicine
University of Edinburgh
2015







DECLARATION

This thesis has been entirely composed by the author Jason Weiss. I have carried out all experiments except where otherwise stated. This work herein has not been submitted for any other degree or professional qualification. Most of this work has been published in the scientific literature and part of it is protected under patent. Printed versions of the primary research communications resulted from this thesis are included in the appendix.

Patent:

Bioorthogonal methods and compounds, PCT/GB2014/051894. Priority date: 21.06.13. Inventors: J. T. Weiss and A. Unciti-Broceta.

Articles:

1. Weiss, J.T., et al., *Extracellular palladium-catalysed dealkylation of 5-fluoro-1-propargyl-uracil as a bioorthogonally activated prodrug approach.* Nature Communications, 2014. **5**, 3277. Featured in Synform, 2014/07 (A90 - A92)
2. Weiss, J.T., et al., *Development and bioorthogonal activation of palladium-labile prodrugs of gemcitabine.* Journal of Medicinal Chemistry, 2014. **57**(12), 5395-404.
3. Weiss, J.T., et al., *N-alkynyl derivatives of 5-fluorouracil: susceptibility to palladium-mediated dealkylation and toxigenicity in cancer cell culture.* Frontiers in Chemistry, 2014. **2**, 56.
4. Weiss, J.T., Carragher, N.O. & Unciti-Broceta, A. *Palladium-mediated dealkylation of N-propargyl-floxuridine as a bioorthogonal oxygen-independent prodrug strategy*. Scientific Reports, 2015. **5**, 9329

Jason T. Weiss
Sept. 2014

ABSTRACT

Chemotherapy is widely used to treat various forms of cancer. However, some chemotherapeutic drugs, due to their antineoplastic properties, also act upon healthy cells which normally replicate rapidly causing a plethora of undesirable side effects. One rising and promising therapeutic strategy is the development of prodrugs. Prodrugs are derivatives of the pharmaceutically active drugs but require an enzymatic or biochemical transformation within a certain biological space in order for it to become activated and capable of exerting the desired pharmacological effect. As a novel prodrug approach, this thesis describes the pioneering use of a bioorthogonal organometallic (BOOM) activation strategy to develop spatially-controlled anticancer treatments.

Bioorthogonal reactions are selective chemical processes between two abiotic reagents in a biological system that do not interfere with the system's biotic components. In BOOM reactions, one of the reagents is a metal catalyst, which if immobilized, could in principle allow for the local transformation of a continuous flow of a bioorthogonal chemo-substrate indefinitely. To exploit the benefits of this paradigm in anticancer therapy, this thesis reports the design, synthesis and screening of a set of prodrugs masked with bioorthogonal protecting groups sensitive to activation by a catalysts-based "activating device". Specifically, it describes the synthesis of palladium (Pd^0) functionalized resins (the activating device) capable of activating cytotoxic pyrimidine analogue prodrugs masked with Pd^0-labile protecting groups. Both the Pd^0 functionalized resins and the BOOM-activated prodrugs are independently non-cytotoxic. However, once in combination together, the Pd^0 is capable of mediating the removal of the masking groups *in situ* and rendering the drugs in their cytotoxic state with comparable antiproliferative properties to the unmodified parental drugs *in vitro*. The Pd^0 resins also display biocompatibility and local catalytic activity inside zebrafish embryos. This approach is intended to generate a more targeted therapeutic treatment regime while minimizing harm to normal healthy tissues through the local generation of prodrugs which are not dependent on intrinsic biological activators but by an external activating device, thus reducing the systemic presence of the drug.

ACKNOWLEDGEMENTS

I have been very fortunate to have an overall truly positive PhD experience. The biggest reason of course is because I have been surrounded by an incredible support staff that has helped me every step of the way. Therefore, I have a lot of people to acknowledge who at the very least deserve my utmost gratitude and appreciation.

First and foremost, thank you Dr. Asier Unciti-Broceta. You are truly wonderful supervisor who took a chance on me to undertake this amazing project. Your patience, counsel and brilliance throughout my three years have been instrumental for the success of this project and shaping me into the competent graduate student I am today.

A special thank you to Craig Fraser, the other founding member of the Unciti-Broceta Lab and Dr. John Dawson of the Carragher Lab. Craig, your thorough chemistry knowledge has been both inspirational and beneficial for me and the laughs we've shared both inside and outside of the lab won't be forgotten. John, your seemingly boundless biology knowledge and ability to both run and fix any piece of equipment have thoroughly contributed to the success of this project. It has been an honour and privilege to work with you both.

A big thank you to Dr. Neil Carragher and all the members of the Carragher and Unciti-Broceta Lab with special mention to Dr. Belén Rubio-Ruiz, Sam Myers, Richard Crispin, Kenneth Macleod and Alison Munro, you all have been monumental in one way or another throughout my schooling. Thank you Dr. Liz Patton and Witold Rybski for all your incredible Zebrafish work. I would also like to mention Jan, the lovely ECRC receptionist, for always seamlessly arranging all the necessary accommodation and transportation for all my conferences. You all will be thoroughly missed.

This section would not be complete without mentioning all of the amazing friends I have made throughout my time here (you know who you are). Your humour, support, distractions, brain storming and at times collaborative misery have made my time here truly memorable.

A most special thank you goes to my family and Christina. To my parents Judy and Dennis, and my brother Adam, your constant love and belief in me have been like a beacon of light. I am forever grateful. Thank you to my parents-in-law, Bruce and Cyndi, for their support and kindness. To my beloved Christina, you came with me to Scotland four years ago and have been a relentless supporter every step of the way. They say happiness is only real when shared, my time in Edinburgh has been one of the greatest and happiest times of my life and I can think of no one better to have shared this experience with. I will always love you. You all have helped shape the man I am today and this thesis is dedicated to you.

CONTENTS

DECLARATION *2*

ABSTRACT *3*

ACKNOWLEDGEMENTS *4*

CONTENTS *6*

LIST OF FIGURES *10*

LIST OF TABLES *12*

ABBREVIATIONS *13*

CHAPTER 1 ..... *15*

Introduction *15*

1.1 Broad Treatment Options for Cancer Patients 15

1.2 Targeted Therapy 16

1.3 Prodrugs 18

1.4 Bioorthogonal Chemistry 23

1.5 Transition Metals in Bioorthogonal Chemistry 26

1.6 BOOM Chemistry for Chemotherapy 30

1.7 Design of Bioorthogonal Pd-labile Prodrugs 31

1.8 Aims 32

CHAPTER 2 ..... *34*

Methods *34*

2.1 CHEMISTRY 34

2.1.1 Chemicals 34

2.1.2 Chromatography 34

2.1.3 Nuclear Magnetic Resonance Spectroscopy (NMR) 34

2.1.4 Mass Spectroscopy 35

2.2 EXPERIMENTAL – CHAPTER 3 35

2.2.1 Synthesis of Pd^0 Resins and Characterization 35

2.3 EXPERIMENTAL – CHAPTER 4 36

2.3.1 Synthesis of Carbonate Gemcitabine Prodrugs (**2, 3, 4**) 36

2.3.2 Synthesis of Carbamate Gemcitabine Prodrugs Intermediates (**6, 7, 8**) 39

2.3.3 Synthesis of Carbamate Gemcitabine Prodrugs (**9, 10, 11**) 42

2.3.4 Synthesis of Non-Fluorescent Probes (**13, 14, 15**) 45
2.4 EXPERIMENTAL – CHAPTER 5 47
2.4.1 Synthesis of 5FU Prodrugs (**All, Pro, Bn-5FU**) 47
2.4.2 Synthesis of 1-propargyl-2-pyridone (**21**) 49
2.4.3 Synthesis of 1-propargyl-4-pyridone (**23**) 50
2.5 EXPERIMENTAL – CHAPTER 6 50
2.5.1 Synthesis of N1-Functionalized 5FU Derivatives (**24, 25, 26** and **27**) 50
2.5.2 Synthesis of 3-propargyl-5-fluorouracil (**30**) 53
2.6 EXPERIMENTAL – CHAPTER 7 55
2.6.1 Synthesis of Compound **33** 55
2.7 BIOLOGY – GENERAL METHODS 57
2.7.1 Cell Culture 57
2.7.2 Non-Biological Pd^0-mediated Conversion Study 58
2.7.3 Bioorthogonal Comparative Study of Prodrug to Parental Drug 58
2.7.4 Pd^0-mediated Activation of Pd-labile Prodrugs in vitro 59
2.7.5 Time-Lapse Imaging Study 59
2.8 METHODS – CHAPTER 3 59
2.8.1 Pd^0 Biocompatibility in vitro 59
2.8.2 Pd^0 Biocompatibility inside Zebrafish Embryos 60
2.9 METHODS – CHAPTER 4 60
2.9.1 DNA Damage Study 60
2.9.2 Pd^0 Catalytic Activity Inside Zebrafish Embryos 61
2.10 METHODS – CHAPTER 5 61
2.10.1 Combination Study with 5FU and Increasing Concentrations of Pro-5FU 61
2.10.2 Catalytic Study With Pd^0 Resins in vitro 62
2.10.3 Zeptosens Reverse Phase Protein Microarray Analysis 62
2.10.4 Western Blot Analysis 63
2.10.5 Mouse Xenograft Assay 64
2.11 METHODS – CHAPTER 6 65
2.11.1 BOOM Activation Comparison of Prodrugs **18** and **30** in Various Cancer Cells 65
2.12 METHODS – CHAPTER 7 65
2.12.1 Pd^0-mediated Activation of Pro-FUdR in vitro Under Hypoxic Conditions 65

CHAPTER 3 ..... *66*

Functionalized Pd^0 Resins *66*

3.1 INTRODUCTION 66

3.2 RESULTS 67

3.2.1 Design and Synthesis of Functionalized Pd^0 Resins 67

3.2.2 Image Analysis of Pd^0 Resins 68

3.2.3 Characterisation of Pd^0 Resins 69

3.2.4 Pd^0 Resins Biocompatibility Both in vitro and in vivo 71

3.3 CONCLUSIONS 72

CHAPTER 4 ..... *74*

Pd-Labile Gemcitabine Prodrugs *74*

4.1 INTRODUCTION 74

4.2 RESULTS 76

4.2.1 Design and Synthesis of Pd^0-labile Gemcitabine Prodrugs 76

4.2.2 Gemcitabine Prodrug Bioorthogonal Comparative Study 77

4.2.3 Non-biological Pd^0-mediated Conversion Study 79

4.2.4 Pd^0-mediated Conversion of Prodrugs in vitro 80

4.2.5 Cytotoxic Mode of Action Analysis 83

4.2.6 Pd^0 Resins Catalytic Activity in Zebrafish 84

4.3 CONCLUSIONS 87

CHAPTER 5 ..... *89*

Pd-Labile 5-Fluorouracil Prodrug *89*

5.2 RESULTS 92

5.22 Pd^0–mediated Conversion of Prodrugs into 5FU Under Biocompatible Conditions 93

5.23 Bioorthogonality of Pro-5FU 96

5.24 Biological Conversion Assay with Pd^0 / Pro-5FU Combination 99

5.25 Phenotypic Evaluation of Pd^0 / Pro-5FU Combination 102

5.26 In Vivo Mice Xenograft Assay 106

5.3 CONCLUSIONS 107

CHAPTER 6 ..... *110*

N-Alkynyl Derivatives of 5-Fluorouracil *110*

6.1 INTRODUCTION 110

6.2 RESULTS 111
6.2.1 Synthesis of Alkynyl-modified 5FU Derivatives 111
6.2.2 Pd^0-lability of 5FU Alkynyl Derivatives 112
6.2.3 Pd^0-lability of N3- vs. N1-propargyl 5FU Prodrugs 113
6.2.4 Pd^0-lability of N3- vs. N1-propargyl 5FU Prodrugs at Varying pH 114
6.2.5 Bioorthogonality of N3- vs. N1-propargyl 5FU Prodrugs 115
6.2.6 Pd^0-mediated activation of N3- vs. N1-propargyl 5FU prodrugs in vitro 116
6.3 CONCLUSIONS 119
CHAPTER 7 ..... *121*
Pd-Labile Floxuridine Prodrug *121*
7.1 INTRODUCTION 121
7.2 RESULTS 124
7.2.1 Synthesis of Pro-FUdR 124
7.2.2 Evaluation of the Efficacy of the Deactivation Strategy of Pro-FUdR 125
7.2.3 Non-Biological Pd^0-mediated Conversion Study 126
7.2.4 Pd^0-mediated Conversion of Pro-FUdR in vitro 128
7.2.5 Phenotypic Evaluation of Pd^0 / Pro-FUdR Combination 129
7.2.6 Pd^0-mediated Conversion of Pro-FUdR in vitro in Hypoxia 130
7.3 CONCLUSION 132
CHAPTER 8 ..... *134*
Discussion *134*
CHAPTER 9 ..... *143*
References *143*
APPENDIX *153*

LIST OF FIGURES

Chapter 1

Figure 1.1. *Mechanism for Immunotherapy for Cancer Treatment* 17
Figure 1.2. *Schematic for Directed Enzyme Prodrug Therapy (DEPT)* 19
Figure 1.3. *Photo-activatable prodrug and photopharmacology Strategies* 22
Figure 1.4. *Bioorthogonal Chemical Reporter Strategy* 23
Figure 1.5. *Staudinger Ligation with Azides* 24
Figure 1.6. *Cycloaddition with a Strained Cyclooctyne and an Azide* 25
Figure 1.7. *Envisioned antibody-drug-conjugate (ADC) bound to cancer cell* 26
Figure 1.8. *BOOM Chemistry Using a Pd-microsphere Heterogeneous Catalyst Inside HeLa Cells* 27
Figure 1.9. *Palladium mediated cross coupling and cleavage reactions in E. coli cells* 29
Figure 1.10. *BOOM Chemistry as a Chemotherapeutic Concept* 31

Chapter 3

Figure 3.1. *SEM and TEM images of Pd^0 resin* 69
Figure 3.2. *Pd^0 resins X-ray diffraction spectra* 70
Figure 3.3. *Pd^0 resins biocompatibility in vitro and in vivo* 72

Chapter 4

Figure 4.1. *Targeted functional groups and cytotoxic mode of action of Gemcitabine* 75
Figure 4.2. *Bioorthoganol study of Gemcitabine prodrug library* 78
Figure 4.3. *Non-biological conversion assay with carbamate Gemcitabine prodrugs* 80
Figure 4.4. *Preliminary Boom activation comparison of Gemcitabine prodrugs 9, 10 and 11* 81
Figure 4.5. *BOOM activated Gemcitabine prodrugs and cell growth kinetics* 82
Figure 4.6. *DNA damage study* 84
Figure 4.7. *Pd0 mediated carbamate cleavage of fluorescent probes inside zebra fish embryos* 86
Figure 4.8. *Bioactivation of compound 14 inside digestive system of zebra fish embryos* 87

Chapter 5

Figure 5.1. *5FU Prodrug BOOM Activation Strategy and Cytotoxic Mode of Action* 91
Figure 5.2. *5FU conjugate bases* 92
Figure 5.3. *5FU conjugate bases, 5FU prodrugs and non-biological conversion assay* 94
Figure 5.4. *Reaction Scheme of Pro-5FU + Pd^0 and Mass Spec. Analysis Post Reaction* 95
Figure 5.5. *Study of Pro-5FU Bioorthogonality* 98
Figure 5.6. *Study of pharmacological interactions between 5FU and Pro-5FU and Acetol Bioorthogonality* 99
Figure 5.7. *Catalytic study of Pd^0 resins and BOOM activation comparison of 5FU prodrugs* 100
Figure 5.8. *BOOM generation of 5FU in cancer cell culture* 101
Figure 5.9. *Phenotypic effect of BOOM generation of 5FU in cancer cell culture* 103
Figure 5.10. *Zeptosens Reverse Phase Protein Microarray analysis* 105
Figure 5.11. *Western blot analysis of total p53, phosphorylated p53 and phosphorylated Akt* 105

***Figure 5.12**. Mean Tumour Volume Analysis from HCT116 Xenograft Mice.....106*

Chapter 6

***Figure 6.1**. Non-biological conversion assay of compounds 18, 30 and 31..... 114*
***Figure 6.2**. N3- vs. N1-propargyl 5FU prodrug comparison of bioorthogonality and Pd^0 mediated cytotoxicity 1 17*
***Figure 6.3**. Boom activation comparison of prodrugs 18 and 30 in various cancer cells 119*

Chapter 7

***Figure 7.1**. Palladium labile prodrugs 122*
***Figure 7.2**. Study of Pro-FUdR Bioorthogonality 126*
***Figure 7.3**. Non-biological conversion assay with Pro-FUdR..... .....127*
***Figure 7.4**. BOOM Generation of Pro-FUdR in cancer cell culture..... .....129*
***Figure 7.5**. Cell Growth Kinetics and Phenotypic Evaluation of BOOM generated FUdR.....130*
***Figure 7.6**. BOOM Generation of Pro-FUdR in HCT116 Cells Under Hypoxic Conditions.....131*

LIST OF TABLES

Chapter 2

Table 2.1. *Library of primary antibodies used for the Zeptosens reverse phase protein microarray analysis..... ....63*

Chapter 6

Table 6.1. *Percentages of conversion of 5FU alkynyl precursors mediated by Pd^0 catalysis 113*
Table 6.2. *Percent conversion of 5FU alkynyl precursors mediated by Pd^0 catalysis in varying pH ranges..... .... 115*

Chapter 7

Table 7.1. *Palladium-mediated conversion of Pro-FUdR into FUdR..... ....128*

ABBREVIATIONS

^{13}C NMR	Carbon-13 Nuclear Magnetic Resonance
^{1}H NMR	Proton Nuclear Magnetic Resonance
δ	Chemical Shift
Alloc	Allyloxycarbonyl
Ar*H*	Aromatic Hydrogen
br s	Broad Singlet
C-C	Carbon-Carbon
Cbz	Carboxybenzyl
d	Doublet
DCM	Dichloromethane
dd	Double Doublet
ddd	Doublet of Doublet of Doublets
DMEM	Dulbecco's Modified Eagle Media
DMF	*N,N*-Dimethylformamide
DMSO	Dimethyl sulfoxide
dq	Doublet Quartet
dpf	Days Post-fertilisation
dt	Double Triplet
eq.	Equivalents
ESI	Electrospray Ionisation
EtOAc	Ethyl Acetate
hpf	Hours Post-fertilisation
HPLC	High Performance Liquid Chromatography
HRMS	High Resolution Mass Spectrometry
HRP	Horseradish Peroxidase
Hz	Hertz
ICP-OES	Inductively Coupled Plasma Optical Emission Spectrometry
J	Coupling Constant
LRMS	Low Resolution Mass Spectrometry
m	multiplet
m/z	Mass-to-charge ratio
MCF7	Human Breast Adenocarcinoma Cell Line
MeOH	Methanol
MHz	Mega Hertz
MS	mass spectrometry
MW	Molecular Weight
nm	Nanometer
NMR	Nuclear Magnetic Resonance
PAGE	Polyacrylamide Gel Electrophoresis
PBS	Phosphate Buffered Saline
Pd	Palladium
Pd^{0}	Palladium with an Oxidation State of 0
Pd^{2+}	Palladium with an Oxidation State of 2
$Pd(OAc)_2$	Palladium(II) Acetate
PEG	Polyethylene Glycol

Poc	Propargyloxycabonyl
POD ECL	Peroxidase Enhanced Chemiluminescence
PS	Polystyrene
PVDF	Polyvinylidene fluoride
q	Quartet
qt	Quartet of Triplets
R_f	Retention Factor
rpm	Revolutions Per Minute
RPMI	Roswell Park Memorial Institute Medium
RT	Room Temperature
s	Singlet
SDS	Sodium Dodecyl Sulfate
SEM	Scanning Electron Microscopy
TEM	Transmission Electron Microscope
TG	Tenta Gel
THF	Tetrahydrofuran
TLC	Thin Layer Chromatography

CHAPTER 1

Introduction

1.1 Broad Treatment Options for Cancer Patients

Cancer is a devastating disease that needs little introduction. It affects millions of people and in fact it is one of the leading causes of death from a non-contagious disease worldwide.[1] It has plagued humanity since as long as we came to be. Treatment is frustratingly complex because it is not a single disease but rather hundreds of diseases. An effective treatment option for one type of cancer can be rendered useless to another. However, as our knowledge of the causes and progression of cancer grows, so too does our ability to cure it.

To date, cancer patients have a wide array of treatment options to choose from which best serve their treatment needs. The most common treatment options are: surgery; radiation; chemotherapy; or a combination of any of the three. However, with the exception of surgery (although even this is sometimes not the case), radiation and chemotherapy are typically non-specific and affect not only the cancerous tissues but healthy tissues as well. This then results in a number of undesirable and unpleasant side effects.

Radiation and surgical treatments for cancer can be a successful means for the control and eradication of local tumours. However, they become obsolete once the cancer has metastasised. Chemotherapy can fill this void because it can treat the patient systemically.[2,3] Although many different classes of chemotherapeutic drugs exist - alkylating agents, antimetabolites, kinase inhibitors, topoisomerase inhibitors and tubulin-binding drugs to name a few - most share a common trait which is to hinder the cancer cells neoplasticity.[4] However, because most chemotherapeutics are not very selective for cancer cells and therefore also affect healthy cells which are

normally fast-growing such as skin cells, hair follicles, cells within the digestive tract and the reproductive system, unpleasant side effects are commonly associated with this type of treatment regime. This has led to a subclass of chemotherapy aimed to minimize these unwanted side effects termed targeted therapy.

1.2 Targeted Therapy

Our growing understanding of tumour biology and our use of genetic and molecular approaches to understand fundamental differences between normal cells and cancer cells has spawned the development of targeted therapy.[2] Targeted therapy aims to exploit these differences through inhibition of molecular pathways which are critical solely for tumour growth and maintenance. The two main categories of targeted therapy are small molecule inhibitors and immunotherapy.[5] Indeed one of the first and landmark examples of targeted therapy was the use of Imatinib to treat chronic myeloid leukaemia (CML). For roughly 90% of patients, CML is the result of the formation of the philadelphia chromosome.[6] This chromosome contains the juxtaposition of two genes called BCR and ABL. The formation of these reverse ordered genes coded for the continuously active tyrosine kinase $P210^{BCR-ABL}$ and thus resulted in the leukemogenesis.[7,8] Imatinib was able to render this type of CML into complete remission through the successful selective targeting and inhibition of the $P210^{BCR-ABL}$ kinase.[6,9] Other examples of targeted small molecule inhibitors are JAK2 inhibitors,[10,11] Src family kinase and mTOR inhibitors, etc.[12]

Immunotherapy for cancer treatment was developed by taking advantage of specific cell surface antigens that are only expressed from certain cancer cells. Monoclonal antibodies (mAbs) through a relatively complex and laborious processes can be used to kill tumour cells directly through tumour receptor blockage, or by the delivery of a cytotoxic drug or radioactive isotope (Fig. 1.1a). These mAbs can also initiate tumour death via immune-mediated cell killing and through the effects that the mAbs can have on tumour vasculature and stroma (Fig. 1.1b).[13] Trastuzumab used to target ERBB2, a member of the epidermal growth factor receptor family[13-15] and Bevacizumab which targets the vascular endothelial growth factor protein

(VEGF)[13,16] are two examples of mAbs currently used in the clinic today. Other antigen targets for immunotherapy include stromal and extracellular matrixes,[17] glycoproteins,[18] and carbohydrates.[19]

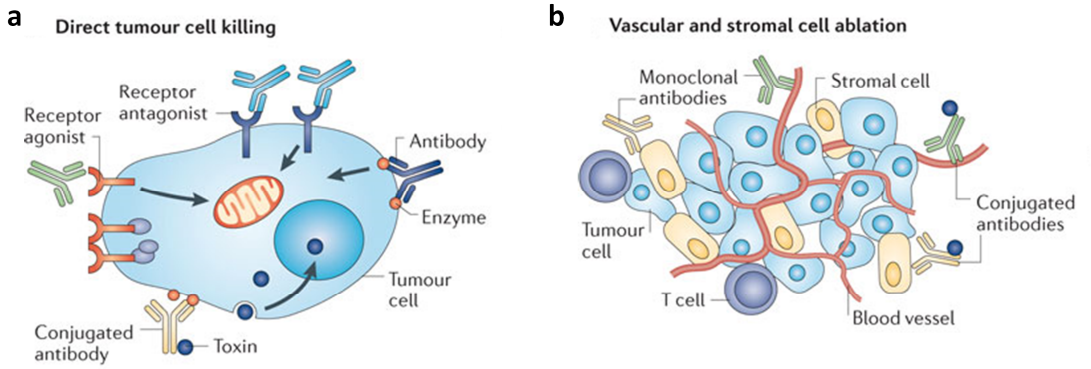

Figure 1.1. Mechanism for Immunotherapy for Cancer Treatment. (**a**) Direct tumour cell killing via immunotherapy can be elicited by conjugated mAbs delivering a payload such as a drug or a radioisotope, by receptor antagonist activity through binding of cell surface receptors and by receptor agonist activity such as activating a tumour cell surface receptor leading to apoptosis. (**b**) The effects mAbs can have on tumour vasculature and stroma can be elicited by vasculature and stroma cell receptor antagonism and by delivering a cytotoxic drug to the vasculature or stroma cells. Reprinted and adapted with permission from reference[13], copyright (2012), Macmillan Publishers Ltd.

Although targeted therapy is a much more direct therapeutic approach compared to conventional chemotherapy and radiation, this therapeutic regime is not without its drawbacks and limitations. Most targeted small molecule inhibitors are tyrosine kinase inhibitors which although can be effective cancer killers, are not always specific at inhibiting a specific kinome family. This lack of specificity also leads to unpleasant side effects during treatment. Killing cancer cells with mAbs that target specific cancer cell antigens is also challenging because many targeted antigens between primary tumours and metastatic legions and even between individual metastatic legions lack homogeneity. The antigens are not always specific to the cancer cells and can also be expressed by healthy cells. Severe toxicity can arise when the mAbs bind to those healthy cells also expressing the same targeted antigens. Also, the process for developing mAbs for clinical use is complex, time consuming and expensive.[20]

1.3 Prodrugs

Another means to improve chemotherapy's efficiency and targeting are the development of prodrugs. Prodrugs are derivatives of the pharmaceutically active drug compounds. They contain promoieties that mask key functional groups within the drug molecule which are responsible for the drug's pharmacological effect. If the masking of the functional group is successful, it will render the prodrug inactive or at least their cytotoxicity will be significantly reduced. The prodrugs are designed to be enzymatically or chemically activated once administered inside the body to improve upon the active compounds' pharmacokinetic and pharmacodynamic properties, and reduce systemic toxicity to healthy tissues by increasing the drugs activation in a more selective manner.[21-23]

When designing prodrugs, there are important aspects to consider. One is to determine what are the key functional groups within the drug responsible for its activation and are they susceptible to chemical prodrug derivatization. Another is the promoiety used. It is important that after the prodrug derivatization has taken place, the side products produced are non-toxic and ideally are rapidly excreted from the organism. This will greatly reduce any off target effects caused by potentially toxic by-products produced during the prodrug's activation process.[22]

Prodrugs activated through enzymatic hydrolysis currently occupy most prodrugs found on the market today (≈ 50%)[24]. However, some are activated solely through chemical transformations like varying pH environments.[25] One major challenge with these activation strategies regarding cancer therapy is finding tumours with high enough expression levels of the activating enzymes in order to achieve selectivity over healthy tissues. One prodrug technology aimed at improving prodrug selectivity is called directed enzyme prodrug therapy (DEPT). This technology uses enzymes artificially introduced into the body to activate the prodrug. This process works in two parts. First, the exogenous enzyme has to be directed to the tumour site or expressed. The second is the administration of the prodrug which is to become locally activated once in contact with the enzyme (Fig. 1.2).[26] The major challenge for this therapeutic approach is targeting the exogenous enzyme to the tumour. There are several varieties of enzyme delivery methods. One is the delivery of the genes

which encode for the activating enzyme to the tumour which will then express the enzyme (GDEPT).[27] This can be achieved by traditional gene therapeutic means (e.g. electroporation, cationic lipids, etc.)[28] or using viral vectors as gene carriers (VDEPT).[29] Another more commonly used method is targeting the actual enzyme to the tumour using mAbs (ADEPT), which again is dependent on reliable tumour specific antigens.[30] Although DEPT is an attractive technology especially from an academic prospective, clinically it has suffered and never been approved for medical use. The main reason for its limitations is because the expression levels of the activating enzymes are poor, resulting in inadequate active drug quantities required to reach lethal concentrations.[26]

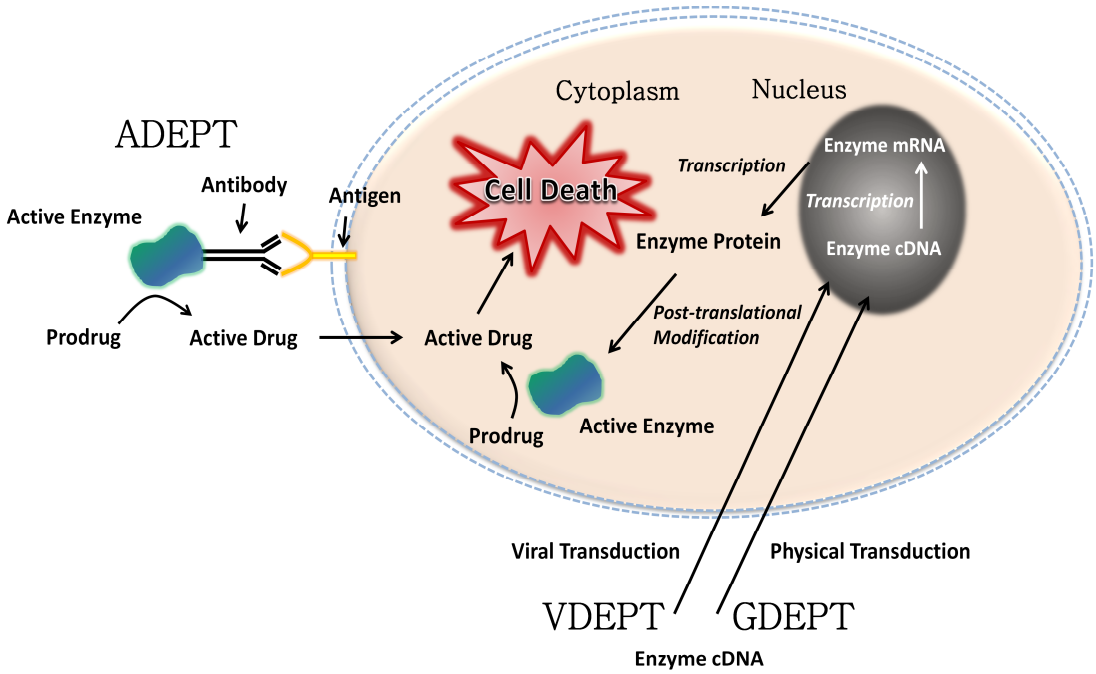

Figure 1.2. Schematic for Directed Enzyme Prodrug Therapy (DEPT). There are two major classes for delivery methods of an exogenous enzyme-prodrug strategy. The first is the genes which encode for the exogenous enzyme can be delivered virally (VDEPT) or physical delivery of the genes using various techniques such as liposomal gene delivery (GDEPT). The other method is direct delivery of the enzyme to cancer cells using mAbs which bind to specific antigens expressed on the tumour cells. Reprinted and adapted from reference,[26] copyright (2001), American Association for Cancer.

Overall, one of the major challenges using prodrugs within the clinic is discriminating their activation in tumour cells and healthy cells. Prodrugs mostly rely on innate biochemical processes for their activation and obtaining bioselective

activation within the tumour environment has proven to be difficult. Significant progress, however, has been made to overcome this issue through the use of benign non-biological means to activate drug precursors. In analogy to the concept of bioorthogonality developed by Bertozzi *et al*, these prodrugs, which ought to be biochemically stable (= bioorthogonal), are subject to activation by non-native, non-biological, non-perturbing means.

Photodynamic therapy (PDT) is an example of this type of non-biological prodrug activation technology.[31,32] PDT involves the administration of photo-labile cytotoxic prodrugs termed photosensitizers. Following the administration of the photosensitizers, the tumour is then illuminated with light at the appropriate wavelength which can activate the prodrug. This activation results in the transfer of energy to oxygen molecules which leads to the formation of reactive oxygen species. Reactive oxygen species can cause a plethora of local damage to many biomolecules within the cancer cells which invariably leads to cancer cell death. However, one major drawback to PDT is the requirement for oxygen as many advanced and aggressive tumours contain hypoxic regions.[33]

Photoactivatable prodrug therapy negates this problem of requiring the presence of oxygen in order to exert the desired cytotoxic effect. These are prodrugs masked with photo-sensitive promoieties, which similar to PDT, are activated upon exposure to light. However, unlike photosensitizers, once the promoiety has been cleaved the now activated drug exerts its pharmacological effect directly and not through the transfer of energy to oxygen.[33] This technology has been applied to many platinum based chemotherapeutic drugs[33,34], Floxuridine[35] and the natural product duocarmycin,[36] to name a few. This technology has however encountered significant issues because most photo-sensitive promoieties are only activated by short wavelengths which are inefficient at penetrating deep into the tissues of the tumour and have shown susceptibility towards biological reducing agents such as glutathione i.e. lacking bioorthogonality.[33]

Advancing this technology to allow more dynamic control over a drug's local activation, the chemotherapeutic technique photopharmacology has been developed. This technique uses bioactive compounds modified with photo-switchable moieties

within the drug's molecular structure. Unlike conventional prodrugs, the photoswitches are designed to undergo reversible molecular transformations when exposed to varying photons. This ability allows the drug to be converted back to its inactive state, further reducing any off target cytotoxicity (Fig 1.3a). The two most basic designs that have shown the most promise for biological applications are the azobenzenes[37] (Fig. 1.3b-i) and the diarylethenes (Fig. 1.3b-ii).[38] Photopharmacology is ideal for localized diseases within locations such as the skin or eyes where light can easily penetrate.[39] Advances are being made for developing molecular photoswitches sensitive to more penetrating red light. This would certainly increase the scope of this niche treatment regime to include denser localized tissues such as solid tumours.

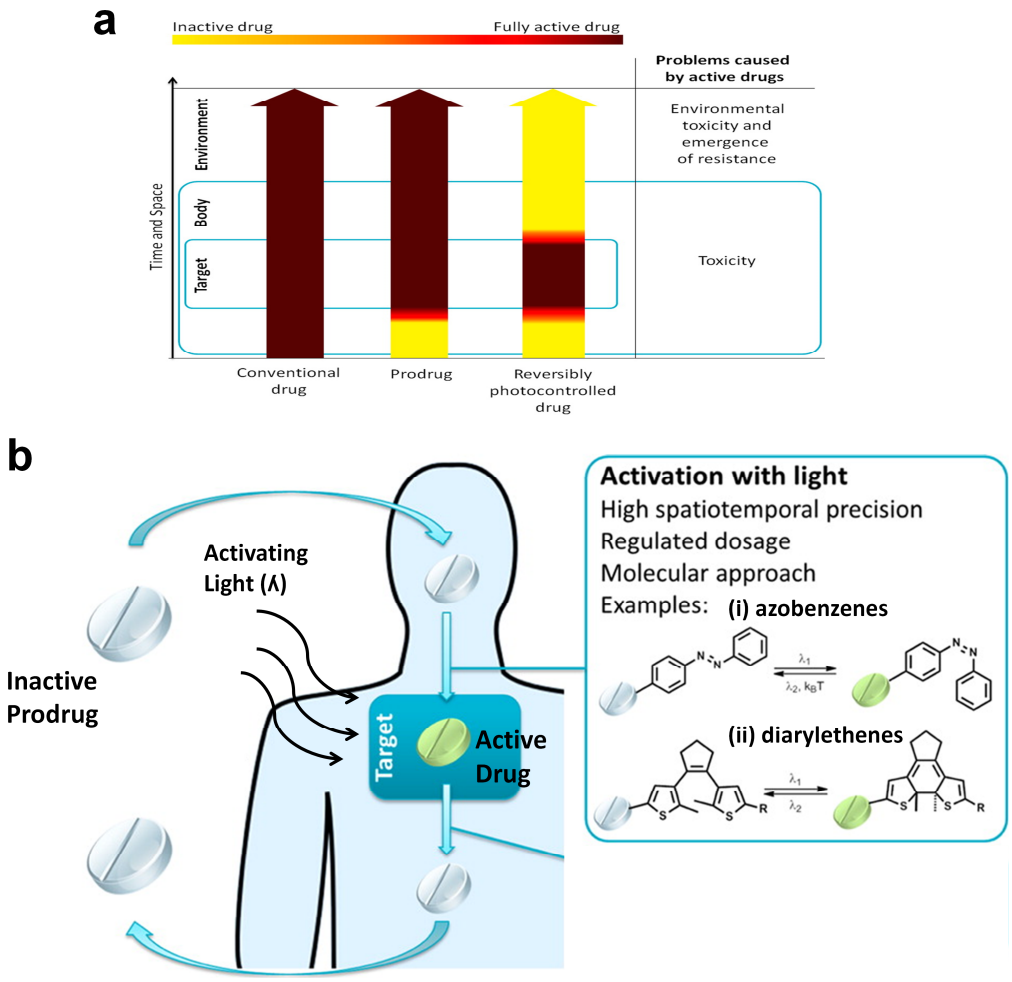

Figure 1.3. Photo-activatable Prodrug and Photopharmacology Strategies. (**a**) Comparison of drug activity over time and space for a conventional drug, a prodrug (including non-reversible photoactivatable prodrugs), and a reversibly photo-controlled drug. (b) Patient is administered with a non-active prodrug which contains photo switchable moieties. Upon exposing the prodrug to a light source, the drug becomes locally activated. Due to the reversibility of the process, in the absence of the light source the active drug is again converted into its inactive form. Two common examples of photo switchable moieties are the (**b-i**) azobenzenes and (**b-ii**) diarylethenes. Reprinted and adapted with permission from reference[39], copyright (2014), American Chemical Society.

Another example of prodrugs activated by non-biological means is from a recent study by Dyson *et al*., who used various anti-cancer drugs and modified them with a fluorous chain. This fluorous modification equipped the drug derivatives with thermoresponsive capabilities. They were able to demonstrate that by inducing slight hyperthermia within various cancer cell lines (40- 42°C vs. normal temperatures of 37 °C), they were able to exert selective cytotoxicity.[40,41]

1.4 Bioorthogonal Chemistry

Bioorthogonal chemistry, a term developed by Bertozzi in the early 2000s,[42,43] is formed by a subset of artificial synthetic chemical reactions between two chemospecific reactive partners that can be conducted in a biological environment, while separately neither of these reagents interact with nor interfere with any biological systems. Initially, bioorthogonal reactions were developed to probe many biomolecules in their native state (nucleic acids, lipids, glycans, etc.) through the selective conjugation of two biologically inert functional groups which would normally be difficult to target by traditional means such as genetically encoded reporters like fluorescent proteins (Fig 1.4).[44,45]

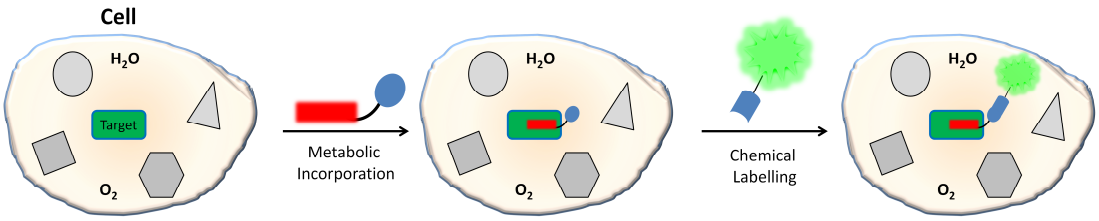

Figure 1.4. Bioorthogonal Chemical Reporter Strategy. A bioorthogonal functional group (blue circle) is linked to a substrate (green box) and is introduced into a biomolecule of interest either through metabolism or genetic incorporation. In the second step, the substrate is conjugated to an exogenously delivered probe (green shape) through the chemospecific reaction with another bioorthogonal functional group (blue cylinder). Both bioorthogonal functional groups must avoid side reactions with non-target biomolecules (grey shapes, H_20 and O_2). Reprinted and adapted with permission from reference[44], copyright (2005), Nature Publishing Group.

Due to the exclusive nature of the bioorthogonal concept, the range of chemical reactions that fit these criteria is relatively limited. To date, the best known bioorthogonal reactions are the Staudinger ligation (Fig. 1.5a)[46] and cycloadditions between "spring-loaded" reactive partners (metal-free click chemistry). The copper-free modification of the 1,3-dipolar cycloaddition (also known as the Huisgen cycloaddition) proceeds with the reaction of azides with ring-strained cyclooctynes. The strained conformation of the cyclooctynes as well as the effects of other modifications to its structure such as fluorination (Fig. 1.6a)[47] and aryl ring fusion[48], led to a spring-loaded reagent that reacts specifically with alkyl azides without the

need for a potentially toxic copper catalyst. This has allowed for further bioorthogonal mediated labelling and probing of biological systems.[44,45,49,50] More recent contributions to the bioorthogonal repertoire are the trans-cycloocetene tetrazine ligation[51] and the nitrone-cyclooctyne 1,3-dipolar cycloaddition[52], both of which have improved reaction kinetics.

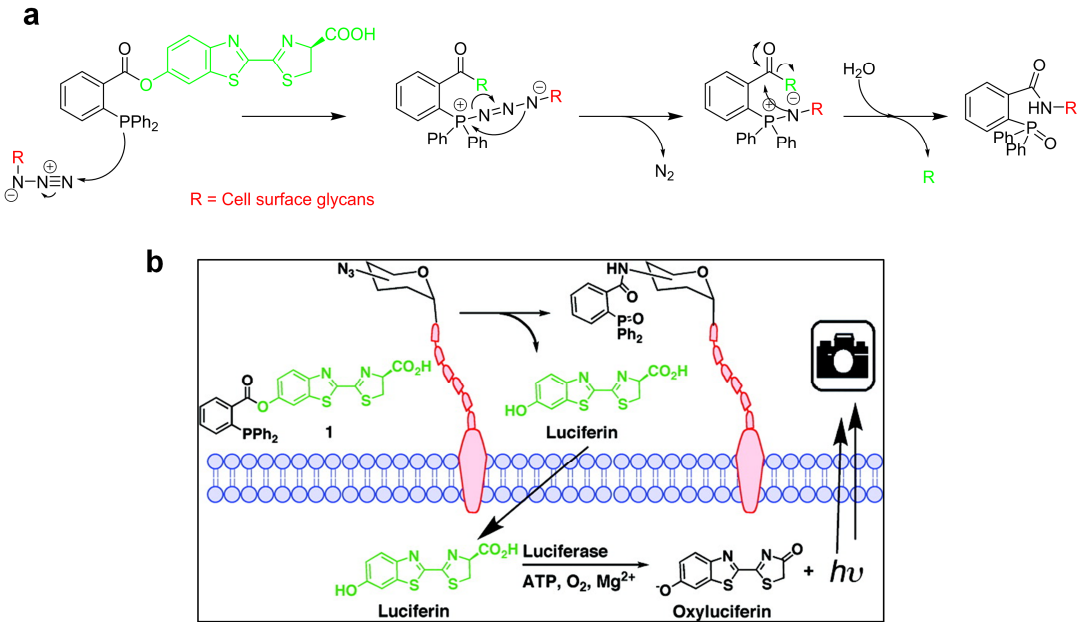

Figure 1.5. Staudinger Ligation with Azides. (**a**) Mechanism of Staudinger ligation with a luciferin molecule (green) containing a phosphine moiety whereupon it selectively reacts with an azide labelled glycan (red R group). (**b**) Scheme for bioluminescence imaging of cell surface azidoglycans. Upon Staudinger ligation of compound 1 with the azide functional group within the cell surface glycan (red), the luciferin (green) is released and enters into the cell. The intercellular luciferin is catalysed by luciferase into oxyluciferin which gives off a bioluminescence. Reprinted and adapted with permission from reference[50], copyright (2010), American Chemical Society.

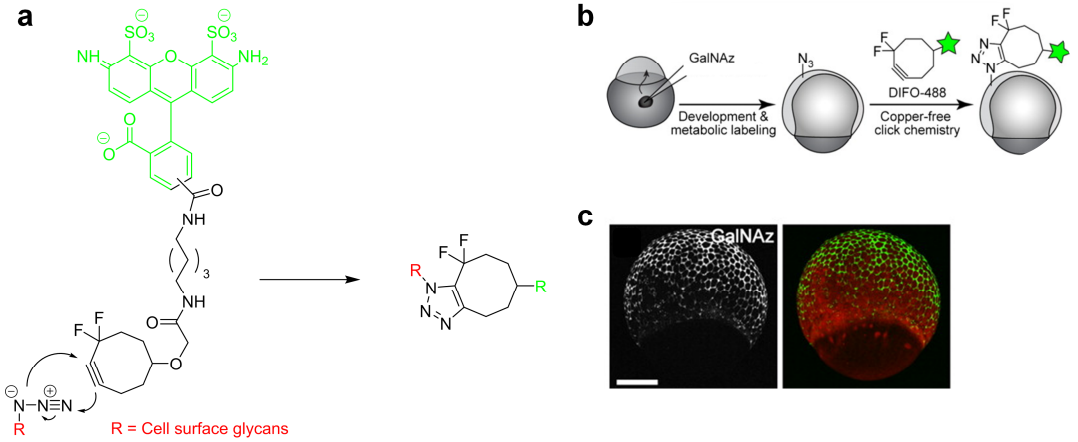

Figure 1.6. Cycloaddition with a Strained Cyclooctyne and an Azide. (**a**) Mechanism of a cycloaddition with a fluorophore-488 (green) conjugated to a difluorinated cyclooctyne (DIFO). (**b**) Scheme for the *in vivo* imaging of glycans within zebrafish embryos. The process works by first microinjecting the *N*-Azidogalactosamine (GalNAz) into the zebrafish embryos, followed by treatment with the DIFO-488 probe. The glycans are labelled with the fluorophore-488 through the selective reaction between the two bioorthogonal reactants as displayed in (**a**). (**c**) zebrafish embryos 7 hours post-fertilization (hpf) treated with both the GalNAz and the DIFO-488 probe (green fluorescence) and counter stained with rhodamine-dextran (red fluorescence), imaged by confocal microscopy. Reprinted and adapted from reference[47], copyright (2010), National Academy of Sciences.

Progressing the bioorthogonal paradigm further, a proof of concept study from Robillard *et al* demonstrated the potential to target and activate a prodrug through a bioorthogonal reaction wherein one of the reagents is bound to a mAb antigen expressed by a tumour cell. Through the development of a new bioorthogonal elimination reaction, the spontaneous release of a drug can be facilitated from trans-cyclooctene following a tetrazine ligation (Fig. 1.7).[53]

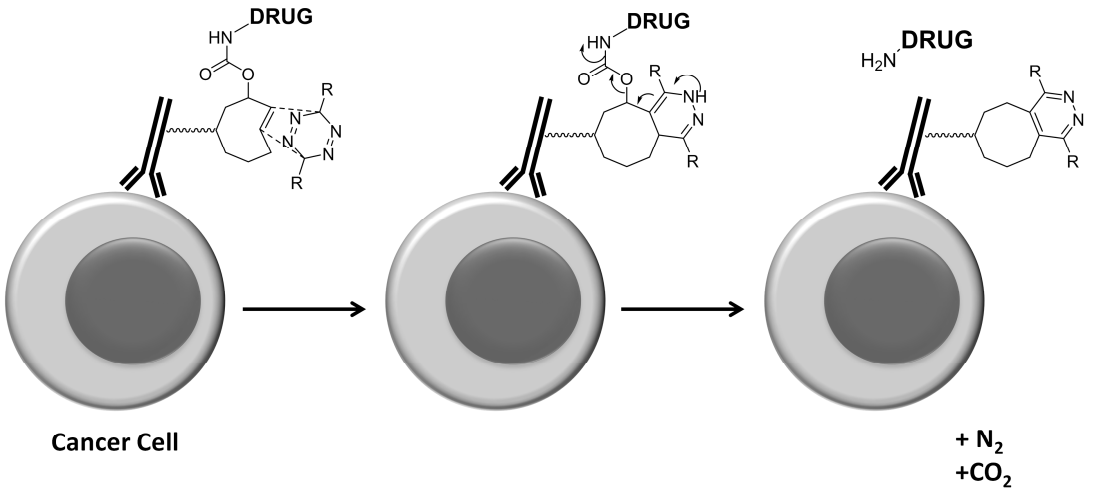

Figure 1.7. Envisioned Antibody-drug-conjugate (ADC) Bound to Cancer Cell. Upon interaction with an administered tetrazine compound to the ADC, the drug is locally released though the inverse-Diels Alder elimination reaction. Reprinted and adapted with permission from reference[53], copyright (2013), Wiley-VCH Verlag GmbH & Co.

1.5 Transition Metals in Bioorthogonal Chemistry

As a new prominent alternative to the bioorthogonal field, the use of transition metals to functionalize biomolecules or mediate the activation of probes in a biological system has emerged. Transition metals have been widely utilised in organic chemistry as an extremely powerful tool capable of mediating chemical transformations in a chemospecific manner. The synthetic flexibility facilitated from transition metals provides very attractive possibilities from a bioorthogonal chemical perspective. The use of non-biotic transition metals to mediate bioorthogonal chemistry are known as bioorthogonal organometallic (BOOM) reactions.[54] However, despite the numerous variety of transition metal catalysed reactions reported in the literature, few are capable of proceeding under biocompatible conditions (37 °C and physiological pH) such as palladium mediated cleavage reactions for example.[55,56] However, this isn't to say that all transition metals are incapable of bioorthogonal reactions within cells. In 2006, Streu and Meggers[57] described the first application of a ruthenium based catalyst capable of carrying out the deprotection of a bis-*N*,*N*′-allyloxycarbonyl caged rhodamine 110 fluorophore inside human cells with no adverse effects on the cell's viability. This seminal study led the way to Yusop and co-workers to investigate biocompatible palladium (Pd) functionalized microspheres capable of catalysing various chemospecific

transformations. These Pd microspheres were readily taken up by the cells and once inside mediated *N*-allyloxycarbonyl (*N*-Alloc) deprotection and Suzuki-Miyaura cross-coupling reactions within the cytoplasm of the cell, all without causing any observable cytotoxicity (Fig. 1.8).[54,58]

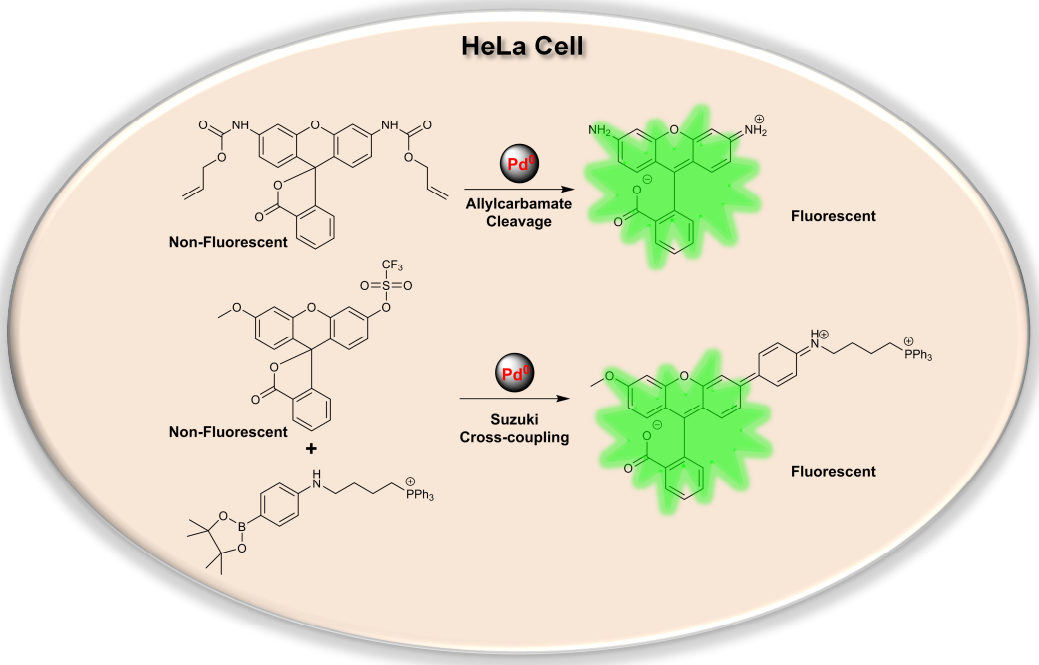

Figure 1.8. BOOM Chemistry Using a Pd-microsphere Heterogeneous Catalyst Inside HeLa Cells. Intercellular Pd-microsphere catalysed Allylcarbamate deprotection and Suzuki cross-coupling reactions to yield fluorescent products.[58]

Since then, many applications for palladium catalysed reactions within the chemical biological field have been reported. Most of these Pd-mediated reactions have involved the Suzuki-Miyaura or Sonogashira cross-coupling reactions with water soluble palladium catalysts and these reactions have predominately taken place within bacterial cells.[59] Such examples include a palladium ligand complex capable of mediating Sonogashira cross-coupling reaction to fluorescently probe a metabolically encoded alkyne-containing ubiquitin protein to an aryl iodide probe in *Escherichia coli* (*E. coli)* (Fig. 1.9b).[60] Another example performed by Davis and co-workers was the fluorescently tagged, genetically modified, porin channels within *E.coli* (Fig. 1.9a). The channels contained aryl halides within various non-perturbing

sites of the protein and they were probed through Pd-mediated Suzuki-Miyaura cross-coupling reaction with a fluorescent boronic acid within the cell surface.[61] Progressing the use of Pd catalysed bioorthogonal reactions, Chen and co-workers were able to control protein function through palladium-triggered chemical rescue (Fig. 1.9c).[62,63] Specifically, the authors incorporated a propargyloxycarbonyl (Poc)-lysine residue within a critical position of an OspF phosphothreonine lyase enzyme of *Shigella flexneri* (a species of gram negative bacteria) critical for its enzymatic activity. OspF is a secretion effector enzyme that irreversibly catalyses the dephosphorylation of Erk, which consequently leads to an accumulation of damaged Erk substrate within the host cell. This accumulation of phosphorylated Erk results in altered host inflammatory transcriptional responses causing a repression in innate immunity from the host.[64] Once the host cell was treated with the membrane permeable palladium reagent, the Poc caging group was effectively cleaved, restoring the OspF activity. Using this bioorthogonal palladium mediated reaction, the authors were able to confirm that indeed this lysine residue is critical for OspF function and that this enzyme is responsible for the subcellular localization of phospho-Erk, giving further insight into the effects OspF has on cellular signalling pathways as part of *Shigella flexneri's* infection processes.

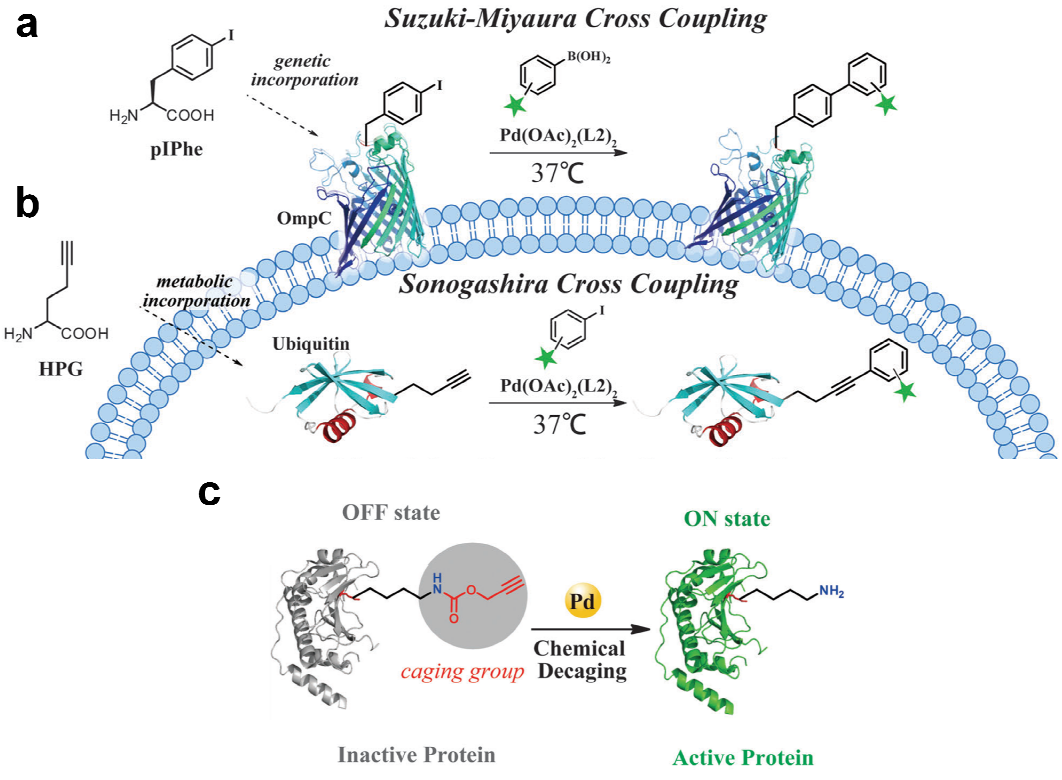

F

igure 1.9. Palladium Mediated Cross Coupling and Cleavage Reactions in *E. coli* Cells. (**a**) Suzuki-Miyaura cross coupling was conducted to probe porin channels within the membrane of *E. coli*. The channels contained an aryl iodide (pIPhe) functional group which was coupled to a fluorescent boronic acid. (**b**) Sonogashira cross coupling reaction was conducted to probe ubiquitin protein expressing a homopropargylglycine (HPG) functional group which was coupled to an aryl iodide fluorophore inside *E. coli* cells. (**c**) Palladium mediated cleavage reaction for protein activation. The propargyloxycarbonyl (Poc)-caged lysine residue can be genetically and site-specifically incorporated into a lysine dependent protein which generates an "OFF" state mutant. Upon entering the cell, the biocompatible palladium catalyst can cleave the Poc moiety within the lysine residue switching the protein activity to an "ON" state. Reprinted and adapted with permission from reference[65], copyright (2014), The Royal Society of Chemistry.

The capacity to create C-C bonds using transition metals within living biological systems has opened up new and exciting opportunities for chemical biology and medicinal chemistry. The utilization of transition metals for facilitating bioorthogonal chemistry has expanded this important field from stoichiometric reactions to catalytic cycles, further expanding the applications of bioorthogonal chemistry.[65,66]

1.6 BOOM Chemistry for Chemotherapy

To date, the majority of these metal catalysed bioorthogonal reactions require the use of genetically modified proteins which express the bioorthogonal functional groups in order to probe their locations or modulate their activity. Although this has greatly improved our understanding of protein localization and function, this greatly limits this application for therapeutic means. Herein, this thesis reports the first steps towards the use of BOOM chemistry for cancer therapy through the development of prodrugs susceptible to bioorthogonal reactions catalysed by a non-biological heterogeneous Pd metal source in an attempt to obtain more localized and efficient cancer therapies with fewer side effects.[67-70]

Based on the unique catalytic properties and biocompatibility of Pd as mentioned above, we hypothesized that we could mediate, in a spatially controlled manner, the chemospecific activation of a systemically administered Pd-labile prodrug into its pharmaceutically active form through a Pd functionalized implant inside a tumour (Fig. 1.10). This would vary significantly from traditional prodrugs which are normally activated intra or extracellularly by metabolic or chemical means; the Pd-labile prodrugs would be activated exclusively from the action of this transition metal. Therefore, the prodrug would remain systemically intact, greatly reducing adverse side effects within healthy tissues. Local activation of small molecule prodrugs would reinvigorate the therapeutic use of approved drugs plagued by poor safety profiles or promising drug candidates which failed in clinical trials due to pharmacokinetic issues. Local activation would also allow for increase dosing inside the disease tissue which makes this therapeutic regime ideal for tumours which, for whatever reason, cannot be resected surgically.

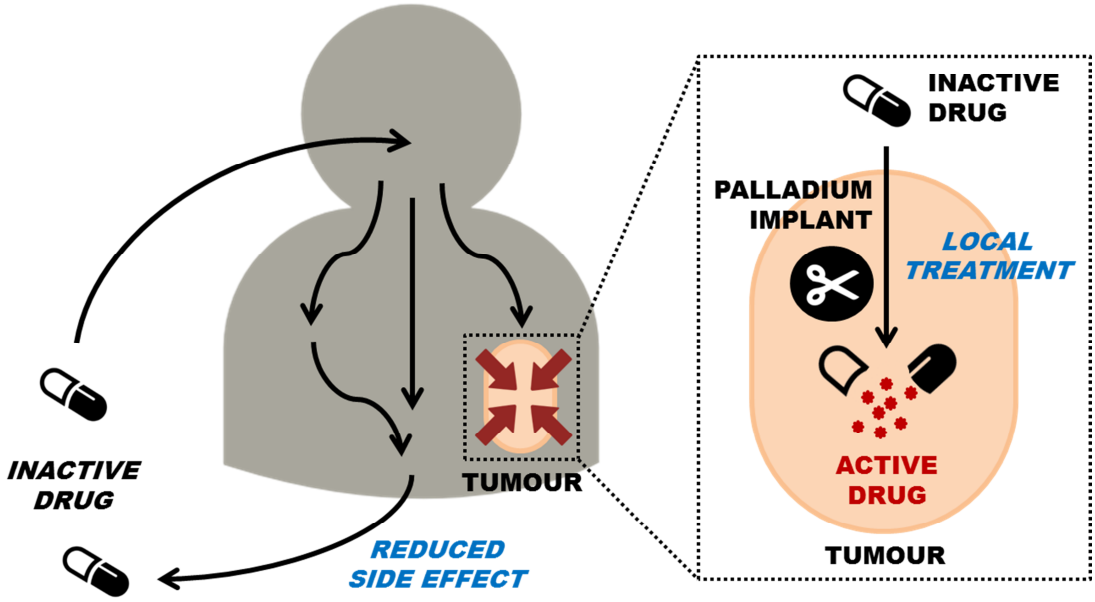

Figure 1.10. BOOM Chemistry as a Chemotherapeutic Concept. Pd-labile prodrugs would be administered systemically wherein they would remain inert within the patient until locally and exclusively activated by a heterogeneous Pd insert within a tumour. The Pd activating device would be surgically implanted inside the tumour prior to treatment with the prodrug.

This new prodrug approach warrants expanding the classical prodrug concept to two fundamentally different classes: biolabile prodrugs prone to transformations by biological means such as the many examples described above; and bioorthogonal prodrugs which encompass physiological stable prodrugs subject to activation by non-biological, non-native means.[69] This bioorthogonal prodrug class would therefore include prodrugs activated by benign light sources,[39] mild hyperthermia,[40,41] metal free click chemistry,[53] or the above described BOOM chemistry.[54,67-70]

1.7 Design of Bioorthogonal Pd-labile Prodrugs

When designing prodrugs susceptible to palladium activation, one must take into consideration several important features. First, extensive knowledge is required about how the drug exerts its cytotoxic effect and what the relevant biological targets of the drug are. This knowledge can then be used to modify the drug with chemical "masking groups" at a position within the drug that is mechanistically relevant to its pharmacological activity. Second, the masking group must be sensitive to palladium

mediated cleavage but bioorthogonally and chemically stable enough so that it is not recognized by human enzymes capable of removing it and activating the drug systemically. Third, the bioorthogonal prodrug must not competitively compete with the same enzymes responsible for forming the active metabolites of the now activated drug. With initial dosing, this would not be a problem. However, with continuous dosing of the prodrug, if the prodrug competitively competed against the activated drug, eventually the active drug would lose potency because the relevant enzymes would become saturated with the prodrug. The effective masking strategy should ideally render the prodrug at least 100 fold less cytotoxic then the active drug. Once cleaved, the Pd-labile masking group should also be non-toxic to prevent any cytotoxic off target effects. And finally, the Pd activating device should also be biocompatible (ideally bioorthogonal) at concentrations capable of activating the prodrug under physiological conditions (aqueous environment, physiological temperatures, pH, etc.). Preferably, the Pd device should be catalytic in order implement a repetitive dosing regimen without the constant need to surgically implant the Pd device.

1.8 Aims

The aim of this thesis is to develop a targeted and localized prodrug activated chemotherapeutic strategy whereby the prodrug activation is mediated by a non-biological palladium-based activating device. A library of pyrimidine analogue prodrugs will be designed, synthesized and tested to determine which masking groups (the promoiety) and which functional groups to be masked will result in a prodrug that is not only bioorthogonal but also highly sensitive to palladium mediated activation. Specifically:

1. To develop an easy to handle palladium activated device that could mediate the activation of Pd-labile prodrugs and probes within the extracellular space both *in vitro* and *in vivo*.

2. To investigate the masking of the pharmacological properties of cytotoxic drugs by modifying key functional groups with Pd-sensitive promoieties that

would render them significantly less cytotoxic in the absence of the Pd activating device. However, in the presence of the device, their cytotoxicity would be restored to comparable levels to the parental drug. The cytotoxic drugs to be investigated for BOOM chemistry are the pyrimidine analogues Gemcitabine, 5-fluorouracil and Floxuridine.

3. To develop a promoiety with appropriate reaction kinetics in the presence of palladium and biochemical resiliency in the absence of palladium.

CHAPTER 2

Methods

2.1 CHEMISTRY

2.1.1 Chemicals

All chemicals used were purchased from Sigma-Aldrich, VWR International Ltd. or Fisher Scientific UK Ltd. unless otherwise stated. Gemcitabine HCl was purchased from Shan Dong Boyuan Pharmaceutical Co. All chemicals were used as received.

2.1.2 Chromatography

Compounds were purified by manual flash column chromatography with commercially available silica gel (220 – 440 mesh, Sigma-Aldrich). Column size and solvents used to elute and purify the products varied depending on the amount of starting material used and polarity of compounds. R_f values were determined on Merck aluminium backed TLC Silica gel 60 F254 sheets. Compounds were visualized using a UV6L-58 Mineralight UV emitter at 254 nm. Reverse phase analytical high-performance liquid chromatography (RP HPLC) was performed using an Agilent 1100 Chemstation, and compounds were detected using an evaporative light scattering detector (ELSD) and a UV detector (280 and 254 nm). All solvents used were HPLC grade. Method: eluent A, water and formic acid (0.1%); eluent B, acetonitrile and formic acid (0.1%); A/B = 95:5 to 5:95 in 3 min, isocratic 1 min, 5:95 to 95:5 in 1 min, and isocratic 1 min.

2.1.3 Nuclear Magnetic Resonance Spectroscopy (NMR)

^{1}H and ^{13}C NMR spectra were recorded at ambient temperature on a Bruker Avance III 400 MHz and 500 MHz spectrometer from the School of Chemistry at the

University of Edinburgh. All chemical shifts are reported as parts per million (δ) relative to solvent peak. MestReNova software was used to interpret the spectra.

2.1.4 Mass Spectroscopy

Low Resolution Mass Spectra (LRMS) was obtained using an Agilent 1100 HPLC Modular System coupled to an Agilent Technologies 6130 Quadrupole LC/MS Mass Spectrometer under electron spray ionisation (ESI) conditions. High Resolution Mass Spectra (HRMS) were obtained using Bruker 3.0 T Apex II Spectrometer.

2.2 EXPERIMENTAL – CHAPTER 3

2.2.1 Synthesis of Pd^0 Resins and Characterization

NovaSyn TG amino resin HL (1,000 mg, 0.39 mmol NH_2 per gram) and palladium acetate (263.0 mg, 1.17 mmol) were added into a 25 ml Biotage microwave vial (Biotage). Next, toluene (10 ml) was added to the vial and heated to 80 °C under stirring for 10 min. The mixture was then stirred at room temperature (RT) for an additional 2 h. The resins were then filtered and washed with dichloromethane (DCM) (5 x 20 ml) and methanol (MeOH) (5 x 20 ml). Resins were dispersed in 10% hydrazine monohydrate in MeOH (10 ml) and stirred at room temperature for 25 min. The resins were again filtered and washed with MeOH (5 x 20 ml) and DCM (5 x 20 ml). Resins were added to a solution of Fmoc-Glu(OH)-OH (216 mg, 0.59 mmol), Oxyma (166 mg, 1.17 mmol), N,N'-diisopropylcarbodiimide (DIC) (148 mg, 1.17 mmol) with DCM/dimethylformamide (DMF) (2:1, 9ml) and stirred for 2 h at RT. The resins were filtered and washed with DCM (5 x 20 ml), MeOH (5 x 20 ml) and H_2O (5 x 20 ml) and dried in an oven at 40 °C for 3 days. Complete coupling was verified by the ninhydrin test after the last MeOH wash. Scanning electron microscope/transmission electron microscope images were performed by Stephen Mitchell from the School of Biological Sciences and Pd^0 quantification (by inductively coupled plasma-optical emission spectrometry) was performed by Dr. Lorna Eades from the School of Chemistry. Resins were characterized using X-ray diffractometry (Bruker D2 PHASER with LYNXEYE detector (Bruker), Cu

radiation source at 30 kV, 10mA and a Ni filtre). This was performed by Dr. Carmen Torrez-Sanchez from the Additive Manufacturing Research Group at Loughborough University before and after Pd^0-functionalization. Without any extra preparation or post-processing, samples were mounted on a 1 inch diameter standard holder. The phase constituents were identified as per Fig 3.2.

*2.2.1.1 Synthesis of 2-(9H-fluoren-9-ylmethoxycarbonylamino)pentanedioic acid (**Fmoc-Glu(OH)-OH**)*

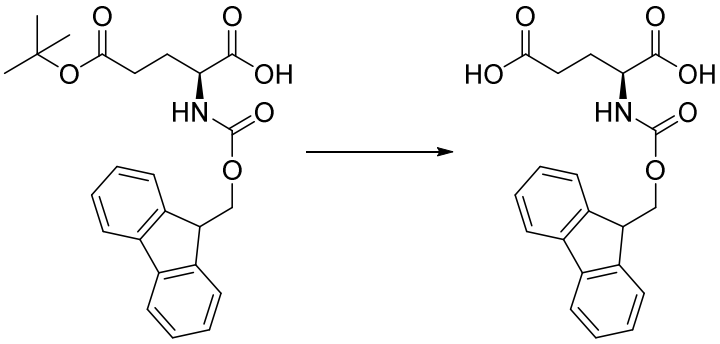

Fmoc-Glu(OtBu)-OH (1g, 2.4 mol) is dissolved in DCM (15 ml) with 20% TFA (5 ml). The mixture was stirred for 3.5 hrs. The solvent was removed *in vacuo* and purified via ether titration yielding a white solid (491 mg, 58%), R_f 0.12 (15% MeOH in DCM).^{1}H NMR (500 MHz, MeOD) δ 7.79 (d, J = 7.5, 0.9 Hz, 2H, Ar*H*), 7.67 (t, 2H, Ar*H*), 7.39 (t, 2H, Ar*H*), 7.31 (td, J = 7.5, 6.8, 1.2 Hz, 2H, Ar*H*), 4.35 (dd, J = 7.1, 2.5 Hz, 1H, O–C*H*$_2$–CH), 4.26 – 4.18 (m, 2H, C–C*H*–NH; O–CH$_2$–C*H*), 2.41 (t, J = 7.5 Hz, 2H, CH–CH$_2$–C*H*$_2$), 2.25 – 2.13 (m, 1H, CH–C*H*$_2$–CH$_2$), 1.98 – 1.88 (m, 1H, CH–C*H*$_2$–CH$_2$).^{13}C NMR (126 MHz, MeOD) δ 176.38 (C), 175.36 (C), 158.70 (C), 145.35 (C), 145.19 (C), 142.58 (C), 128.78 (CH), 128.17 (CH), 126.28 (CH), 120.89 (CH), 68.02 (CH_2), 54.65 (CH), 48.42 (CH), 31.22 (CH_2), 27.90 (CH_2). MS (ESI) m/z 368.0 $[M-H]^-$.[71]

2.3 EXPERIMENTAL – CHAPTER 4

*2.3.1 Synthesis of Carbonate Gemcitabine Prodrugs (**2, 3, 4**)*

Gemcitabine HCl (**1**) (150 mg, 0.5 mmol) was dissolved in dry DMF (3 mL) with 1,8-diazabicyclo[5.4.0]undec-7-ene (DBU) (194 µL, 1.30 mmol) under N_2

atmosphere. The mixture was then cooled to 4 °C in an ice bath. Allyl, propargyl, or benzyl chloroformate (0.75 mmol) was added dropwise to the mixture. The mixture was stirred overnight and allowed to warm up to RT. The solvents were then removed *in vacuo*, the crude redissolved with 25% isopropanol (IPA) in $CHCl_3$ (20 mL), and washed with H_2O (20 mL). The aqueous layer was washed with 25% IPA in $CHCl_3$ (3 × 20 mL) and the combined organic layers dried over $MgSO_4$, filtered, and concentrated *in vacuo*.

*2.3.1.1 4-Amino-1-(2-deoxy-2,2-difluoro-5-O-[allyloxycarbon-yl]-β-D-erythro-pentofuranosyl)pyrimidin-2(1H)-one] (**2**)*

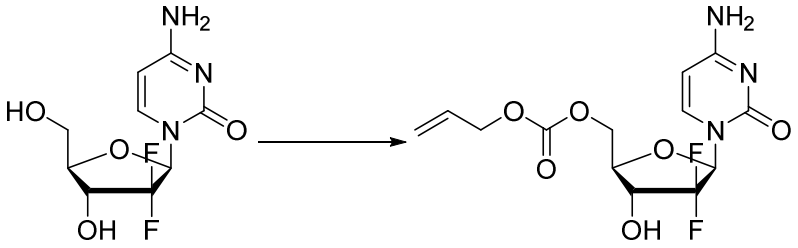

The crude was purified by column chromatography with 8% MeOH in DCM (R_f 0.29, 10% MeOH in DCM) which yielded a light green solid (90 mg, 52% yield). ^{1}H NMR (500 MHz, DMSO) δ 7.50 (d, *J* = 7.5, 1H, Ar*H*), 7.42 (d, *J* = 5.7, 2H, N*H*$_2$), 6.44 (d, *J* = 6.3, 1H, CH–O*H*), 6.17 (s, 1H, Ar*H*), 5.99 – 5.89 (m, 1H, –C*H*=), 5.79 (d, *J* = 7.5, 1H, Ar*H*), 5.38 – 5.23 (m, 1H, =C*H*$_2$), 4.63 (dt, *J* = 5.5, 1.3, 2H, C*H*$_2$–CH=), 4.47 – 4.37 (m, 2H, C*H*$_2$–O), 4.18 (s, 1H, Ar*H*), 4.07 – 4.00 (m, 1H, Ar*H*). ^{13}C NMR (126 MHz, DMSO) δ 165.63 (C), 154.48 (C), 154.07 (C), 141.16 (CH), 132.02 (CH), 122.60 (t, $J_{C\text{-}F}$ = 264.6, C), 118.56 (CH_2), 94.87 (CH), 83.89 (CH), 77.22 (CH), 70.09 (t, $J_{C\text{-}F}$ = 25.2, CH), 68.16 (CH_2), 66.31 (CH_2). MS (ESI) m/z 346.0 [M-H]$^-$. HRMS (m/z): [M - H]$^-$ calcd for $C_{13}H_{14}O_6N_3F_2$, 346.0856; found 346.0859.

*2.3.1.2 4-Amino-1-(2-deoxy-2,2-difluoro-5-O-[propargyloxy-carbonyl]-β-D-erythro-pentofuranosyl)pyrimidin-2(1H)-one] (**3**).*

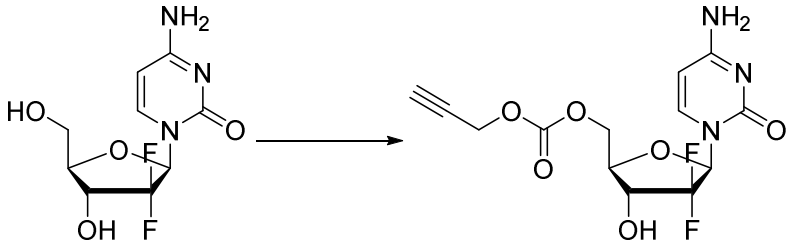

The crude was purified by column chromatography with 10% MeOH in DCM (R_f 0.23, 10% MeOH in DCM) which yielded a pale yellow solid (81 mg, 47%)**.** ^{1}H NMR (500 MHz, DMSO) δ 7.65 (d, *J* = 7.5, 1H, Ar*H*), 7.44 (d, *J* = 13.0, 2H, N*H*$_2$), 6.24 (s, 1H, Ar*H*), 5.81 (d, *J* = 7.5, 1H, Ar*H*), 5.28 – 5.26 (m, 2H, Ar*H*, CH–O*H*), 4.88 (s, 2H, C*H*$_2$–C≡CH), 4.22 – 4.16 (m, 1H, Ar*H*), 3.79 – 3.62 (m, 3H, C≡C*H*, C*H*$_2$). ^{13}C NMR (126 MHz, DMSO) δ 165.71 (C), 154.41 (C), 152.63 (C), 141.43 (CH), 121.48 (t, J_{C-F} = 262.1, C), 94.83 (CH), 83.76 (CH), 79.16 (CH), 78.11 (CH), 77.25 (C), 73.39 (t, J_{C-F} = 26.5, CH), 59.18 (CH_2), 56.37 (CH_2). MS (ESI) m/z 379.9 $[M+Cl]^-$. HRMS (m/z): $[M - H]^-$ calcd for $C_{13}H_{12}O_6N_3F_2$, 344.0700; found 344.0728.

*2.3.1.3 4-Amino-1-(2-deoxy-2,2-difluoro-5-O-[benzyloxy-carbonyl]-β-Derythro- pentofuranosyl)pyrimidin-2(1H)-one] (**4**).*

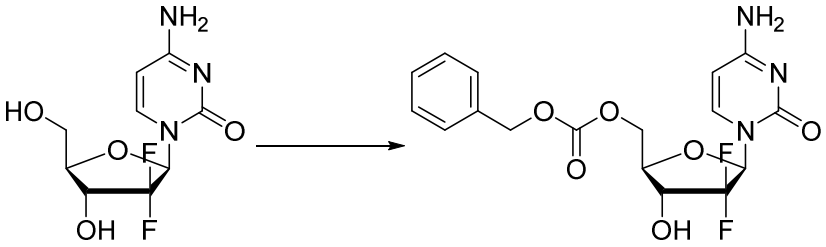

The crude was purified by column chromatography with 6% MeOH in DCM (R_f 0.05, 4% MeOH in DCM) which yielded a white solid (70 mg, 53% yield). ^{1}H NMR (500 MHz, DMSO) δ 7.49 (d, *J* = 7.5, 1H, Ar*H*), 7.44 – 7.33 (m, 7H, Ar*H,* N*H*$_2$), 6.44 (d, *J* = 6.2, 1H, CH–O*H*), 6.17 (s, 1H, Ar*H*), 5.76 (d, *J* = 7.5, 1H, Ar*H*), 5.17 (s, 2H, C*H*$_2$–Ph), 4.52 – 4.35 (m, 2H, C*H*$_2$–O), 4.18 (s, 1H, Ar*H*), 4.03 (t, *J* = 6.1, 1H, Ar*H*). ^{13}C NMR (126 MHz, DMSO) δ 165.60 (C), 154.45 (C), 154.20 (C), 141.15 (CH), 135.04 (C), 128.50 (CH), 128.42 (CH), 128.17 (CH), 122.57 (t, J_{C-F} = 258.3, C), 94.83 (CH), 83.86 (CH), 77.18 (CH), 70.10 (t, J_{C-F} = 23.4, CH), 69.22 (CH_2),

66.39 (CH_2). MS (ESI) m/z 398.0 $[M+H]^+$. HRMS (m/z): $[M - H]^-$ calcd for $C_{17}H_{16}O_6N_3F_2$, 396.1013; found 396.1016.

*2.3.2 Synthesis of Carbamate Gemcitabine Prodrugs Intermediates (**6, 7, 8**).*

*2.3.2.1 Synthesis of Compound **5**.*

1 (500 mg, 1.67 mmol) was dissolved in dry DMF (5 ml) with imidazole (397 mg, 5.84 mmol) and *Tert*-butyldimethylsilyl chloride (TBS-Cl) (302 mg, 2.0 mmol) stirred at RT overnight. The mixture was then concentrated *in vacuo*. The mixture was then dissolved in EtOAc (50 ml) and washed with H_2O (50 ml). The aqueous layer was then washed two more times with EtOAc. The organic layer was then washed with brine (150 ml) and dried over $MgSO_4$. The product was then purified by column chromatography with 8% MeOH in DCM.

*2.3.2.2 4-amino-1-(2-deoxy-2,2-difluoro-5-O-[tertbutyl(dimethyl)silyl]-β-D erythropentofuranosyl)pyrimidin-2(1H)- one] (**5**)*

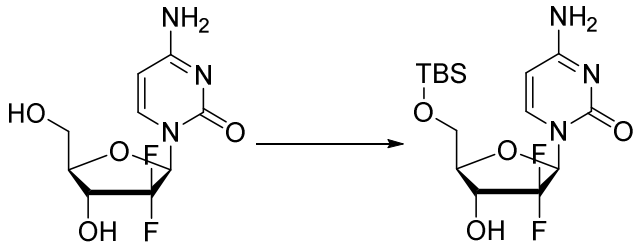

552 mg, 88% yield. ^{1}H NMR (500 MHz, DMSO) δ 7.63 (d, *J* = 7.5, 1H, Ar*H*), 7.38 (s, 2H, N*H*$_2$), 6.31 (d, *J* = 5.1, 1H, CH–O*H*), 6.14 (t, *J* = 7.7, 1H, Ar*H*), 5.76 (d, *J* = 7.5, 1H, Ar*H*), 4.19 – 4.06 (m, 1H, Ar*H*), 3.95 (d, *J* = 11.8, 1H, Ar*H*), 3.90 – 3.77 (m, 2H, C*H*$_2$– OH), 0.90 (s, 9H, C-(C*H*$_3$)$_3$), 0.09 (d, *J* = 2.1, 6H, Si-(C*H*$_3$)$_2$). ^{13}C NMR (126 MHz, DMSO) δ 165.58 (C), 154.56 (C), 139.91 (CH), 122.95 (t, $J_{C\text{-}F}$ = 258.3, C), 94.51 (CH), 83.45 (t, $J_{C\text{-}F}$ = 31.5, CH), 79.76 (CH), 68.23 (t, $J_{C\text{-}F}$ = 22.7, CH), 60.72 (CH_2), 25.71 (CH_3), 17.99 (C), -5.52(CH_3), -5.63 (CH_3). MS (ESI) m/z: 378.0 $[M+H]^+$.

*2.3.2.3 Synthesis of Intermediate **6**.*

Compound **5** (100 mg, 0.27 mmol) was dissolved in dry THF (2.5 mL) with pyridine (61 µL, 0.75 mmol) and the mixture cooled to 4 °C in an ice bath. Allyl chloroformate (55 µL, 0.52 mmol) was added dropwise to the mixture and stirred for 1 h. The solvent was removed *in vacuo* and purified via flash chromatography (eluent: 3% MeOH in DCM) to yield compound **6** as a white solid.

*2.3.2.4 4-(Allyloxycarbonylamino)-1-(2-deoxy-2,2-difluoro-5-O-[tertbutyl(dimethyl)silyl]-β-D-erythro-pentofuranosyl)pyrimidin-2(1H)- one] (**6**).*

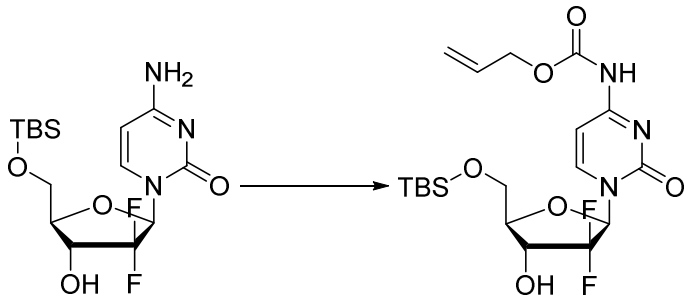

83 mg, 69% yield (R_f 0.53, 10% MeOH in DCM). ^{1}H NMR (500 MHz, MeOD) δ 8.29 (d, *J* = 7.7, 1H, Ar*H*), 7.32 (d, *J* = 7.6, 1H. Ar*H*), 6.25 (t, *J* = 6.7, 1H, Ar*H*), 6.04 – 5.94 (m, 1H, –C*H*=), 5.39 (dq, *J* = 17.2, 1.5, 1H, =CH_2), 5.27 (dq, *J* = 10.5, 2.6, 1.3, 1H, =CH_2), 4.70 (dt, *J* = 5.6, 1.4, 2H, CH_2–C=), 4.33 – 4.24 (m, *J* = 12.5, 8.8, 1H, Ar*H*), 4.10 (d, *J* = 12.0, 1H, Ar*H*), 4.03 – 3.89 (m, 2H, CH_2-O), 0.97 (s, 9H, C–(CH_3)$_3$), 0.17 (s, 6H, Si-(CH_3)$_2$). ^{13}C NMR (126 MHz, MeOD) δ 165.38 (C), 157.33 (C), 154.35 (C), 144.81 (CH), 133.24 (CH), 123.87 (t, J_{C-F} = 259.7, C), 118.88 (CH_2), 96.95 (CH), 86.22 (t, J_{C-F} = 32.8, CH), 82.46 (CH), 69.56 (t, J_{C-F} = 23.9, CH), 67.56 (CH_2), 61.68 (CH_2), 26.37 (CH_3), 19.26 (C), -5.35 (CH_3), -5.45 (CH_3). MS (ESI) m/z 462.0 $[M+H]^+$.

*2.3.2.5 Synthesis of Intermediates **7** and **8***

Compound **5** (100 mg, 0.27 mmol) was dissolved in dry DMF (2.5 mL) with pyridine (61 µL, 0.75 mmol) and the mixture cooled to 4 °C in an ice bath. Propargyl (63 µL, 0.65 mmol) or benzyl chloroformate (56 µL, 0.39 mmol) was added dropwise to the mixture. The mixture was stirred at RT overnight (for **8**) or for 48 h (for **7**). The

solvents were removed and the mixture redissolved with EtOAc (30 mL) and washed with H_2O (30 mL). The aqueous layer was washed twice more with EtOAc (30 mL each) and the combined organic layers dried over $MgSO_4$ and concentrated *in vacuo*. The crude was purified via flash chromatography (eluent: 3% MeOH in DCM) to yield compounds **7** and **8** as white solids.

*2.3.2.6 4-(Propargyloxycarbonylamino)-1-(2-deoxy-2,2-difluoro-5-O-[tert-butyl(dimethyl)silyl]-β-D-erythro-pentofuranosyl)pyrimidin-2(1H)-one] (**7**).*

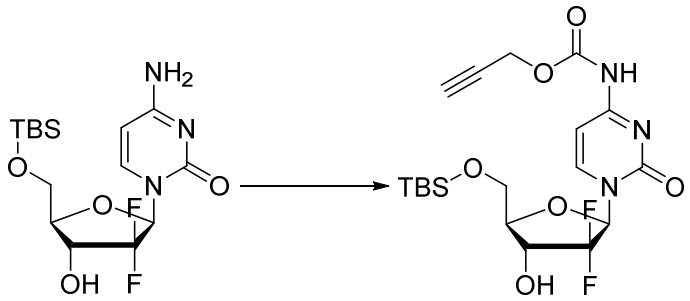

53 mg, 44% (R_f 0.6, 10% MeOH in DCM)**.** ^{1}H NMR (500 MHz, MeOD) δ 8.30 (d, *J* = 7.6, 1H, Ar*H*), 7.29 (d, *J* = 7.6, 1H, Ar*H*), 6.25 (t, *J* = 6.7, 1H, Ar*H*), 4.84 (d, *J* = 2.5, 2H, CH_2–C≡CH), 4.33 – 4.24 (m, 1H, Ar*H*), 4.10 (d, *J* = 12.0, 1H, Ar*H*), 4.03 – 3.90 (m, 2H, CH_2–OH), 2.99 (t, *J* = 2.3, 1H, C≡C*H*), 0.98 (s, 9H, C– (CH_3)$_3$), 0.17 (s, 6H, Si-(CH_3)$_2$). ^{13}C NMR (126 MHz, MeOD) δ 165.28 (C), 157.29 (C), 154.57 (C), 144.97 (CH), 123.88 (t, J_{C-F} = 259.6, C), 96.93 (CH), 86.15 (t, J_{C-F} = 32.8, CH), 82.49 CH), 77.70 (C), 76.92 (CH), 69.57 (t, J_{C-F} = 22.7, CH), 61.69 (CH_2), 54.34 (CH_2), 26.36 (CH_3), 19.26 (C), -5.36 (CH_3), -5.46 (CH_3). MS (ESI) m/z 460.2 $[M+H]^+$.

*2.3.2.7 4-(Benzyloxycarbonylamino)-1-(2-deoxy-2,2-difluoro-5-O-[tertbutyl(dimethyl)silyl]-β-D-erythro-pentofuranosyl)pyrimidin-2(1H)-one] (**8**).*

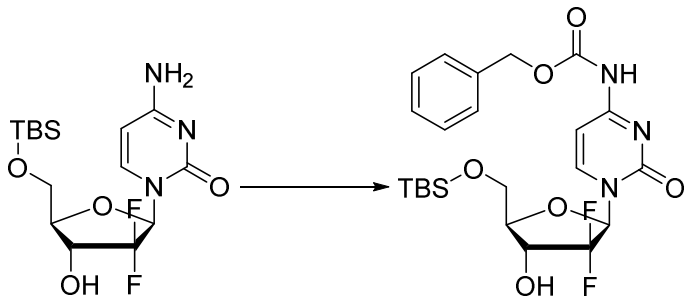

86 mg, 42% (R_f 0.53, 10% MeOH in DCM). ^{1}H NMR (500 MHz, CDCl3) δ 8.11 (d, *J* = 7.5, 1H, Ar*H*), 7.40 – 7.32 (m, 5H, Ar*H*), 6.40 – 6.32 (m, 1H, Ar*H*), 5.22 (s, 2H, C*H*$_2$–Ph), 4.41 – 4.31 (m, 1H, Ar*H*), 4.07 – 4.00 (m, 2H, Ar*H* + C*H*$_2$), 3.90 (dd, *J* = 11.9, 2.2, 1H, C*H*$_2$), 0.93 (s, 9H, C– (C*H*$_3$)$_3$), 0.12 (s, 6H, Si-(C*H*$_3$)$_2$). ^{13}C NMR (126 MHz, DMSO) δ 162.90 (C), 154.93 (C), 152.35 (C), 144.42 (CH), 135.02 (C), 128.85 (CH), 128.43 (CH), 122.32 (t, J_{C-F} = 258.3, C), 95.54 (CH), 84.56 (t, J_{C-F} = 32.8, CH), 81.62 (CH), 69.31 (t, J_{C-F} = 26.5, CH), 68.22 (CH_2), 60.69 (CH_2), 25.97 (CH_3), 18.5 (C), -5.37 (CH_3).). MS (ESI) m/z 534.1 $[M+Na]^+$.

*2.3.3 Synthesis of Carbamate Gemcitabine Prodrugs (**9, 10, 11**)*

Compounds **6, 7** and **8** (48 mg, 0.1 mmol; 31 mg, 0.07 mmol; 73 mg, 0.14 mmol respectively) and TBAF solution (1.5 equiv. for **6** and **8** and 2.5 equiv for **7**) were dissolved in anhydrous THF (3 mL) and stirred at room temperature for 3 h (for **10**) or overnight (for **9, 11**). The resulting mixture was concentrated *in vacuo* and purified via flash chromatography (6% MeOH in DCM) to yield compounds **9, 10** and **11** as white solids.

2.3.3.1 4-(Allyloxycarbonylamino)-1-(2-deoxy-2,2-difluoro-β-Derythropento-furanosyl)pyrimidin-2(1H)-one ***(9)***.

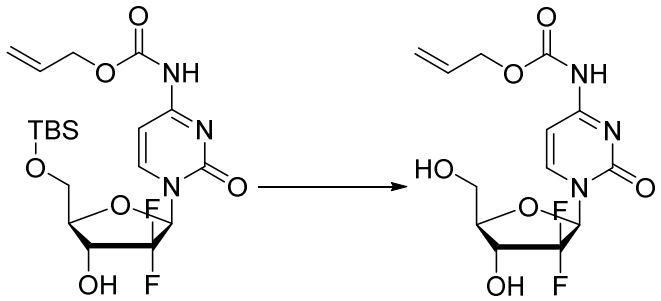

32 mg, 92% (R_f 0.27, 10% MeOH in DCM). ^{1}H NMR (500 MHz, DMSO) δ 10.96 (s, 1H, CH_2–O*H*), 8.23 (d, *J* = 7.6, 1H, Ar*H*), 7.10 (d, *J* = 7.6, 1H, Ar*H*), 6.31 (d, *J* = 6.5, 1H, CH–O*H*), 6.16 (t, *J* = 7.5, 1H, Ar*H*), 6.00 – 5.89 (m, 1H, –C*H*=), 5.42 – 5.21 (m, 3H, =C*H*$_2$, N*H*), 4.64 (d, *J* = 5.3, 2H, C*H*$_2$–C=), 4.24 – 4.13 (m, 1H, Ar*H*), 3.88 (dt, *J* = 8.5, 3.1, 1H, Ar*H*), 3.84 – 3.61 (m, 2H, C*H*$_2$– OH). ^{13}C NMR (126 MHz, DMSO) δ 163.40 (C), 153.99 (C), 152.82 (C), 144.45 (CH), 132.39 (CH), 122.94 (t, $J_{C\text{-}F}$ = 258.3, C), 118.04 (CH_2), 94.82 (CH), 84.07 (t, $J_{C\text{-}F}$ = 32.8, CH), 80.98 (CH), 68.37 (t, $J_{C\text{-}F}$ = 22.7, CH), 65.64 (CH_2), 58.79 (CH_2).). MS (ESI) m/z 346.0 $[M\text{-}H]^-$. HRMS (m/z): $[M - H]^-$ calcd for $C_{13}H_{14}O_6N_3F_2$, 346.0856; found 346.0853.[72]

*2.3.3.2 4-(Propargyloxycarbonylamino)-1-(2-deoxy-2,2-difluoro-β-D-erythro-pentofuranosyl)pyrimidin-2(1H)-one (**10**)*

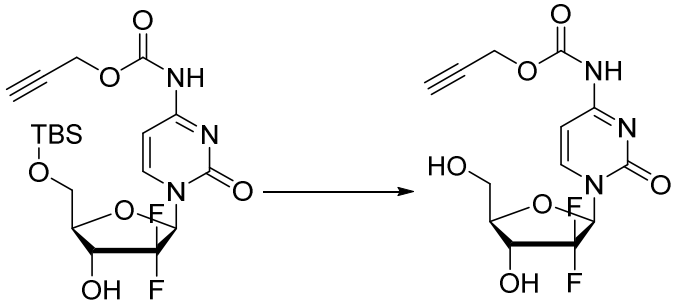

39 mg, 81% (R_f 0.41, 10% MeOH in DCM). ^{1}H NMR (500 MHz, DMSO) δ 11.06 (s, 1H, CH_2– O*H*), 8.25 (d, *J* = 7.6, 1H, Ar*H*), 7.08 (d, *J* = 7.5, 1H, Ar*H*), 6.30 (d, *J* = 6.5, 1H, CH–O*H*), 6.16 (t, *J* = 7.4, 1H, Ar*H*), 5.29 (t, *J* = 5.5, 1H, N*H*), 4.80 (d, *J* = 2.4, 2H, C*H*$_2$–C≡CH), 4.26 – 4.13 (m, 1H, Ar*H*), 3.89 (dt, *J* = 8.5, 3.1, 1H, Ar*H*), 3.84 – 3.63 (m, 2H, C*H*$_2$), 3.62 (t, *J* = 2.4, 1H, C≡C*H*). ^{13}C NMR (126 MHz,

DMSO) δ 163.26 (C), 153.93 (C), 152.37 (C), 144.61 (CH), 122.92 (C), 94.80 (CH), 84.09 (CH), 81.01 (CH), 78.21 (CH), 78.18 (C) 68.37 (CH), 58.78 (CH), 53.01 (CH_2). MS (ESI) m/z 344.0 $[M-H]^-$. HRMS (m/z): $[M - H]^-$ calcd for $C_{13}H_{12}O_6N_3F_2$, 344.0700; found 344.0719.

*2.3.3.3 4-(Benzyloxycarbonylamino)-1-(2-deoxy-2,2-difluoro-β-D-erythro-pentofuranosyl)pyrimidin-2(1H)-one (**11**)*

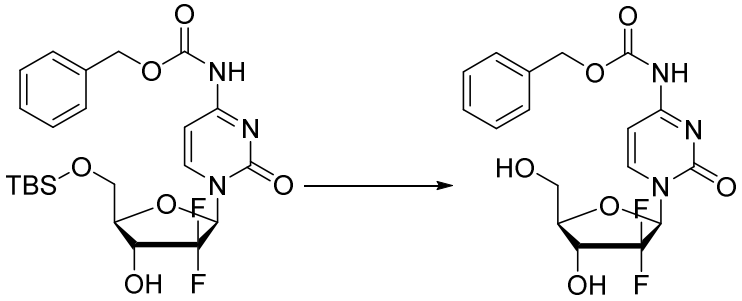

51 mg, 92% yield (R_f 0.33, 10% MeOH in DCM). ^{1}H NMR (500 MHz, DMSO) δ 10.98 (s, 1H, CH_2–O*H*), 8.23 (d, *J* = 7.6, 1H, Ar*H*), 7.45 – 7.32 (m, 5H, Ar*H*), 7.11 (d, *J* = 7.6, 1H, Ar*H*), 6.31 (d, *J* = 6.5, 1H, CH–O*H*), 6.16 (t, *J* = 7.4, 1H, Ar*H*), 5.29 (t, *J* = 5.5, 1H, N*H*), 5.20 (s, 2H, C*H*$_2$–Ph), 4.25 – 4.13 (m, 1H. Ar*H*), 3.88 (dt, *J* = 8.5, 3.1, 1H, Ar*H*), 3.84 – 3.62 (m, 2H, C*H*$_2$– OH). ^{13}C NMR (126 MHz, DMSO) δ 163.38 (C), 153.99 (C), 153.00 (C), 144.46 (CH), 135.81 (C),), 128.48 (CH), 128.19 (CH), 127.96 (CH), 122.93 (t, J_{C-F} = 259.6, C), 94.86 (CH), 84.08 (t, J_{C-F} = 30.2, CH),80.98 (CH), 68.37 (t, J_{C-F} = 22.7, CH), 66.67 (CH_2), 58.78 (CH_2). MS (ESI) m/z 396.1 $[M-H]^-$. HRMS (m/z): $[M - H]^-$ calcd for $C_{17}H_{16}O_6N_3F_2$, 396.1013; found 396.1016.

*2.3.4 Synthesis of Non-Fluorescent Probes (**13, 14, 15**)*

*2.3.4.1 Synthesis of Non-Fluorescent Probe bis-N,N'-allyloxycarbonylrhodamine 110 (**13**)*

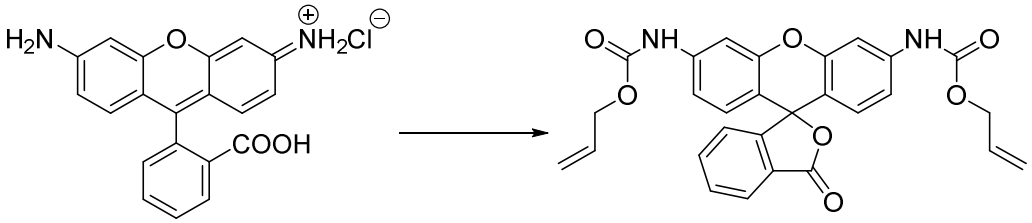

Rhodamine 110 (**12**) (250 mg, 0.68 mmol) is dissolved in dry DMF (1.5 ml) under N_2 atmosphere. and cooled to 4 ˚C. Separately, allyl chloroformate (492 µl, 4.08 mmol, 6 eq.), diluted in dry DMF (1 ml) and pyridine (496 µl, 6.12 mmol, 9 eq.) are simultaneously added dropwise to the rhodamine 110 solution. The reaction mixture is allowed to warmup to RT while stirring overnight. The solvent is then removed *in vacuo*. The mixture is resuspended in 25% IPA in $CHCl_3$ (20 ml) and washed with 5% HCl. The aqueous layer is then washed twice more with 25% IPA in $CHCl_3$ (20 ml X2). The combined organic layer is washed with 5% HCl (60 ml X3), $NaHCO_3$ (60 ml X1). The organic layer was then washed with charcoal for 10-15 min to decolorize any impurities. The organic layer was then filtered, dried over $MgSO_4$ and filtered again. Product was purified via flash chromatography (hexane/ethyl acetate [2:1]) which yielded bis-N,N'-allyloxycarbonylrhodamine 110 (**12**) as a white solid 121 mg (36% yield), R_f 0.2 (hexane/ethyl acetate [2:1]). ^{1}H NMR (500 MHz, MeOD) δ 8.02 (d, *J* = 7.6, 1H, Ar*H*), 7.77 (t, *J* = 7.5, 1H, Ar*H*), 7.71 (t, *J* = 7.5, 1H, Ar*H*), 7.61 (s, 2H, Ar*H*), 7.21 (d, *J* = 7.7, 1H. Ar*H*), 7.07 (dd, *J* = 8.7, 1.9, 2H, Ar*H*), 6.67 (d, *J* = 8.7, 2H, Ar*H*), 6.00 (m, 2H, –C*H*=), 5.38 (dd, *J* = 17.2, 1.1, 2H, =CH_2), 5.24 (d, *J* = 10.5, 2H, =CH_2), 4.66 (d, *J* = 5.5, 4H, CH_2–C=). ^{13}C NMR (126 MHz, MeOD) δ 171.37 (C), 155.31 (C), 154.46 (C), 153.21 (C), 142.91 (C), 136.72 (CH), 134.07 (CH), 131.25 (CH), 129.42 (CH), 127.80 (C), 125.87 (CH), 125.19 (CH), 118.06 (CH_2), 115.55 (CH), 114.21 (C), 106.94 (CH), 84.58 (C), 66.64 (CH_2). MS (ESI) m/z 496.9 $[M-H]^-$.[57]

*2.3.4.2 Synthesis of Non-Fluorescent Probe bis-N,N'-propargyloxycarbonylrhodamine 110 (**14**)*

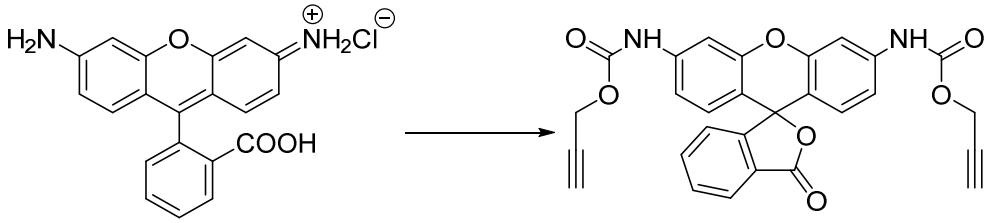

12 (250 mg, 0.68 mmol) is dissolved in dry DMF (4 ml) under nitrogen atm. Separately, Propargyl chloroformate (265 µl, 2.72 mmol, 4 eq.), and triethylamine (474 µl, 3.4 mmol, 5 eq.) are simultaneously added dropwise to the rhodamine mixture. The reaction mixture is stirred at RT for 48h. The solvent is then removed *in vacuo*. The mixture is resuspended in 25% IPA in DCM (20 ml) and washed with H_2O. The aqueous layer is then washed 5 more with 25% IPA in DCM (20 ml X5). The combined organic layer was then dried over $MgSO_4$ and filtered. Next, the organic layer was washed with charcoal for 10-15 min to decolorize any impurities and filtered again. Product was purified via flash chromatography (hexane/ethyl acetate [2:1]) which yielded bis-N,N'-propargyloxycarbonylrhodamine 110 (**14**) as a white solid, 67 mg (20% yield), R_f 0.13 (hexane/ethyl acetate [2:1]). ^{1}H NMR (500 MHz, MeOD) δ 8.02 (d, J = 7.6, 1H, ArH), 7.77 (td, J = 7.5, 1.1, 1H, ArH), 7.71 (td, J = 7.5, 0.9, 1H, ArH), 7.61 (d, J = 1.9, 2H, ArH), 7.21 (d, J = 7.6, 1H, ArH), 7.08 (dd, J = 8.7, 2.2, 2H, ArH), 6.68 (d, J = 8.7, 2H, ArH), 4.78 (d, J = 2.4, 4H, CH_2–C≡CH), 2.94 (t, J = 2.4, 2H, C≡CH). ^{13}C NMR (126 MHz, MeOD) δ 171.35 (C), 154.59 (C), 154.43 (C), 153.18 (C), 142.65 (C), 136.74 (CH), 131.27 (CH), 129.47 (CH), 127.76 (C), 125.89 (CH), 125.19 (CH), 115.60 (CH), 114.42 (C), 107.04 (CH), 84.48 (C), 79.08 (C), 76.22 (C), 53.40 (CH_2). MS (ESI) m/z 495.2 $[M+H]^+$.[62,67]

*2.3.4.3 Synthesis of Non-Fluorescent Probe bis-N,N'-benzyloxycarbonylrhodamine 110 (**15**)*

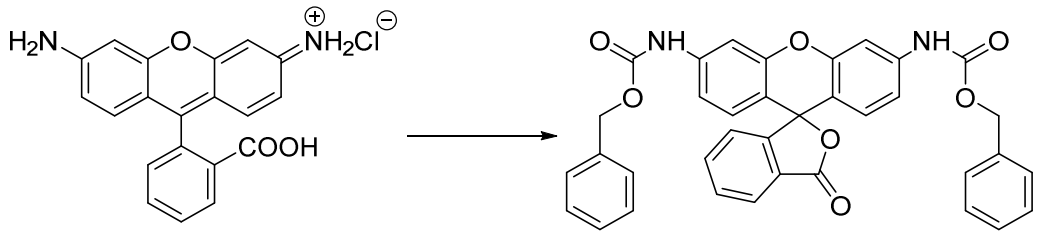

Under N_2 atmosphere, **12** (150 mg, 0.41 mmol) was dissolved in dry DMF (4 mL). Separately, benzyl chloroformate (350 µL, 2.45 mmol) and pyridine (298 µL, 3.69 mmol) were dissolved in DMF (1 mL) and added dropwise to the mixture. The reaction mixture was stirred at RT for 48 h, solvents removed *in vacuo*, and the resulting crude resuspended in 25% isopropanol in CHCl3 (30 mL) and washed with H2O. The aqueous layer was then washed 5 times with 25% isopropanol in CHCl3 (30 mL). The combined organic layers were dried over anhydrous $MgSO_4$ and the solids filtered off and concentrated *in vacuo*. The crude was purified via flash chromatography (hexane/EtOAc 2:1) to yield bis-N,N'-benzyloxycarbonylrhodamine 110 (**15**) as a white solid 31 mg (13% yield), R_f 0.23 (hexane/ethyl acetate [2:1]). ^{1}H NMR (500 MHz, DMSO) δ 10.12 (s, 2H, N*H*), 8.01 (d, *J* = 7.6, 1H, Ar*H*), 7.78 (t, *J* = 7.1, 1H, Ar*H*), 7.72 (t, *J* = 7.3, 1H, Ar*H*), 7.58 (d, *J* = 1.7, 2H, Ar*H*), 7.45 – 7.33 (m, 10H, Ar*H*), 7.27 (d, *J* = 7.6, 1H, Ar*H*), 7.20 – 7.12 (m, 2H, Ar*H*), 6.70 (d, *J* = 8.7, 2H, Ar*H*), 5.18 (s, 4H, C*H*$_2$–Ph). ^{13}C NMR (126 MHz, DMSO) δ 168.66 (C), 153.25 (C), 152.51 (C), 150.94 (C), 141.43 (C), 136.31 (C), 135.71 (CH), 130.21 (CH), 128.53 (CH), 128.47 (CH) 128.19 (CH), 125.71 (C), 124.77 (CH), 123.95 (CH), 114.46 (CH), 112.48 (C), 105.10 (CH), 81.94 (C), 66.07 (CH_2).MS (ESI) m/z 597.2 $[M-H]^-$. HRMS (m/z): $[M + H]^+$ calcd for $C_{35}H_{27}O_7N_2$, 599.1813; found 599.1795.

2.4 EXPERIMENTAL – CHAPTER 5

*2.4.1 Synthesis of 5FU Prodrugs (**All, Pro, Bn-5FU**)*

5FU (**16**) (200 mg, 1.54 mmol) and DBU (269 ml, 1.80 mmol) were dissolved in dry DMF (2 ml) under N_2 atmosphere and cooled to 4 °C. Either allyl, propargyl or

benzyl bromide (1.54 mmol) were dissolved in dry DMF (0.5 ml). The solution was then added dropwise to the mixture and stirred at RT overnight. Solvents were then removed under reduced pressure and the crude purified via flash chromatography (3% MeOH in DCM).

*2.4.1.1 1-allyl-5-fluorouracil (**All-5FU; 17**)*

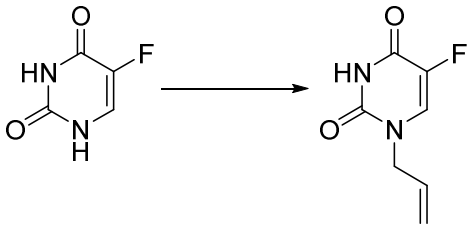

80 mg, 31% yield (R_f 0.5, 6% MeOH in DCM). ^{1}H NMR (500 MHz, DMSO) δ 11.80 (br s, 1H, N*H*), 8.01 (d, *J* = 6.7, 1H, Ar*H*), 5.88 (ddt, *J* = 17.0, 10.5, 5.3, 1H, N–CH_2–C*H*), 5.19 (m, 2H, CH_2–CH–CH_2), 4.24 (d, *J* = 5.3, 2H, N–CH_2–CH). ^{13}C NMR (126 MHz, DMSO) δ 157.45 (d, J_{C-F} = 25.7, C), 149.46 (C), 139.68 (d, J_{C-F} = 229.3, C), 132.63 (CH), 129.79 (d, J_{C-F} = 33.2, CH), 117.64 (CH_2), 49.34 (CH_2). MS (ESI) m/z 169.2 $[M-H]^-$. HRMS (m/z): $[M + H]^+$ calcd for $C_7H_7O_2N_2F_1$ 170.0486 found 170.0489.

*2.4.1.2 1-propargy-5-fluorouracil (**Pro-5FU; 18**)*

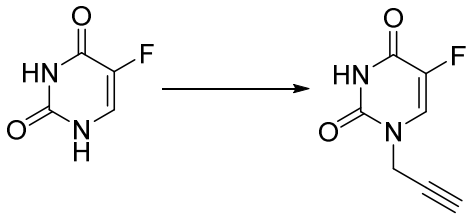

104 mg, 40% yield (R_f 0.35, 6% MeOH in DCM). ^{1}H NMR (500 MHz, DMSO) δ 11.91 (br s, 1H, N*H*), 8.13 (d, *J* = 5, 1H, Ar*H*), 4.46 (d, *J* = 2.5, 2H, N–CH_2–C), 3.44 (t, *J* = 2.5, 1H, C≡C*H*). ^{13}C NMR (126 MHz, DMSO) δ 157.35 (d, J_{C-F} = 25.9, C), 149.11 (C), 139.80 (d, J_{C-F} = 230.4, C), 128.95 (d, J_{C-F} = 33.9, CH), 78.40 (C), 76.15

(CH), 37.00 (CH_2). MS (ESI) m/z 167.2 $[M-H]^-$. HRMS (m/z): $[M + H]^+$ calcd for $C_7H_5O_2N_2F$ 168.0332 found 168.0330.

*2.4.1.3 1-benzyl-5-fluorouracil (**Bn-5FU; 19**)*

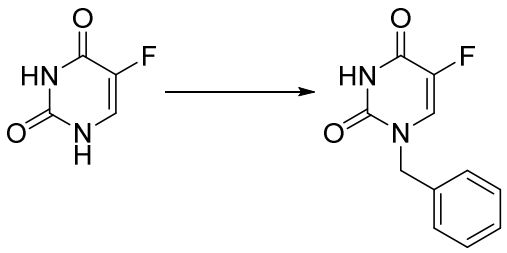

133 mg, 38% yield (R_f 0.44, 6% MeOH in DCM). ^{1}H NMR (500 MHz, DMSO) δ 11.86 (br s, 1H, N*H*), 8.22 (d, *J* = 6.7, 1H, Ar*H*), 7.39 – 7.28 (m, 5H, Ar*H*), 4.83 (s, 2H, N–CH_2–Ph). ^{13}C NMR (126 MHz, DMSO) δ 157.42 (d, J_{C-F} = 25.6, C), 149.68 (C), 139.62 (d, J_{C-F} = 227.9, C), 136.52 (C), 130.08 (d, J_{C-F} = 33.4, CH), 128.67 (CH), 127.75 (CH), 127.49 (CH), 50.63 (CH_2). MS (ESI) m/z 219.2 $[M-H]^-$. HRMS (m/z): $[M + H]^+$ calcd for $C_{11}H_9O_2N_2F$ 220.0643 found 220.0643.

*2.4.2 Synthesis of 1-propargyl-2-pyridone (**21**)*

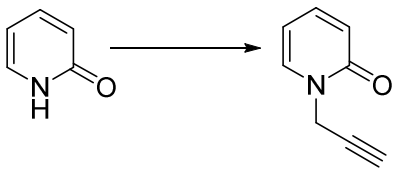

2-hydroxypyridine (**20**) (170 mg, 1.3 mmol) was dissolved in dry DCM (4 ml) containing DBU (291.6 µl, 2.0 mmol). Propargyl bromide solution (166.8 µl, 1.6 mmol) was added dropwise to the mixture. Reaction was stirred at RT overnight. The solvent was then removed and the product was dissolved with EtOAc (20 ml) and washed with H_2O (20 ml). The aqueous layer was then washed twice more with EtOAc (20 ml each). The combined organic layers were then washed with brine (60 ml X2) and dried over $MgSO_4$ and concentrated *in vacuo.* The product was purified via flash chromatography (EtOAc 2:1 Hexane), which yielded a yellow oil, 123 mg (71% yield), R_f 0.2 (EtOAc 2:1 Hexane). ^{1}H NMR (500 MHz, CDCl3) δ 7.61 (dd, *J*

= 6.9, 1.9, 1H, Ar*H*), 7.32 (ddd, *J* = 8.8, 6.6, 2.0, 1H, Ar*H*), 6.54 (d, *J* = 9.2, 1H, Ar*H*), 6.22 (td, *J* = 6.8, 1.2, 1H, Ar*H*), 4.73 (d, *J* = 2.6, 2H, N–CH_2–C), 2.47 (t, *J* = 2.6, 1H, C≡C*H*). ^{13}C NMR (126 MHz, CDCl3) δ 162.10 (C), 139.91 (CH), 135.93 (CH), 120.69 (CH), 106.48 (CH), 76.99 (C), 75.47 (CH), 37.71 (CH_2). MS (ESI) m/z 134.2 $[M+H]^+$.[73]

*2.4.3 Synthesis of 1-propargyl-4-pyridone (**23**)*

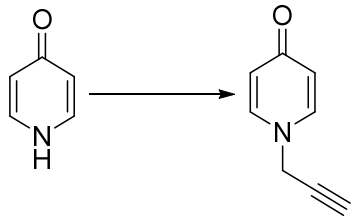

4-pyridone (**22**) (300 mg, 3.15 mmol) was dissolved in dry DCM (4 ml) containing DBU (1413 µl, 9.45 mmol, 3.0 eq). The reaction mixture was cooled to 4 °C. Afterwards, propargyl bromide solution (674 µl, 6.3 mmol, 2 eq.) was added dropwise to the mixture. Reaction was stirred at RT for 2 h. The solvent was then removed and the product was dissolved in $CHCl_3$ with 25% IPA (40 ml) and washed with H_2O (40 ml). The aqueous layer was then washed four times more. The combined organic layers were then washed with brine (200 ml X2) and dried over $MgSO_4$ and concentrated *in vacuo.* The product was purified via flash chromatography (8% MeOH in DCM), which yielded a clear oil, 104 mg (25% yield), R_f 0.4 (10% MeOH in DCM). ^{1}H NMR (500 MHz, CDCl3) δ 7.45 – 7.36 (m, 2H, Ar*H*), 6.41 – 6.31 (m, 2H, Ar*H*), 4.57 (d, *J* = 2.6, 2H, N–CH_2–C), 2.62 (t, *J* = 2.6, 1H, C≡C*H*). ^{13}C NMR (126 MHz, CDCl3) δ 179.06 (C), 139.22 (CH), 119.03 (CH), 77.13 (C), 75.45 (CH), 45.50 (CH_2). MS (ESI) m/z 134.2 $(M+H)^+$.[74]

2.5 EXPERIMENTAL – CHAPTER 6

*2.5.1 Synthesis of N1-Functionalized 5FU Derivatives (**24, 25, 26** and **27**)*

16 (100 mg, 0.77 mmol) was dissolved in acetonitrile (MeCN) (2 ml) with DBU (115 µl, 1 eq.). The mixture was then cooled to 4 ˚C in an ice bath. The corresponding

alkylbromide (0.77 mmol) was added dropwise to the mixture. The mixture was stirred overnight and allowed to warm up to RT. The solvents were then removed *in vacuo* and the product was purified via flash chromatography (1.5% MeOH in DCM), which yielded compounds **24, 25, 26** and **27** as white solids.

*2.5.1.1 1-(1-butyn-3-yl)-5-fluorouracil (**24**)*

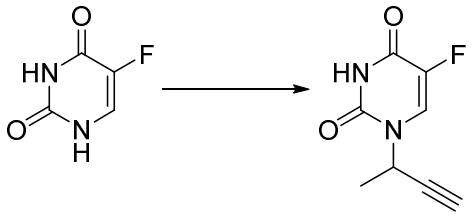

75 mg, 54% yield (R_f 0.55, 10% MeOH in DCM). ^{1}H NMR (500 MHz, DMSO) δ 11.89 (s, 1H, N*H*), 8.15 (d, *J* = 6.8, 1H, Ar*H*), 5.40 – 5.30 (m, 1H, C*H*–CH_3), 3.61 (d, *J* = 2.4, 1H, C≡C*H*), 1.47 (d, *J* = 7.0, 3H, CH–C*H*$_3$). ^{13}C NMR (126 MHz, DMSO) δ 157.01 (d, *J* = 26.0, C), 148.69 (C), 140.19 (d, $J_{C\text{-}F}$ = 231.4, C), 125.97 (d, $J_{C\text{-}F}$ = 33.8, CH), 81.34 (C), 76.53 (CH), 42.92 (CH), 20.47 (CH_3). MS (ESI) m/z 181.0 $[M\text{-}H]^-$. HRMS (m/z): $[M - H]^-$ calcd for $C_8H_6O_2N_2F_1$, 181.0412; found 181.0419.

*2.5.1.2 1-(2-butyn-1-yl)-5-fluorouracil (**25**)*

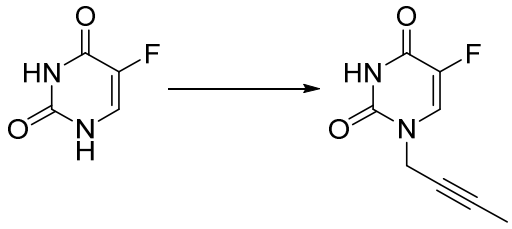

63 mg, 45% yield (R_f 0.53, 10% MeOH in DCM). ^{1}H NMR (500 MHz, DMSO) δ 11.86 (s, 1H, N*H*), 8.11 (d, *J* = 6.7, 1H, Ar*H*), 4.41 (q, *J* = 2.3, 2H, C*H*$_2$–C≡C), 1.82 (t, *J* = 2.4, 3H, C≡C–C*H*$_3$). ^{13}C NMR (126 MHz, DMSO) δ 157.30 (d, $J_{C\text{-}F}$ = 25.9, C), 149.04 (C), 139.71 (d, $J_{C\text{-}F}$ = 230.2, C), 128.93 (d, $J_{C\text{-}F}$ = 33.8, CH), 81.61 (C), 73.39 (C), 37.30 (CH_2), 3.07 (CH_3). MS (ESI) m/z 181.0 $[M\text{-}H]^-$. HRMS (m/z): $[M - H]^-$ calcd for $C_8H_6O_2N_2F_1$, 181.0419; found 181.0409.

*2.5.1.3 1-(2-pentyn-1-yl)-5-fluorouracil (**26**)*

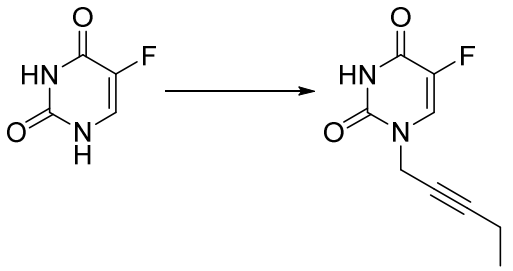

56 mg, 37% yield (R_f 0.53, 10% MeOH in DCM). ^{1}H NMR (500 MHz, DMSO) δ 11.86 (s, 1H, N*H*), 8.10 (d, *J* = 6.6, 1H, Ar*H*), 4.43 (t, *J* = 2.2, 2H, N–C*H*$_2$), 2.21 (qt, *J* = 7.5, 2.2, 2H, C–C*H*$_2$–CH$_3$), 1.06 (t, *J* = 7.5, 3H, C–CH$_2$–C*H*$_3$). ^{13}C NMR (126 MHz, DMSO) δ 157.31 (d, J_{C-F} = 25.9, C), 149.03 (C), 139.71 (d, J_{C-F} = 230.2, C), 128.87 (d, J_{C-F} = 33.7, CH), 87.05 (C), 73.53 (C), 37.27 (CH$_2$), 13.45 (CH$_3$), 11.60 (CH$_2$). MS (ESI) m/z 195.0 [M-H]$^-$. HRMS (m/z): [M - H]$^-$ calcd for $C_9H_8O_2N_2F_1$, 195.0575; found 195.0571.

*2.5.1.4 1-(3-phenyl-1-propargyl)-5-fluorouracil (**27**)*

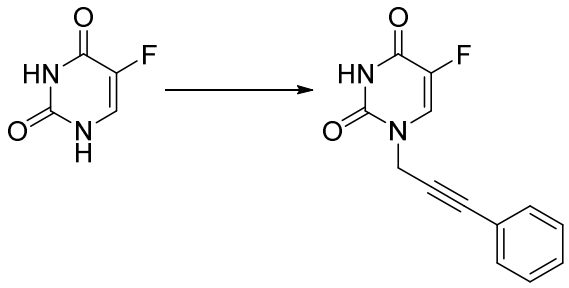

66 mg, 35% yield (R_f 0.66, 10% MeOH in DCM). ^{1}H NMR (500 MHz, DMSO) δ 11.92 (s, 1H, N*H*), 8.22 (d, *J* = 6.6, 1H, Ar*H*), 7.49 – 7.36 (m, 5H, Ar*H*), 4.73 (s, 2H, C*H*$_2$–C≡C). ^{13}C NMR (126 MHz, DMSO) δ 157.35 (d, J_{C-F} = 25.9, C), 149.12 (C), 139.83 (d, J_{C-F} = 230.4, C), 131.53 (CH), 129.01 (d, J_{C-F} = 34.0, CH), 129.04 (CH), 128.69 (CH), 121.60 (C), 84.38 (C), 83.79 (C), 37.64 (CH$_2$). MS (ESI) m/z 243.0 [M-H]$^-$. HRMS (m/z): [M - H]$^-$ calcd for $C_{13}H_8O_2N_2F_1$, 243.0575; found 243.0574.

*2.5.2 Synthesis of 3-propargyl-5-fluorouracil (**30**)*

*2.5.2.1 Synthesis of Compound **28***

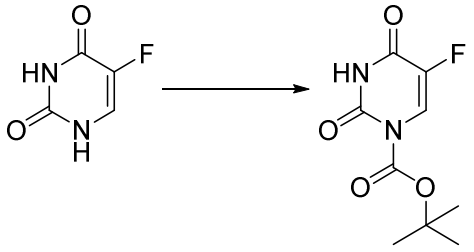

16 (100 mg, 0.77 mmol) was dissolved in a mixture of MeCN (2 ml) and DMF (1 ml). Next, Di-*tert*-butyl dicarbonate (Boc_2O) (252 mg, 1.16 mmol) and DMAP (19 mg, 0.15 mmol) were added to the mixture. The mixture was stirred overnight at RT. The solvents were then removed *in vacuo* and the product was purified via flash chromatography (hexane/ EtOAc 3:1), which yielded a white solid (70 mg, 40%). ^{1}H NMR (500 MHz, DMSO) δ 10.60 (s, 1H, N*H*), 7.64 (d, J = 4.7, 1H, Ar*H*), 1.62 (s, 9H, CH_3). ^{13}C NMR (126 MHz, DMSO) δ 159.21 (d, $J_{C\text{-}F}$ = 24.4, C), 150.70 (C), 139.59 (d, $J_{C\text{-}F}$ = 224.8, C), 123.02 (d, $J_{C\text{-}F}$ = 31.6, CH), 61.45 (C) 29.35 (CH_3).

*2.5.2.2 Synthesis of Compound **29***

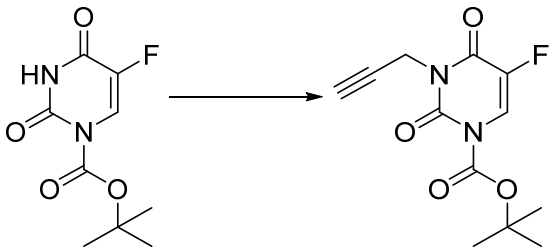

Compound **28** (56 mg, 0.24 mmol) was dissolved in dry DCM (2 ml) with DBU (55 µl, 0.36 mmol) and propargyl bromide solution (31 µl, 0.29 mmol). The mixture was stirred at RT for 4 h. The solvent was then removed *in vacuo* and the product was purified via flash chromatography (hexane/ EtOAc 5:1), which yielded an oil (43 mg, 67%). ^{1}H NMR (500 MHz, CDCl3) δ 7.40 (d, J = 4.6, 1H, Ar*H*), 4.45 (d J = 2, 2H,

N–CH_2–C), 2.49 (t, J = 2.6, 1H, C≡CH), 1.68 (s, 9H, CH_3). ^{13}C NMR (126 MHz, CDCl3) δ 159.08 (d, $J_{C\text{-}F}$ = 24.3, C), 150.31 (C), 140.51 (d, $J_{C\text{-}F}$ = 233.9, C), 123.13 (d, $J_{C\text{-}F}$ = 33.9, CH), 76.22 (C), 75.88 (CH), 64.18 (C), 38.01 (CH_2), 29.76 (CH_3).

*2.5.2.3 Synthesis of Compound **30***

Compound **29** (28 mg, 0.1 mmol) was dissolved in MeOH containing K_2CO_3 (7 mg, 0.5 eq.). The mixture was stirred at RT for 3 h. The solvent was then removed *in vacuo* and the product was purified via flash chromatography (3% MeOH in DCM), which yielded a white solid.

*2.5.2.4 3-propargy-5-fluorouracil (**30**)*

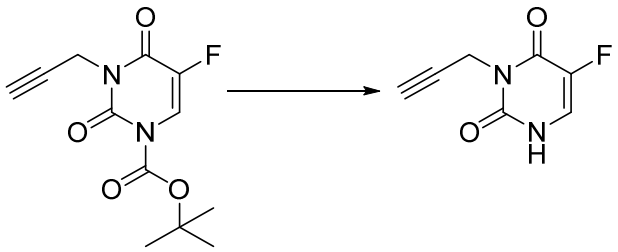

12 mg, 71% yield. ^{1}H NMR (500 MHz, MeOD) δ 7.61 (d, J = 5.2, 1H), 4.64 (dd, J = 2.5, 0.5, 2H), 2.57 (t, J = 2.5, 1H). ^{13}C NMR (126 MHz, MeOD) δ 158.82 (d, $J_{C\text{-}F}$ = 25.8, C), 151.06 (s, C), 141.35 (d, $J_{C\text{-}F}$ = 229.9, C), 125.88 (d, $J_{C\text{-}F}$ = 32.1, CH), 78.65 (C), 71.94 (CH), 31.06 (CH_2). MS (ESI) m/z 167.0 $[M\text{-}H]^-$. HRMS (m/z): $[M - H]^-$ calcd for $C_7H_4O_2N_2F_1$, 167.0262; found 167.0252.

*2.5.2.5 Synthesis of Compound **31***

16 (100 mg, 0.8 mmol) was dissolved in dry DMF (2 ml) containing DBU (345 µl, 2.3 mmol) under N_2 atm. and cooled to 4 °C. Propargyl bromide solution (170 µl, 1.7 mmol) was dissolved in dry DMF (0.5 ml). The solution was then added dropwise to the mixture. Reaction was stirred at RT overnight. The solvent was then removed and the product was purified via flash chromatography (1.5% MeOH in DCM) to yield compound **7** as a white solid.

*2.5.2.6 1,3-dipropargy-5-fluorouracil (**31**)*

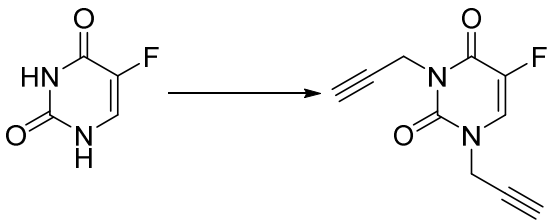

136 mg, 86% yield. ^{1}H NMR (500 MHz, CDCl3) δ 7.60 (d, *J* = 5.3, 1H, Ar*H*), 4.72 (d, *J* = 2.4, 2H, N–C*H*$_2$–C), 4.61 (d, *J* = 2.6, 2H, N–C*H*$_2$–C), 2.56 (t, *J* = 2.6, 1H, C≡C*H*), 2.20 (t, *J* = 2.5, 1H, C≡C*H*). ^{13}C NMR (126 MHz, CDCl3) δ 156.19 (d, $J_{C\text{-}F}$ = 26.0, C), 148.92 (C), 140.26 (d, $J_{C\text{-}F}$ = 237.3, C), 125.33 (d, $J_{C\text{-}F}$ = 33.7, CH), 77.24 (C), 76.74 (CH), 75.47 C), 71.51 (CH), 38.18 (CH_2), 31.27 (CH_2). MS (ESI) m/z 435.2 $[2M+Na]^+$. HRMS (m/z): $[M - H]^-$ calcd for $C_{10}H_6O_2N_2F_1$, 205.0419; found 205.0414.

2.6 EXPERIMENTAL – CHAPTER 7

*2.6.1 Synthesis of Compound **33***

Floxuridine (**32**) (300 mg, 1.22 mmol) and imidazole (605 mg, 8.89 mmol) were added to anhydrous DMF (8 ml) and the resulting mixture stirred at RT for 5 min. TBS-Cl (643 mg, 4.27 mmol) was then added to the mixture and the reaction was stirred for 2 h. The solvents were removed *in vacuo*, re-dissolved in EtOAc (20 ml) and washed with H_2O (20 ml). The aqueous layer was then washed two more times with EtOAc, the organic layer was then washed with brine (60 ml) and dried over anhydrous $MgSO_4$. The product was then purified by column chromatography with 2:1 EtOAc/hexane to yield compound **5** as a white solid.

*2.6.1.1 3'-O,5'-O-bis[(tert-butyl)dimethylsilyl]-5-fluoro-3-propargyldeoxyuridine (**33**)*

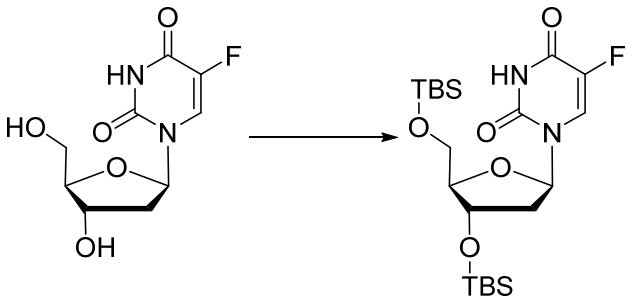

552 mg, 95% yield. ^{1}H NMR (500 MHz, CDCl3) δ 9.31 (d, *J* = 3.9, 1H, N*H*), 8.04 (d, *J* = 6.3, 1H, Ar*H*), 6.29 (td, *J* = 6.3, 1.6, 1H, Ar*H*), 4.44 – 4.38 (m, 1H, Ar*H*), 3.96 – 3.90 (m, 2H, CH_2– OH), 3.77 (t, *J* = 6.0, 1H), 2.32 (ddd, *J* = 13.3, 6.1, 3.8, 1H), 2.09 – 2.01 (m, 1H), 0.94 – 0.91 (m, 9H), 0.90 – 0.87 (m, 9H), 0.12 (t, *J* = 3.2, 6H), 0.07 (t, *J* = 2.8, 6H). ^{13}C NMR (126 MHz, CDCl3) δ 157.05 (d, J_{C-F} = 26.9, C), 148.98 (C), 140.63 (d, J_{C-F} = 236.6, C), 124.43 (d, J_{C-F} = 34.0, CH), 88.23 (CH), 85.67 (CH), 71.67 (CH), 62.82 (CH_2), 41.95 (CH_2), 26.02 (CH_3), 25.85 (CH_3), 18.55 (C), 18.12 (C), -4.61 (d, J_{Si-CH3} = 31.1, CH_3), -5.45 (d, J_{Si-CH3} = 3.2, CH_3). LC-MS (m/z): 475.4 $[M+H]^{+}$.[75]

*2.6.1.2 Synthesis of Compound **35***

Compound **33** (150 mg, 0.32 mmol) and DBU (168 µl, 1.12 mmol) in dry DCM (3 ml) was stirred for 5 min before adding dropwise a 1 mL solution of propargyl bromide (120 µl, 0.93 mmol). The reaction was stirred for 30 min and monitored by TLC. Afterwards, additional 16 ml of DCM was added and the mixture was washed once with H_2O (20 ml). The aqueous layer was then washed twice more with DCM (20 ml). The organic layers were collected, washed twice with brine (60 ml), dried over $MgSO_4$ and concentrated *in vacuo.* Without further purification, the product (**34**) was dissolved in a 1 M TBAF solution in THF (2.5 ml) and stirred for 1 h. The mixture was concentrated *in vacuo*, dissolved in 25% IPA in $CHCl_3$ (20 ml) and washed once with H_2O (20 ml). The aqueous layer was then washed twice more with 25% IPA in $CHCl_3$ (20 ml). The organic layers were collected, dried over $MgSO_4$ and the resulting crude purified by column chromatography using 6% MeOH in DCM as eluent to yield compound **35** as a colourless sticky solid.

*2.6.1.3 5-fluoro-3-propargyldeoxyuridine (**35**)*

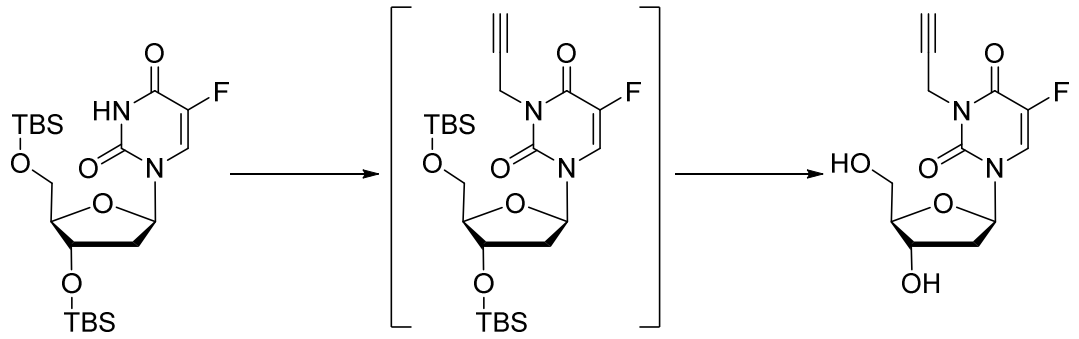

52 mg, 58% yield. ^{1}H NMR (500 MHz, DMSO) δ 8.36 (d, *J* = 7.0, 1H, Ar*H*), 6.18 (td, *J* = 6.4, 1.5, 1H, Ar*H*), 5.28 (d, *J* = 4.3, 1H, CH_2–O*H*), 5.19 (t, *J* = 4.9, 1H, CH–O*H*), 4.54 (t, *J* = 2.0, 2H, C*H*$_2$-C≡CH), 4.25 (dt, *J* = 8.7, 4.3, 1H, Ar*H*), 3.81 (q, *J* = 3.3, 1H, Ar*H*), 3.61 (qdd, *J* = 11.9, 4.9, 3.5, 2H, *CH*$_2$–OH), 3.18 (t, *J* = 2.4, 1H, C≡C*H*), 2.19 – 2.12 (m, 2H, Ar*H*$_2$). ^{13}C NMR (126 MHz, DMSO) δ 155.63 (d, $J_{C\text{-}F}$= 26.4, C), 148.28 (C), 139.29 (d, $J_{C\text{-}F}$ = 228.6, C), 124.04 (d, $J_{C\text{-}F}$ = 34.6, CH), 87.72 (CH), 85.68 (CH), 78.41 (C), 73.52 (CH), 69.93 (CH), 60.86 (CH_2), 39.94 (CH_2), 30.49 (CH_2). LC-MS (m/z): 319.0 $[M+Cl]^-$. HRMS (m/z): $[M + Cl]^-$ calcd for $C_{12}H_{13}O_5N_2F_1Cl_1$, 319.0497; found 319.0502.

2.7 BIOLOGY – GENERAL METHODS

2.7.1 Cell Culture

Cell lines were grown in culture media supplemented with serum (10% fetal bovine serum) and L-glutamine (2 mM) and incubated in a Heracell 240i tissue culture incubator at 37 °C and 5% CO_2. Human colorectal carcinoma HCT116 cells (a kind gift from Dr Van Schaeybroeck), human hepatocyte carcinoma HepG2 cells (purchased from Sigma-Aldrich), Human breast adenocarcinoma MCF7 cells (purchased from ATCC), human ovarian carcinoma PE04 cells (a kind gift from Prof Charlie Gourley), human breast cancer R-SKBR3a cells and human pancreatic carcinoma Mia PaCa-2 cells (a kind gift from Dr. Simon Wilkinson) were cultured in Dulbecco's Modified Eagle Media (DMEM). Human pancreas adenocarcinoma

BxPC-3 cells (a kind gift from Dr Mark Duxbury) was cultured in Roswell Park Memorial Institute (RPMI) media.

2.7.2 Non-Biological Pd^0-mediated Conversion Study

All stock drug samples (100 mM in DMSO) were dissolved in PBS (1 mL) for a final concentration of 100 μM (30 μM for Pro-FUdR – chapter 7) with 1 mg of Pd^0 resins (0.67 mg for Pro-FUdR – chapter7) and shaken at 1400 rpm (1200 rpm for chapters 6 and 7) at 37 °C in a Thermomixer. Reaction crudes were monitored at 0, 4, 6, 8, 24, and 48 h by analytical HPLC (Agilent) using an UV detector at 280 nm to avoid the detection of PBS salts. HPLC method described above.

2.7.3 Bioorthogonal Comparative Study of Prodrug to Parental Drug

Cells were seeded in a 96-well plate format at the appropriate cell concentration (3,000 cells in chapters 2 and 5 and 1,000 cells per well in the rest of the chapters for HCT116 cells; 3,000 cells in chapters 2 and 5 and 2,500 cells per well in the rest of the chapters for BxPC-3 cells; 4,000 cells per well for HepG2 cells and 1,000 cells per well for MIA PaCa-2 cells) and incubated for 48 h before treatment. Each well was then replaced with fresh media containing parental drug (0.3 nM to 1mM) with DMSO (0.1% v/v); or Prodrug (0.3 nM to 1 mM) with DMSO (0.1% v/v) and incubated for 5 days (4 days for MIA PaCa-2 treated cells). Untreated cells were incubated with DMSO (0.1% v/v). PrestoBlue cell viability reagent (10% v/v) was added to each well and the plates incubated for 60 - 90 min depending on the cell line. Fluorescence emission was detected using a PerkinElmer Victor2 multilabel reader in chapter 4 and a PerkinElmer EnVision 2101 multilabel reader in the rest of the chapters (excitation filter at 540 nm and emissions filter at 590 nm). All conditions were normalized to the untreated cells (100%) and blank wells containing just media and PresoBlue (10%). Curves were fitted using GraphPad Prism software using a sigmoidal variable slope curve.

2.7.4 Pd^0-mediated Activation of Pd-labile Prodrugs in vitro

Cells were seeded in a 96-well plate format at the appropriate cell concentration as described above and incubated for 48 h before treatment. Each well was then replaced with fresh media containing: Pd^0 resins (0.67 mg/ml for all cell lines except HCT116 cells from chapter 5 which contained 1 mg/ml) with DMSO (0.1% v/v); Prodrug (0.3 nM – 100 μM) with DMSO (0.1%, v/v); parental drug (0.3 nM – 1μM) with DMSO (0.1%, v/v) or combination of Pd^0 resins + prodrug (0.3 nM – 100 μM) with DMSO (0.1%, v/v). Untreated cells were incubated with DMSO (0.1% *v/v*). Cells both treated and non-treated were incubated for 5 days. PrestoBlue cell viability reagent (10% v/v) was added to each well and the plate incubated for 60 – 90 min. Fluorescence emission was detected and results normalized as described above.

2.7.5 Time-Lapse Imaging Study

Cells were seeded and treated as described above in a Nunc 96 well plate (cat. no. 165306). Each well was imaged every 2 h (chapter 5) or 3 h (remaining chapters) over 5 days under standard incubation conditions using an IncuCyte ZOOM microscope (placed inside the incubator). Imaged-based analysis of cell confluence was carried out using the IncuCyte software.

2.8 METHODS – CHAPTER 3

2.8.1 Pd^0 Biocompatibility in vitro

HCT116 and BxPc-3 cells were seeded in a 96 well plate format as described above (3,000 cells/well). After 48 hours each well was replaced with fresh media containing Pd^0 resins (0.2 – 3 mg/ml) and Non-active (naked) resins (0.2 – 3 mg/ml). All cells both treated and untreated were incubated with DMSO (0.1% *v/v*) (Fig. 3.3a and b).

2.8.2 Pd^0 Biocompatibility inside Zebrafish Embryos

Wild-type zebrafish embryos were collected from AB-TPL breeding pairs and reared at 28 °C in E3 embryo media. 24 hours post fertilization (h.p.f), embryos were treated with tricaine (anesthetic) and pierced in the yolk with a fine needle. A single Pd^0 resin was then rapidly inserted into the yolk opening to minimize loss of yolk. Embryos that lost significant yolk in the procedure were removed from the experiment. Embryos were then gently transferred to fresh E3 medium (n = 5), returned to 28 °C and monitored over 3 days by microscopy (Fig. 3.3c). This was performed by Dr. E. Elizabeth Patton from the Edinburgh Cancer Research Centre (ECRC).

2.9 METHODS – CHAPTER 4

2.9.1 DNA Damage Study

MIA PaCa-2 cells were seeded in an 8 well chamber slide with a density of 2,000 cells per well and incubated for 48 h prior to treatment. Each well was then replaced with fresh media containing 0.1% DMSO (*v/v*) and the following treatments: Pd^0 resins (0.67 mg/ml); **7** (300 nM); Gemcitabine (300 nM) or combination of Pd^0 resin + **10** (300 nM). The combination of **10** and Pd^0 resins were incubated together for 24 h at 37 °C prior to treatment with cells to allow time for the Pd^0-mediated dealkylation process to take place. After 24 h of treatment, all treated cells were fixed with paraformaldehyde (4%, 20 min). Permeabilised (Triton X-100, 0.1%) cells were then treated with rabbit monoclonal antibody against Phospho-Histone H2AX (Ser139) (1:400, Cell Signaling Technologies, cat. no. 9718) for 1 h at RT. This was followed by 1 h incubation at RT with secondary Alexa Fluor® 488 linked antibody (1:1000, goat anti-rabbit, IgG, Life Technologies), Hoechst 33342 (1:8000, Life Technologies) and Alexa Fluor® 594 Phalloidin (1:500, Life Technologies). Cells were imaged using on an Olympus FV1000 microscope and images analysed using ImageJ software (Fig. 4.6).

2.9.2 Pd^0 Catalytic Activity Inside Zebrafish Embryos

Either a non-active (naked) resin or a Pd^0 resin was implanted in 24 hpf zebrafish embryos (n = 5) following the same procedure described in 2.8.2 and gently transferred to fresh E3 medium. Embryos were incubated for another 24 h after implantation at 28 °C to ensure the embryos survived the surgical procedure. Embryos that lost significant yolk in the procedure were removed from the experiment. The corresponding probes (**13, 14** and **15**) were separately added to the embryo medium (final concentration 5 μM) and the treated fish were incubated for an additional 24 h at 31 °C to increment the probe activation rate. Fish were imaged using fluorescent microscopy (Olympus Scan-R) (Fig. 4.7b and c). It is important to note that the zebrafish embryos appeared older than 3 days post-fertilization (dpf). This was probably due to the increased incubation temperature (31 °C) which may have increased their developmental rate. Experiments were repeated three times. The fold change in fluorescence with the Pd^0 resin + 8p in comparison to that with the inactive resin + 8p were quantified using ImageJ software. A line was drawn horizontally over the yolk sac of the embryo encompassing both the resin beads and the area surrounding them. The pixel intensities along the lines were calculated (Fig. 4.7d). Zebrafish husbandry and experiments were performed under Home Office License in compliance with the Animals (Scientific Procedures) Act 1986, and approved by the University of Edinburgh Ethics Committee. The surgical implantation of both the Pd^0 and naked resins were again performed by Dr. E. Elizabeth Patton and Witold Rybski, both from the ECRC.

2.10 METHODS – CHAPTER 5

2.10.1 Combination Study with 5FU and Increasing Concentrations of Pro-5FU

HCT116 and BxPC-3 were seeded as described above (3000 cells/well). Cells were treated with a combination of varying concentrations of Pro-5FU (0.1 μM – 1000 μM) and 5FU (10 μM and 1 μM for HCT116 and BxPC-3 respectively) and were incubated for 5 days under standard incubation conditions described above. Cell viability was determined using PrestoBlue as described above (Fig. 5.5a and b).

2.10.2 Catalytic Study With Pd^0 Resins in vitro

HCT116 and BxPC-3 were seeded as described above (3000 cells/well). Cells were treated with either 5FU or Pro-5FU (100 and 30 μM for HCT116 and BxPC-3 respectively) or a combination of varying concentrations of Pd^0 resins (0.007 – 1 mg/ml) with Pro-5FU. Treated cell were then incubated and cell viability was determined as described above (Fig. 5.6c and d).

2.10.3 Zeptosens Reverse Phase Protein Microarray Analysis

Cells were plated in a 6-well plate at a density of 440,000 and 480, 000 cells per well for HCT116 and BxPC-3 cells respectively and incubated for 48 h. Before adding the prodrug to the HCT116 cells, combination of Pro-5FU (100 μM) and Pd^0 resins (1 mg/ml) were incubated in media at 37 °C for 24 h to overcome the time delay required to convert Pro-5FU into 5FU, which was seen to have a relevant effect in this cell type. This pre-incubation procedure was not carried out for the treated BxPC-3 cells (30 μM). Pd^0 resin/Pro-5FU combination and the controls (untreated cells; Pd^0 resins; Pro-5FU and 5FU) were incubated with each cell line for 6 and 24 h (n = 2). Afterwards, the cells were washed with PBS (2 X 3 ml) and lysed with Zeptosens CLB1 lysis buffer (90 μl). Samples were analysed by Zeptosens RPPA (Zeptosens) as previously described[76] using the following specific conditions. Tumour cell lysates were normalized to a uniform protein concentration with spotting buffer CSBL1 (Zeptosens-Bayer) before preparing a final fourfold concentration series of 0.2, 0.15, 0.1 and 0.05 mg/ml. The diluted concentration series of each sample was printed onto Zeptosens protein microarray chips (ZeptoChip, Zeptosens-Bayer) under environmentally controlled conditions (constant 50% humidity and 14 °C temperature) using a non-contact printer (Nanoplotter 2.1e, GeSiM). A single 400 pl droplet of each lysate concentration was deposited onto the Zeptosens chip (thus representing four spots per each biological replicate). A reference grid of Alexa Fluor-647 conjugate BSA consisting of 4 column X 22 rows was spotted onto each sub-array. Each sample concentration series were spotted in between reference columns. After array printing, the arrays were blocked with an aerosol of BSA solution using a custom designed nebulizer device (ZeptoFOG, Zeptosen-Bayer) for 1 h. The protein array chips were subsequently washed in

double-distilled H_2O and dried before performing a dual antibody immunoassay comprising of a 24 h incubation of primary antibody (the library of primary antibodies used is in Table 2.1 from reference[67] and were purchased from Cell Signaling Technologies) followed by 2.5 h incubation with secondary Alexa Fluor-conjugated antibody detection reagent (anti-rabbit A647 Fab; Invitrogen). Following secondary antibody incubation and a final wash step in BSA solution, the immunostained arrays were imaged using the ZeptoREADER instrument (Zeptosens-Bayer). For each sub-array, five separate images were acquired using different exposure times ranging from 0.5 to 10 s. Microarray images representing the longest exposure without saturation of fluorescent signal detection were automatically selected for analysis using the ZeptoView 3.1 software (Zeptosens-Bayer). A weighted linear fit through the fourfold concentration series was used to calculate relative fluorescence intensity (RFI) value for each sample replicate. Local normalization of sample signal to the reference BSA grid was used to compensate for any intra- or inter-array/chip variation. Local normalized RFI values were used for all subsequent analysis. Calculated by the ZeptoView 3.1 software, abundance levels of total p53 protein, phosphorylated p53 (Serine 15) and phosphorylated Akt (Serine 473) were plotted as RFI data using GraphPad software (Fig. 5.9). The protein microarray was performed and analysed by Dr. Neil Carragher and Kenneth Macleod from the ECRC.

Table 2.1. Library of primary antibodies used for the Zeptosens reverse phase protein microarray analysis.

4E-BP1 P Ser65	Bcl-2	Bcl-x
4E-BP1 P thr37, Thr46	Caspase 3 cleaved	B-Catenin P Ser33, Ser37, Thr41
ATM	Cyclin D1 P Thr286	ATM/ATR Substrate P Ser/Thr
Bad P Ser136	p38 MAPK	Prohibitin
Beta-Catenin P Thr41, Ser45	p38 MAPK PThr180, Tyr182	p53
GSK 3 B	p53 P Ser15	GSK-3-alpha/beta P Ser21/Ser9
NFkB p65 Ser536	PARP cleaved Asp214	Akt P Ser473
Akt	Bax	XIAP
Bad P Ser112	NFkB p105/p50	Histone H2AX P Ser139
Bak	p21 CIP/WAF1 p Thr145	Cyclin D1

2.10.4 Western Blot Analysis

Cell lysates from HCT116 and BxPC-3 cells that were prepared as described above for the Zeptosens analysis were used for this study. The protein samples (35 μg) and

SeeBlue® Plus2 Pre-Stained Standard (7.5 µg) were separated by SDS PAGE (BioRad 4-15% gels) and transferred to PVDF membranes (GE). Western blotting was performed using rabbit monoclonal antibodies against human p53 (HCT116), p53-phospho-serine 15 (both cell lines) and Akt-phospho-serine 473 (BxPC-3) (1:1000, Cell Signaling Technologies, cat. no. 9282, 9284 and 9271 respectively) at 4 °C, overnight. This was followed by 1 hour incubation at room temperature with secondary Horseradish peroxidase (HRP) linked antibody (1:10,000, anti-rabbit IgG, Sigma). The loading control, actin, was mouse monoclonal antibody (1:40,000, Calbiochem, cat. no. CP01) followed by a secondary HRP linked antibody treatment (1:40,000, anti-mouse IgM, Calbiochem). HRP was detected by addition of peroxidase enhanced chemiluminescence (POD ECL - Roche) and bands visualized using a ChemiDoc^{TM} MP Imager (BioRad).

2.10.5 Mouse Xenograft Assay

6-10 week old female CD-1 nude mice were obtained from Harlen Laboratories. Colorectal HCT116 cells in Hanks Balanced Salt Solution, were injected subcutaneously into the flank, bilaterally, at 2 x 10^6 cell concentration alone or with metallic palladium beads (0.1 mg/ml per implant). Once tumours reached palpable size, mice were randomised into groups of 5 and each group was treated as follows:

Gp. A – No Beads Control (Saline)

Gp. B – No Beads + Pro-5FU 5mg/ml (50 mg/kg)

Gp. C – No Beads + 5FU 5mg/ml (50 mg/kg)

Gp. D – Pd^0 Resins Beads Control (Saline)

Gp. E – Pd^0 Resin Beads + Pro-5FU 5mg/ml (50 mg/kg)

Drug treatment commenced on day 0 (3 days after tumour inoculation) by intraperitoneal (ip) injection with either 5FU or Pro-5FU (made up in saline) depending on the treatment group. All drug treatments were administered biweekly. The tumours were measured by callipers and the tumour volume was calculated from these measurements. This was the work performed by Dr. John Dawson from the ECRC.

2.11 METHODS – CHAPTER 6

*2.11.1 BOOM Activation Comparison of Prodrugs **18** and **30** in Various Cancer Cells*

Cells were seeded in a 96 well plate format (HCT116 – 1000 cell/well; BxPC-3 – 2500 cells/well; MCF7 – 2000 cells/well; PE04 – 1000 cells/well; r-SKBR3a – 156 cells/well). After 48 h, cells were treated with fresh media containing either Pd^0 resins (0.67 mg/ml) with DMSO (0.1% v/v); compounds **18**, or **30** (3, 10, 30 and 100 μM) with DMSO (0.1% v/v); 5FU (3, 10, 30 and 100 μM) with DMSO (0.1% v/v); or combination of Pd^0 resins + **18** or **30** (3, 10, 30 and 100 μM) with DMSO (0.1% v/v). Untreated cells were incubated with DMSO (0.1% v/v). This assay undertaken with BxPC-3 cells was performed by Dr. Belén Rubio-Ruiz; MCF7 cells by Craig Fraser; PE04 cells by Richard Crispin and r-SKBR3a cells by Sam Myers. All of whom are situated at the ECRC.

2.12 METHODS – CHAPTER 7

2.12.1 Pd^0-mediated Activation of Pro-FUdR in vitro Under Hypoxic Conditions

HCT116 cells were seeded in a 96 well plate format as described above (1000 cells/well). After 48 h the cells were treated with the combination of Pd^0 resins and Pro-FUdR (0.003 μM – 30 μM) and the appropriate controls as described above. Immediately following treatment cells were placed inside a hypoxic chamber (Whitley H35 Hypoxystation), which was flushed by a gas mixture of 0.5% O_2, 5% CO_2, 95% N_2 for 5 days. Cell viability determination was performed as described above.

CHAPTER 3

Functionalized Pd^0 Resins

3.1 INTRODUCTION

Transition metals such as zinc, nickel and copper are widely used by a certain class of enzymes called metalloproteins to aid in structure formation e.g. zinc fingers or to drive catalysis e.g. superoxide dismutase.[77] These transition metals or trace elements are utilized by enzymes as cofactors to aid in facilitating many different types of enzymatic reactions. Their use in medicinal chemistry, such as cisplatin, a drug containing platinum(II) which intercalates within DNA and causes cell death, have been exploited for quite some time. However, their use to mediate chemo-selective reactions within cells or whole organisms is a recent addition to the chemical biology field.[54,57,58,60]

Streu and Meggers, first introduced the concept of using a ruthenium based catalysts capable of carrying out the Alloc deprotection of a caged fluorophore within human cells[57]. Adding to this concept, the use of palladium (Pd) as a heterogeneous catalyst proved not only capable of mediating more diverse chemo-selective reactions but was also more biocompatible.[54,58]

For a long time Pd has been instrumental in organic chemistry as a catalyst able to mediate a myriad of chemical transformations such as hydrogenation, dehydrogenation, oxidation, hydrogenolysis and cross-coupling reactions. In the last years it is perhaps most celebrated for its use in the Heck, Negishi and Suzuki cross-coupling reactions, from which the 3 scientist received the Nobel Prize in Chemistry in 2010, although it is widely employed in other processes resulting in the formation of new C-C bonds such as the Sonogashira coupling or the Stille reaction.[78,79, 81] Pd has 4 common oxidation states but Pd^{2+} and Pd^0 have the most abundant catalytic properties. Whereas Pd^{2+} is mainly used as an oxidising agent, Pd^0 is a much versatile

catalyst and has the safest toxicity profile among all Pd species. It is used for dental restoration and to produce jewellery.[80,81]

One drawback when using Pd^0 for catalytic purposes is the issue of purifying the desired product from the Pd and its ligand. One way to overcome this problem is to use Pd nanoparticles and immobilize them onto solid supports such as charcoal, silica and alumina.[82-84] The advantage of using the Pd nanoparticles as a heterogeneous catalyst is the excellent surface-to-volume ratio which allows for greater physical contact of the Pd catalyst with the desired reactants.[85] More recently, a number of groups including the Bradley group have investigated immobilizing Pd nanoparticles onto / into polymer beads, most notably polyethylene glycol-polystyrene (PEG-PS) based polymers.[54,86,87] In this context, the Pd nanoparticles are much more secured into the PEG-PS polymer due to both the chemical interactions and the physical protection caused by the solid support.[88] In the approach used to generate heterogeneous Pd catalyst for this project, the nanoparticles can then be further secured by cross-linking carbon chains to the vacant amino tails within the polymer (Scheme 3.1).[86]

This chapter describes the synthesis and characterization of Pd^0 functionalized PEG-PS resins (Pd^0 resins). The resins' biocompatibility was investigated both *in vitro* and *in vivo*.

3.2 RESULTS

3.2.1 Design and Synthesis of Functionalized Pd^0 Resins

The Pd^0 resins were synthesized following the protocol developed by Bradley and coworkers[86] with minor modifications. Briefly, the NovaSyn TG amino resins were treated with $Pd(OAc)_2$ which caused the resins to turn into dark orange colour. The $Pd(OAc)_2$ bound within the resins was then reduced to Pd^0 using a 10% hydrazine monohydrate solution in MeOH, consequently turning the resins to a distinct black colour. The Pd^0 was then physically entrapped to the resin by cross-linking Fmoc-Glu(OH)-OH to the free amino groups within the resins. This was performed using a

standard coupling mixture (Scheme 3.1). Complete coupling was verified by the ninhydrin test.

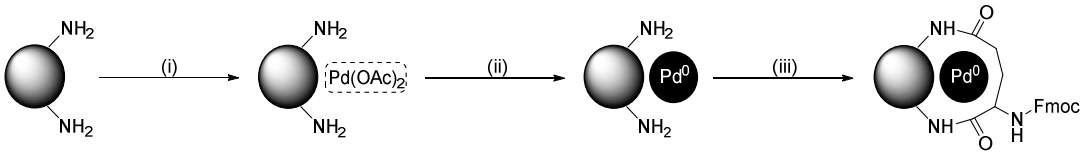

Scheme 3.1. Synthesis of Pd^0 resin. Reagents and conditions (i) $Pd(OAc)_2$ (3 equiv.) and toluene at 80 °C for 10 min followed by RT for 2 hr; (ii) 10% NH_2NH_2 in MeOH at RT in a thermomixer for 25 min; (iii) Fmoc-Glu(OH)-OH (1.5 equiv.), Oxyma (3 equiv.), DIC (3 equiv.) and DCM:DMF (2:1) at RT for 2 hr.

3.2.2 Image Analysis of Pd^0 Resins

The structural integrity of the resin beads after Pd functionalization was verified using scanning electron microscope (SEM), where they appeared to maintain their spherical shape (Fig. 3.1a, b). The presence of Pd^0 nanoparticles (5-10 nm) within and around the resins were verified using transmission electron microscopy (TEM). The Pd^0 nanoparticles are identified as well dispersed dense dark spots within the cross sectioned resin beads (Fig. 3.1c, d).

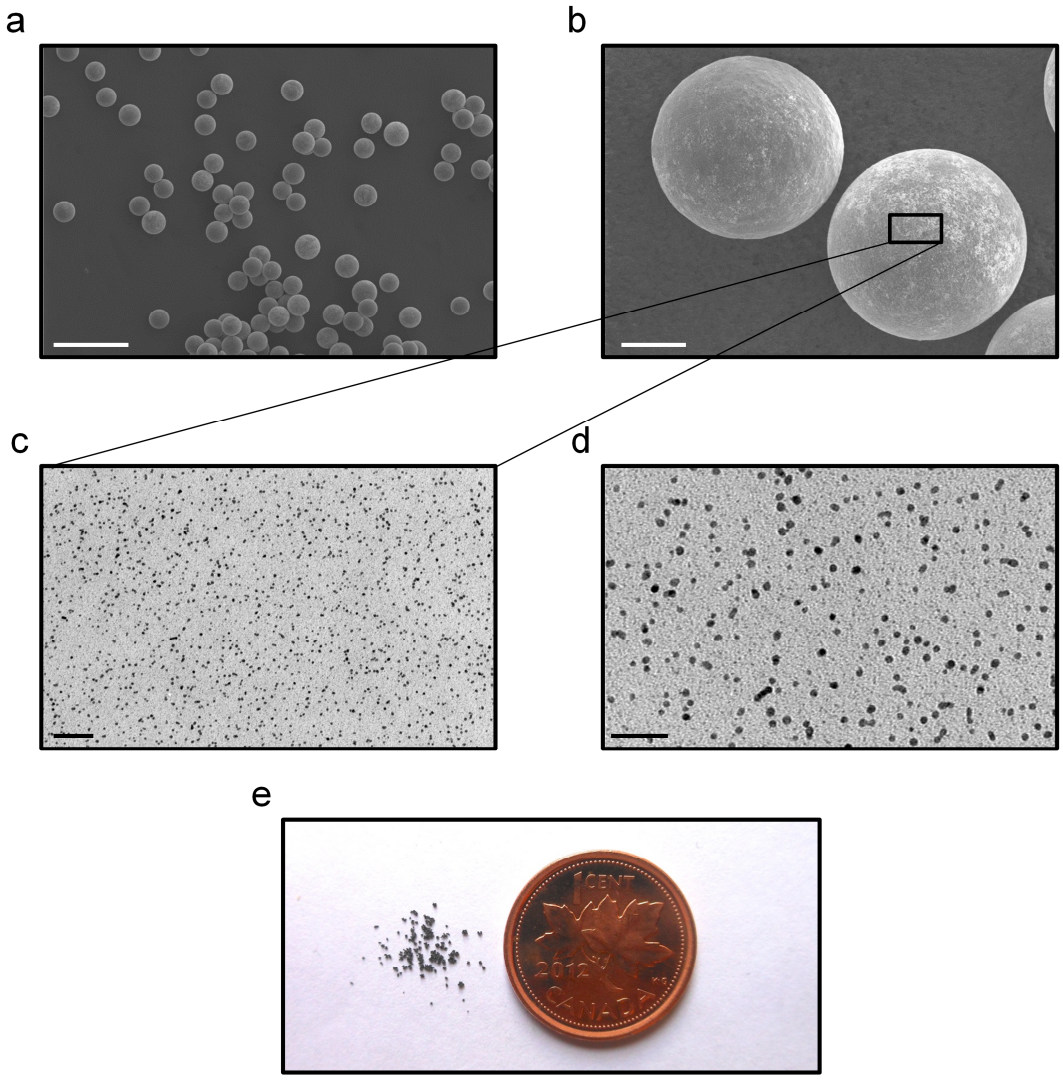

Figure 3.1. SEM and TEM images of Pd^0 resin. (**a-b**) SEM images of Pd^0 resins. (**a**) Pd^0 resins at approximately 22 magnification (scale bar: 500 µm); (**b**) Pd^0 resins at approximately 180 magnification (scale bar: 50 µm) (**c-d**) TEM cross section of Pd^0 resin. (**c**) cross section at approximately 6 X 10^5 magnification (scale bar: 100 nm) (**d**) cross section at approximately 1.6 X 10^6 magnification (scale bar: 50 nm). (**e**) Image of Pd^0 resins next to a 1 cent Canadian coin (19.05 mm in diameter).

3.2.3 Characterisation of Pd^0 Resins

The Pd^0 resins were visually differentiated from the non-active (naked) resins because of the black colour of the former (Fig. 3.1e). Successful reduction of $Pd(OAc)_2$ was verified using powder X-ray diffraction spectra. This was performed by Dr. Carmen Torres at Loughborough University, wherein the data presented the

distinctive pattern of the face-centred cubic lattice of Pd^0 with 4 peaks between 40 – 82 degrees (Fig. 3.2).[58,89]

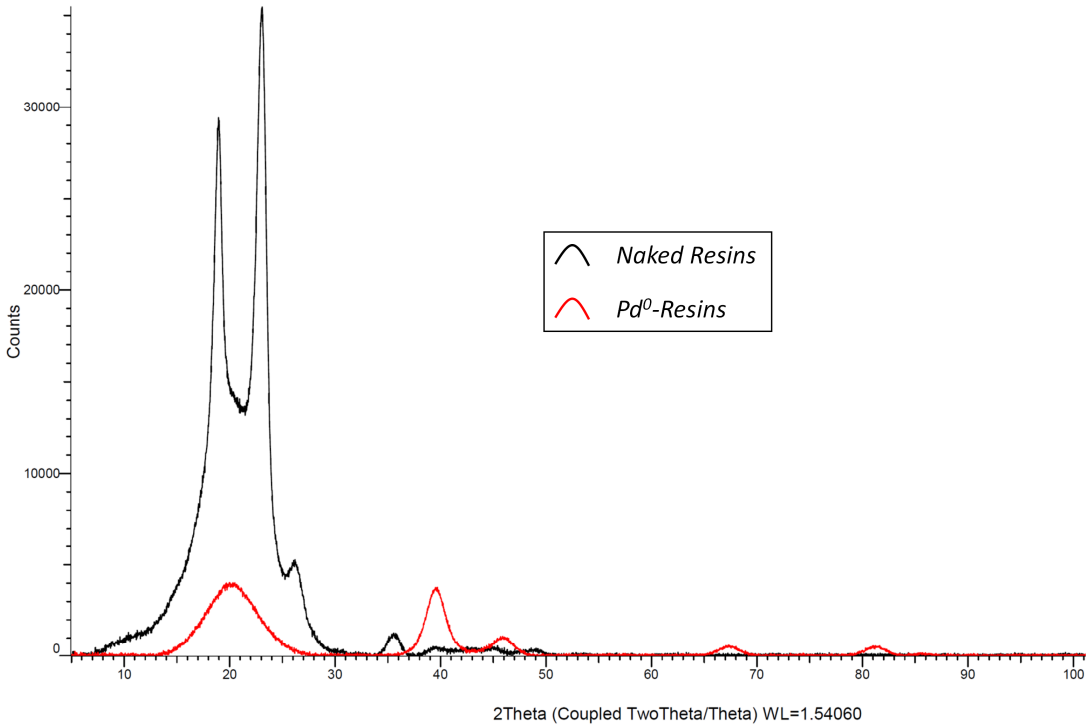

Figure 3.2. Pd^0 resins X-ray diffraction spectra. X-ray diffraction spectra of non-active (naked) resins (black) compared to Pd^0 functionalized resins (red). The Pd^0 resins spectra displayed the distinctive pattern of crystalline Pd^0 with 4 peaks at approximately 40, 46, 67 and 81 degrees. Both samples contained a strong peak at 20 degrees representing the semi-amorphous structure of the PEG-PS matrix.

The content of palladium in the Pd^0 resins was determined by inductive coupled plasma optical emission spectrometry (ICP-OES). This analytical technique is commonly used for the detection of trace metals within various samples of interest.[90] This type of emission spectroscopy relies on inductively coupled plasma (produced by electromagnetic induction) which when the sample (in this case the dissolved Pd^0 resins in nitric acid) is pumped into the high temperature plasma, the atoms from the sample become excited and emit electromagnetic radiation of known characteristic elemental wavelengths (the Pd^0 metal). The content is determined by comparing the intensity of the emission given off by the sample to previously measured intensities of known concentrations of the elements. In this case, the content of Pd^0 was found

to be 2.83% *w/w* for the first batch of synthesised Pd^0 resins used in this chapter and chapter 5 and 4.4% *w/w* from the second batch used in the remaining chapters. Based on this quantification, a solution containing 1 mg/ml of Pd^0 resins (with a 2.83% *w/w* content of Pd) would therefore contain 263 µM of Pd^0 (0.028 g / 106.42 g/mol) or a solution with 0.67 mg/ml of Pd^0 resins (with a 4.4% *w/w* content of Pd) would contain 277 µM of Pd^0.

Sample calculation for 2.83% *w/w* Pd^0 *content*:

Atomic Weight of Pd = 106.42 g/mol; Pd^0 content in 1 g of Pd^0 resins = 0.028 g

$$\textit{(i)} \quad \textit{Moles of } Pd^0 = \frac{0.028\ g}{106.42\ g/mol}$$

$$= 2.63 \times 10^{-4} moles$$

$$\textit{(ii)} \quad Pd^0 \textit{Molar Conc.} = \frac{2.63 \times 10^{-4}\ moles}{1\ L}$$

$$= 2.63 \times 10^{-4} M \text{ or } \boldsymbol{263\ \mu M}$$

3.2.4 Pd^0 Resins Biocompatibility Both in vitro and in vivo

In order for the resins to successfully mediate BOOM chemistry, they have to be biocompatible within the respective biological system. This was therefore assessed both in cell based models and whole organisms. The cell lines chosen for this assessment were the HCT116 colorectal and BxPC-3 pancreatic cancer cell lines. The maximum tolerated concentration of Pd^0 resins was calculated by simply incubating the cells with increasing quantities of resins and monitoring cell viability after 5 days using PrestoBlue reagent and analysed by spectrofluorometery (Fig. 3.3a, b). It was determined that concentrations of 2 mg/mL of Pd^0 resins were cytotoxic to the cells and that the maximum tolerated amount for HCT116 cells were 1 mg/ml (≈ 266 µM of Pd^0) and 0.67 mg/ml for BxPC-3 cells. The biocompatibility of the Pd^0 resins in a whole organism was investigated by implanting a single Pd^0 resin bead inside the yolk sac of a 24 h old zebrafish embryo. The development of the embryo was then monitored for 3 days. As displayed in Fig. 3.3c, the embryo containing the implanted Pd^0 resin (red arrow) developed normally into the larval

stage without any altered phenotype or toxicity illustrating the resins biocompatibility *in vivo*.

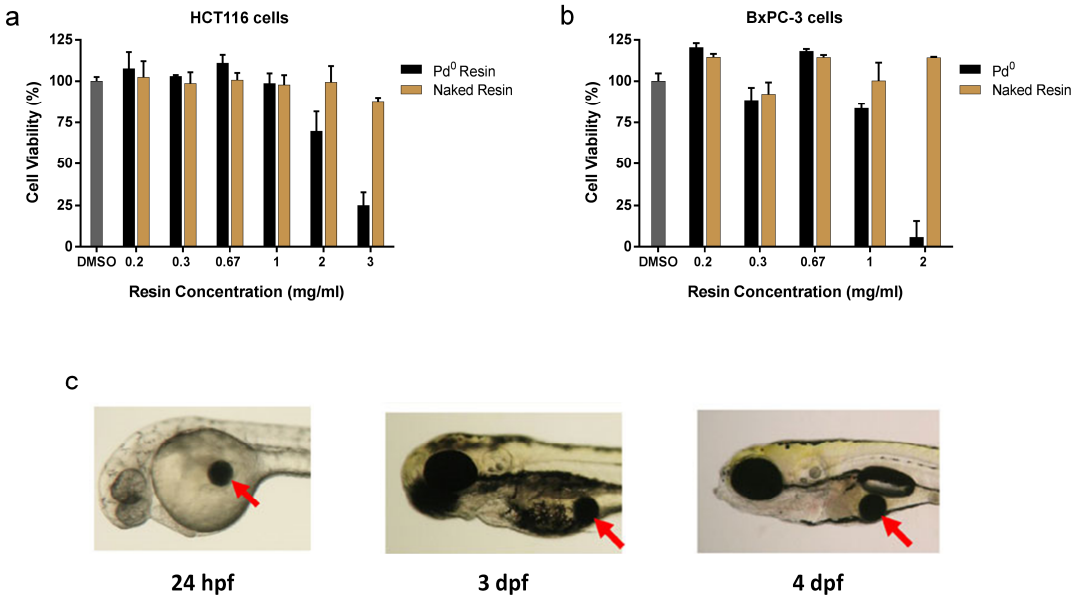

Figure 3.3. Pd^0 resins biocompatibility *in vitro* and *in vivo*. (**a-b**) Study of unspecific cytotoxic effect induced by Pd^0 resins. Pd^0 resins (active resins) and naked (in-active resins) were incubated with cells for 5 days with increasing quantities (0.2 – 3 mg/ml) and cell viability (PrestoBlue^{TM} assay) determined. (**c**) Images of zebrafish embryos containing a single Pd^0 resin implanted within the yolk sac (red arrow) at different stages of development. Fish were imaged at 24 hpf, 3 and 4 dpf.

3.3 CONCLUSIONS

The Pd^0 resins were successfully synthesised using a slightly modified procedure reported by Cho *et al.*[86]. The structural integrity of the Pd^0 resins after the functionalization process was maintained as illustrated by SEM images and the presence of the tiny well dispersed Pd^0 nanoparticles were visualized from TEM images. The successful reduction of $Pd(OAc)_2$ to Pd^0 was confirmed by X-Ray diffraction spectra wherein the typical distinctive pattern of crystalline Pd^0 was detected.

The results indicate that the resins are biocompatible both *in vitro* and *in vivo* by incubating them directly with HCT116 and BxPC-3 cancer cell lines and by surgically implanting a single bead inside the yolk sac of a zebrafish. Although the

biocompatibility displayed by the Pd^0 resins are a critical criteria for BOOM chemistry, whether or not they are catalytically competent at these concentrations (1 – 0.67 mg/ml for the *in vitro* assay and 1 single Pd^0 resins bead for the *in vivo* assays) is a critical factor for this novel treatment regime concept. Their catalytic potential is investigated thoroughly in chapters 4 and 5.

The results presented in this chapter have been previously published as Weiss et al. Nat. Commun. 2014. 5, 3277 (reference 67).

CHAPTER 4

Pd-Labile Gemcitabine Prodrugs

4.1 INTRODUCTION

The first drug candidate to be developed for BOOM chemistry was Gemcitabine. This commercially available antineoplastic drug is used for the treatment of many difficult to treat cancers including non-small cell lung,[91] ovarian[92] and metastatic breast cancers[93] either independently or in combination. It is also the first-line therapy option for the treatment of pancreatic cancer.[94-96]

The drug is classed as a pyrimidine anti-metabolite and is an analogue of deoxycytidine (dC), a nucleoside used intrinsically for DNA synthesis. The sole difference in comparing the two is the presence of two fluorine atoms bound to carbon 2' (C2') (Fig. 4.1). Fluorinated drugs are common in anti-metabolites because they display an increase resistance to biological decay; making them ideal candidates for inhibiting DNA, RNA and enzymatic processes[97]. Gemcitabine is converted into its therapeutically active metabolites through successive phosphorylation of the OH on C5' of the deoxyribose analogue. When di-phosphorylated, it can inhibit ribonucleotide reductase,[98-100] an important enzyme for regulating the overall rate of DNA synthesis[101]. In its tri-phosphorylated state, the drug damages DNA though partial DNA chain termination and stalling of replication forks.[102,103]

In order for the active metabolites to form, Gemcitabine must become phosphorylated by Deoxycytidine Kinase (dCK) which adds the phosphate groups to the OH on C5'. The amine within the cytosine base on C4 is a key component used by dCK to discriminate dC from other DNA nucleosides such as deoxythymidine and deoxyuridine. Both of these nucleosides are unable to form stable hydrogen bonding interactions with the amino acid aspartic acid (Asp) 133, located within the activation

site of dCK.[104,105] The amine group is also the position metabolically attacked by cytidine deaminase. This enzyme is responsible for the detoxification of Gemcitabine via the hydrolytic deamination, which is predominantly mediated within the liver whereby it catalyses the irreversible conversion of Gemcitabine into its inactive metabolite difluoro-deoxyuridine.[106,107]

Based on Gemcitabine's metabolic methods of activation and deactivation, it was hypothesised that by masking the OH on C5' or the NH_2 on C4 with Pd^0 sensitive masking groups (SMG), in theory, the drug's cytotoxicity could be reduced until in the presence of Pd^0. Pd^0 SMGs bound to the OH could have the potential to inhibit the drugs interaction with dCk thus preventing the incorporation of the phosphate groups.[105,108] Eliminating the phosphorylation steps effectively eliminates the overall activation pathway of the drug through the prevention of its two cytotoxic forms. Pd^0 SMGs within the amine could not only affect the drugs interaction with dCk's active site but also could have the added benefit of improving the drugs pharmacokinetics through the prevention of premature liver deactivation.

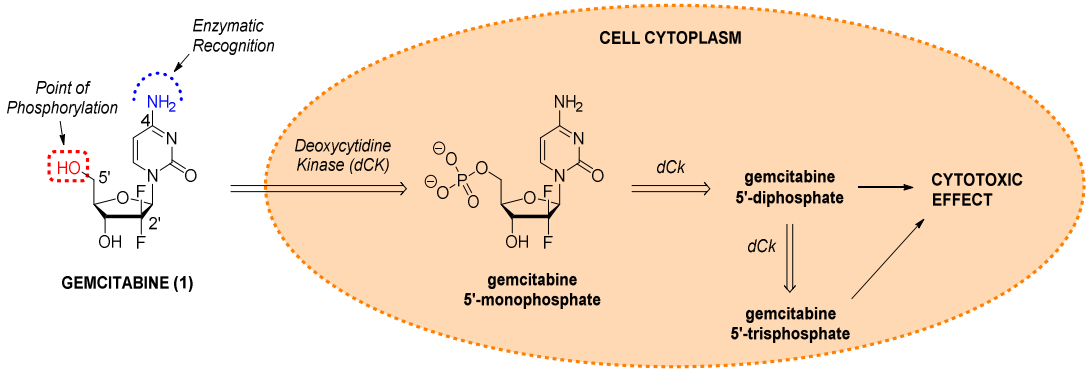

Figure 4.1. Targeted functional groups and cytotoxic mode of action of Gemcitabine. Following entry into the cell, Gemcitabine is successively phosphorylated by dCk at its 5' – OH position to generate cytotoxic metabolites. Reprinted and adapted with permission from reference[68], copyright (2014), American Chemical Society.

This chapter investigates the application of BOOM chemistry for chemotherapy, tailoring it towards creating a more efficient and localized cancer treatment regime. Through masking of Gemcitabine's key functional groups with Pd^0 SMGs, we were able to significantly reduce the drugs cytotoxicity *in vitro*. The carbamate

functionalized prodrugs proved to be the more bioorthogonal and remarkably, the N-propargyloxycarbonyl (N-Poc) promoiety was the most sensitive to Pd^0-mediated catalysis. Zebrafish models confirmed that the Pd^0 resins are not only biocompatible *in vivo* but are also catalytically viable. Treating zebrafish embryos containing a single Pd^0 resin bead within its yolk sac with caged rhodamine 110 fluorescent probes confirmed that N-Poc was the most suitable masking group for BOOM chemistry.

4.2 RESULTS

4.2.1 Design and Synthesis of Pd^0-labile Gemcitabine Prodrugs

Allyloxycarbonyl (Alloc) and propargyloxycarbonyl (Poc) groups were chosen as the Pd^0 SMGs for their proven susceptibility to Pd^0 catalysis[109-112] under biocompatible conditions.[54,58,62,67] The carboxybenzyl (Cbz) group was chosen for its sensitivity to Pd^0-mediated catalytic hydrogenation[113]. This protecting group was expected to be more resilient than Alloc or Poc because of an additional hydrogen source required to drive the Pd^0-mediated cleavage reaction.

The Gemcitabine prodrugs were synthesized using a semisynthetic strategy. First, the carbonate prodrugs (5' – OH) were synthesized by treating Gemcitabine (**1**) with either allyl, propargyl or benzyl chloroformate in the presence of DBU (Scheme 4.1) which yielded compounds **2, 3** and **4** in moderate yields. The carbamate prodrugs were synthesized by first silylating the primary 5' – OH group with TBS-Cl in the presence of imidazole, followed by the treatment of the corresponding alkyl chloroformates (compounds **6, 7** and **8**). The TBS protecting group was then removed through TBAF mediated cleavage which yielded compounds **9, 10** and **11** in moderate to good yields (Scheme 4.1).

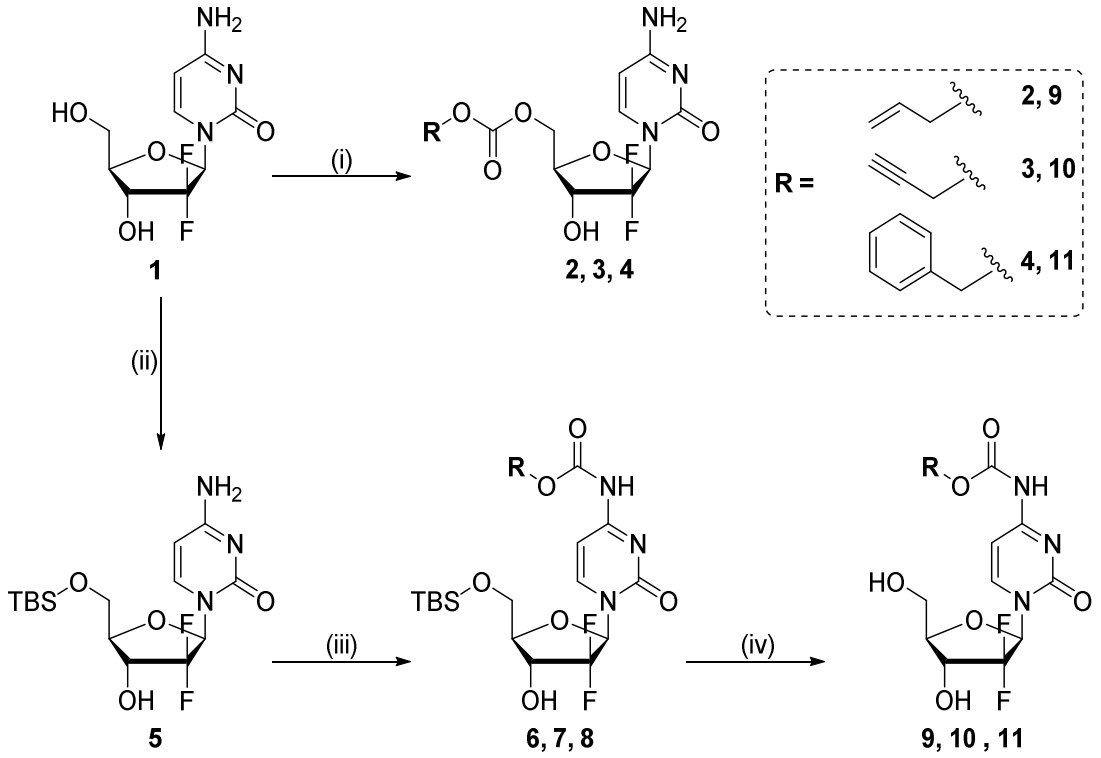

Scheme 4.1. Synthesis of Gemcitabine prodrugs. Reagents and conditions: (i) DBU (2.5 equiv.), DMF, addition of alkyl chloroformate (1.5 equiv.) at 4 °C, then RT overnight (47−53%); (ii) TBS-Cl (1.1 equiv.), imidazole (3.5 equiv.), DMF, RT, 2.5 h (88%); (iii) pyridine (3.2 equiv.), DMF or THF, addition of alkylchloroformate (1.5 equiv.) at 4 °C, then RT. overnight 12−48h (42−69%); (iv) TBAF (2.5 equiv.), THF, RT, overnight (62−92%).

4.2.2 Gemcitabine Prodrug Bioorthogonal Comparative Study

The first step was to determine which masked functional group provided the most bioorthogonality. In theory the masking of both functional groups should have a significant impact on the drugs cytotoxicity; however, one of the key factors for BOOM chemistry is the Pd^0 SMGs resiliency to enzymatic metabolism. With this in mind, the prodrug library was tested in a dose response manner against Gemcitabine in pancreatic adenocarcinoma BxPC-3 and MIA PaCa-2 cell lines. Pancreatic cancer cell lines were chosen due to Gemcitabine's clinical relevancy as a first line of defence for treating this type of cancer. As displayed in Figure 4.2, the carbamate protected prodrugs were the best at reducing Gemcitabine's cytotoxic properties, with a significant (69 - 23 fold) reduction in cytotoxicity compared to unmodified Gemcitabine, verifying the validity of the amine masking strategy, whereas the carbonate protected prodrugs had dose response curves similar to Gemcitabine which

indicated that the carbonate bond is more sensitive to metabolic activation. This result is in accordance with the weaker nature of the carbonate bond in comparison to the carbamate bond.[114,115] It was then concluded that compounds **2, 3** and **4** were not suitable for BOOM applications and therefore only compounds **9, 10** and **11** were examined further in this study.

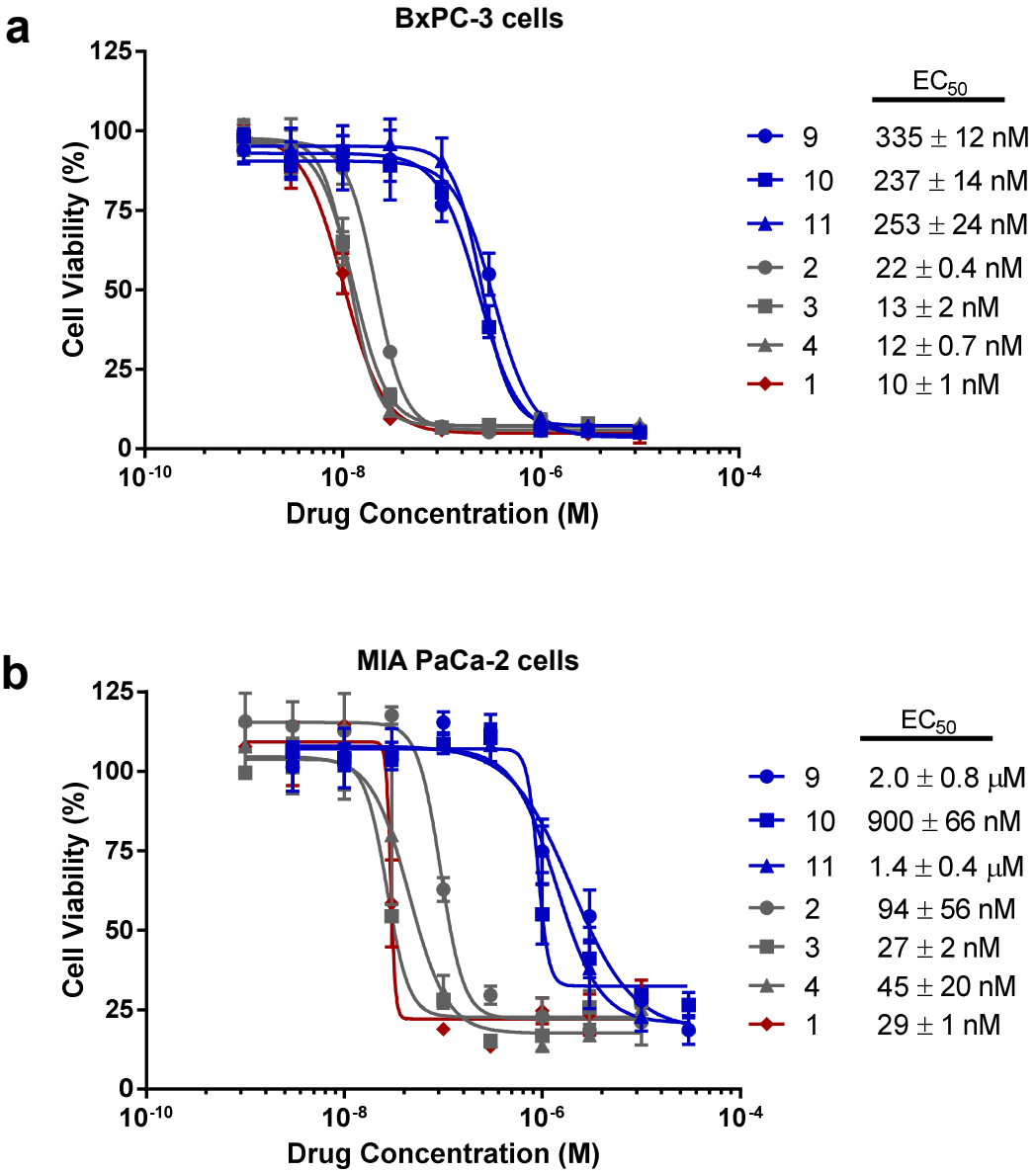

Figure 4.2. Bioorthogonal study of Gemcitabine prodrug library. Cytotoxic effect of carbamate and carbonate protected prodrugs in comparison to Gemcitabine. Cells were incubated with increasing concentrations of drugs (0.003 – 30 μM) for either 5 days (BxPC-3 cells) or 4 days (MIA Paca-2 cells). Cell viability was determined by plotting semi logged dose response curves to determine EC_{50} values. (**a**) BxPC-3 cancer cells. (**b**) MIA PaCa-2 cancer cells. Error bars represent ± standard deviation from *n* = 3

4.2.3 Non-biological Pd^0-mediated Conversion Study

9, 10 and **11** (100 μM) were then tested in a non-biological conversion assay under biocompatible conditions to test their susceptibility to Pd^0-mediated cleavage (Fig. 4.3a). This was done by incubating them (100 μM) in a thermomixer at 1400 rpm, 37 °C for 6 and 24 h with 1 mg/ml of Pd^0 resins (4.4% w/w of Pd^0, as discussed in chapter 3) in 1 ml of PBS (Pd^0 resins were synthesized as described in chapter 3 of this thesis). The resulting Gemcitabine produced from the Pd^0-mediated reaction was detected by comparing the retention time (0.94 sec.) of unmodified Gemcitabine from HPLC analysis (Fig. 4.3b). As expected, **11** was non-responsive to Pd^0 catalysis producing negligible amounts of Gemcitabine (Fig. 4.3e). Again, this was expected due to the lack of an additional hydrogen source required to drive the reductive cleavage of Cbz moieties.[113,116] In contrast, **9** and **10** showed excellent reactivity with the Pd^0 resins (Fig. 4.3c, d), leading to the significant generation of Gemcitabine within 24 h. Remarkably, the *N*-Poc deprotection of **10** proceeded in the fastest and cleanest manner, obtaining a reaction half-life of less than 6 h. This result is in accordance with previous observations, which have demonstrated the superior sensitivity of *O*-propargylated derivatives to Pd catalysis over *O*-allylated derivatives under biocompatible conditions.[62,112,117]

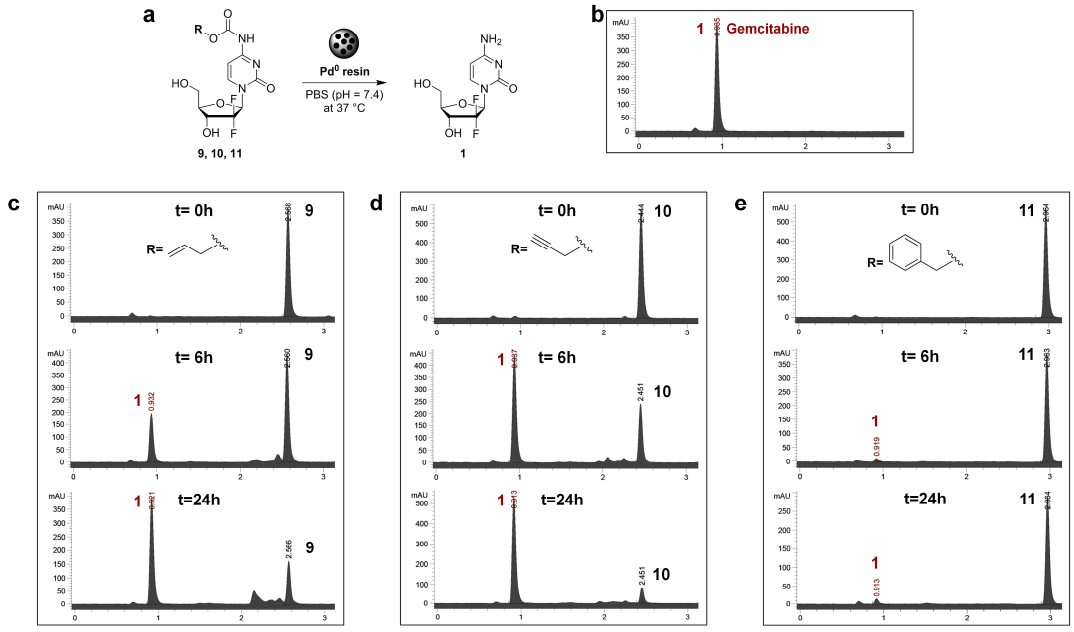

Figure 4.3. Non-biological conversion assay with carbamate Gemcitabine prodrugs. (**a**) Schematic of Pd^0 resin mediated conversion of compounds 9, 10 and 11 under biocompatible conditions. (**b**) HPLC chromatogram of compound 1 (Gemcitabine). (**c - e**) HPLC chromatogram (280 nm) of Pd^0 resin mediated conversion of compound 9 (**c**), compound 10 (**d**) and compound 11 (**e**) at 37 °C for 0 h (top panels), 6 h (middle panels) and 24 h (bottom panels).

4.2.4 Pd^0-mediated Conversion of Prodrugs in vitro

Using BxPC-3 cells, compounds **9, 10 and 11** were incubated with Pd^0 resins in order to assess the prodrugs/Pd^0 combination's cytotoxic capabilities in comparison to unmodified Gemcitabine (Fig. 4.4). While neither the Pd^0 resins nor any of the prodrugs separately displayed any cytotoxicity, in combination, compounds **9** and **10** significantly displayed antiproliferative capabilities. This confirmed the *in situ* bioorthogonal synthesis (BOOM activation) of cytotoxic Gemcitabine. The combination with compound **11** was again ineffective because of the reasons mentioned above. As a consequence only compounds **9** and **10** were further evaluated.

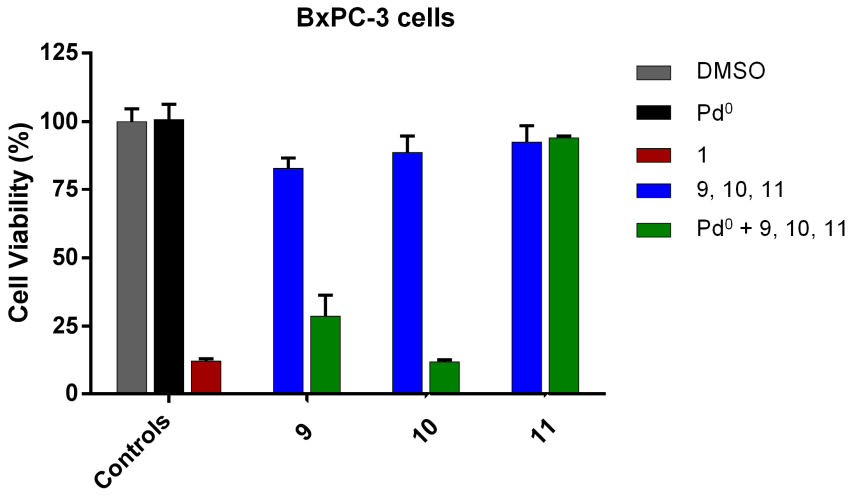

Figure 4.4. Preliminary Boom activation comparison of Gemcitabine prodrugs 9, 10 and 11. Experiments: 0.1% (v/v) DMSO (untreated cell control, gray); 0.67 mg/mL of Pd^0 resins (negative control, black); Gemcitabine (100 nM, positive control, red); prodrug 9, 10 and 11 (100 nM, negative control, blue); and 0.67 mg/mL of Pd^0 resins + prodrug 9, 10 and 11 (100 nM, BOOM activation, green). Cell viability was measured at day 5 using PrestoBlue reagent. Error bars: ± SD from n = 3.

To further evaluate the use of Alloc vs. Poc as Pd^0 SMGs for the BOOM activation, dose response studies were carried out with **9** and **10** in combination or without Pd^0 resins in two pancreatic carcinoma cell lines: BxPC-3 (Fig. 4.5a) and MIA PaCa-2 cells (Fig. 4.5b). As initially demonstrated in Fig. 4.4 and further reinforced in Fig. 4.5, both **9** and **10** when in combination with Pd^0 displayed antiproliferative capabilities; however, only **10** was able to consistently demonstrate its effect at comparative levels to unmodified Gemcitabine at all concentrations tested. This indicates that the propargyl moiety is the superior Pd^0 SMG. **10** showed consistent cytotoxic levels to Gemcitabine despite the cell line used or media in which the Pd^0-mediated deprotection reaction took place (BxPC-3 cells were cultured in RPMI media and MIA PaCa-2 cells in DMEM). In stark contrast, the allyl moiety within **9** displayed inconsistent Pd-triggered cytotoxicity. Although **9**/Pd^0 combination displayed significant cytotoxic levels at higher concentrations (30 and 100 nM) when tested with the BxPC-3 cells, the combination displayed virtually no effect with the MIA PaCa-2 cells. This indicated that the Pd^0-mediated *N*-Alloc cleavage is affected by cell type or cell culture conditions, an undesirable trait for BOOM activation.

Cell growth kinetics of BxPC-3 cells was monitored by time-lapse imaging using an IncuCyte ZOOM™ microscope to compare the effect of each prodrug/catalyst

combination upon cell growth (Fig. 4.5c). The negative controls (**9** and **10** without Pd^0) displayed standard growth curves up to 100% cell confluency (blue curves). The positive control, Gemcitabine treatment, displayed competent suppression of cell proliferation within 24 h (red curve). In accordance with the dose response combination study, *N*-Poc was the more responsive Pd^0 SMG. **10**/Pd^0 combination affected cell proliferation with the same efficacy and kinetic response as Gemcitabine indicating the cytotoxic levels of the drug were rapidly generated. Contrastingly, although the combination of **9**/Pd^0 affected the proliferation of BxPC-3 cells as made evident by the differential growth curve compared to the negative controls, was inferior at producing cytotoxic levels of the drug as compared to **10**/Pd^0 combination and Gemcitabine.

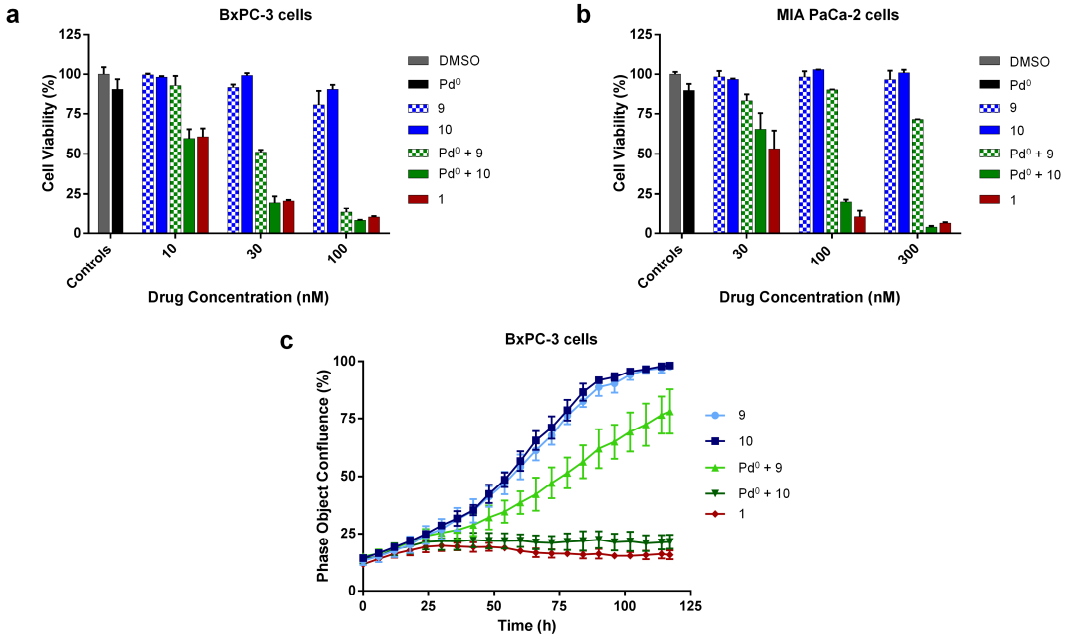

Figure 4.5. BOOM activated Gemcitabine prodrugs and cell growth kinetics. Toxigenic effect of bioorthogonally activated Gemcitabine prodrugs in a dose response manner in (**a**) BxPC-3 and (**b**) MIA PaCa-2 cells. Experiments: 0.1% (v/v) DMSO (untreated cell control, gray); 0.67 mg/mL Pd^0 resins (negative control, black); Gemcitabine (positive control, red); prodrug 9, 10 (negative control, blue); and 0.67 mg/mL of Pd^0 resins + prodrug 9, 10 (BOOM activation, green). (**c**) Cell confluency study in BxPC-3 cells monitored for 120 h. Drug and prodrug concentrations – 30 nM, Pd^0 resins - 0.67 mg/ml. Error bars: ± SD from n = 3.

4.2.5 Cytotoxic Mode of Action Analysis

Double stranded breaks caused by DNA damage induces phosphorylation of the variant histone of the H2A protein family, H2AX. Phosphorylated ɣ-H2AX is responsible for recruiting and localizing the DNA repair mechanism.[118] Gemcitabine damages DNA through partial DNA chain termination and stalling of replication forks[102]. In order to assess the toxigenic effect of the prodrug/catalyst combination at the molecular level to unmodified Gemcitabine, immunofluorescence studies were conducted to probe for ɣ-H2AX as a marker of DNA damage in the MIA PaCa-2 cells (Fig. 4.6). Figure 4.6 demonstrates that only the combination and the unmodified Gemcitabine treated cells expressed high levels of ɣ-H2AX (Fig. 4.6c, d, green fluorescence), whereas both the negative controls (Pd^0 and **10**) separately did not (Fig. 4.6a, b). These expression levels of ɣ-H2AX further illustrate the analogous toxigenic activity of the prodrug/catalyst combination to unmodified Gemcitabine.

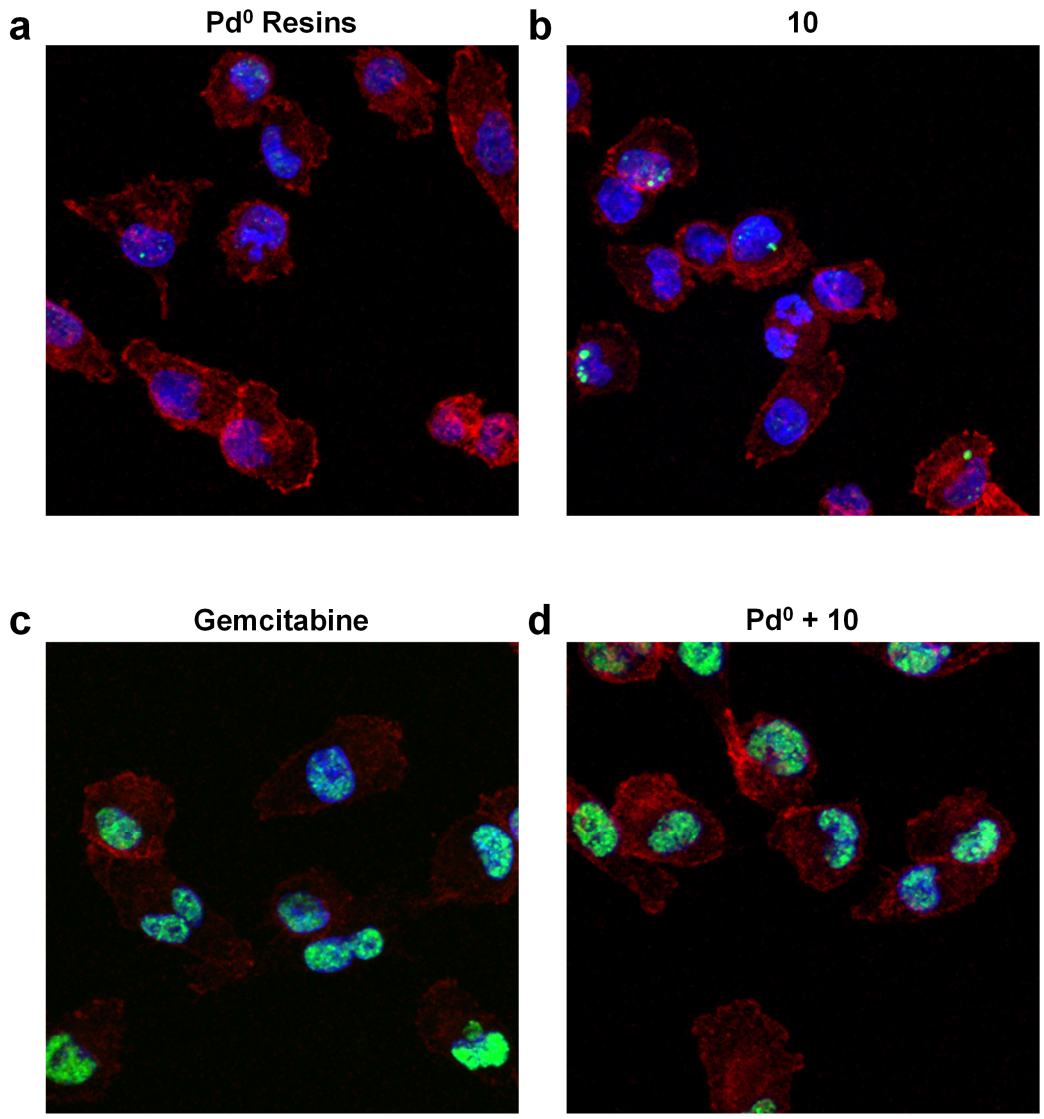

Figure 4.6. DNA damage study. Merge fluorescent images of MIA PaCa-2 cells after 24 h of treatment. (**a**) Pd^0 resins (0.67 mg/ml). (**b**) 10 (300 nM). (**c**) Gemcitabine (300 nM). (**d**) Pd^0 resins/10 combination (BOOM activation assay). Fluorescent labels: Hoechst 33342 for cell nuclei (blue), Alexa Fluor 594 phalloidin for F-actin (red), and anti-phospho-histone γ-H2AX + Alexa Fluor 488 secondary antibody for phosphorylated γ-H2AX (green).

4.2.6 Pd^0 Resins Catalytic Activity in Zebrafish

In chapter 3, the biocompatibility of a single Pd^0 resin was demonstrated by surgically implanting a bead inside a zebrafish embryo yolk sac. The development of the fish was then monitored for several days with no apparent development of phenotype or hindrance of normal embryonic development as a result of palladium induced toxicity. However, in order for the BOOM activation strategy to be successful, not only do the beads have to be biocompatible but also their potential to

mediate chemical transformations is equally important. In order to assess their catalytic proficiency, several Pd^0-labile fluorescent probes were synthesized (Scheme 4.2) and incubated with the zebrafish containing either an active Pd^0 resin or a non-active (no Pd^0 present) resin bead (Fig. 4.7b, c). Carbamate-protected probes (compounds **13, 14** and **15**) were synthesized using rhodamine 110 chloride (**12**) and treating it with the corresponding alkyl chloroformates in the presence of either Et_3N or pyridine in dry DMF (Scheme 4.2). The resulting non-fluorescent probes (5 μM) were then incubated with 2 dpf zebrafish embryos which contained either of the two types of resin beads. The enhanced lipophilic property of the probes meant that they could readily diffuse across biological barriers such as the embryos' epidermis; whereas the fluorescent rhodamine 110 produced from the BOOM activation reaction, due to its hydrophilicity, would remain trapped in the physiological compartment wherein the reaction took place, i.e. the zebrafish yolk sac.[54,57,58] After treating the zebrafish with the probes for 24 h at 32 °C, they were analysed by fluorescence microscopy. Treating the zebrafish with the various probes also presented the opportunity to test the bioorthogonality of each Pd^0 SMG *in vivo*. The embryos containing the non-active resins treated with the **15** (Cbz) and **14** (Poc) displayed decent biochemical stability (Fig. 4.7b - bottom and middle panels respectively), with detectable fluorescence only in the digestive system (yellow arrow). When those probes were incubated with embryos containing a Pd^0 resin, expectedly, **15** remained unresponsive to palladium mediated catalysis (Fig. 4.7c - bottom panel); while an increase in fluorescence intensity was clearly evident from the embryos incubated with **14**, thus suggesting the palladium mediated generation of rhodamine 110 (Fig. 4.7c, middle panel). In fact, an image analysis of the area encompassing both the Pd^0 resin bead and the area surrounding it (blue line which measured pixel intensity along that area) measured up to a 4 fold increase in fluorescence intensity (Fig. 4.7d). Comparing this to the area surrounding the non-active resin treated with **14** (red line), apart from the auto-fluorescence obtained from the non-active polystyrene-made resin, no increment in fluorescence was observed in the area nearby the resin. Interestingly, the zebrafish embryos treated with **13** (*N*-Alloc), regardless of whether they contained the Pd^0 bead or the non-active bead, displayed high levels of fluorescence within the yolk sac and the digestive system

(Fig. 4.7b and c – top panels). Due to the poor chemical stability of compound **13**, the production of rhodamine 110 produced by palladium catalysis was imperceptible. This was a strong indication of the poor bioorthogonality *N*-Alloc groups possess within this *in vivo* model.

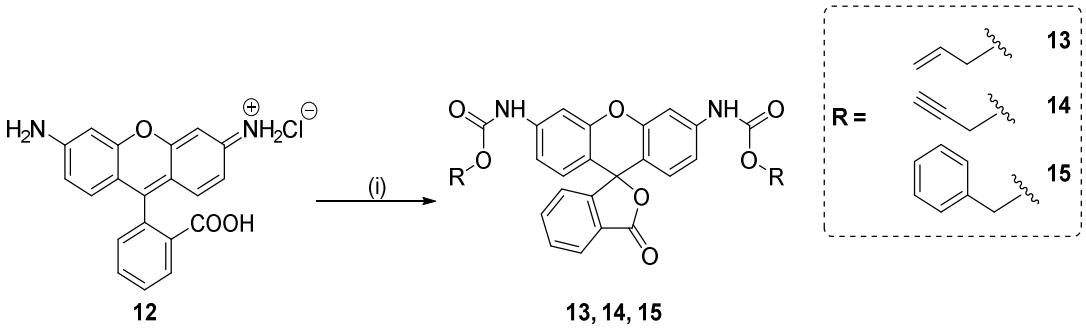

Scheme 4.2. Synthesis of non-fluorescent Pd^0-labile probes. Reagents and conditions: (i) Et_3N or pyridine (9 equiv.), DMF, addition of alkylchloroformate (6 equiv.) at RT overnight (13-36%).

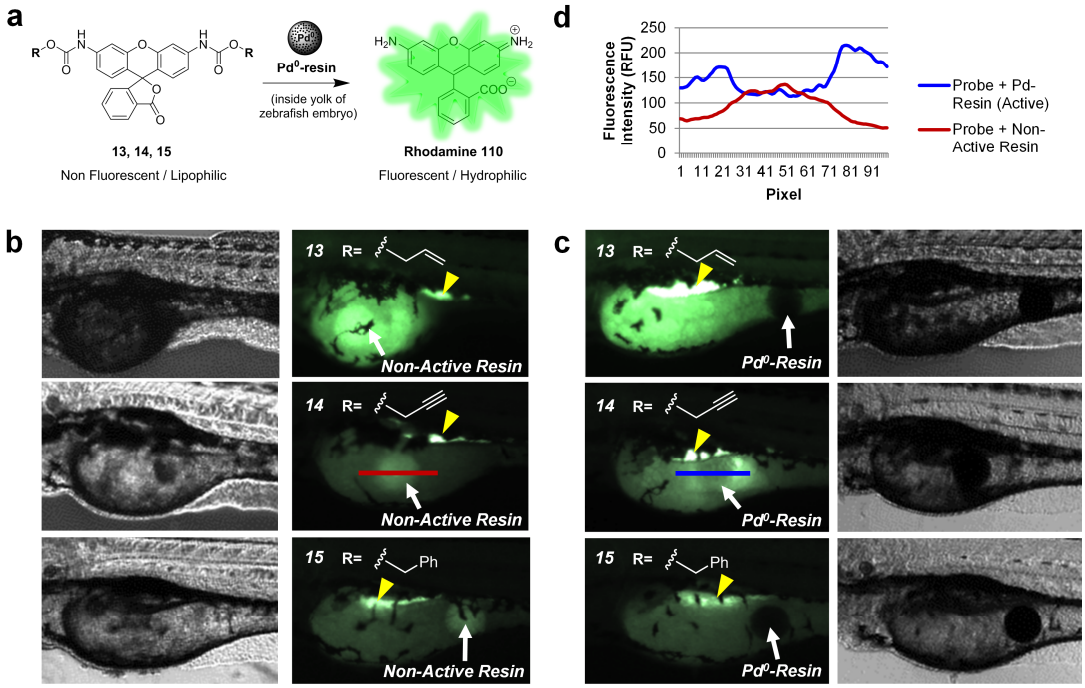

Figure 4.7. Pd^0-mediated carbamate cleavage of fluorescent probes inside zebrafish embryos. (**a**) Schematic of BOOM conversion of nonfluorescent lipophilic compounds 13, 14 and 15 into fluorescent hydrophilic rhodamine 110. (**b, c**) 3-dpf zebrafish embryos (n = 5) after incubation with 5 µM of compounds 13 (top), 14 (middle), and 15 (bottom) for 24 h at 31 °C. (**b**) Fish containing a non-active resin within the yolk sac (white arrows). (**c**) Fish containing a Pd^0 resin within the yolk sac (white arrows). Fish were imaged by phase contrast and fluorescent microscopy (Ex / Em: 488 / 521 nm). (**b**) Analysis of fluorescence intensity/pixel across a horizontal line of approximately 300 µm drawn in the yolk sac of the zebrafish embryos and encompassing both the resin and the area surrounding it. Note: the red and blue lines represent the areas of fluorescence intensity profile

measured over the inactive resin (**b**, middle left panel) and the Pd^0 resin (c, middle right panel), respectively.

Regardless of which probe the zebrafish were treated with and which type of bead they contained within their yolk sacs, strong fluorescence signals were observed within the digestive system (Fig. 4.8, red, yellow and white arrows).[119,120] This suggests that the carbamate bonds, although much more resistant to enzymatic metabolism *in vitro* compared to the carbonate bond, were still susceptible to the digestive enzymes within the gut. This indicates that prodrugs masked with chemical moieties containing carbamate bonds would not be suitable for oral administration for the BOOM activation strategy.

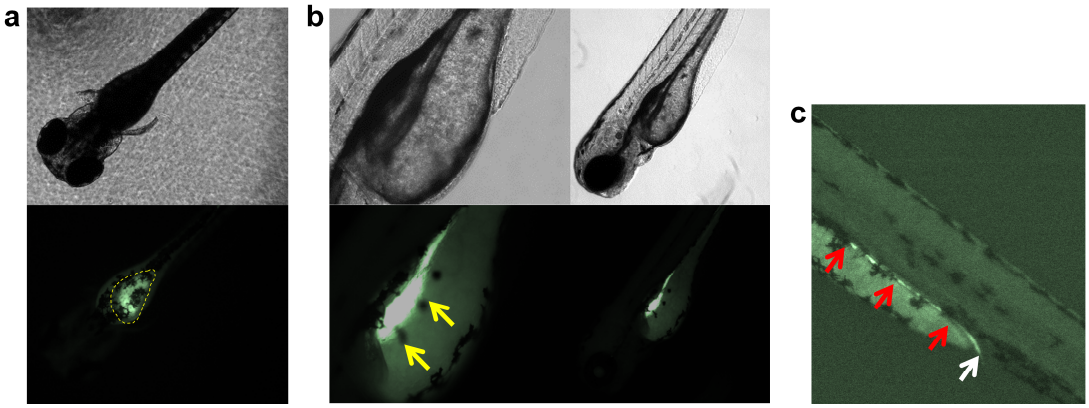

Figure 4.8. Bioactivation of compound 14 inside digestive system of zebrafish embryos. Zebrafish embryos (3 dpf, *n* = 5) were incubated with compound 14 (5 µM) for 24 h at 31 °C and imaged using fluorescent microscopy (Ex / Em: 488 / 521 nm). (**a**) Ventral view of a 4 dpf zebrafish embryo, in brightfield or with the fluorescent signal from the developing intestinal bulb outlined (yellow dashed line, possibly including the exocrine pancreas). (**b, c**) Lateral view of a zebrafish embryo showing the fluorescent signal from the developing intestinal bulb (yellow arrow), along the intestinal tract (red arrows) to the anus (white arrow).

4.3 CONCLUSIONS

The strategy to mask the amino group on C4 compared to the OH on C5' of the Gemcitabine molecule proved to be the most successful route at significantly reducing drug's cytotoxicity. Of the three carbamates derivatives investigated, *N*-Poc was the more susceptible to Pd^0-mediated cleavage both in cell culture and in the non-biological conversion assay. Through cell viability assays, cell growth kinetics

assays and DNA damage assays it was confirmed that indeed Gemcitabine was the product produced from the combination of extracellular Pd^0 resins and compound **10**. When comparing the bis-protected rhodamine 110 derivatives (compounds **13, 14** and **15**), only the bis-*N,N*'-Poc-rhodamine (**14**) was locally activated by the single Pd^0 resin bead within the yolk sac of the zebrafish. Compound **13** was too susceptible to enzymatic metabolism to quantify Pd^0-mediated rhodamine 110 activation and compound **15** was non-responsive to Pd^0 catalysis. These *in vivo* results further strengthened the Poc-carbamate's candidacy for use in development of BOOM activation strategies. A recent study by Chen *et al*.,[62] which used Pd^0 to control the activation of an enzyme intracellularly, also concluded that in terms of comparing Alloc vs Poc carbamates against palladium sensitivity, Poc is superior.

Although using Poc-carbamates proved to be a successful first entry for the BOOM activation strategy with excellent palladium mediated deprotection kinetics comparable to unmodified Gemcitabine at all concentrations tested, the bioorthogonality of the *N*-Poc moiety leaves room for improvement. While a 23 fold decrease in cytotoxicity is of significance for some applications, ideally the difference should be much greater to be considered a strong bioorthogonal prodrug candidate for reducing systemic adverse effects of anticancer treatment. Within the zebrafish model, the *N*-Poc revealed a poor chemical stability within the digestive system. This brings into question how well a Poc-prodrug used for the BOOM activation strategy would translate within a more complex organism such as mice or humans. Ideally, a more chemically stable and thus more bioorthogonal Pd^0 SMG would be required for progressing this treatment regime further such as the Pd^0 SMG investigated in chapter 5.

The results presented in this chapter have been previously published as Weiss et al. J. Med. Chem. 2014. 57, 5395 (reference 68)

CHAPTER 5

Pd-Labile 5-Fluorouracil Prodrug

3.1 INTRODUCTION

The previous chapter confirmed the extraordinary challenge of developing prodrugs able to bypass the cell metabolism while still maintaining susceptibility to Pd-mediated transformation. Therefore, we searched for promoieties with high biochemical stability that could still remain sensitive to palladium catalysis. The use of *N*-alkyl groups was then investigated, since there are not enzymatic pathways specifically designed to metabolize these groups and are very stable under basic and acidic environments. While allyl and propargyl phenolic ethers have demonstrated sensitivity to palladium species under biocompatible conditions,[112,121,122] reports of palladium-mediated *N*-dealkylations indicated that this process would only occur under biologically unfavourable environs.[56] Despite this, we hypothesized that the relatively low pKa of endocyclic NH groups with lactam/lactim tautomery could allow for the *N*-deakylation process to take place under biocompatible conditions. Significantly, this kind of chemical group is found in several cytotoxic pyrimidine derivatives such as uracil analogues.

5-fluorouracil (5FU) was therefore nominated as the next chemotherapeutic drug used for the BOOM treatment strategy. This well-established drug has been used for many years in oncology to treat a range of various cancers either on its own or in combination. Its use for the treatment of colorectal cancers is where it has had its greatest impact.[123] However, the response rate for this patient population when treated with 5FU as a first line of defence is still only 10 -15%. This is primarily due to the drug's limited safety profile.[124]

5FU like Gemcitabine is classed as an antimetabolite. It is analogous to uracil with the exception that 5FU contains a fluorine atom at *C*5. Once 5FU is converted into

one of its several cytotoxic antimetabolitic forms, it causes the disruption of essential biosynthetic processes. When 5FU is metabolised to fluorodeoxyuridine monophosphate (FdUMP), it inhibits thymidylate synthase (TS). This is a well conserved enzyme across many species and is involved in DNA synthesis and repair[125]. The other antimetabolic form is fluorouridine triphosphate (FUTP). FUTP is responsible for causing RNA damage by preventing subsequent RNA processing once it has been incorporated into the growing strand.[126-128]

Another drawback to 5FU is its limited bioavailability. More than 80% of the administered 5FU in a patient is catabolised in the liver by an enzyme called dihydropyrimidine dehydrogenase (DPD). DPD reduces 5FU to dihydrofluorouracil which renders the drug ineffective. The 5FU molecule binds to the active site of the enzyme through hydrogen bonds via the carbonyl and nitrogen atoms within 5FU and asparagine residues within the active site.[129]

The nitrogen atom at position *N*1 within the 5FU molecule is where the functionalization takes place for the conversion of 5FU into its cytotoxic nucleotidic metabolites (Fig. 5.1). In addition, similarly to phenolic OH, this endocyclic nitrogen possesses a pKa of 9 due to lactam/lactim tautomery[130] (Fig. 5.2). Based on this mode of action, it was hypothesized that by incorporating a metabolically stable group at this position, the intracellular activation of 5FU would be greatly hindered and consequently, so too would its cytotoxic capabilities.[123] Importantly, the pharmacological activity of 5FU should be restored locally within the tumour by an intratumoral Pd activating device. This strategy may also have the added benefit of increasing the drugs bioavailability by hindering its interaction with DPD through the prevention of one of the key hydrogen binding interactions between the *N*1 and asparagine 609.[129] The bulkier modified 5FU prodrug may also decrease the binding affinity within the active pocket of DPD, further increasing its bioavailability.

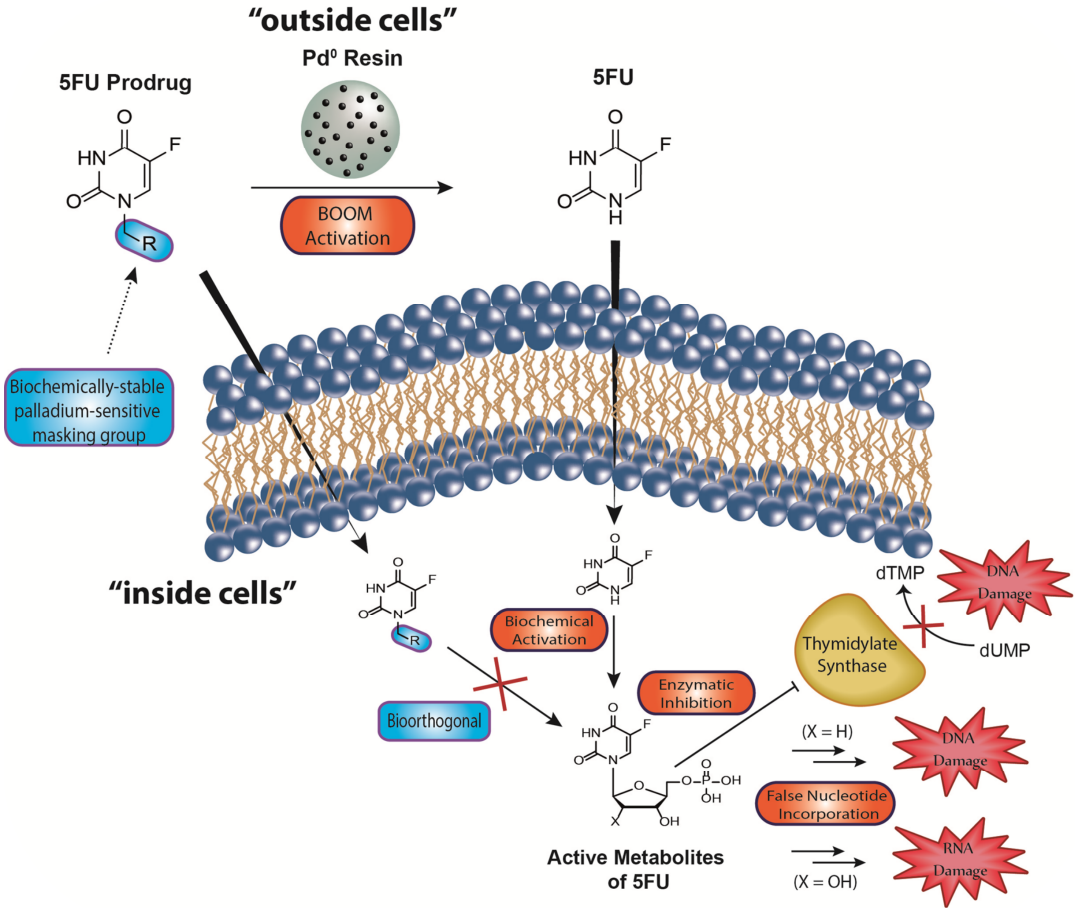

Figure 5.1. 5FU prodrug BOOM activation strategy and cytotoxic mode of action. Masking N1 position of 5FU with a Pd-labile promoiety would impede 5FU intracellular pharmacological activity. However, in the presence of the Pd^0 activating device, the device would bioorthogonally cleave the masking group effectively activating 5FU. This would be a local activation within the tumour where the device has been surgically implanted. This local treatment of the disease would reduce systemic side effects from 5FU. dTMP – thymidine monophosphate; dUMP – deoxyuridine monophosphate.

To obtain bioorthogonal palladium-labile 5FU prodrugs, the protecting groups incorporated at *N*1 again had to fulfil two criteria: 1) sensitive to palladium mediated cleavage and 2) in the absence of palladium, biochemically stable so that the prodrug's cytotoxicity is several times less cytotoxic (ideally greater than 100 fold).[54] Following the hypothesis that the relatively low pKa values due to the charge delocalization of 5FU's aromatic conjugate bases[130] could promote 5FU's leaving group properties (Fig. 5.2), biochemically-stable allyl and propargyl moieties were investigated (All-5FU - **17** and Pro-5FU - **18** respectively) to mask 5FU's intracellular activation. The benzyl moiety (Bn-5FU - **19**) was chosen again as a

negative control based on its resistance to palladium mediated cleavage demonstrated in chapter 4 (Scheme 1). These compounds were classed as 5FU prodrugs.

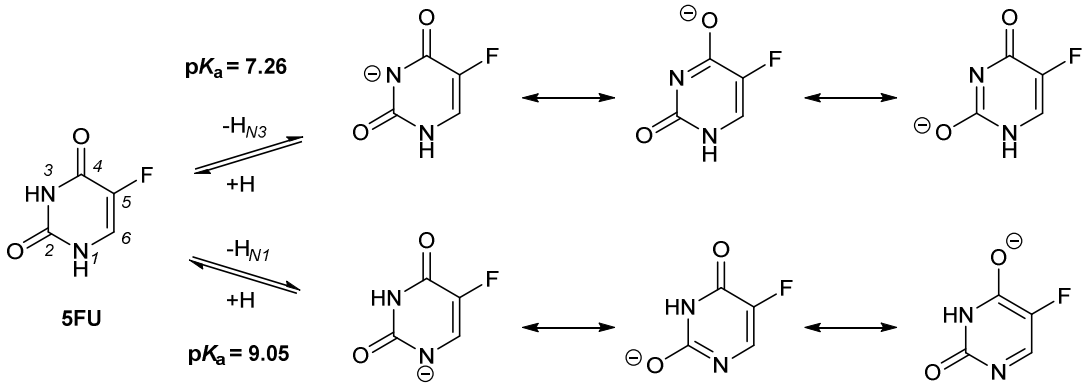

Figure 5.2. 5FU conjugate bases. The low experimental pK_a of 5FU is in part due to the delocalization of the resulting negative charge across the π system.[130]

5.2 RESULTS

5.21 Synthesis of 5FU Prodrugs

All 5FU prodrugs were synthesized in one step by reacting 5FU with the corresponding alkyl bromide in the presence of DBU using DMF as the solvent (Scheme 5.1).

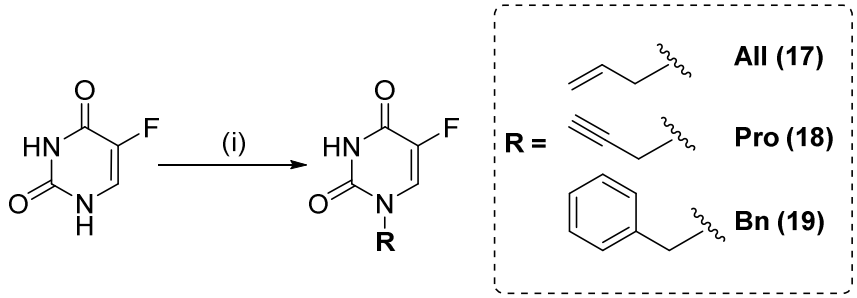

Scheme 5.1. Synthesis of 5FU prodrugs. Reagents and conditions: (i) DBU (1.2 equiv.), DMF, alkylbromide (1 equiv.), 4 °C, then RT overnight (31-40%).

5.22 Pd^0–mediated Conversion of Prodrugs into 5FU Under Biocompatible Conditions

The sensitivity of the prodrugs to Pd^0 resins were investigated under biocompatible conditions. All three 5FU derivatives (100 μM) were incubated in a thermomixer at 1400 rpm, 37 °C for 6, 24 and 48 h with 1 mg/ml of Pd^0 resins ([Pd] = 266 μM) in 1 ml of PBS. Conversion rates were analysed by HPLC using an UV detector to avoid the visualization of salts. As expected, the Bn-5FU showed virtually complete stability in the presence of Pd^0 after 48 h (Fig. 5.3c, right panel). Remarkably, conversion from Pro-5FU to 5FU was almost 40% after just 6 h, with complete conversion observed within 24 h (Fig. 5.3b). More surprising was the inactivity displayed from All-5FU (Fig. 5.3c, middle panel). This suggests that electronic and/or conformational aspects may be essential for efficient metal coordination and dealkylation (Fig. 5.4a), features which only the propargyl group seemed to be able to provide. The successful conversion to 5FU from Pro-5FU was verified by mass spectrometer. Also, as observed previously[56] and verified by mass spectrometry, the by-product of the oxidative cleavage of the propargyl group was acetol (1-hydroxyacetone) (Fig. 5.4b; Scheme 5.2). Acetol is a natural compound biologically used for glycogenesis.[131] Compounds 1-propargyl-2-pyridone (**21**) and 1-propargyl-4-pyridone (**23**) were synthesized and treated under the same conditions as described above to test whether this *N*-depropargylation process could be applied to other heterocyclic compounds with similar lactam/lactim tautomery (Fig. 5.4c). Verified by TLC, after 24 h exposure with the Pd^0 resins, both **21** and **23** starting materials were completely converted to the desired products, 2-pyridone and 4-pyridone (compounds **20** and **22**, respectively). This indicated that this deprotection process can be applied to similar heterocyclic systems. The proposed mechanism for this reaction is illustrated in Scheme 5.2.

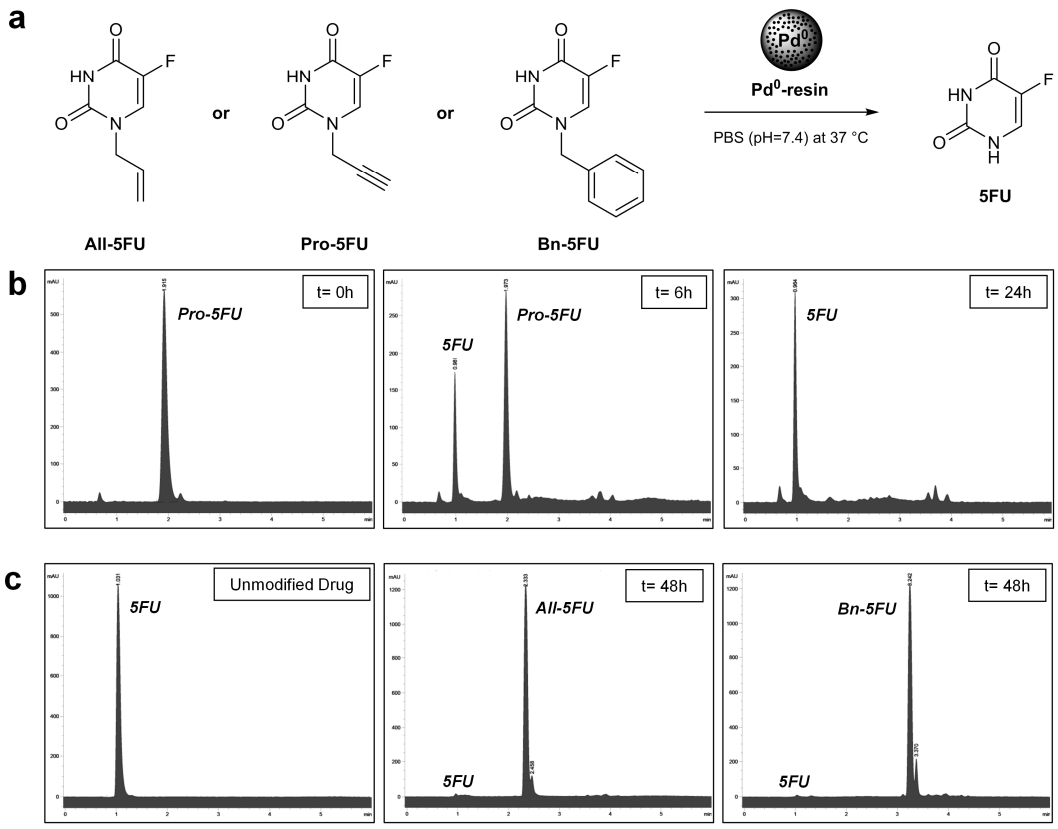

Figure 5.3. **5FU conjugate bases, 5FU prodrugs and non-biological conversion assay**. (**a**) 5FU prodrugs and Pd^0-mediated dealkylation under biocompatible conditions (37 °C, isotonic media and physiological pH). (**b**) HPLC traces of Pd^0-mediated conversion of Pro-5FU, into 5FU. HPLC traces of reaction crude were analysed using an UV detector (280 nm) at t = 0 h (left), t = 6 h (central) and t = 24 h (right). (**c**) Treatment of All-5FU and Bn-5FU with Pd^0-resins. Reaction crude was monitored by HPLC using the UV detector (280nm): left panel, commercial 5FU; central panel, All-5FU experiment; right panel, Bn-5FU experiment.

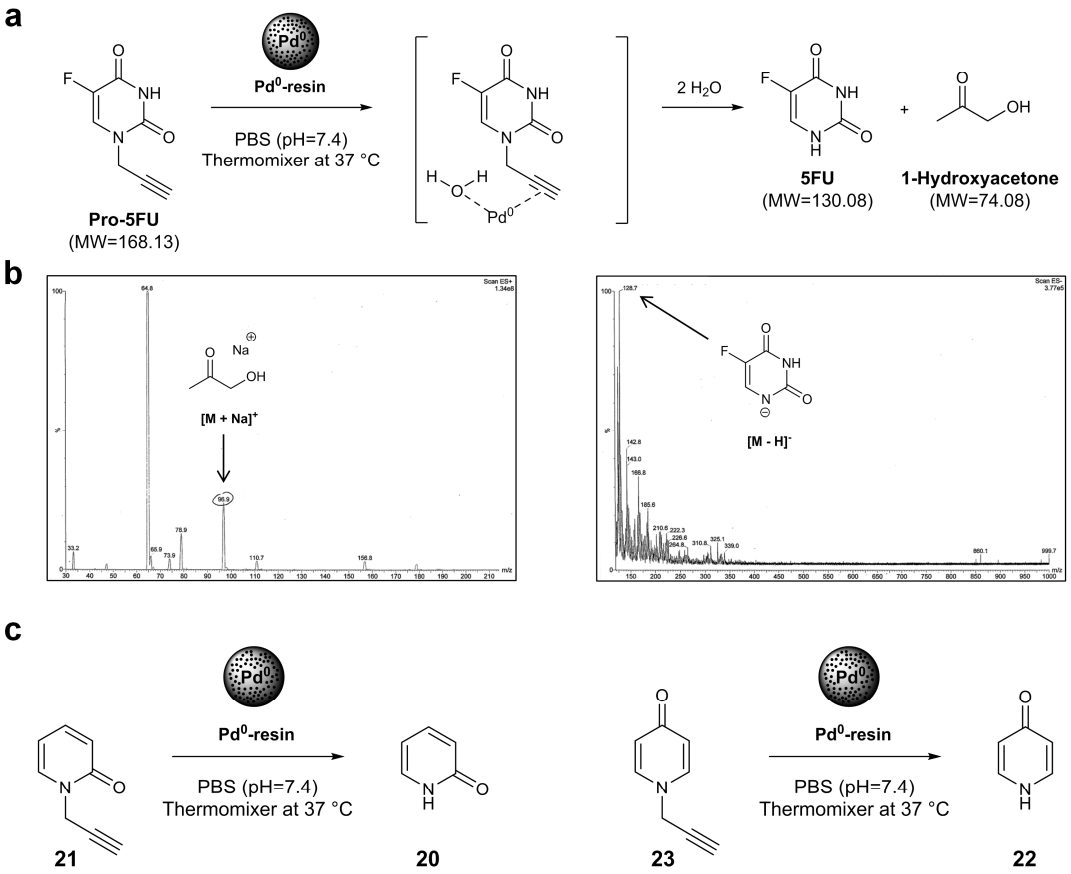

Figure 5.4. Reaction scheme of Pro-5FU + Pd^0 and mass spec. analysis post reaction. (**a**) Schematic of Pd^0-mediated conversion of Pro-5FU into 5FU and acetol in isotonic media. (**b**) low resolution mass spec (ESI) analysis of reaction crude following reaction completion – acetol $[M + Na]^+$ (left panel) and 5FU $[M - H]^-$ (right panel). (**c**) Pd^0-mediated depropargylation of 1-propargyl-2-pyridone (21) and 1-propargyl-4-pyridone (23). Pd^0 resins (1 mg / ml) were dispersed into a solution of compounds 21 or 23 (100 µM) in 0.1% (v/v) DMSO in PBS and incubated at 37 °C. After 24 h, TLC showed no traces of starting material and the formation of deprotected compounds 20 and 22.

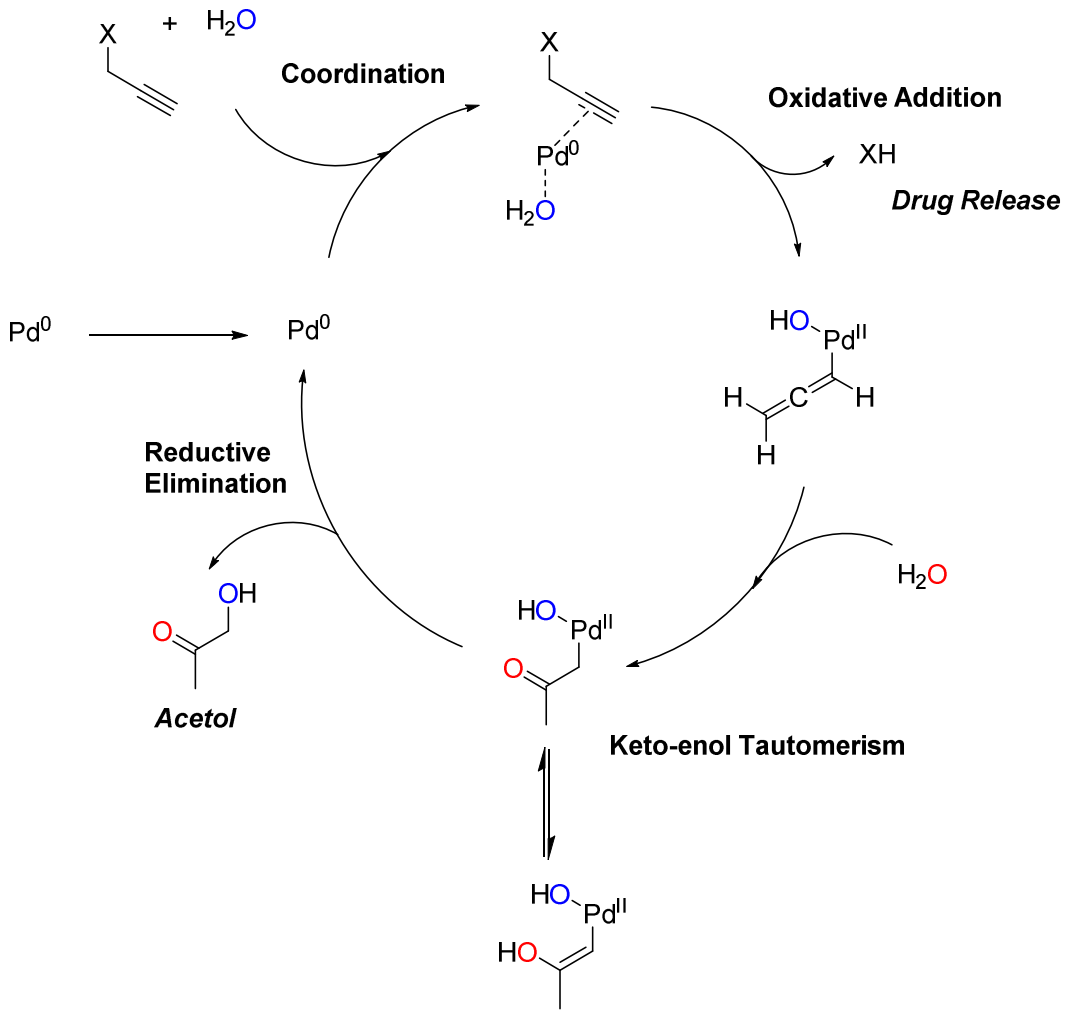

Scheme 5.2. Proposed mechanism for the Pd^0-catalyzed cleavage of O/N-propargyl groups in water. X represents drug.

5.23 Bioorthogonality of Pro-5FU

In the clinic, 5FU is used systemically to treat many different types of cancers including colorectal and pancreatic cancers.[123] For this reason colorectal (HCT116) and pancreatic (BxPC-3) cancer cell lines were chosen for anti-proliferative and mechanism of action analysis. The Pro-5FU was tested *in vitro* in the absence of Pd^0 to determine the degree of bioorthogonality of this 5FU precursor, the second criteria required for BOOM chemistry. Cell viability assay using both cancer cell lines ranging from 10 nM – 1 mM, were carried out using PrestoBlue reagent and analysed by spectrofluorometry. Remarkably, at all concentrations tested in both cell lines, Pro-5FU displayed no cytotoxicity compared to 5FU which had an EC_{50} value of 0.14 and 2 µM (BxPC-3 and HCT116, respectively; Fig. 5.5a, b). By comparison,

Pro-5FU was greater than 500 times less toxic then 5FU proving the effectiveness of the masking strategy at the *N*1 position. The masking strategy was further evaluated in liver HepG2 cells which have a higher metabolic capacity, to further test the structural integrity of Pro-5FU. However, despite hepatocytes' greater metabolic rate, Pro-5FU again displayed no cytotoxic effects whereas 5FU was significantly cytotoxic at low micromolar concentration (EC_{50} – 1.4 μM; Fig. 5.5c). This further illustrated Pro-5FU's resistance to enzymatic cleavage.

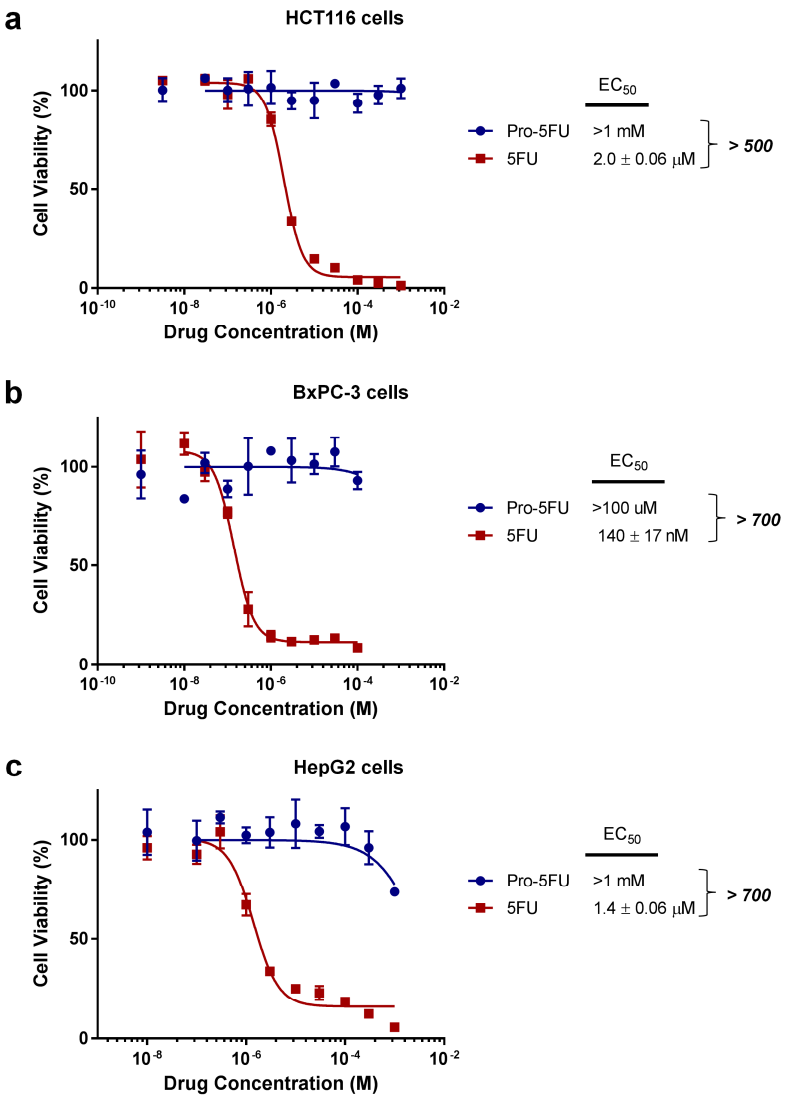

Figure 5.5. Study of Pro-5FU Bioorthogonality. Cytotoxic effect of Pro-5FU in comparison to unmodified **5FU**. Cells were incubated with increasing concentrations of **Pro-5FU** and **5FU** (0.01-1,000 µM) for 5 days and cell viability measured through semi log dose response curves to determine the corresponding EC_{50} values. (**a**) colorectal HCT116 cancer cells. (**b**) pancreatic BxPC-3 cancer cells. (**c**) liver HepG2 cancer cells. Error bars represent ± standard deviation from *n* = 3.

One foreseeable concern based on the structural similarity between 5FU and Pro-5FU was the potential for the prodrug to inhibit 5FU's pharmacological effects through its interaction with the same enzymes responsible for 5FU's activation. However, these concerns were put to rest by testing 5FU in combination with varying concentrations of Pro-5FU. Despite a prodrug/drug ratio of 100:1, Pro-5FU did not inhibit 5FU's antiproliferative capabilities (Fig. 5.6a, b). This indicates that in a continuous dosing regime with Pro-5FU in a patient, Pro-5FU would not eventually

inhibit the deprotected 5FU from exerting its desired cytotoxic effect. Furthermore, the by-product produced from the *N*-depropargylation reaction, acetol, was also non-cytotoxic in both cell lines (Fig. 5.6c, d). This ruled out any potential toxicity caused by the by-product produced from the palladium mediated reaction.

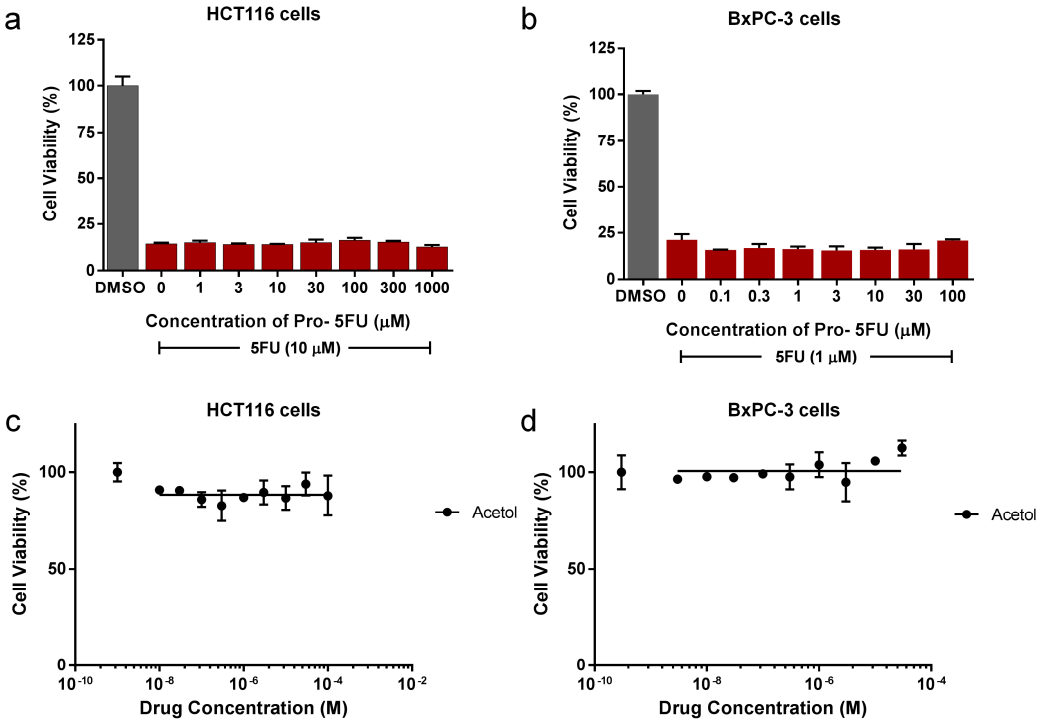

Figure 5.6. Study of pharmacological interactions between 5FU and Pro-5FU and acetol bioorthogonality. (**a, b**) study of Pro-5FU ability to inhibit 5FU at varying concentrations. Cells were incubated with 5FU (10 μM and 1μM for HCT116 and BxPC-3 cells respectively with increasing concentrations of Pro-5FU (0.1 – 1,000 μM), and cell viability determined. (**c, d**) Study of cytotoxic effect of acetol in HCT116 (**c**) and BxPC-3 (**d**) cells. Cells were incubated with increasing concentrations of acetol (0.003 – 100 μM) for 5 days and cell viability measured. Error bars represent ± standard deviation from *n* = 3.

5.24 Biological Conversion Assay with Pd^0 / Pro-5FU Combination

Next, the Pro-5FU/Pd^0 combination was accessed as a BOOM prodrug strategy. First, a preliminary cell screening assay with all 5FU prodrugs with and without Pd^0 resins was carried out. Cell viability analysis demonstrated that only Pro-5FU is sensitive of Pd^0-mediated activation into 5FU and capable of exerting a cytotoxic

effect (Fig. 5.7a, b), confirming the results observed from the non-biological conversion assays.

In order to see the range of Pd^0 required to elicit a comparable antiproliferative response to 5FU, a concentration range of resins either on their own or in combination with Pro-5FU at either 100 or 30 µM concentrations (HCT116 and BxPC-3 cells respectively) was evaluated (Fig. 5.7c, d). Based on the results it was concluded that the concentrations of Pd^0 resins used for the original BOOM activation assay (Fig. 5.7a, b) were still the optimal concentrations to yield comparable antiproliferative effects to unmodified 5FU (1 mg/ml - 266 µM for HCT116 cells and 0.67 mg/ml - 177 µM for BxPC-3 cells).

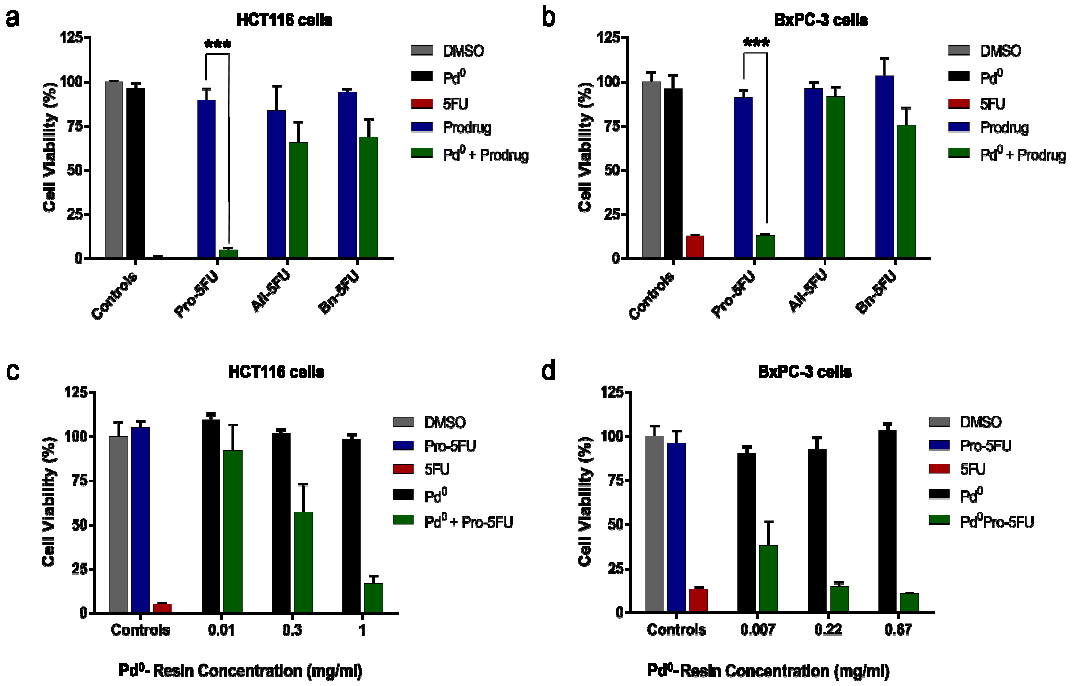

Figure 5.7. Catalytic study of Pd^0 resins and BOOM activation comparison of 5FU prodrugs. (**a, b**) Determination of optimal Pd^0 resins concentration (0.007 – 1 mg / ml) to generate cytotoxic effect of Pro-5FU (100 and 30 µM for HCT116 and BxPC-3 respectively) comparable to unmodified 5FU (100 and 30 µM for HCT116 and BxPC-3 respectively) via Pro-5FU dealkylation. (**c, d**) Preliminary BOOM activation comparative study with 5FU prodrugs. Experiments: 0.1% (v/v) DMSO in media (untreated cell control); 1 or 0.66 mg / mL of Pd^0 resins (negative control, HCT116 and BxPC-3 respectively); prodrug (100 µM for HCT116 cells and 30 µM for BxPC-3 cells - negative control); and Pd^0 resins (1 or 0.66 mg / mL) + prodrug (100 µM for HCT116 cells and 30 µM for BxPC-3 cells - BOOM conversion assay). Following 5 days of treatment, cell viability (PrestoBlue™ assay) was determined and compared to analyse significant effects. *** = $p < 0.001$ (n=3). Error bars represent ± standard deviation from $n = 3$.

The BOOM activation strategy was further assessed comparing the combination to 5FU in a dose response manner (Fig. 5.8a, b). The combination displayed comparative cytotoxic effects to 5FU at all concentrations in both cell lines. At the lower concentrations the difference in toxicity is presumably attributed to the time lapse required for the Pd^0-mediated *N*-depropargylation to take place before the newly-formed deprotected 5FU can elicit a cytotoxic response. This was difficult to achieve to comparable levels at concentrations where 5FU is less responsive. Nonetheless, the combination displayed similar EC_{50} values compared to 5FU (Fig. 5.8c, d). It is worth mentioning that on their own, neither the Pd^0 resins nor Pro-5FU at any concentrations tested exhibited antiproliferative activity, validating the bioorthogonality of this strategy.

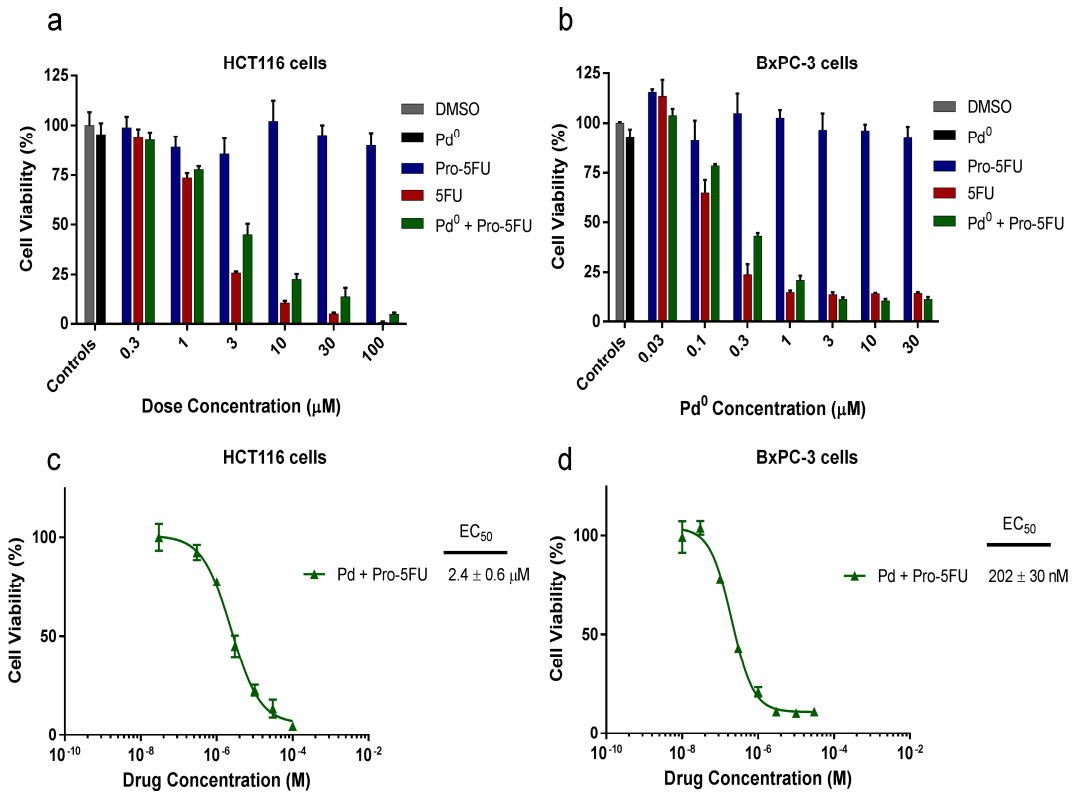

Figure 5.8. BOOM generation of 5FU in cancer cell culture. (**a, b**) Study of BOOM activation in a dose response study of cell viability after 5 days of treatment. Experiments: 0.1% (v/v) dimethylsulphoxide (DMSO, untreated cell control; in grey), Pd^0 resins (negative control; in black); 0.01–100 mM of Pro-5FU (negative controls; in blue); 0.01–100 mM of 5FU (positive controls; in red) and Pd^0 resins + Pro-5FU (bioorthogonal organometallic conversion assay; in green). Cells were incubated with Pd^0 resins (1 mg / mL for HCT116 cells and 0.66 mg / mL for BxPC-3 cells). (**c, d**) Dose response study of Pd^0 resins + Pro-5FU combinations plotted from values obtained from (**a**) and (**b**)

(bioorthogonal organometallic conversion assay; in green) to determine the corresponding EC_{50} values. Error bars represent ± standard deviation from *n* = 3.

5.25 Phenotypic Evaluation of Pd^0 / Pro-5FU Combination

The phenotypic effect from the prodrug / metal combination was monitored in real-time using an IncuCyte ZOOM® (Fig. 5.9a, b). This device automatically quantifies cell growth kinetics through image-based analysis based on cell confluency as a function of time. The negative controls (DMSO, Pd^0 and Pro-5FU) exhibited standard growth curves for both cell lines, while the growth curve from the cells treated with 5FU decreased rapidly after 24 hours of treatment. The growth curve from the combination treatment for the HCT116 cells displayed a 24 hour time lapse before the growth curve fell towards cytotoxic levels comparable to 5FU. This distinct growth curve was not observed for the BxPC-3 cells but instead both curves for the 5FU and combination were nearly identical, indicating that the cytotoxic levels of the drug for this cell line are rapidly generated. As observed in the microscopy images shown in Fig. 5.9c and d, treatment induced changes to cell morphology were the same with the combination and 5FU for both cell lines.

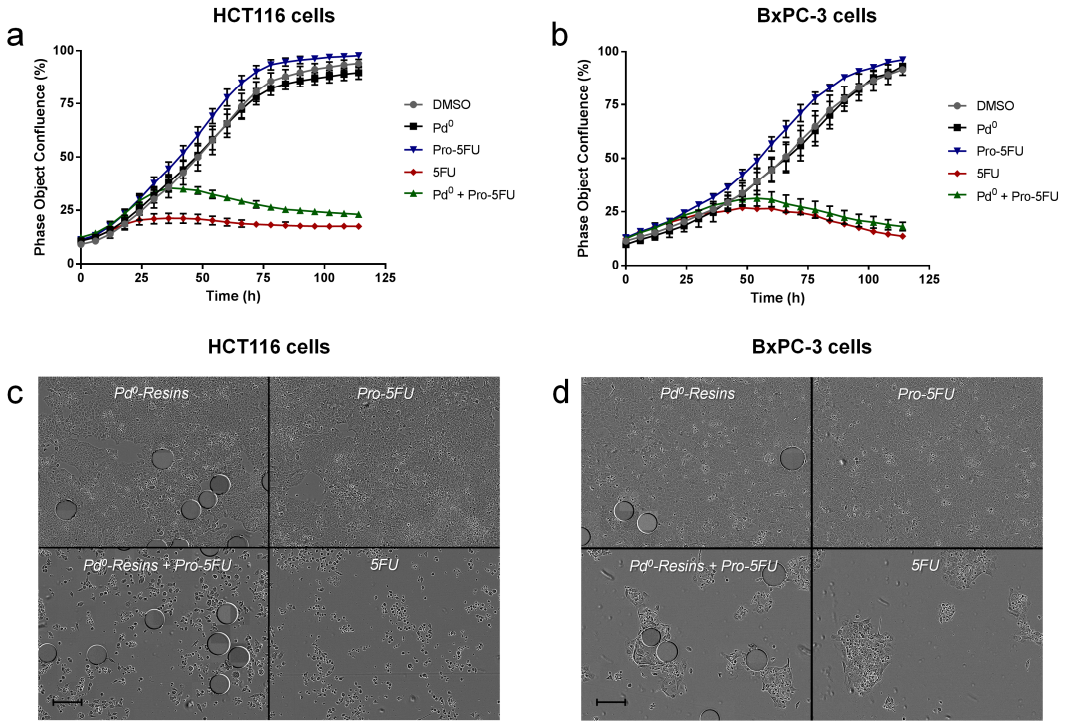

Figure 5.9. Phenotypic effect of BOOM generation of 5FU in cancer cell culture. (**a, b**) Study of real-time cell confluency. Cell population was monitored over 5 days (120 h) using an IncuCyte ZOOM microscope inside an incubator (5% CO_2, 37 °C) treated with either Pro-5FU, Pd^0 resins, 5FU or combination of Pd^0 resins + Pro-5FU. Experiments: 0.1% (v/v) dimethylsulphoxide. Drug/prodrug concentrations: 100 mM, for HCT116 cells, and 30 mM, for BxPC-3 cells. (**c, d**) Phase contrast images of cells after 4 days of treatment (96 h). Scale bar – 150 µM. Pd^0 resins are identified as spheres of an average of 150 µM. Error bars represent ± standard deviation from *n* = 3.

The phenotypic response at the molecular level of total expression and post-translational modifications of cancer relevant pathways were analysed using a Zeptosens Reverse Phase Protein Microarray (RPPA). This high throughput antibody-based protein microarray technique allows the quantitative measurement of protein expression levels in a number of biological samples across dose- and time-series studies.[76,132,133]

As described in section 5.1, one of 5FU's cytotoxic mechanism-of-action is characterized by incorporation of its cytotoxic metabolites into DNA and RNA.[123] Once incorporated, this elicits the DNA damage response signal which subsequently arrests cell cycle progression resulting in apoptosis. The p53 tumour suppressor protein plays a critical role in mediating DNA damage response signaling and apoptosis induction.[134,135] Studies have shown that 5FU treatment induces the p53 response pathway through stabilization and phosphorylation of the protein.[136]

Akt is another biomarker for apoptosis. This serine/threonine protein kinase plays an important role in many cellular pathways most notably apoptosis. It is involved in cellular survival pathways through the inhibition of the apoptotic processes.[137,138]

Using RPPA, to assess multiple pathways (Table 2.1), we were able to identify the post translation modification of total and Ser15-phosphorylated p53 for HCT116 cells (Fig. 5.10a, c) and Ser15-phosphorylated p53 and Ser473-phosphorylated Akt for BxPC-3 cells (Fig. 5.10b, d) treated with 5FU, the Pro-5FU/Pd^0-resin combination and the necessary controls.

As displayed in Fig. 5.10a and c, the levels of total and phosphorylated p53 were greatly increased after 24 hours of exposure to the Pd^0/Pro-5FU combination which is comparable to the DNA damage response elicited by 5FU. The negative controls however, displayed no increase in p53 expression levels. A decrease in phospho-Akt expression was observed after 24 h with the combination, which was again comparable to 5FU activity (Fig. 5.10b, d). A decrease in Akt expression is indicative of cells undergoing apoptosis. All the negative controls maintained high levels of Akt expression.[137,138]

To verify that the protein expression levels generated from the RPPA were accurate and not as a consequence of unspecific primary or secondary Ab binding, the results were validated by Western blotting. This is a widely employed analytical technique used to detect specific proteins using mAbs from in this case, treated cells. As displayed in Figure 5.11, all the affected protein expression levels obtained from the RPPA analysis were corroborated via Western blot. Only the combination and 5FU treated cells expressed increased levels of both total and phosphorylated p53 levels and with the BxPC-3 treated cells, a decrease in phosphor-Akt expression.

Both the RPPA and Western blot results further indicate that the desired product produced from the combination treatment is indeed the desired 5FU product made evident from the analogous phenotypic responses at the molecular level.

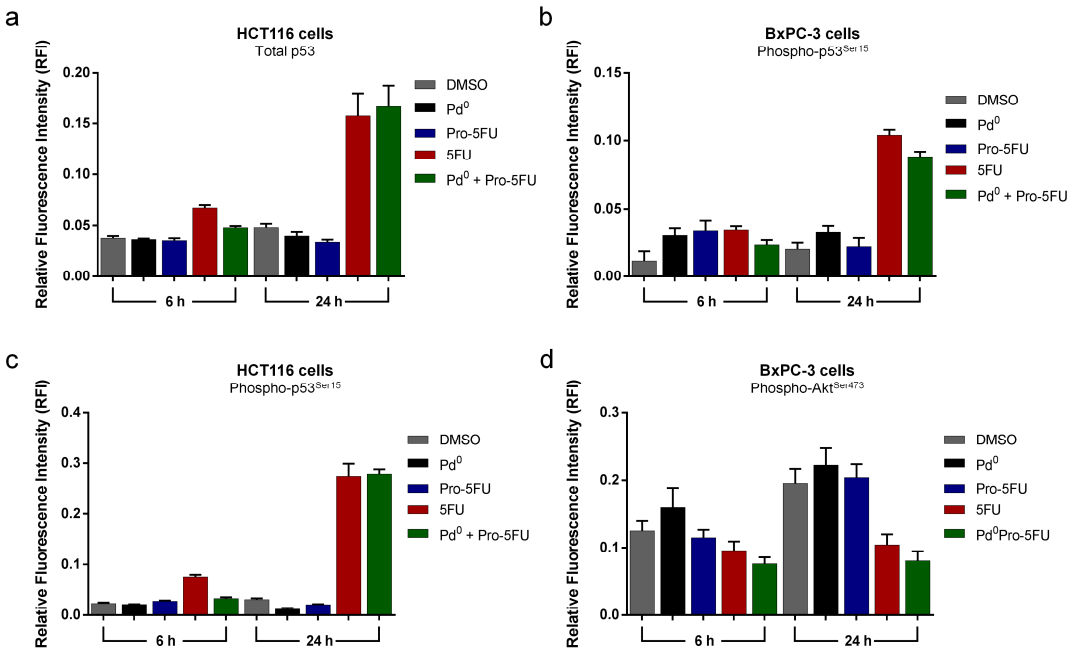

Figure 5.10. Zeptosens Reverse Phase Protein Microarray analysis. Relative abundance of total and phosphorylated p53 levels (HCT116 cells – **a, c**) and phosphorylated p53 and phosphorylated Akt levels (BxPC-3 cells – **b, d**) expressed across DMSO, Pd^0 resins and Pro-5FU treated cells (negative controls), 5FU treated (positive controls) and the combination of Pd^0 resins + Pro-5FU treated cells at 6 and 24 h treatment exposures. Bar graphs represent the median relative fluorescence intensity (RFI) values and standard deviation calculated across a 4-fold protein concentration series extracted from each sample.

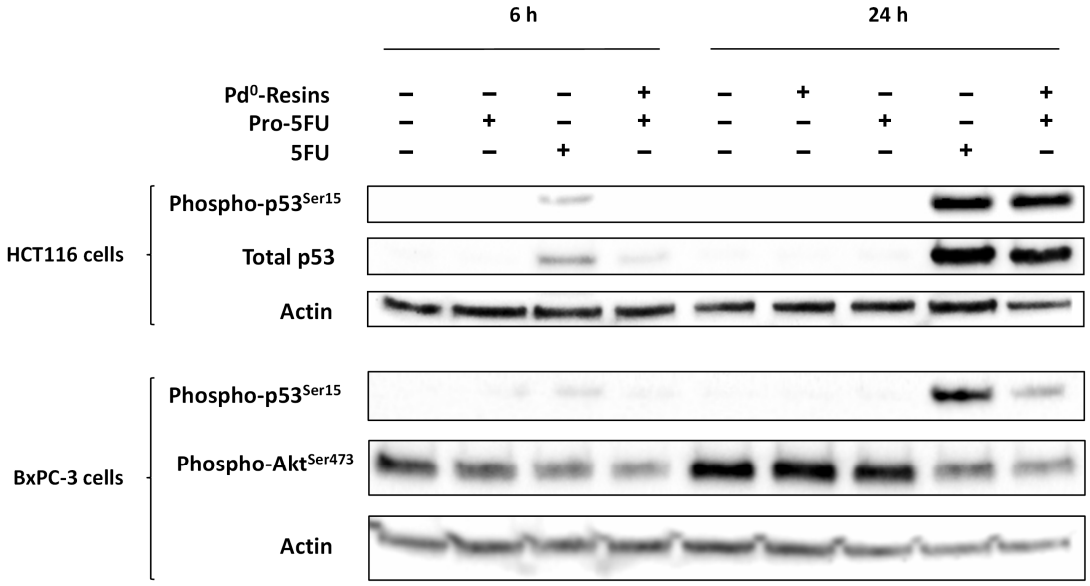

Figure 5.11. Western blot analysis of total p53, phosphorylated p53 and phosphorylated Akt. Relative protein expression within HCT116 and BxPC-3 cells across DMSO, Pd^0 resins and Pro-5FU treated cells (negative controls), 5FU treated (positive controls) and the combination of Pd^0 resins + Pro-5FU treated cells at 6 and 24 h treatment exposures.

5.26 In Vivo Mice Xenograft Assay

The effectiveness of this BOOM prodrug strategy was further assessed using mice xenograft tumour models using the HCT116 colorectal cancer cell line. All mice were implanted with the cell line either on its own or in combination with the Pd resin beads. Either Pro-5FU or 5FU were injected biweekly into the peritoneum. The volume of the tumours and the overall weight of the mice were also recorded biweekly. Unfortunately, once the untreated tumours had exceeded their allowable limit, there was no noticeable reduction of tumour volumes when comparing the mice samples treated with the Pd^0 resin / Pro-5FU combination to the untreated mice. The mice treated with Pd^0 and Pro-5FU separately also had comparable tumour sizes to the untreated mice. The mice treated with 5FU did however show a moderate reduction in tumour volume (Fig. 5.12).

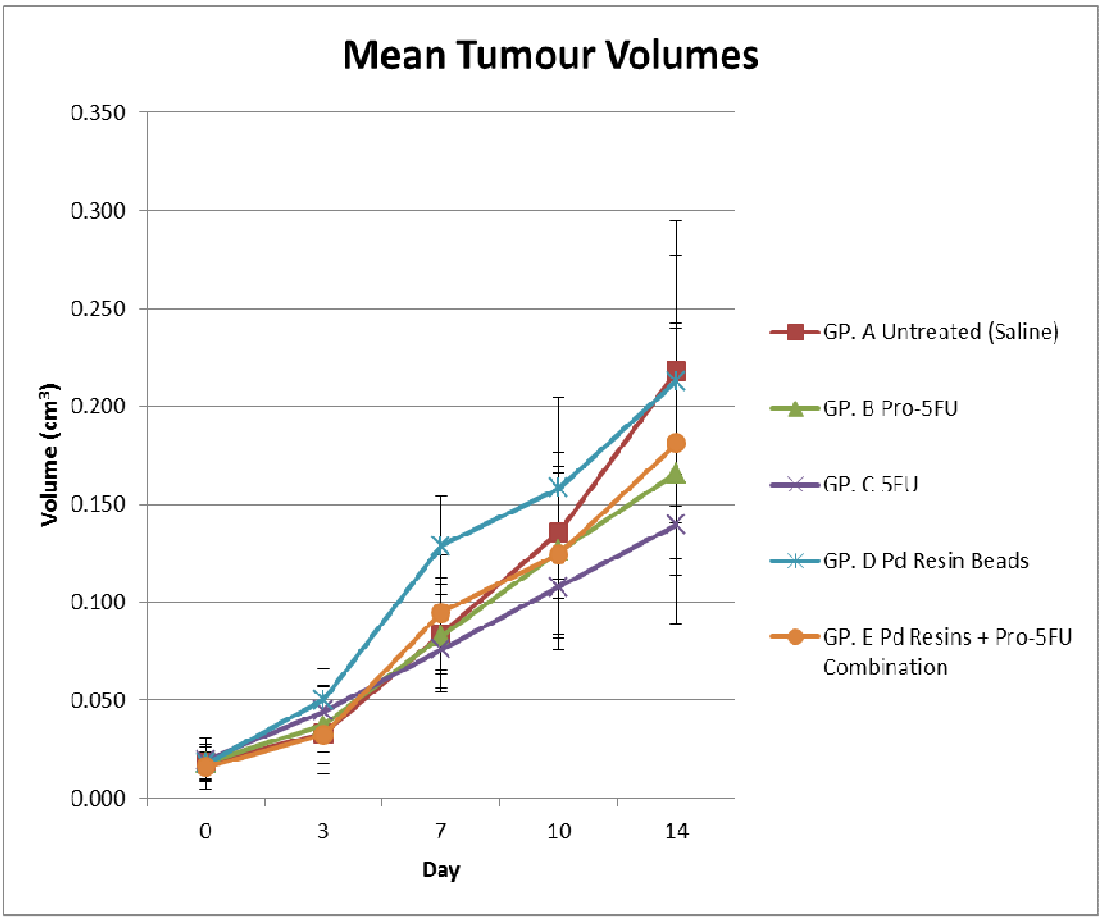

Figure 5.12. Mean Tumour Volume Analysis from HCT116 Xenograft Mice. 5 mice within each group were treated at day 0 with either Pro-5FU prodrug (50 mg/kg); 5FU (50 mg/kg); Pd Resin Beads (0.1 mg/ml per implant) or a combination of Pro-5FU + Pd Resins (same concentrations). Untreated mice were administered saline. Tumour volumes were measured using a calliper. Error bars: ± SD from n = 5.

Due to the available animal license of our collaborators (Prof Brunton and Dr. J Dawson) for performing the xenograft assay with the mice, the Pd^0 resin beads could only be administered at the same time as the HCT116 cells which were administered subcutaneously into both the left and right flanks of the mice. Histological analysis of the tumours cross sections at the conclusion of the assay revealed very little presence of the beads within the tumour. Due to the density of the beads and lack of ability to float in suspension, it was hypothesized that perhaps the beads clumped together at the periphery of the tumour xenograft. A lack of sufficient Pd beads within the tumour mass would not facilitate the activation of the Pro-5FU prodrug in the right place. This is perhaps why there was no decrease in tumour volume from the combination treatment compared to the untreated mice. It is also important to note that the effect mediated by 5FU was very weak.

Going forward, it would be optimal to implant the Pd beads inside the xenograph after the tumours have been allowed to develop for several days. This way there would be a greater chance of adequately distributing the beads throughout the tumour and increasing the likelihood of BOOM activation of the prodrug within the tumour.

Repetition of this *in vivo* assay with the combination treatment will extend to examining total expression and post-translational modifications of cancer relevant pathways such as p53 expression levels within the tumours in conjunction to measuring tumour volumes and growth rates. However, as an initial proof of concept study, the results were unfavourable and it is believed that the method for treating the tumours with Pd^0 resin beads must first be optimized before hope of achieving any therapeutic effect *in vivo* from the combination of Pd^0 resins beads with Pro-5FU.

5.3 CONCLUSIONS

We have discovered a novel BOOM reaction, i.e. palladium-mediated *N*-depropargylation of endocyclic NH groups with lactam/lactim tautomery, the first Pd-catalyzed C-N cleavage able to occur under biocompatible conditions. The application of this novel chemistry allowed for the elimination of 5FU's cytotoxic properties while enabling the palladium-mediated restoration of its cytotoxicity in

cancer cell culture. Based on the mechanism of action of 5FU,[123] the addition of the palladium sensitive chemical moieties at *N*1 proved to be an effective strategy for completely reducing the drugs ability to exert its cytotoxic effect. This demonstrated that the alkyl groups in this type of heterocyclic system are resilient to enzymatic cleavage within a cellular environment. In the presence of Pd^0, the chemical stability of the benzyl moiety within Bn-5FU came as no surprise due to the additional hydrogen source required to complete the reaction. [121] However, a drastic difference between Pro-5FU and All-5FU's sensitivity to Pd^0 was evident in both in the non-biological conversion and *in vitro* assays. Furthermore, the by-product produced from this reaction, acetol, is a natural occurring compound. The inertness displayed by acetol within both cell lines, indicated that any off target effects caused by harmful by-products as a result of the activation process are greatly reduced. This makes for a much more controlled and predictive outcome within the clinic.

The prodrug / metal combination displayed all the attributes required for a successful BOOM activation. Both the Pd^0 resins and Pro-5FU separately were not cytotoxic but when combined displayed similar potency to unmodified 5FU. This was made apparent when comparing the EC_{50} value from the combination to 5FU within both cell lines (5FU - 2.0 μM vs. combination - 2.4 μM for HCT116; 5FU – 140 nM vs. combination - 202 nM for BxPC-3). The difference in cell viability at the lower concentrations is presumably attributed to the time delay for the Pd^0-mediated cleavage of the propargyl moiety to produce 5FU and illicit its cytotoxic response. This is difficult to achieve to comparable levels at concentrations where 5FU is less responsive. This time delay was observed from the time-lapse imaging analysis using the IncuCyte during the treatment of the HCT116 cells. The growth curve from the combination treatment displayed a 24 hour time lag before the growth curve fell towards cytotoxic levels comparable to 5FU. This delay correlates nicely with the time required for the Pd^0 to convert the prodrug to the active drug form as observed from the non-biological HPLC conversion assay. The similarity of growth curves within the BxPC-3 cells can perhaps be attributed to their greater sensitivity to 5FU.

In accordance with the comparable cytotoxicity observed from the combination and 5FU, the immunoassay studies showed analogous cell death induction mechanisms

between the two treatments. This further illustrated that the cytotoxicity observed from the combination treatment was a result of the BOOM synthesis of 5FU *in vitro*.

Although this BOOM prodrug strategy proved to be very successful at creating a more chemically stable and consequently, a more bioorthogonal prodrug compared to the Gemcitabine prodrugs, the 5FU drug itself lacked potency. Therefore a more evolved BOOM prodrug would have the bioorthogonality of Pro-5FU but the potency of Gemcitabine. This type of BOOM prodrug would be the ideal candidate to progress the BOOM strategy into mice models.

The results presented in this chapter have been previously published as Weiss et al. Nat. Commun. 2014. 5, 3277 (reference 63).

CHAPTER 6

N-Alkynyl Derivatives of 5-Fluorouracil

6.1 INTRODUCTION

In chapter 5, a propargylated-5FU derivative was shown to be an effective bioorthogonal Pd-labile prodrug. When in combination with Pd^0 resins in cell culture, its cytotoxic response was comparable to unmodified 5FU at nearly all drug dose concentrations tested.[67] The secondary amine at position 1 (*N*1) is the functional group whereby the sugar moiety is coupled to the drug. This consequently leads to the production of 5FU's cytotoxic nucleotidic metabolites.[123] Based on this mode of action, it was first hypothesized and later proven (using cell based models) that by masking *N*1 with a chemically stable protecting group, one could significantly limit 5FU of any cytotoxic activation. The 5FU prodrug was then switched on through Pd^0-mediated cleavage of the propargylated masking group. Due to unprecedented nature of the *N*-propargylation process, further investigations were warranted to further improve upon the reaction kinetics. We were particularly interested in determining how the presence of substituents in the propargyl moiety would affect the cleavable properties of the masking group. Therefore, several *N*-alkynyl derivatives were used as masking groups and their sensitivity to Pd^0 was tested and ranked.

Another direction pursued to improve the BOOM activation of 5FU was to investigate other functional groups of 5FU. Keeping in mind the criteria required for successful BOOM activation – the BOOM prodrug must be pharmaceutically inactive in the absence of palladium, the masking of the *N*3 position was also investigated. As described in chapter 5, based on the lactam/lactim tautomery of 5FU, both NH groups have unusually low pKa values for a secondary amine (Fig. 5.2).[130] In fact, *N*3 has a lower pKa (7.26) compared to *N*1 (9.05) and it was therefore

believed that coupling the propargly moiety at *N*3 could also improve upon the reaction kinetics of the Pd^0-mediated catalysis. This of course provided it had the same anti-cytotoxic effects.

In summary, this chapter investigates the development and use of additional *N*-alkynyl derivatives to test their sensitivity to Pd^0 catalysis under biocompatible conditions. In addition, the comparison of *N*1 vs. *N*3-propargyl 5FU derivatives against biocompatibility and Pd^0 susceptibility has been carried out.

6.2 RESULTS

6.2.1 Synthesis of Alkynyl-modified 5FU Derivatives

Pro-5FU (**18**) was synthesized as previously described in chapter 5 and used as a positive control. Compounds **24, 25, 26** and **27** were synthesized in one step by reacting 5FU with the corresponding alkyl bromide in the presence of DBU using dry MeCN as the solvent (Scheme 6.1). The synthesis of the *N3*-functionalized propargyl derivative (**30**) was carried out in 3 steps. First a ^{t}Boc protecting group was coupled to *N*1 of 5FU in the presence of a catalytic amount of DMAP using a 2:1 mixture of MeCN and DMF. The resulting product was treated with propargyl bromide solution in the presence of DBU using dry DCM as the solvent. This was followed by the removal of the Boc protecting group in the presence of K_2CO_3 using MeOH as the solvent (Scheme 6.2). Compound **31** was synthesized by reacting 5FU with propargyl bromide solution in the presence of DBU using dry DMF as the solvent (Scheme 6.2).

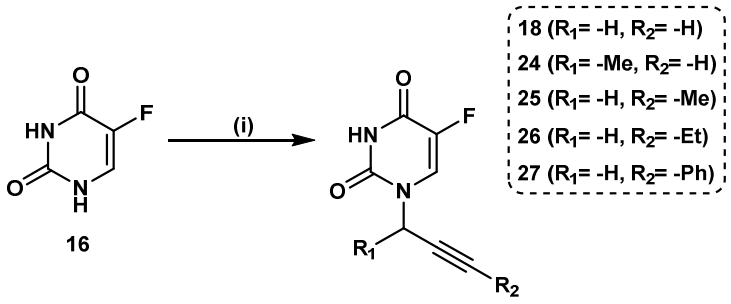

Scheme 6.1. Synthesis of *N1*-functionalized 5FU alkynyl derivatives. Reagents and conditions: (i) DBU (1 equiv.), dry MeCN, alkyl bromide (1 equiv.), 4 °C, then RT overnight (35-54%).

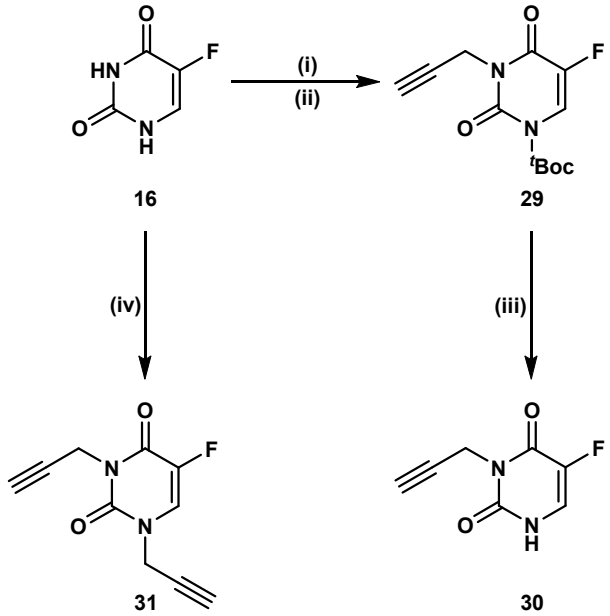

Scheme 6.2. Synthesis of 5-fluoro-3-propargyluracil and 1,3-dipropargyl-5-fluorouracil. Reagents and conditions: (i) ^{t}Boc (1.5 equiv.), MeCN:DMF (2:1 equiv.), DMAP (0.2 equiv), RT overnight (40%). (ii) propargyl bromide (1.2 equiv.), dry DCM, DBU (1.5 equiv.), RT 4 h (67%). (iii) K_2CO_3 (0.5 equiv.), MeOH, RT 3 h (71%). (iv) propargyl bromide (2.1 equiv.), dry DMF, DBU (3 equiv.), 4 °C, then RT overnight (86%).

6.2.2 Pd^0-lability of 5FU Alkynyl Derivatives

A quick and simple method to assess and quantify the alkynyl derivatives sensitivity to Pd^0-mediated catalysis is by incubating the derivatives with the Pd^0 resins under biocompatible conditions described in previous chapters (Scheme 6.3). Using the same methodology (1 mg of Pd^0 resins, 100 μM of prodrug together in 1 ml of PBS shaken at 37 °C), the amount of 5FU produced from **24, 25, 26** and **27** via the Pd^0-

mediated reaction after 24 h was analysed (by HPLC) and compared to the well-established Pro-5FU prodrug (**18**). As expected and previously reported, **18** was completely converted to 5FU within 24 h. However, compound **24, 25, 26** and **27** generated considerably lower levels of 5FU within the same time span (Table 6.1). **24** (methyl group at R_1) had the second best conversion rate with 26% conversion to 5FU after 24 h. For compounds **25, 26** and **27** (containing methyl, ethyl and benzyl groups at position R_2), their conversion to 5FU was inversely proportional to the size of the moiety within the terminal carbon of the triple bond. These results strongly indicate that the limiting factor for the reaction kinetics is largely dependent on steric constraints, hindering Pd^0 coordination with the triple bond. This would then suggest that the non-substituted propargyl moiety is the optimal choice to generate bioorthogonal compounds that have the greatest reaction kinetics to Pd^0 catalysis.

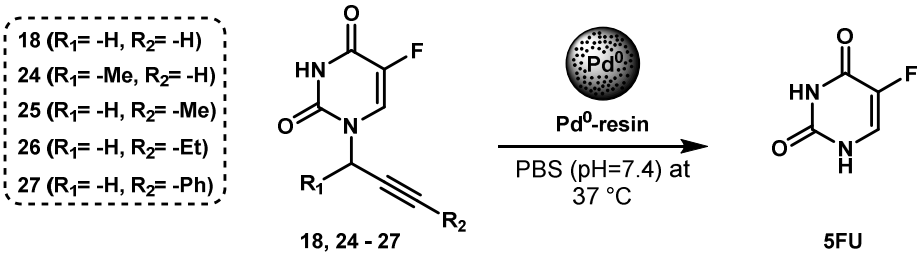

Scheme 6.3. Non-biological conversion assay with 5FU alkynyl precursors. Reagents and conditions: alkynyl derivatives (100 µM), Pd^0 resins (1 mg), PBS, 37 °C, 1200 rpm, 24 h (100 – 4%).

Table 6.1. Percentages of conversion of 5FU alkynyl precursors mediated by Pd^0 catalysis. Relative values calculated from integrated chromatographic peak values.

5FU Precursor	Product	Yield (%)
18	5FU	100
24	5FU	26
25	5FU	12
26	5FU	10
27	5FU	4
30	5FU	85
31	5FU	43 (**30**) and 26 (5FU)

6.2.3 Pd^0-lability of N3- vs. N1-propargyl 5FU Prodrugs

Once the optimal propargyl moiety for Pd^0-lability was established, the optimal position within the 5FU molecule to obtain a bioorthogonal palladium-labile prodrug

was further analysed. As explained in chapter 5, the tautomerism of 5FU causes the two NH groups within the molecule to possess relatively low p*K*a values than would normally be expected for more basic amines.[130] Specifically, the *N*3 position has a lower p*K*a value than the *N*1 position and therefore, it was hypothesized that this lower value would have a positive effect in its properties as a better leaving group. To aid in this investigation, not only was **30** synthesized and tested but also **31** (*bis*-propargylated 5FU precursor). Using the same methodology for the non-biological conversion assay, the yield of 5FU from the precursors was again obtained (Table 6.1). Contrary to our hypothesis, **30** underwent depropargylation at a slower rate (85% conversion) after 24 h (Fig. 6.1, middle panel). The 24 h reaction with **31** resulted in the generation of 5FU (26%) and **30** (43%) (Fig. 6.1, right panel). This 43% production of **30** confirmed that the dealkylation of the propargyl group proceeds faster at *N*1 than *N*3. This suggested that perhaps the presence of the two oxo groups on either side of the *N*3 position limited the Pd^0/triple bond interaction, reinforcing the relevance of steric and conformational effects on this reaction's kinetics.

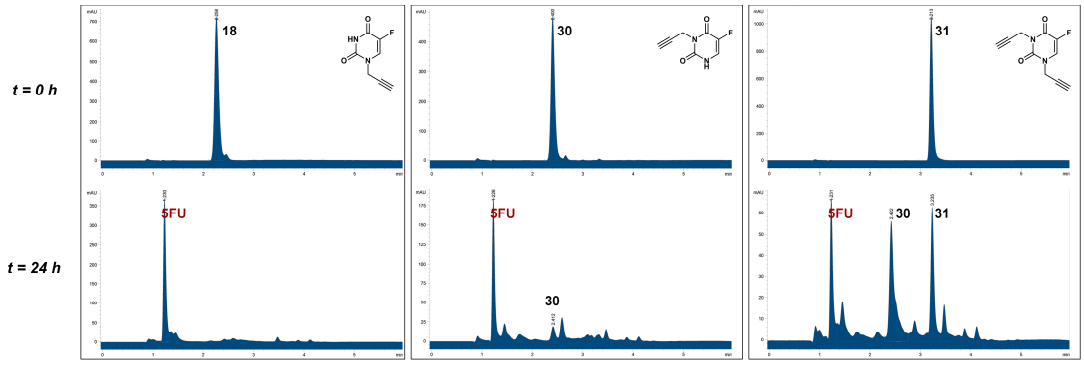

Figure 6.1. Non-biological conversion assay of compounds 18, 30 and 31. HPLC traces of Pd^0-mediated conversion of 18 (left panel), 30 (middle panel) and 31 (right panel) into 5FU. HPLC traces of reaction crude were analysed using an UV detector (280 nm) at t = 0 h (top panels) and t = 24 h (bottom panels).

6.2.4 Pd^0-lability of N3- vs. N1-propargyl 5FU Prodrugs at Varying pH

Since the BOOM treatment regime strategy is intended for the treatment of locally advanced tumors which would normally be unresectable, logically it made sense to

test the *N*-depropargylation reaction of both *N*1 and *N*3 at the pH expected to be found in those tumours. Due to hypoxic regions and glucose deprivation within solid tumours, the extracellular pH levels are estimated in the order of 0.5 units lower compared to normal healthy tissues.[139,140 141] Therefore, *N*-depropargylation reactions were performed as described above at a pH range of 6.5, 7.0 and 7.5. The reactions were monitored by HPLC at 6 and 24 h. Interestingly, the pH had a noticeable effect on the reaction rates, most notably after short incubation periods with the Pd^0 resins (Table 6.2). Despite complete conversion of prodrug **18** at all pH ranges, within 6 h, the reaction kinetics were more favourable at the more basic pH range (7.5). This same trend was observed for prodrug **30**. However, despite the varied conversion rates at the varying pH ranges, this study demonstrates that the *N*-depropargylation reaction required to activate 5FU is compatible within the extracellular space of solid tumours.

Table 6.2. Percent conversion of 5FU alkynyl precursors mediated by Pd^0 catalysis in varying pH ranges. Relative values calculated from integrated chromatographic peak values.

	t = **6 h**			t = **24 h**		
Prodrug	**pH=6.5**	**pH=7.0**	**pH=7.5**	**pH=6.5**	**pH=7.0**	**pH=7.5**
18	28.9%	33.7%	44.4%	100%	100%	100%
30	21.3%	33.4%	39.1%	75.6%	76.9%	80.6%

6.2.5 Bioorthogonality of N3- vs. N1-propargyl 5FU Prodrugs

The strategy to inhibit 5FU's cytotoxicity by masking either or both NH groups within 5FU was evaluated using dose response viability studies with HCT116 colorectal cancer cells. As displayed in Figure 6.2a, none of the propargylated 5FU prodrugs (**18, 30** and **31**) exhibited any antiproliferative activity at any concentrations tested. This confirmed that masking either functional group renders 5FU derivatives pharmaceutically inactive.

6.2.6 Pd^0-mediated activation of N3- vs. N1-propargyl 5FU prodrugs in vitro

The rate of activation of compounds **18, 30** and **31** was further evaluated in cancer cell culture using an IncuCyte ZOOM device by incubating HCT116 cells with the prodrugs either in the presence or absence of the Pd^0 resins, as described in the previous two chapters (Fig. 6.2b). To obtain maximum differentiation among all prodrugs tested, the cells were seeded at a density that would allow them to reach maximum confluency within 5 days (the end point of the assay). As expected based on the previous results displayed above, Pd^0 resin combination with **18** displayed the greatest sensitivity to BOOM heterocatalysis as made evident by the significantly smaller bell shaped curve and overall comparable cytotoxicity to 5FU. Although the combination with **30** still inhibited cell growth by more than 50%, it appeared to lack the depropargylation kinetics required to compete with prodrug **18**. Prodrug **31**, due to the presence of two propargyl moieties, obtained a poor cytotoxic effect with an overall 65% cell confluency measurement after 5 days. These results were confirmed by phase contrast images obtained from the IncuCyte ZOOM (Fig. 6.2c), which displayed combination with **18** having a similar cytotoxic effect to 5FU, whereas combinations with **30** and **31** had significantly lower cytotoxic effects.

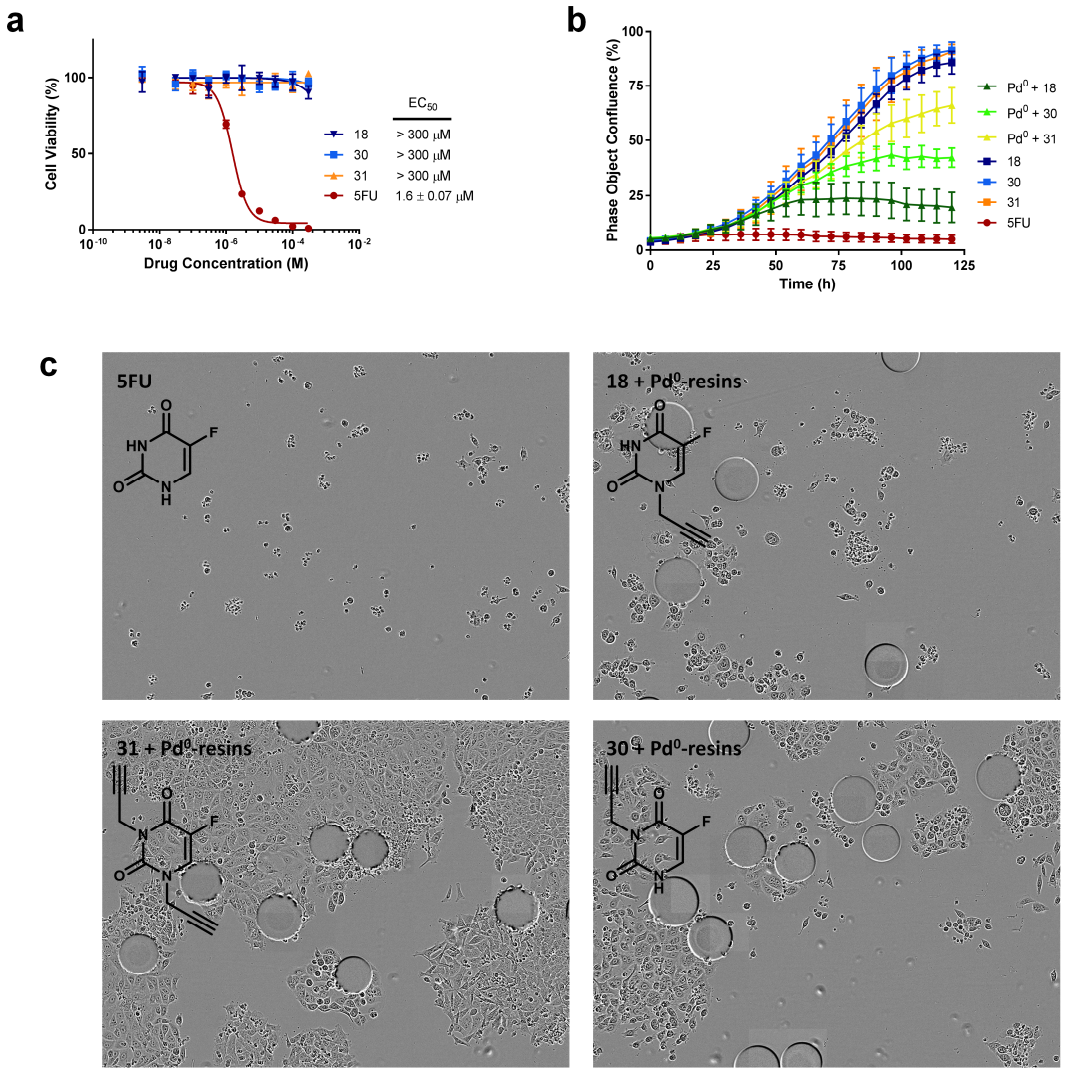

Figure 6.2. *N*3- vs. *N*1-propargyl 5FU prodrug comparison of bioorthogonality and Pd^0-mediated cytotoxicity. (**a**) Study of prodrugs' bioorthogonality. Semi Log dose response curves and calculated EC50 values of prodrugs 18, 30 and 31 in comparison to unmodified 5FU in HCT116 cells. Cell viability was measured at day 5 using PrestoBlue cell viability reagent. (**b**) Bioorthogonally-activated cytotoxic effect in HCT116 cells: time lapse cell confluence study. The cell population was monitored for 5 days using an IncuCyte ZOOM system in an incubator (5% CO_2 and 37 °C). Drug/prodrug concentration: 100 µM; Pd^0 resins concentration: 0.67 mg/mL. (**c**) Phase contrast images of cells after 5 days of treatment with: 100 µM of 5FU (top left); 0.67 mg/mL Pd^0 resins + 100 µM of 31 (bottom left); 0.67 mg/mL Pd^0 resins + 100 µM of 18 (top right); 0.67 mg/mL Pd^0 resins + 100 µM of 30 (bottom right). Pd^0 resins are identified as spheres of 150 µm (average diameter). Error bars: ± SD from *n* = 3.

The Pd^0-mediated activation of prodrugs **18** and **30** were further exemplified in a dose response manner using a range of human cancer cell types – colorectal HCT116 cancer cells, pancreatic BxPC-3 cancer cells, ovarian carcinoma PE04 cancer cells, ER overexpressing MCF-7 breast cancer cells and HER2 overexpressing R-SKBR3a breast cancer cells with induced resistance to AZD8931 (Fig. 6.3).[142] Again, cells

were seeded to obtain maximum cell confluency within 5 days and to augment the cytotoxic effect of 5FU treatment to more effectively discriminate the rate of prodrug activation. In accordance with previous observations, although prodrug **18** and **30** in the absence of Pd^0 were bioorthogonal at all concentrations tested, in the presence of Pd^0, prodrug **18** further epitomised its greater sensitivity to Pd^0 activation. This was evident in all cell lines tested where prodrug **18** was the more cytotoxic compound. In pancreatic cells, however, the similarity in cytotoxicity produced between **18** and **30** in combination was presumably attributed to the increased sensitivity of the BxPC-3 cell line to 5FU (Fig. 6.3b). BxPC-3's heightened 5FU sensitivity therefore required less 5FU generation from the prodrug/Pd^0 combination in order to elicit a significant antiproliferative response. The opposite trend is observed within cell lines that are less sensitive to 5FU, i.e. HCT116 and MCF-7 cells (Fig. 6.3a and c respectively). The difference in the activation rates between both combinations was clearly evident with prodrug **30** displaying less cytotoxicity.

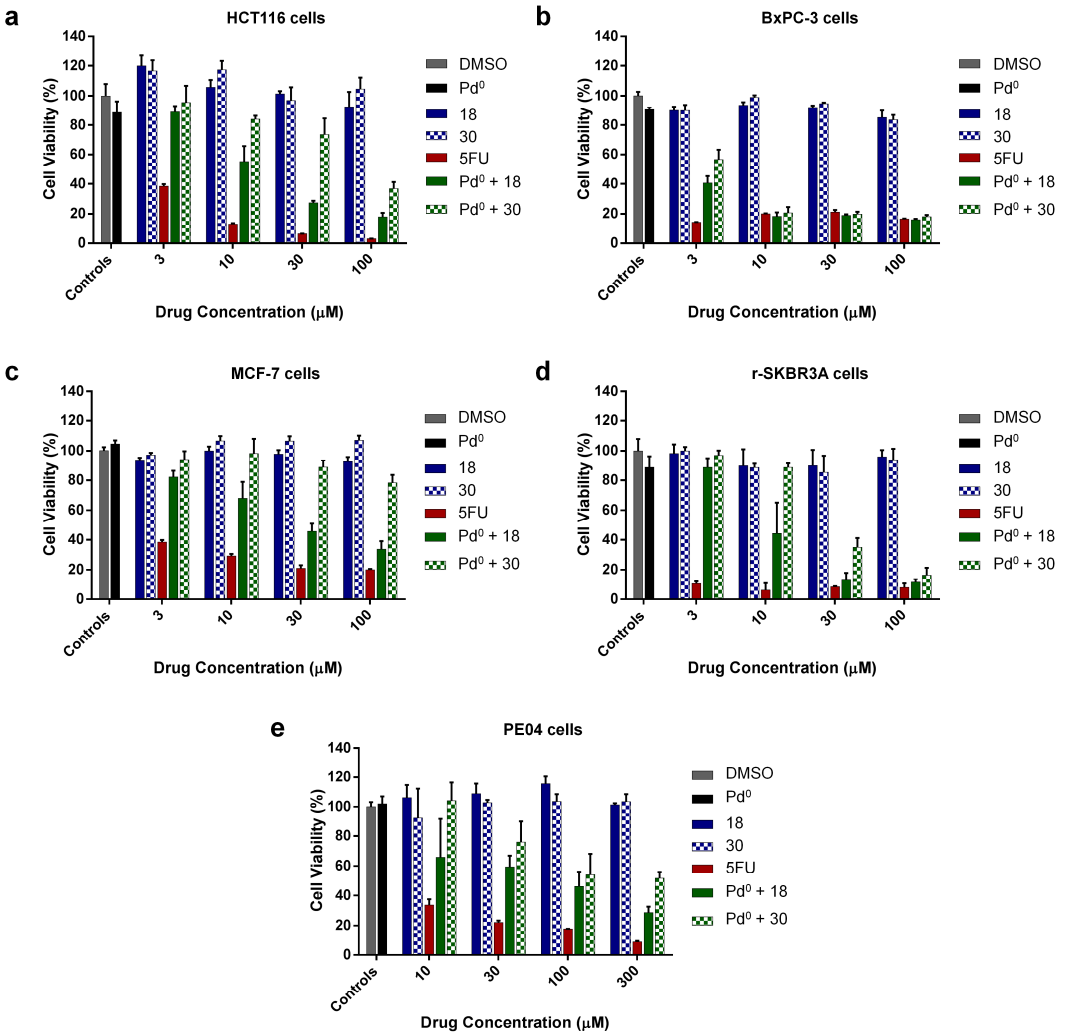

Figure 6.3. Boom activation comparison of prodrugs 18 and 30 in various cancer cells. Cytotoxic effect of bioorthogonally activated prodrug 18 and 30 comparison in a dose response manner in (**a**) HCT116 and (**b**) BxPC-3 (**c**) MCF-7 (**d**) r-SKBR3A and (**e**) PE04 cancer cells. Experiments: 0.1% (v/v) DMSO (untreated cell control, gray); 0.67 mg/mL Pd^0 resins (negative control, black); 5FU (positive control, red); prodrug 18 and 30 (negative control, blue); and 0.67 mg/mL of Pd^0 resins + prodrug 18 and 30 (BOOM activation, green). Error bars: ± SD from *n* = 3.

6.3 CONCLUSIONS

In an attempt to improve the reaction kinetics of prodrug **18**, a set of 2-alkyn-1-yl (containing a triple bond in position 2 relative to the point of connection to 5FU) prodrug derivatives were synthesized and investigated. In addition, the comparison of alkylating *N*3 vs. *N*1 with a propargyl moiety in terms of bioorthogonality and reaction kinetics was also investigated. Despite the production of 5FU from the non-biological Pd^0-mediated conversion assays with the prodrug derivative library, it was

evident that the size of the moiety at the terminal carbon of the triple bond inversely affects the rate of activation; meaning, that the more the Pd^0/triple bond interaction is hindered the slower the BOOM reaction occurs. This suggests that the reaction kinetics is largely dependent on the accessibility of the catalyst to the triple bond.

Once the propargyl moiety was established as the more Pd-labile masking group, its position with regards to masking the functional groups of 5FU was investigated. Despite the lower pKa value of *N*3 in comparison to *N*1, the reaction kinetics of the Pd^0-mediated cleavage proceeded faster at *N*1. This was evident both in the non-biological conversion assay and the various *in vitro* assays. Not only was the yield of 5FU greater after 24 h of incubation with Pd^0 resins with prodrug **18** than with **30** under biological conditions but also prodrug **31** (*bis*-propargylated 5FU precursor) after 24 h generated prodrug **30** and 5FU as the resulting products. This indicated that the propargyl group at *N*1 was the first to be cleaved. Varying the pH range slightly affected the rate of reaction for both compounds. The more basic the pH, the faster the *N*-depropargylation reaction proceeded.

The masking of both 5FU functional groups successfully resulted in complete biocompatibility; however, again it was prodrug **18** in combination with the Pd source which consistently had the more comparable cytotoxicity to unmodified 5FU in all cell types tested.

In conclusion, to date, the propagylation at position *N*1 of 5FU is the best strategy for this type of BOOM activation. This study strongly suggests that the key limiting factors for Pd^0-labile prodrugs to be successfully introduced into the clinic is the rate of activation and the potency of the cytotoxic drug. In order to achieve antiproliferative effects equal to the unmodified drug in a sustained and effective manner, either the rate of activation has to be superior to the rate of cancer cell proliferation or the resulting drug is cytotoxic enough that despite the slower reaction kinetics, the activated drug is still capable of killing the cancer cell.

The results presented in this chapter have been previously published as Weiss et al. Front. Chem., 2014. 2, 56. (reference 65).

CHAPTER 7

Pd-Labile Floxuridine Prodrug

7.1 INTRODUCTION

In chapters 4 and 5, the synthesis and application of two BOOM activated prodrugs were described. The first was the *N*-propargyloxycarbonyl Gemcitabine (*N*-Poc-gem, Fig. 7.1a).[68] This prodrug underwent rapid carbamate cleavage in the presence of the Pd^0 functionalized resin beads, via Pd^0 catalysis. This resulted in the rapid and efficient generation of the potent Gemcitabine anticancer drug, which had an EC_{50} value in the low nanomolar range with treated BxPC-3 cells. However, it was the use of the *N*-propargyloxycarbonyl masking group which limited the prodrug's applicability. The masking group lacked biochemical stability and as a result was only ≈ 23 fold less cytotoxic relative to the parental drug. This insufficient dissimilarity would represent a significant limitation for *in vivo* use, since it would fail to fulfil one of the important aspects of the BOOM therapeutic treatment regime which is to enable an increment of the local concentration of a therapeutic substance within a target tissue while minimizing systemic presence. Nevertheless, *N*-Poc-gem was an excellent proof of concept drug but warranted investigating a more biochemically stable promoiety.

The second described BOOM prodrug was 5-fluoro-1-propargyluracil (Pro-5FU, Fig. 7.1a).[67,69] It was a drastic improvement to the former *N*-Poc-gem, with remarkable biochemical stability (>500 fold less cytotoxic than the 5FU). The propargyl promoiety was not only highly resilient to enzymatic cleavage but also displayed high Pd-lability. Both of these features are ideal characteristics for implementing BOOM therapy. However, because 5FU is a cytotoxic nucleobase of relatively low antiproliferative potency (EC_{50} value in the high nanomolar range within BxPC-3

cells), clinically speaking, the dosing concentrations required to induce a therapeutic response could become a limiting factor.

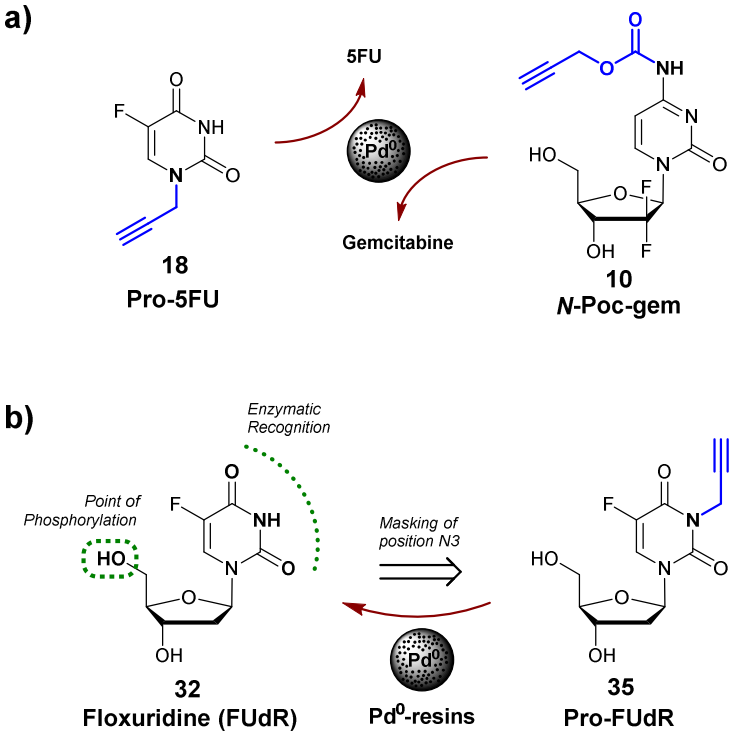

Figure 7.1. Palladium labile prodrugs. (**a**) Palladium labile prodrugs of 5FU and Gemcitabine (Pro-5FU and *N*-Poc-gem, respectively) described in chapters 5 and 4. **(b)** FUdR, (**32**), and the proposed palladium-labile prodrug Pro-FUdR (**35**). Reprinted and adapted with permission from reference,[70] copyright (2015), Nature Publishing Group.

Therefore a BOOM prodrug with potent antiproliferative potential similar to Gemcitabine but with the bioorthogonality of Pro-5FU was sought-after. Due to the superior bioorthogonal properties of *N*-alkyl promoieties and their high sensitivity to Pd^0-mediated cleavage coupled to an endocyclic nitrogen within a heterocyclic group,[67,69] naturally, this promoiety was the obvious choice to investigate drugs of higher structural complexity like nucleoside analogues which are generally more cytotoxic compared to nucleobases.[143-145] Based on its structural similarity to 5FU, i.e. it contains a endocyclic nitrogen capable of being masked with a propargyl promoiety, and its demonstrated superior cytotoxic properties both *in vitro* and *in vivo*,[143,144] the clinically used anticancer drug floxuridine (FUdR, **32**, Fig. 7.1b) was nominated as the BOOM prodrug to be developed and investigated with the potential to possess all the important prodrug characteristics required for BOOM technology.

FUdR is classed as an antimetabolite. It is one of the metabolites generated by 5FU. Its mechanism of action is mediated by the transformation of FUdR into its monophosphorylated and triphosphorylated state. The monophosphorylated-FUdR inhibits thymidylate synthetase (TS).[145,146] This causes a decrease in overall thymidine nucleosides which impedes DNA synthesis. Triphosphorylated-FUdR when incorporated into DNA also results in the disruption of DNA synthesis and cytotoxicity.[145,146] Whereas 5FU is more readily incorporated into RNA[147], FUdR is predominately incorporated into DNA[148], which could account for one of the reasons for the comparative difference in cytotoxicity between the two antimetabolites.

FUdR is commonly administered to patients suffering from advance colorectal, stomach and kidney cancer. FUdR is also favoured for hepatic arterial infusion (HAI) therapy used to treat patients in which the primary gastrointestinal tumour has metastasized to the liver where surgery is not an option.[146] HAI is a medical procedure which delivers chemotherapy from a pump through a catheter which is connected directly to the hepatic artery which leads directly to the liver. FUdR is favoured for this treatment option due to its steep dose response curves and high liver extraction.[149] Systemic treatment of FUdR is however limited by several severe side effects which include dose limiting toxicities upon diarrhea[150] and neutropenia.[151]

Due to FUdR's poor toxicity profile, several FUdR prodrugs have been developed to increase the drug's selectivity. One in particular has been designed with a phosphoramidate promoiety bound to the primary OH group of FUdR (point of phosphorylation, Fig. 7.1b) which undergoes intercellular activation.[152] A lot of work by Nishimoto, Tanabe and co-workers over that last several years have intensively investigated a range of FUdR prodrugs with promoieties bound to the *N*3 position which are predominately activated under hypoxic radiation conditions.[153-156] This class of prodrug are designed for selective activation within hypoxic regions of tumours in combination with electromagnetic radiation. Such promoieties used for this class of prodrug include 2-oxoalkyl groups,[153] an indolequinone group,[154] azide methyl groups[155] and oxo-linkers which upon irradiation releases two FUdR molecules.[156] However, the majority of these hypoxic irradiated activated FUdR prodrugs are either insufficiently activated to cause antiproliferative effects

comparable to the parental drug or the prodrug in the absence of the activating device is only moderately less cytotoxic than unmodified FUdR. Therefore, there is still an unmet medical need for FUdR prodrugs with improved pharmacokinetics and targeted potency.

The importance to treat hypoxic tumours is undeniable. When a tumour develops hypoxic regions, these types of tumours tend to be in the latter stages of development and express a strong malignant phenotype.[157,158] Hypoxic tumours contain low levels of O_2. These types of tumours are particularly difficult to treat for a number of reasons. Radiotherapy is predominately ineffective because since there are low levels of O_2, consequently there are low levels of reactive oxygen species produced from the radiation, the primary source for killing cancer cells.[159] Hypoxic tumours are resistant to many anticancer drugs because of their distance from blood vessels, the primary delivery system of most chemotherapeutics.[158] Hypoxic tumours have decreased cellular proliferation, the primary target of most chemotherapeutics[160] and they have been shown to upregulate genes involved in drug resistance.[158,161] Several different treatment options have been investigated to treat hypoxic tumours which include hypoxic prodrugs which become activated within this unique reductive environment.[162,163]

Herein, this chapter describes the synthesis and application of our most bioorthogonal and potent BOOM prodrug to date, Pro-FUdR (**35**, Fig. 7.1b). The prodrug's activation in the presence of the functionalized Pd^0 resins was investigated *in vitro* under different cancer-like environs.

7.2 RESULTS

7.2.1 Synthesis of Pro-FUdR

Pro-FUdR (**35**) was synthesized in 3 steps from FUdR (**32**). First, in the presence of imidazole, TBS-Cl protected the hydroxyl groups of FUdR at positions 3' and 5', which yielded the bis-silylated precursor (**33**). Second, *N*-alkylation at position *N*3 using propargyl bromide in the presence of DBU afforded intermediate **34**. Without

purification, this was followed by the immediate last step, desilylation of **34** with TBAF solution in THF, yielding Pro-FUDR (**35**) in an overall moderate yield (Scheme 7.1).

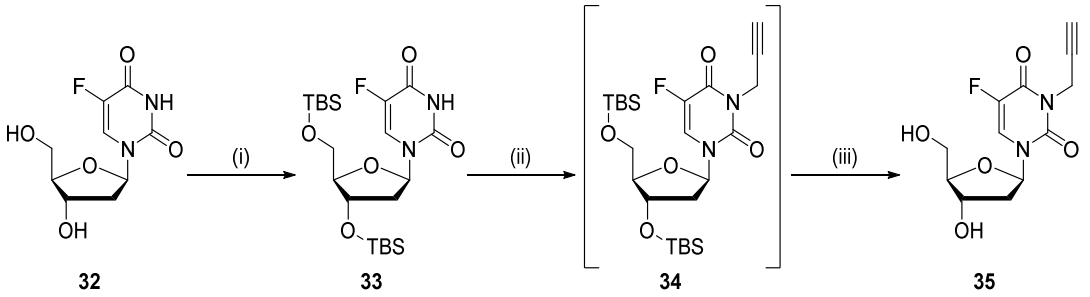

Scheme 7.1. Synthesis of Pro-FUdR. Reagents and conditions: (i) TBS-Cl (3.5 equiv.), imidazole (7.3 equiv.), DMF at RT for 2 h (95%); (ii) DBU (3.5 equiv.), DMF, addition of propargyl bromide solution (3.0 equiv.) at RT for 30 min; (iii) TBAF solution (2.5 equiv.), THF at RT for 1 h (58 %).

7.2.2 Evaluation of the Efficacy of the Deactivation Strategy of Pro-FUdR

Based on the successful masking strategy of both 1 and 3-propargyl-5-fluorouracil (chapter 6),[67,69] it was hypothesised that propargylation at the *N*3 position of FUdR would have a similar effect in terms of biochemical stability, bioorthogonality and susceptibility to Pd^0 catalysed depropargylation. This hypothesis was tested in cell culture by performing dose response assays with Pro-FUdR and FUdR in two human cancer cell lines: the clinically relevant colorectal HCT116 and the pancreatic BxPC-3 cell line. BxPC-3 was chosen because this cell line has been consistently tested in all previous chapters for both the Gemcitabine and 5FU prodrugs and therefore the efficiency and reaction kinetics of all Pd-labile BOOM prodrugs could be accurately compared from this cell line. As displayed in Fig. 7.2, Pro-FUdR's cytotoxicity was vastly reduced relative to the parental FUdR. The difference in antiproliferative activity between the two (EC_{50}-Pro-FUdR / EC_{50}-FUdR) was ≈ 6,250 fold.

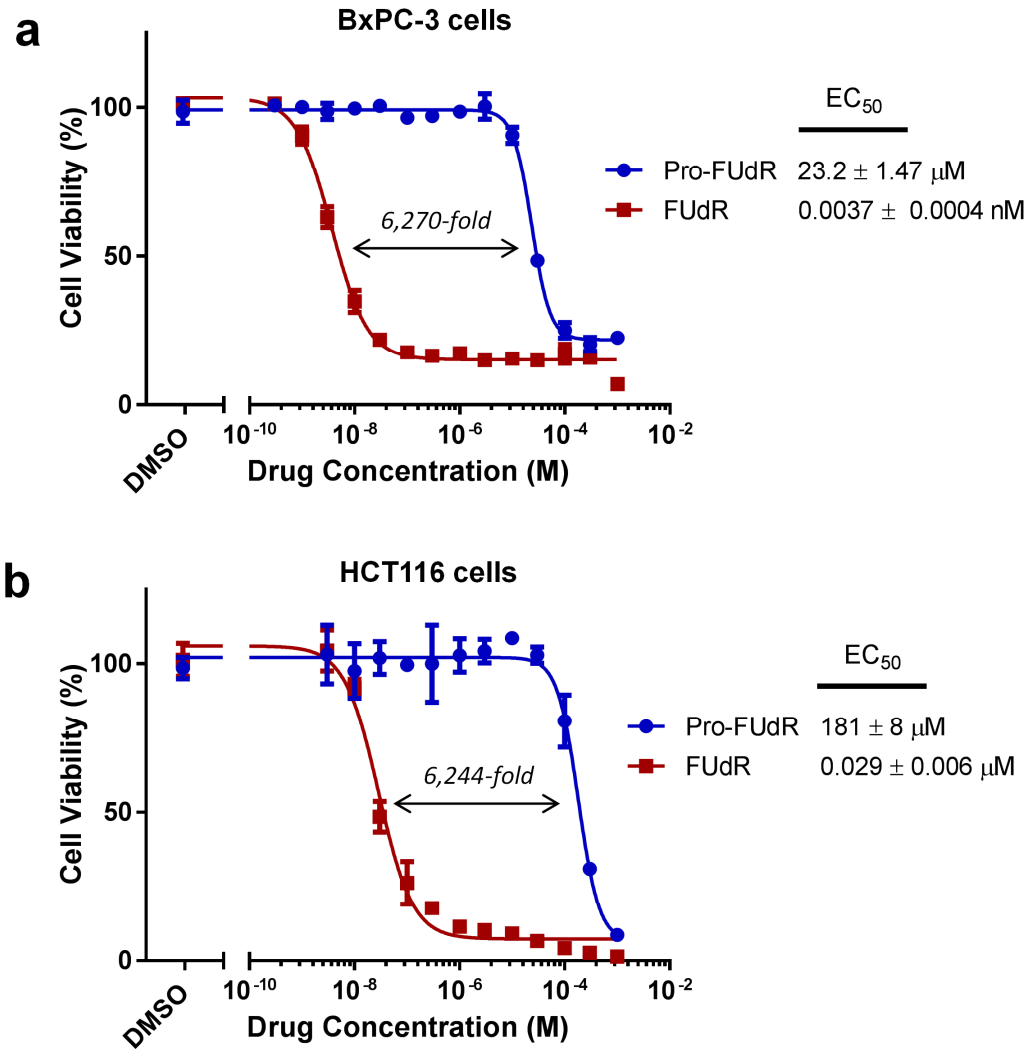

Figure 7.2. Study of Pro-FUdR bioorthogonality. Cytotoxic effect of Pro-FUdR (blue) in comparison to unmodified FUdR (red) measured through Semi Log dose response curves of increasing drug concentrations (0.0003 - 1,000 μM) to calculate corresponding EC_{50} values. **(a)** BxPC-3 and **(b)** HCT116 cells. Cell viability was determined at day 5 using PrestoBlue™ reagent and a fluorescent microplate reader. Error bars: ± SD from *n* = 3.

7.2.3 Non-Biological Pd^0-mediated Conversion Study

Similarly to the previous three chapters, Pro-FUdR (30 μM) was incubated with Pd^0 resins (0.67 mg) in 1 ml of PBS of either pH of 6.5 or 7.5 in a thermomixer at 37 °C, 1200 rpm for a total of 24 h. The reaction crudes were analysed at 3 different time points, 4, 8 and 24 h, by HPLC with a 280 nm UV detector (Fig. 7.3; Table 7.1). The slightly acidic pH of 6.5 was chosen because advance solid tumours have been shown to have a slightly acidic extracellular pH, in the range of 0.5 – 1.0 units below physiological pH within healthy tissues.[139,140,164] Therefore, it was important to test

the reaction kinetics of *N*-dealkylation of Pro-FUdR within both the pH ranges of cancer-like and normal physiological extracellular environs.

As displayed in Fig. 7.3c and quantified in Table 7.1, in the absence of the Pd^0 activating device, Pro-FUdR was fully stable. In the presence of the Pd^0 resins, regardless of the pH, within 24 h, Pro-FUdR completely disappeared yielding FUdR as the main reaction product (Fig. 7.3b – right panel). The effect of pH was evident within the shorter incubation periods (4 and 8 h), with the reaction kinetics of *N*-dealkylation happening faster at the slightly more alkaline pH (7.5) (Fig. 7.3b – left and middle panel; Table 7.1).

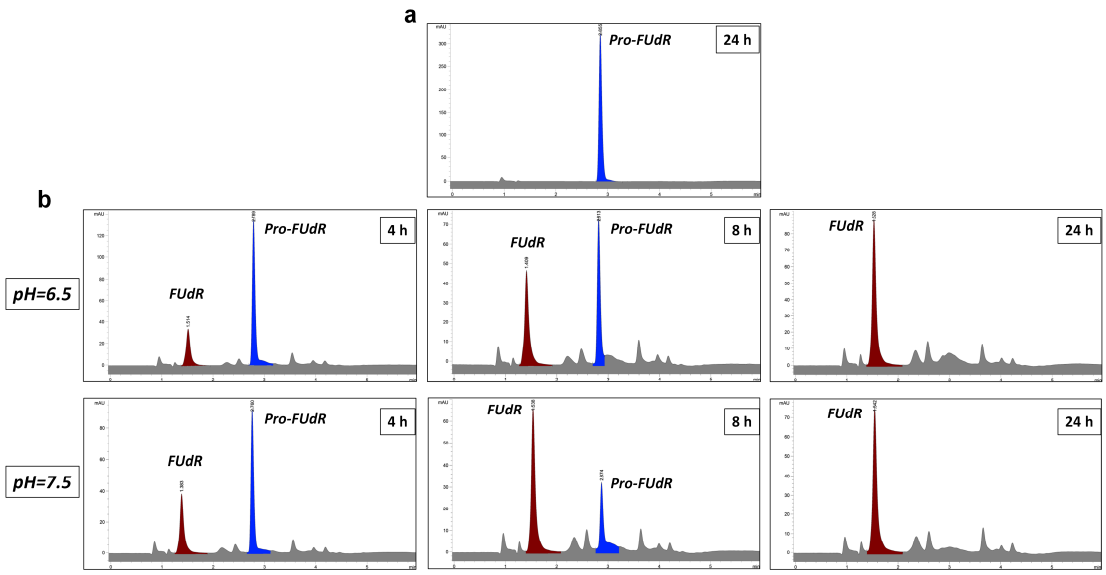

Figure 7.3. Non-biological conversion assay with Pro-FUdR. (**a**) HPLC chromatogram (280 nm) of Pro-FUdR after 24 h without Pd^0 resins. (**b**) HPLC chromatogram (280 nm) of Pd^0 resin mediated conversion of Pro-FUdR in PBS at pH 6.5 and 7.5, at 37 °C for 4 h (left panels), 8 h (middle panels) and 24 h (right panels).

Table 7.1. Palladium-mediated conversion of Pro-FUdR into FUdR. Relative percentages as calculated by chromatogram peak integration obtained from HPLC using a 280 nm detector.

		REACTANTS			
		Pro-FUdR		Pro-FUdR + Pd^0	
	Time	pH=6.5	pH=7.5	pH=6.5	pH=7.5
Product of FUdR (%)	at t= 4 h	N/D	N/D	26.6%	37.3%
	at t= 8 h	N/D	N/D	49.0%	65.9%
	at t= 24 h	0%	0%	100%	100%

7.2.4 Pd^0-mediated Conversion of Pro-FUdR in vitro

The combination of Pro-FUdR with the heterogeneous Pd^0 catalyst was then evaluated *in vitro*. BxPC-3 and HCT116 cells were treated with a range of concentrations of Pro-FUdR (0.0003 – 30 μM; blue) with Pd^0 resins (0.67 mg/ml; black) separately (negative controls) and in combination (BOOM activation assay; green). The combination was compared to unmodified FUdR with the same dose range (positive control; red). As expected, based on the results obtained from Fig. 7.2 and previous chapters, the independently administered Pro-FUdR and Pd^0 resins did not exhibit any antiproliferative effect on the treated cells (Fig. 7.4a, c). Remarkably, the combination displayed a comparative antiproliferative effect to cells treated with FUdR, indicating the *in situ* generation of FUdR (Fig. 7.4a, c). The combination of Pd^0 resins and Pro-FUdR manifested an EC_{50} value of 0.319 μM from the HCT116 cells (Fig. 7.4d – green curve). When compared to FUdR (0.045 μM; Fig. 7.4d – red curve), this is only a 7 fold difference in cytotoxicity and compared to the EC_{50} value in the absence of the Pd^0 resins (181.1 μM; Fig. 7.2b – blue curve), the difference in biological properties is >560 fold. This difference was even more impressive for the more sensitive BxPC-3 treated cells. The combination (Pd^0 + Pro-FUdR) produced an EC_{50} value of 0.016 μM (Fig. 7.4b – green curve), which is only ≈ 2 fold difference compared to the unmodified drug (0.009 μM; Fig. 7.4b – red curve). Remarkably, when compared to the EC_{50} value obtained from the solo treated Pro-FUdR (23.2 μM; Fig. 7.2a – blue curve) the disparity between the inactive and reactive prodrug is an astonishing 1,450 fold difference.

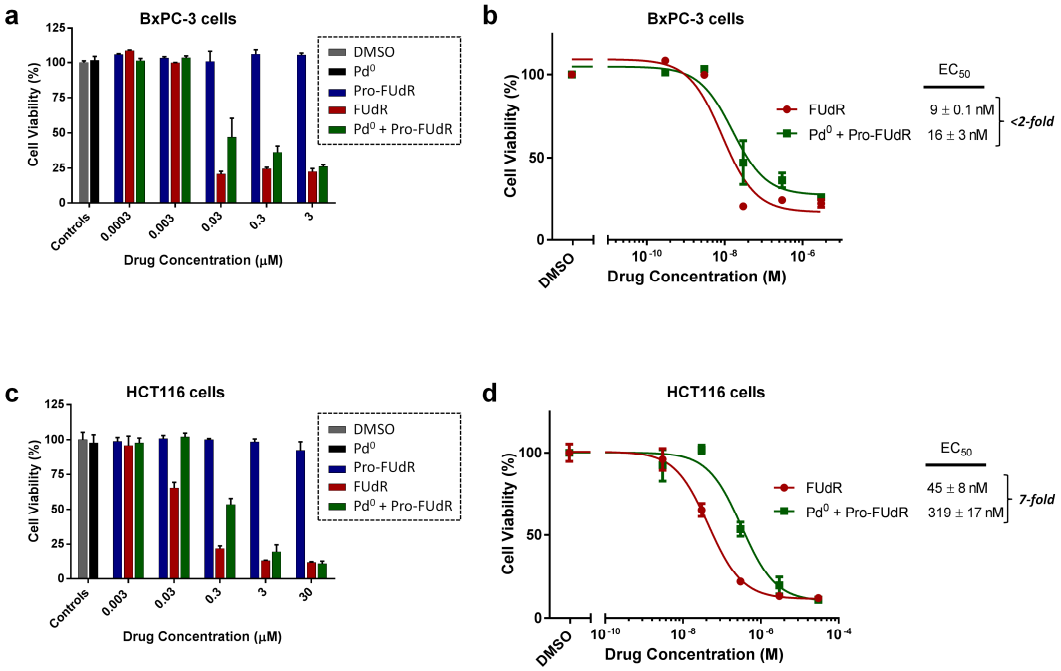

Figure 7.4. BOOM generation of Pro-FUdR in cancer cell culture. (**a, c**) Study of BOOM activation in a dose response study of cell viability after 5 days of treatment with (**a**) BxPC-3 and (**c**) HCT116 cells. Experiments: 0.1% (v/v) DMSO (untreated cell control; in grey), 0.67 mg/ml of Pd^0 resins (negative control; in black); 0.0003 – 30 µM of Pro-FUdR (negative controls; in blue); 0.0003 – 30 µM of FUdR (positive controls; in red) and Pd^0 resins + Pro-FUdR (BOOM generation assay; in green). (**b, d)** Log dose response curves and calculated EC_{50} values of ProFUdR + Pd^0 resins combinations (in green) in comparison to unmodified FUdR (in red) determined from (**a**) and (**c**) respectively. Cell viability was determined at day 5 using PrestoBlue™ reagent. Error bars represent ± standard deviation from *n* = 3.

7.2.5 Phenotypic Evaluation of Pd^0 / Pro-FUdR Combination

Using an IncuCyte ZOOM™ device, the cell growth kinetics were monitored through time-lapse imaging analysis to evaluate the ability of the combination to generate FUdR and exert a comparative cytotoxic effect to the direct treatment with unmodified FUdR. Cells were monitored every 3 hours after drug treatment (Day 0) for a total of 5 days. As displayed in Fig. 7.5a, b, all of the negative controls (blue – Pro-FUdR; black – Pd^0 resins) displayed similar growth curves to the untreated cells (grey – DMSO); whereas the combination (green) exhibited identical bell shaped curves to that of the cells treated with the parental FUdR drug (red). This indicated that the combination affected cell proliferation with the same efficacy and kinetic response as FUdR and at that concentration of Pro-FUdR (3 and 10 µM for BxPC-3 and HCT116 cells, respectively) the drug was rapidly generated *in situ*. Treatment

induced changes to cell morphology from the combination were analogous to the parental drug for both cell lines (Fig. 7.5c, d).

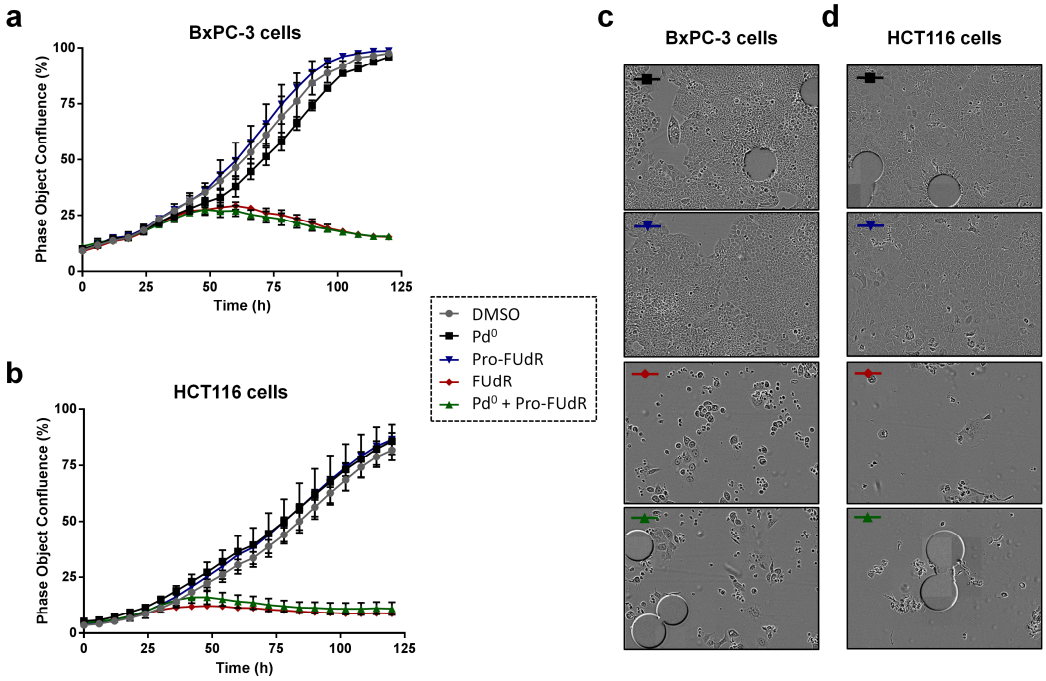

Figure 7.5. Cell Growth Kinetics and Phenotypic Evaluation of BOOM generated FUdR. (**a, b**) Study of real-time cell confluency. Cell population was monitored over 5 days (120 h) using an IncuCyte ZOOM microscope inside an incubator (5% CO_2, 37 °C) treated with either Pro-FUdR, Pd^0 resins, FUdR or combination of Pd^0 resins + Pro-FUdR. Experiments: 0.1% (v/v) DMSO. Drug/prodrug concentrations: 10 µM for HCT116 cells and 3 µM for BxPC-3 cells. (**c, d**) Phase contrast images of cells after 5 days of treatment. Pd^0 resins are identified as spheres of an average of 150 µM. Error bars represent ± standard deviation from *n* = 3.

7.2.6 Pd^0-mediated Conversion of Pro-FUdR in vitro in Hypoxia

Due to the inherent difficulties with treating hypoxic tumours, it was important to evaluate Pro-FUdR's BOOM activation in an oxygen deprived environment (0.5% O_2). This was evaluated by performing the BOOM activation assay with HCT116 cells in a hypoxic chamber. With the exception of growing the cells for 5 days in the hypoxic chamber all other treatment conditions were identical. Importantly, the cytotoxic effect mediated by the combination within the hypoxic chamber (Fig. 7.6a) was found to be equivalent to the one exerted in normoxia. The EC_{50} value obtained from the combination (0.147 µM; Fig. 7.6b – green curve) was only a 9 fold

difference compared to unmodified FUdR (0.015 µM; Fig. 7.6b – red curve) under the same hypoxic conditions. This indicated that the low oxygen levels have minimal or no influence on Pd^0 resins' ability to cleave the *N*-propargyl moiety from Pro-FUdR.

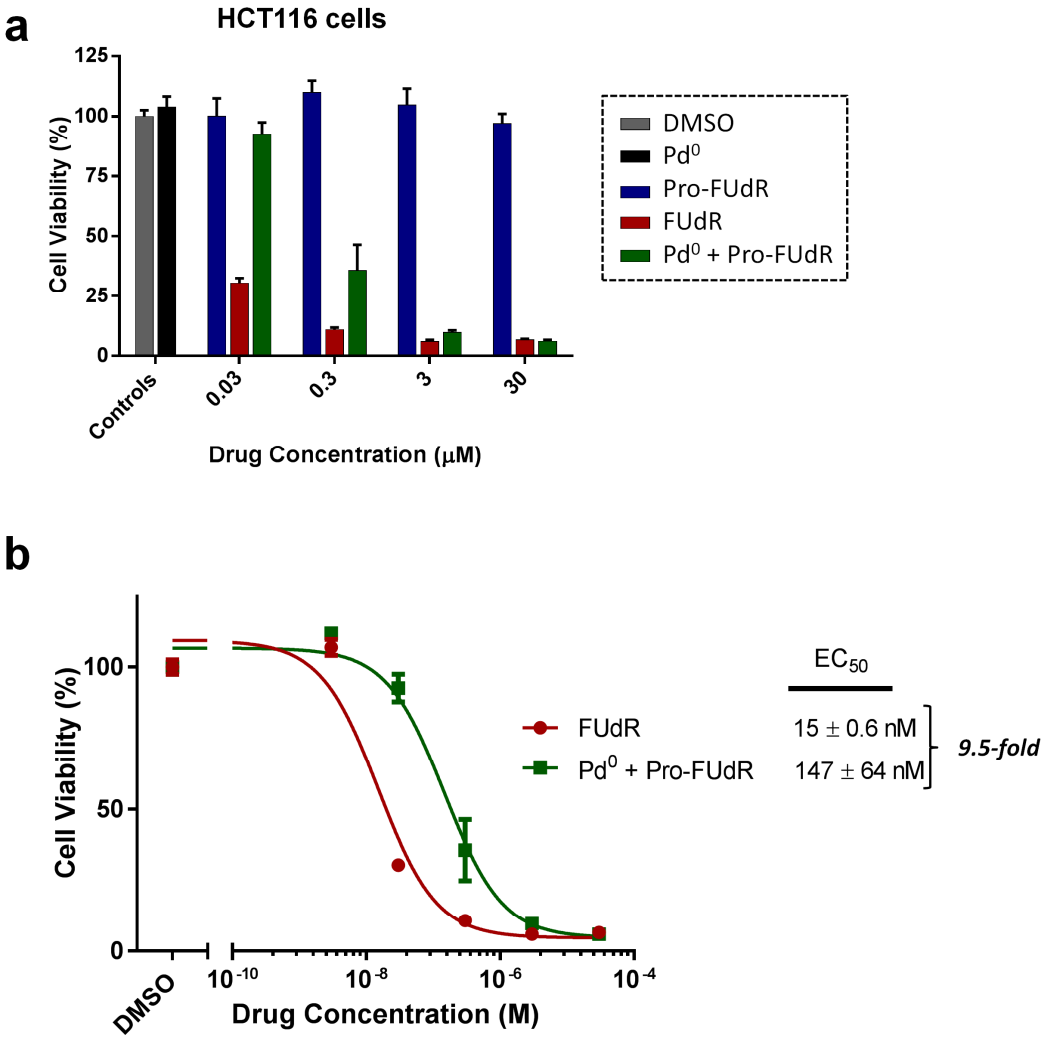

Figure 7.6. BOOM generation of Pro-FUdR in HCT116 cells under hypoxic conditions. (**a**) Study of BOOM activation in a dose response study of HCT116 cell viability after 5 days of treatment in hypoxia. Experiments: 0.1% (v/v) DMSO (untreated cell control; in grey), 0.67 mg/ml of Pd^0 resins (negative control; in black); 0.003 – 30 µM of Pro-FUdR (negative controls; in blue); 0.003 – 30 µM of FUdR (positive controls; in red) and Pd^0 resins + Pro-FUdR (BOOM activation assay; in green). (**b)** Log dose response curves and calculated EC_{50} values of ProFUdR + Pd^0 resins combination (in green) in comparison to unmodified FUdR (in red) determined from (**a**). Cell viability was determined at day 5 using PrestoBlue™ reagent. Error bars represent ± standard deviation from *n* = 3.

7.3 CONCLUSION

The *N*-propargylation of the *N*3 position of the clinically used anticancer drug FUdR successfully created the most relevant BOOM-activated prodrug to date. The coupled promoiety reduced FUdR's cytotoxic activity by ≈ 6,250 fold, demonstrating not only how biochemically stable the proparylation of the NH group is but also the important role this hydrogen donor group plays for enzymatic recognition by the enzymes responsible for producing FUdR's active metabolites (the mono and tri phosphorylated derivatives).

The ability for Pro-FUdR to undergo complete palladium mediated *N*-dealkylation within 24 hours in a range of pHs exhibited within normoxia and hypoxia conditions suggests that this technology could potentially be administered to treat both early and late stage cancer disease. The sensitivity and specificity displayed by the promoiety to Pd^0 catalysis proves that this process is also compatible with the higher complexities of nucleosides.

Chemo-reversible Pro-FUdR, whether in the presence or absence of palladium, displayed a difference in cytotoxicity of 1,450 fold. To the best of our knowledge, this is the greatest therapeutic window displayed by an antimetabolite prodrug *in vitro*.

Analogous bell shaped curves from both the combination of Pd^0 resins with Pro-FUdR and unmodified FUdR treatment was observed from the cell growth kinetics produced from the IncuCyte ZOOM. The antiproliferative effect produced from the combination was comparable to the parental FUdR drug both under normoxic and hypoxic conditions. These results highlight the ability for this prodrug to undergo activation via BOOM chemistry in both physiological and within an oxygen deprived environment and demonstrates the fast and versatile reaction kinetics of palladium mediated *N*-depropargylation to generate an immediate phenotypic effect. It also indicates that this treatment regime would be compatible to treat early stage tumours where oxygen levels are within the normal 21% range and for treating late stage tumours that contain hypoxic regions (on average ≈ 0.7% O_2).[158] This essential

milestone warrants this novel therapeutic approach into more relevant preclinical models of cancer.

The results presented in this chapter have been previously published as Weiss et al. Sci. Rep. 5, 9329. (reference 70)

CHAPTER 8

Discussion

Cytotoxic metabolites such as the ones presented in chapters 4 through 7, although have been widely used for decades for the treatment of various types of cancers, are notorious for causing numerous unpleasant side effects. The mechanism of action employed by these drugs to kill cancer cells (by impairing various biomolecules which the cancer cells required in order to continually divide) equally effect normal fast-dividing healthy cells which can cause many adverse events for the patient.[165] Substantial effort has been brought forth from the industrial and academic community to provide more targeted therapy in an effort to minimise these dreadful side effects; however, selectivity remains a major hurdle.[166,167] The majority of small molecule drugs have failed within clinical trials. This is partly due to their limited therapeutic window and therefore many potential drug candidates which could possess the possibility to treat current untreatable diseases and improve upon current pharmacotherapy are removed from clinical trials. Poor selectivity of current drugs used in the clinic means that in order to minimise unpleasant side effects for the patients, sub optimal levels of the drug are being administered which means the full potential of the drug is not being utilised. This allows more time for the tumour to progress and develop a resistance to the drug. Systems biology has demonstrated that drugs which have multiple targets have greater clinical success.[168] This means that drugs must interact with multiple sites in order to gain maximum effectiveness yet still remain inactive to sites that cause side effects. This immensely challenging paradigm highlight the importance of investigating alternative ways for dynamic control over drug activation.[39]

Bioorthogonal chemistry is generally defined as an artificial chemistry processes undertaken between two chemoselective reactants within a biological system that

separately remain inert to the system. This practical approach has become particularly useful for studying biomolecules in their native state.[45,49] Although using transition metals to mediate bioorthogonal chemistry was initially believed to be problematic due to their potential to be toxic to the living system, significant progress has been made within the last several years in developing biologically tolerated BOOM reactions. The introduction of transition metals to the bioorthogonal paradigm has expanded the limitations of capable chemical reactions within the stringent bioorthogonal parameters. For example BOOM chemistry using a Pd catalyst to perform deprotection reactions can selectively control protein function intracellularly.[65]

The clinical application of using bioorthogonal chemistry for therapeutic means has so far been limited to photodynamic therapy.[31,32] This method relies on the formation of reactive oxygen species which are generated from photosensitizers once irradiated by visible light. The reactive oxygen species cause direct and non-specific damage to various biomolecules within cells, particularly to DNA. This therapeutic technique has become a valuable local treatment option within areas easily penetrated by light.

In an attempt to advance the use of bioorthogonal chemistry for therapeutic purposes by incorporating the unique chemospecific chemical transformations possessed by palladium, this thesis reports the early development of BOOM chemistry as an alternate chemotherapeutic option.

For the work of this thesis, the transition metal chosen for BOOM chemistry technology were heterogeneous Pd^0 nanoparticles captured in a biocompatible polymer matrix (PEG-grafted polystyrene resin beads). These readily generated nanoparticles have high catalytic activity[58,66] and can be immobilized through solid support and chemical interactions to PEG-PS polymers.[88] As previously reported,[65] Pd^0 can mediate many chemical reactions within a biological system without causing any apparent toxicity. We investigated the use of Pd^0 functionalized resin beads, which are larger than human cells (150 μM in diameter), as a heterogeneous catalyst capable of activating Pd-labile prodrugs within the extracellular space. However, before the Pd^0 resins catalytic potential could be tested, as one of the essential requisites for BOOM chemistry, they had to demonstrate biocompatibility. Various

concentrations of the resins were tested in two cancer cell lines (colorectal HCT116 and pancreatic BxPC-3). At high concentrations (2 and 3 mg/ml of resins) anti proliferative effects were observed. At these concentrations perhaps enough Pd^{2+} is generated by oxidation of Pd^0 from the Pd nanoparticles within the resin and has leeched out from the solid polymer support. Pd^{2+} species are DNA and RNA biosynthesis inhibitors and therefore at sufficient concentrations would be toxic to cells.[169,170] Importantly, Pd-resins enabled specific prodrug activation at concentrations that were safe for the cells. This means that, for mediating BOOM chemistry, palladium is required at quantities that are catalytic but not directly toxic.

A single resin bead was successfully implanted into the yolk sac of a zebrafish embryo without hindering any embryonic progression or altering the fish's phenotype. This single bead would later demonstrate to support adequate amounts of Pd^0 nanoparticles to locally activate a Pd-labile fluorescent probe. The biocompatibility and catalytic potential displayed by the Pd^0 resins was an excellent proof of concept to demonstrate the potential of a surgically implantable Pd activating device within a tumour whereupon it could locally activate chemotherapeutic prodrugs.

The content of palladium within the Pd^0 resins was determined by ICP-OES and found to be 2.8% (263 μM for 1 mg/ml of resins in solution) from the first batch used in chapters 3 and 5 and 4.4% (277 μM for 0.67 mg/ml of resins in solution) from the second batch used in chapters 4, 6 and 7. However, based on observations from the cross sectioned Pd^0 resins from the TEM images (Fig. 3.1c, d), the ≈ 5 nm Pd^0 nanoparticles were found to be quite well dispersed throughout the polymer network. Considering the compact polymeric structure of the resins, it was expected that only the heterogeneous Pd^0 nanoparticles near the surface of the beads would actually come into contact with the dissolved chemicals in the liquid phase. As a consequence, a fraction of the Pd^0 nanoparticles would actually be involved with the BOOM catalysis. Therefore, the Pd^0 content of 263 or 277 μM, is in fact more realistically much less of what is involved in mediating the chemical transformations.

When designing prodrugs it is important to understand the functional groups involved in the drugs mechanism of action. The two main functional groups

responsible for Gemcitabine's activity were expected to be the OH group on *C*5' (the phosphorylation site) and NH_2 group on *C*4 (key component for enzyme recognition).[104,105] Both functional groups were masked with potential Pd-labile alkyloxycarbonyl promoieties. However, it was the carbamate Gemcitabine prodrugs which proved to be the more enzymatically stable in cell culture, with an approximate 23 fold decrease in antiproliferative activity compared to unmodified Gemcitabine. Although this was not an ideal decrease, it was still significant and could make a difference in improving the quality of life for a patient during treatment. On the contrary, the carbonate prodrugs had a relatively comparable cytotoxic effect to Gemcitabine. Going forward, based on these results, it is proposed that primary amines are the group of choice to mask when designing a prodrug with alkyloxycarbonyl promoieties. This does not mean that functionalization of the OH group of Gemcitabine could not lead to bioorthogonal prodrugs. Rather, it is the weak nature of the carbonate group which probably resulted in a close-to-null reduction in cytotoxicity. On the other hand, masking the NH_2 group had the added potential benefit of increasing the prodrugs bioavailability by preventing cytidine deaminase from attacking the amine and irreversibly inactivating the drug. [106,107]

The superior Pd sensitivity of the *N*-Poc over *N*-Alloc displayed both in buffered solution and cell culture is worth mentioning because to date most labs have favoured the use of *N*-Alloc groups to implement various coupling and decoupling reactions for BOOM chemistry.[57,66,171-175] Albeit, some of these BOOM chemical reactions using Alloc-moieties have been performed with ruthenium based catalysts and to the best of my knowledge a direct comparison of Poc vs. Alloc using this catalysts has yet to be performed. Nevertheless, in terms of palladium-mediated BOOM reactions, our results have demonstrated that not only is *N*-Poc more Pd-labile than N-Alloc but at least as stable in cells and significantly much more stable and enzyme resistant within zebrafish embryos. The *N*-Alloc protected derivative of rhodamine 110, even in the absence of Pd^0, resulted in a highly fluorescent signal after 24 h incubation with zebrafish embryos. This strongly suggests that it was biochemically activated and therefore, this promoiety is insufficient for bioorthogonal use. However, the *N*-Poc and indeed the *N*-Cbz probes did display fluorescent signal within the gastrointestinal tract of the zebrafish embryos regardless

of whether the Pd^0 resin was present or not. This suggests that the carbamates are susceptible to biochemical cleavages by digestives enzymes and indicates that carbamate's chemical stability as promoities could be compromised if the prodrug was administered orally. Therefore, the prodrugs adminstration would require alternative means such as perhaps intravenous injection.

In order for a prodrug to have success as a BOOM activated prodrug designed for chemotherapy it has to display complete biocompatibility in the absence of the activating device. The 5FU prodrug synthesised with a propargyl protecting group within the endocyclic nitrogen at position *N*1 of the molecule obtained this desired characteristic. It displayed complete resistance to metabolic cleavage but was still highly susceptible to Pd-mediated *N*-dealkylation under biocompatible conditions. The heterogeneous Pd^0 catalyst was able to completely restore the pharmacological activity of 5FU in cell culture.

This novel and unprecedented *N*-depropargylation process, which is the first N-C cleavage process enabled by a metal in a bioorthogonal manner, was further investigated to see if this selective deprotection process could be applied by other heterocyclic systems with lactam/lactim tautomery. *N*-propargyl-2-pyridone and *N*-propargyl-4-pyridone were synthesized and treated under the same conditions as described for the non-biological conversion assay from chapters 4 to 7. Both dealkylated products were obtained within 24 h of exposure to the resins. This indicates that the presence of lactam/lactim tautomery is the essential requisite for the reaction to happen, regardless of the position of the oxo group. Due to its excellent chemoselectivity and stable properties, it is believed that this reaction could be broadly applicable to a range of heterocyclic systems with similar tautomerism for pharmacology. This chemical process also provides a powerful new tool for synthetic chemistry for preparing useful heterocyclic compounds under mild and environmentally friendly conditions.

In an attempt to improve upon the reaction kinetics of the Pd^0-mediated *N*-depropargylation reaction of a 5FU prodrug, two different aspects were considered. The first was testing different *N*1-alkynyl promoieties. It was hypothesised that additional moieties within the terminal carbon of the triple bond should influence the

deprotection process. Significantly, the results indicated that the susceptibility of the *N*1-alkynyl derivatives to cleavage was inversely proportional to the size of the moiety bound to the terminal carbon within the triple bond. This informed that the greater the Pd^0 catalyst coordination to the triple bond is hindered the slower the reaction proceeds; therefore, the original alkynyl promoiety used still is the most Pd-labile.

The second study to investigate the dealkylation rate, was masking the *N*3 functional group within 5FU. It was hypothesized that due to the lower pKa value at this position relative to *N*1, the propargyl cleavage could proceed faster. However, this was not the case and still *N*1-depropargylation had the faster reaction kinetics despite the higher pKa value. This indicated that perhaps because *N*3 is between two ring carbonyl groups, that perhaps the steric constraints caused by the two ring carbonyls slightly hindered efficient Pd^0 coordination. This regioselectivity was observed when 1,3-dipropargyl-5-fluorouracil (**31**) treated with the Pd^0 resins resulted in the production of 5FU and 3-propargyl-5-fluorouracil (**30**) after 24 h with the complete and selective depropargylation at *N*1 occurring first.

Despite the slower reaction kinetics of **30**, it is worth mentioning that clinically speaking it may also have potential for BOOM chemotherapy because of its potential to have improved bioavailablity. With more than 80% of the administered 5FU in a patient becoming irreversibly deactivated in the liver by dihydropyrimidine dehydrogenase (DPD)[176], it is important to design a 5FU prodrug that not only increases the drugs therapeutic window through selective activation but also its bioavailability till it reaches the target tissue where palladium can activate it. *N*3 forms a strong hydrogen bond interaction with an asparagine residue (Asn-736) within the active site[129] and therefore there is great potential to significantly reduce the enzymatic binding affinity with **30** by masking this hydrogen bond interaction. Based on the crystal structure of 5-Iodouracil with DPD[129] preventing the hydrogen bonding between *N*3 with its amino acid residue vs. *N*1 with its amino acid residue, the masking of *N*3 would appear to effect the binding affinity more. Of course **31** with both endocyclic nitrogens masked would have the greatest bioavailability but as displayed in chapter 6, the reaction kinetics with this compound is too slow to obtain

effective antiproliferative effects. If a Pd^0 activating device was synthesized with improved catalytic potential that could activate **31** so that the rate of activation was superior to the rate of cancer cell proliferation, then this compound could become a clinically viable option. However, effects of the three 5FU prodrugs on other ADME (absorption, distribution, metabolism and excretion) properties have not been evaluated to date so, at the current stage of this project, it would not be possible to predict which prodrug could possess the optimal characteristics to reach the targeted tissue.

The propargylation strategy implemented for the chemotherapeutic drug FUdR successfully developed a bioorthogonal palladium labile prodrug of a nucleoside analogue, which can be activated via Pd^0-mediated catalysis despite varying pH ranges and O_2 levels within biologically acceptable parameters. The propargyl moiety coupled to the NH group at position 3 greatly reduced the drug's pharmacological activity. This drastic decrease illustrated 2 important features of the prodrug. The first was the remarkable biochemical stability of the propargyl group coupled to the endocyclic nitrogen group. Based on the difference in EC_{50} values obtained from the comparison of Pro-5FU to 5FU (chapter 5), we were aware that N-propargyl groups had a strong biochemical resiliency, but because 5FU's antiproliferative capability was not as potent as FUdR, the extent of this stability was not fully understood. The second was how relevant this NH group is for FUdR's biological activation. By masking the *N*3 group, we rendered the prodrug essentially unnoticeable, i.e. bioorthogonal, to its activating enzymes and/or the targets responsible for its metabolites, for example thymidine kinase (TK). Although this has not been investigated, this masking strategy may also increase the drug's bioavailability by inhibiting its interaction with thymidine phosphorylase (TP). TP is abundantly present in tissues such as the liver and intestine and is responsible for catabolizing FUdR into 5FU.[177] Therefore by limiting the prodrugs interaction with TP and thus preventing its degradation, the therapeutic effectiveness of the drug can be further improved.[144]

The ability for *N*-dealkylation to take place under hypoxic conditions from a chemical perspective, strongly suggests that this reaction is mediated by the

heterogeneous interaction of the prodrug with Pd^0 and not by soluble Pd^{2+} species. This was logically inferred because the reductive environment within the chamber would strongly favour Pd^0's oxidation state.

Pro-FUdR and Pro-5FU are two excellent drug candidates to progress the BOOM chemotherapeutic regime to more clinically relevant animal cancer models. These *in vivo* models would progress our understanding of how bioorthogonal the prodrugs are systemically and to what extent the local activation of the prodrug takes place, i.e. how far outside the tumour does the activated drug advance and potentially cause damage to surrounding tissues. A greater understanding of the prodrugs ADME properties is required in order to advance to clinical trials. However, unlike most new drugs which are in their initial stages of development, most relevant information pertaining to the activated drug is already well established because these drugs have been on the market and used to treat patients for many years.

A more practical Pd^0 activating device for *in vivo* studies is required so it can easily be implanted inside the tumour. Ideally, it should be a singular device with a strong enough solid support to prevent any Pd^0 nanoparticles from leaching out and causing activation outside the targeted therapeutic range. Also, if the device is porous it should increase the contact between the prodrug and the catalyst which would have a positive effect on the rate of activation of the prodrug.

Finally, with a propargyl promoiety of just 38 atomic mass units, this group is one of the smallest promoieties ever used for a prodrug strategy. Only some examples of ester prodrugs, which release carboxyl-functionalized drugs by hydrolytic enzymes,[22,178] contain smaller promoieties (ethyl groups). Those are of course examples of biolabile prodrugs and therefore are not comparable to the prodrugs described in this thesis.

Besides the desired drug product, the only other product produced from the Pd^0-mediated dealkylation reaction is the natural compound 1-hydroxyacetone (also known as acetol), a natural intermediate also formed during glycogenesis. This assures that the desired pharmacological effect is solely mediated by the *in situ* generation of the drug.

The robustness of this masking strategy, the sensitivity and selectivity of the BOOM reaction and the natural by-product produced, highlight the potential of this novel masking strategy to increase the selectivity and efficacy of some chemotherapeutic agents. This would result in tolerable higher dosing concentrations of the drug which would mean the tumor could enter remission sooner before it could develop a resistance and significantly reduce the adverse effects due to the systemic presence of the drug. This overall would improve the quality of life for patients both during and after treatment.

CHAPTER 9

References

1 World Health Statistics 2014. (World Health Organization Geneva, 2013).

2 Chabner, B. A. & Roberts, T. G. Timeline - Chemotherapy and the war on cancer. *Nature Reviews Cancer* **5**, 65-72, doi:Doi 10.1038/Nrc1529 (2005).

3 DeVita, V. T., Jr. & Chu, E. A history of cancer chemotherapy. *Cancer Research* **68**, 8643-8653, doi:10.1158/0008-5472.CAN-07-6611 (2008).

4 Lind, M. J. Principles of cytotoxic chemotherapy. *Medicine* **36**, 19-23, doi:10.1016/j.mpmed.2007.10.003 (2008).

5 Vanneman, M. & Dranoff, G. Combining immunotherapy and targeted therapies in cancer treatment. *Nature reviews. Cancer* **12**, 237-251, doi:10.1038/nrc3237 (2012).

6 O'Brien, S. G., Guilhot, F., Richard, A. L., Gathmann, I. & Baccarani, M. Imatinib Compared with Interferon and Low-Dose Cytarabine for Newly Diagnosed Chronic-Phase Chronic Myeloid Leukemia. *N Engl J Med* **348**, 994-1004 (2003).

7 Bartram, C. R. *et al.* Translocation of C-Abl Oncogene Correlates with the Presence of a Philadelphia-Chromosome in Chronic Myelocytic-Leukemia. *Nature* **306**, 277-280, doi:Doi 10.1038/306277a0 (1983).

8 Faderl, S., Talpaz, M., Estrov, Z. & Kantarjian, H. M. Chronic myelogenous leukemia: Biology and therapy. *Annals of Internal Medicine* **131**, 207-219 (1999).

9 Gambacorti-Passerini, C. *et al.* Multicenter Independent Assessment of Outcomes in Chronic Myeloid Leukemia Patients Treated With Imatinib. *Journal of the National Cancer Institute* **103**, 553-561, doi:Doi 10.1093/Jnci/Djr060 (2011).

10 Nefedova, Y. *et al.* Activation of dendritic cells via inhibition of Jak2/STAT3 signaling. *Journal of immunology* **175**, 4338-4346 (2005).

11 Lee, H., Pal, S. K., Reckamp, K., Figlin, R. A. & Yu, H. STAT3: A Target to Enhance Antitumor Immune Response. *Cancer Immunology and Immunotherapy* **344**, 41-59, doi:Doi 10.1007/82_2010_51 (2011).

12 Zhang, J., Yang, P. L. & Gray, N. S. Targeting cancer with small molecule kinase inhibitors. *Nature reviews. Cancer* **9**, 28-39, doi:10.1038/nrc2559 (2009).

13 Scott, A. M., Wolchok, J. D. & Old, L. J. Antibody therapy of cancer. *Nature reviews. Cancer* **12**, 278-287, doi:10.1038/nrc3236 (2012).

14 Divgi, C. R. *et al.* Phase I and imaging trial of indium 111-labeled anti-epidermal growth factor receptor monoclonal antibody 225 in patients with squamous cell lung carcinoma. *Journal of the National Cancer Institute* **83**, 97-104 (1991).

15 Hudis, C. A. Drug therapy: Trastuzumab - Mechanism of action and use in clinical practice. *New England Journal of Medicine* **357**, 39-51, doi:Doi 10.1056/Nejmra043186 (2007).

16 Dijkers, E. C. *et al.* Biodistribution of 89Zr-trastuzumab and PET imaging of HER2-positive lesions in patients with metastatic breast cancer. *Clinical pharmacology and therapeutics* **87**, 586-592, doi:10.1038/clpt.2010.12 (2010).

17 Scott, A. M. *et al.* A phase I dose-escalation study of sibrotuzumab in patients with advanced or metastatic fibroblast activation protein-positive cancer. *Clinical Cancer Research* **9**, 1639-1647 (2003).
18 Weiner, L. M., Surana, R. & Wang, S. Z. Monoclonal antibodies: versatile platforms for cancer immunotherapy. *Nature Reviews Immunology* **10**, 317-327, doi:Doi 10.1038/Nri2744 (2010).
19 Xu, Y. F., Sette, A., Sidney, J., Gendler, S. J. & Franco, A. Tumor-associated carbohydrate antigens: A possible avenue for cancer prevention. *Immunology and Cell Biology* **83**, 440-448, doi:DOI 10.1111/j.1440-1711.2005.01347.x (2005).
20 Chames, P., Van Regenmortel, M., Weiss, E. & Baty, D. Therapeutic antibodies: successes, limitations and hopes for the future. *British journal of pharmacology* **157**, 220-233, doi:10.1111/j.1476-5381.2009.00190.x (2009).
21 Huttunen, K. M., Raunio, H. & Rautio, J. Prodrugs--from serendipity to rational design. *Pharmacological reviews* **63**, 750-771, doi:10.1124/pr.110.003459 (2011).
22 Rautio, J. *et al.* Prodrugs: design and clinical applications. *Nature reviews. Drug discovery* **7**, 255-270, doi:10.1038/nrd2468 (2008).
23 Yang, Y.-h., Aloysius, H., Inoyama, D., Chen, Y. & Hu, L.-q. Enzyme-mediated hydrolytic activation of prodrugs. *Acta Pharmaceutica Sinica B* **1**, 143-159, doi:10.1016/j.apsb.2011.08.001 (2011).
24 Ettmayer, P., Amidon, G. L., Clement, B. & Testa, B. Lessons learned from marketed and investigational prodrugs. *Journal of medicinal chemistry* **47**, 2393-2404, doi:Doi 10.1021/Jm0303812 (2004).
25 Du, C. *et al.* A pH-sensitive doxorubicin prodrug based on folate-conjugated BSA for tumor-targeted drug delivery. *Biomaterials* **34**, 3087-3097, doi:10.1016/j.biomaterials.2013.01.041 (2013).
26 Xu, G. & McLeod, H. L. Strategies for enzyme/prodrug cancer therapy. *Clinical Cancer Research* **7**, 3314-3324 (2001).
27 Niculescu-Duvaz, I., Spooner, R., Marais, R. & Springer, C. J. Gene-directed enzyme prodrug therapy. *Bioconjugate Chemistry* **9**, 4-22, doi:Doi 10.1021/Bc970116t (1998).
28 Misra, S. Human gene therapy: a brief overview of the genetic revolution. *J Assoc Physicians India* **61**, 127-133 (2013).
29 McNeish, I. A., Green, N. K., Gilligan, M. G., Ford, M. J. & Mautner, V. Virus directed enzyme prodrug therapy for ovarian and pancreatic cancer using retrovirally delivered E. coli nitroreductase and CB1954. *Gene Therapy* **5**, 1061-1069 (1998).
30 Senter, P. D. & Springer, C. J. Selective activation of anticancer prodrugs by monoclonal antibody-enzyme conjugates. *Advanced drug delivery reviews* **53**, 247-264 (2001).
31 Triesscheijn, M., Baas, P., Schellens, J. H. & Stewart, F. A. Photodynamic therapy in oncology. *Oncologist* **11**, 1034-1044, doi:10.1634/theoncologist.11-9-1034 (2006).
32 Allison, R. R., Bagnato, V. S., Cuenca, R., Downie, G. H. & Sibata, C. H. The future of photodynamic therapy in oncology. *Future Oncol* **2**, 53-71, doi:10.2217/14796694.2.1.53 (2006).
33 Bednarski, P. J., Mackay, F. S. & Sadler, P. J. Photoactivatable platinum complexes. *Anticancer Agents Med Chem* **7**, 75-93 (2007).
34 Farrer, N. J. *et al.* A potent trans-diimine platinum anticancer complex photoactivated by visible light. *Angew Chem Int Ed Engl* **49**, 8905-8908, doi:10.1002/anie.201003399 (2010).
35 Wei, Y., Yan, Y., Pei, D. & Gong, B. A photoactivated prodrug. *Bioorg Med Chem Lett* **8**, 2419-2422 (1998).

36 Tietze, L. F., Muller, M., Duefert, S. C., Schmuck, K. & Schuberth, I. Photoactivatable prodrugs of highly potent duocarmycin analogues for a selective cancer therapy. *Chemistry* **19**, 1726-1731, doi:10.1002/chem.201202773 (2013).
37 Beharry, A. A. & Woolley, G. A. Azobenzene photoswitches for biomolecules. *Chemical Society reviews* **40**, 4422-4437, doi:Doi 10.1039/C1cs15023e (2011).
38 Irie, M. Diarylethenes for memories and switches. *Chemical Reviews* **100**, 1685-1716, doi:Doi 10.1021/Cr980069d (2000).
39 Velema, W. A., Szymanski, W. & Feringa, B. L. Photopharmacology: beyond proof of principle. *Journal of the American Chemical Society* **136**, 2178-2191, doi:10.1021/ja413063e (2014).
40 Clavel, C. M., Păunescu, E., Nowak-Sliwinska, P. & Dyson, P. J. Thermoresponsive organometallic arene ruthenium complexes for tumour targeting. *Chemical Science* **5**, 1097, doi:10.1039/c3sc53185f (2014).
41 Clavel, C. M. *et al.* Thermoresponsive chlorambucil derivatives for tumour targeting. *Angewandte Chemie* **50**, 7124-7127, doi:10.1002/anie.201101133 (2011).
42 Agard, N. J., Prescher, J. A. & Bertozzi, C. R. A strain-promoted [3 + 2] azide-alkyne cycloaddition for covalent modification of biomolecules in living systems. *Journal of the American Chemical Society* **126**, 15046-15047, doi:10.1021/ja044996f (2004).
43 Saxon, E. & Bertozzi, C. R. Cell surface engineering by a modified Staudinger reaction. *Science* **287**, 2007-2010 (2000).
44 Prescher, J. A. & Bertozzi, C. R. Chemistry in living systems. *Nature chemical biology* **1**, 13-21, doi:10.1038/nchembio0605-13 (2005).
45 Sletten, E. M. & Bertozzi, C. R. From mechanism to mouse: a tale of two bioorthogonal reactions. *Accounts of chemical research* **44**, 666-676, doi:10.1021/ar200148z (2011).
46 Chang, P. V., Prescher, J. A., Hangauer, M. J. & Bertozzi, C. R. Imaging cell surface glycans with bioorthogonal chemical reporters. *Journal of the American Chemical Society* **129**, 8400-8401, doi:10.1021/ja070238o (2007).
47 Baskin, J. M. *et al.* Copper-free click chemistry for dynamic in vivo imaging. *Proceedings of the National Academy of Sciences of the United States of America* **104**, 16793-16797, doi:10.1073/pnas.0707090104 (2007).
48 Chenoweth, K., Chenoweth, D. & Goddard, W. A., 3rd. Cyclooctyne-based reagents for uncatalyzed click chemistry: A computational survey. *Organic & biomolecular chemistry* **7**, 5255-5258, doi:10.1039/b911482c (2009).
49 Sletten, E. M. & Bertozzi, C. R. Bioorthogonal chemistry: fishing for selectivity in a sea of functionality. *Angewandte Chemie* **48**, 6974-6998, doi:10.1002/anie.200900942 (2009).
50 Cohen, A. S., Dubikovskaya, E. A., Rush, J. S. & Bertozzi, C. R. Real-time bioluminescence imaging of glycans on live cells. *Journal of the American Chemical Society* **132**, 8563-8565, doi:10.1021/ja101766r (2010).
51 Blackman, M. L., Royzen, M. & Fox, J. M. Tetrazine ligation: Fast bioconjugation based on inverse-electron-demand Diels-Alder reactivity. *Journal of the American Chemical Society* **130**, 13518-+, doi:Doi 10.1021/Ja8053805 (2008).
52 Ning, X. *et al.* Protein modification by strain-promoted alkyne-nitrone cycloaddition. *Angewandte Chemie* **49**, 3065-3068, doi:10.1002/anie.201000408 (2010).
53 Versteegen, R. M., Rossin, R., ten Hoeve, W., Janssen, H. M. & Robillard, M. S. Click to release: instantaneous doxorubicin elimination upon tetrazine ligation. *Angewandte Chemie* **52**, 14112-14116, doi:10.1002/anie.201305969 (2013).
54 Unciti-Broceta, A., Johansson, E. M., Yusop, R. M., Sanchez-Martin, R. M. & Bradley, M. Synthesis of polystyrene microspheres and functionalization with Pd(0)

nanoparticles to perform bioorthogonal organometallic chemistry in living cells. *Nature protocols* **7**, 1207-1218, doi:10.1038/nprot.2012.052 (2012).

55 Pal, M., Parasuraman, K. & Yeleswarapu, K. R. Palladium-catalyzed cleavage of O/N-propargyl protecting groups in aqueous media under a copper-free condition. *Organic letters* **5**, 349-352, doi:10.1021/ol027382t (2003).

56 Rambabu, D., Bhavani, S., Swamy, N. K., Basaveswara Rao, M. V. & Pal, M. Pd/C-mediated depropargylation of propargyl ethers/amines in water. *Tetrahedron Letters* **54**, 1169-1173, doi:10.1016/j.tetlet.2012.12.093 (2013).

57 Streu, C. & Meggers, E. Ruthenium-induced allylcarbamate cleavage in living cells. *Angewandte Chemie* **45**, 5645-5648, doi:10.1002/anie.200601752 (2006).

58 Rahimi M. Yusop, Asier Unciti-Broceta, Emma M. V. Johansson, Sanchez-Martın, R. M. & Bradley, a. M. Palladium-mediated intracellular chemistry. *Nature Chemistry* **3**, 239-243, doi:10.1038/nchem.981

59 Ramil, C. P. & Lin, Q. Bioorthogonal chemistry: strategies and recent developments. *Chemical communications* **49**, 11007-11022, doi:10.1039/c3cc44272a (2013).

60 Li, N., Lim, R. K., Edwardraja, S. & Lin, Q. Copper-free Sonogashira cross-coupling for functionalization of alkyne-encoded proteins in aqueous medium and in bacterial cells. *Journal of the American Chemical Society* **133**, 15316-15319, doi:10.1021/ja2066913 (2011).

61 Spicer, C. D., Triemer, T. & Davis, B. G. Palladium-mediated cell-surface labeling. *Journal of the American Chemical Society* **134**, 800-803, doi:10.1021/ja209352s (2012).

62 Li, J. *et al.* Palladium-triggered deprotection chemistry for protein activation in living cells. *Nature Chemistry* **6**, 352-361, doi:10.1038/nchem.1887 (2014).

63 Qian, K. & Zheng, Y. G. Labeling: palladium brings proteins to life. *Nature chemical biology* **10**, 328-330, doi:10.1038/nchembio.1507 (2014).

64 Arbibe, L. *et al.* An injected bacterial effector targets chromatin access for transcription factor NF-kappaB to alter transcription of host genes involved in immune responses. *Nature immunology* **8**, 47-56, doi:10.1038/ni1423 (2007).

65 Yang, M., Li, J. & Chen, P. R. Transition metal-mediated bioorthogonal protein chemistry in living cells. *Chemical Society reviews*, doi:10.1039/c4cs00117f (2014).

66 Sasmal, P. K., Streu, C. N. & Meggers, E. Metal complex catalysis in living biological systems. *Chemical communications* **49**, 1581-1587, doi:10.1039/c2cc37832a (2013).

67 Weiss, J. T. *et al.* Extracellular palladium-catalysed dealkylation of 5-fluoro-1-propargyl-uracil as a bioorthogonally activated prodrug approach. *Nature communications* **5**, 3277, doi:10.1038/ncomms4277 (2014).

68 Weiss, J. T. *et al.* Development and bioorthogonal activation of palladium-labile prodrugs of gemcitabine. *J Med Chem* **57**, 5395-5404, doi:10.1021/jm500531z (2014).

69 Weiss, J. T. *et al.* N-alkynyl derivatives of 5-fluorouracil: susceptibility to palladium-mediated dealkylation and toxigenicity in cancer cell culture. *Frontiers in Chemistry* **2**, doi:10.3389/fchem.2014.00056 (2014).

70 Weiss, J. T., Carragher, N. O. & Unciti-Broceta, A. Palladium-mediated dealkylation of N-propargyl-floxuridine as a bioorthogonal oxygen-independent prodrug strategy. *Scientific reports* **5**, 9329, doi:10.1038/srep09329 (2015).

71 Harayama, Y., Yoshida, M., Kamimura, D., Wada, Y. & Kita, Y. The efficient direct synthesis of N,O-acetal compounds as key intermediates of discorhabdin A: oxidative fragmentation reaction of alpha-amino acids or beta-amino alcohols by using hypervalent iodine(III) reagents. *Chemistry* **12**, 4893-4899, doi:10.1002/chem.200501635 (2006).

72 Wu, W., Sigmond, J., Peters, G. J. & Borch, R. F. Synthesis and biological activity of a gemcitabine phosphoramidate prodrug. *J Med Chem* **50**, 3743-3746, doi:10.1021/jm070269u (2007).
73 Bowman, W. R. & Bridge, C. F. Regioselective synthesis of N-alkyl pyridones. *Synthetic Commun* **29**, 4051-4059, doi:Doi 10.1080/00397919908085926 (1999).
74 Aubert, C. *et al.* Cobalt-mediated [2+2+2] cycloaddition versus C-H and N-H activation of pyridones and pyrazinones with alkynes: an experimental study. *Chemistry* **13**, 7443-7465, doi:10.1002/chem.200601823 (2007).
75 Moharram, S., Zhou, A., Wiebe, L. I. & Knaus, E. E. Design and synthesis of 3'- and 5'-O-(3-benzenesulfonylfuroxan-4-yl)-2'-deoxyuridines: biological evaluation as hybrid nitric oxide donor-nucleoside anticancer agents. *J Med Chem* **47**, 1840-1846, doi:10.1021/jm030544m (2004).
76 van Oostrum, J. *et al.* Tracing pathway activities with kinase inhibitors and reverse phase protein arrays. *Proteomics Clin Appl* **3**, 412-422, doi:10.1002/prca.200800070 (2009).
77 Waldron, K. J., Rutherford, J. C., Ford, D. & Robinson, N. J. Metalloproteins and metal sensing. *Nature* **460**, 823-830, doi:10.1038/nature08300 (2009).
78 Tsuji, J. *Palladium Reagents and Catalysts - New Perspectives for the 21st Century*. (John Wiley & Sons, Ltd, 2004).
79 Wu, X. F., Anbarasan, P., Neumann, H. & Beller, M. From noble metal to Nobel Prize: palladium-catalyzed coupling reactions as key methods in organic synthesis. *Angewandte Chemie* **49**, 9047-9050, doi:10.1002/anie.201006374 (2010).
80 Kielhorn, J., Melber, C., Keller, D. & Mangelsdorf, I. Palladium--a review of exposure and effects to human health. *International journal of hygiene and environmental health* **205**, 417-432, doi:10.1078/1438-4639-00180 (2002).
81 Rushworth, R. Palladium in Restorative Dentistry: Superior Physical Properties Make Palladium an Ideal Dental Metal. *Platinum Metals Rev.* **48**, 30-31 (2003).
82 Marck, G., Villiger, A. & Buchecker, R. Aryl Couplings with Heterogeneous Palladium Catayst. *Tetrahedron Letters* **35**, 3277-3280 (1994).
83 Macquarrie, D. J., Gotov, B. & Toma, S. Silica-Supported Palladium-Based Catalysts for Clean Synthesis. *Platinum Metals Rev.* **45**, 102-110 (2001).
84 Yamaguchi, S. Preparation of Alumina Supported Palladium-Platinum Catalyst. *Platinum Metals Rev.* **21**, 25-27 (1977).
85 Toshima, N. (Springer US, 2003).
86 Cho, J. K. *et al.* Captured and cross-linked palladium nanoparticles. *Journal of the American Chemical Society* **128**, 6276-6277, doi:10.1021/ja057480k (2006).
87 Najman, R., Cho, J. K., Coffey, A. F., Davies, J. W. & Bradley, M. Entangled palladium nanoparticles in resin plugs. *Chemical communications*, 5031-5033, doi:10.1039/b711978j (2007).
88 Cookson, J. The Preparation of Palladium Nanoparticles. *Platinum Metals Review* **56**, doi:10.1595/147106712x632415 (2012).
89 Navaladian, S., Viswanathan, B., Varadarajan, T. K. & Viswanath, R. P. A Rapid Synthesis of Oriented Palladium Nanoparticles by UV Irradiation. *Nanoscale research letters* **4**, 181-186, doi:10.1007/s11671-008-9223-4 (2008).
90 Hou, X. & Jones, B. T. in *Encyclopedia of Analytical Chemistry* 9468 – 9485 (John Wiley & Sons Ltd, 2000).
91 Sandler, A. & Ettinger, D. S. Gemcitabine: single-agent and combination therapy in non-small cell lung cancer. *The oncologist* **4**, 241-251 (1999).
92 Lorusso, D., Di Stefano, A., Fanfani, F. & Scambia, G. Role of gemcitabine in ovarian cancer treatment. *Annals of oncology : official journal of the European Society for*

Medical Oncology / ESMO **17 Suppl 5**, v188-194, doi:10.1093/annonc/mdj979 (2006).
93 Silvestris, N. *et al.* Role of gemcitabine in metastatic breast cancer patients: a short review. *Breast* **17**, 220-226, doi:10.1016/j.breast.2007.10.009 (2008).
94 Bapat, A. A., Hostetter, G., Von Hoff, D. D. & Han, H. Perineural invasion and associated pain in pancreatic cancer. *Nature reviews. Cancer* **11**, 695-707, doi:10.1038/nrc3131 (2011).
95 Laheru, D. & Jaffee, E. M. Immunotherapy for pancreatic cancer - science driving clinical progress. *Nature reviews. Cancer* **5**, 459-467, doi:10.1038/nrc1630 (2005).
96 Rahma, O. E., Duffy, A., Liewehr, D. J., Steinberg, S. M. & Greten, T. F. Second-line treatment in advanced pancreatic cancer: a comprehensive analysis of published clinical trials. *Annals of oncology : official journal of the European Society for Medical Oncology / ESMO* **24**, 1972-1979, doi:10.1093/annonc/mdt166 (2013).
97 Kirk, K. L. Fluorination in Medicinal Chemistry: Methods, Strategies, and Developments. *Organic Process Research & Development* **12**, 305-321 (2008).
98 Wang, J., Lohman, G. J. & Stubbe, J. Mechanism of inactivation of human ribonucleotide reductase with p53R2 by gemcitabine 5'-diphosphate. *Biochemistry* **48**, 11612-11621, doi:10.1021/bi901588z (2009).
99 Artin, E. *et al.* Insight into the mechanism of inactivation of ribonucleotide reductase by gemcitabine 5'-diphosphate in the presence or absence of reductant. *Biochemistry* **48**, 11622-11629, doi:10.1021/bi901590q (2009).
100 Cerqueira, N. M., Fernandes, P. A. & Ramos, M. J. Understanding ribonucleotide reductase inactivation by gemcitabine. *Chemistry* **13**, 8507-8515, doi:10.1002/chem.200700260 (2007).
101 Herrick, J. & Sclavi, B. Ribonucleotide reductase and the regulation of DNA replication: an old story and an ancient heritage. *Molecular microbiology* **63**, 22-34, doi:10.1111/j.1365-2958.2006.05493.x (2007).
102 Ewald, B., Sampath, D. & Plunkett, W. H2AX phosphorylation marks gemcitabine-induced stalled replication forks and their collapse upon S-phase checkpoint abrogation. *Molecular cancer therapeutics* **6**, 1239-1248, doi:10.1158/1535-7163.MCT-06-0633 (2007).
103 Danesi, R. *et al.* Pharmacogenetics of anticancer drug sensitivity in non-small cell lung cancer. *Pharmacological reviews* **55**, 57-103, doi:10.1124/pr.55.1.4 (2003).
104 Hazra, S., Ort, S., Konrad, M. & Lavie, A. Structural and kinetic characterization of human deoxycytidine kinase variants able to phosphorylate 5-substituted deoxycytidine and thymidine analogues. *Biochemistry* **49**, 6784-6790, doi:10.1021/bi100839e (2010).
105 Sabini, E., Ort, S., Monnerjahn, C., Konrad, M. & Lavie, A. Structure of human dCK suggests strategies to improve anticancer and antiviral therapy. *Nature structural biology* **10**, 513-519, doi:10.1038/nsb942 (2003).
106 Gilbert, J. A. *et al.* Gemcitabine pharmacogenomics: cytidine deaminase and deoxycytidylate deaminase gene resequencing and functional genomics. *Clinical cancer research : an official journal of the American Association for Cancer Research* **12**, 1794-1803, doi:10.1158/1078-0432.CCR-05-1969 (2006).
107 Ciccolini, J., Mercier, C., Dahan, L. & Andre, N. Integrating pharmacogenetics into gemcitabine dosing--time for a change? *Nature reviews. Clinical oncology* **8**, 439-444, doi:10.1038/nrclinonc.2011.1 (2011).
108 Zhang, Y., Secrist, J. A., 3rd & Ealick, S. E. The structure of human deoxycytidine kinase in complex with clofarabine reveals key interactions for prodrug activation.

Acta crystallographica. Section D, Biological crystallography **62**, 133-139, doi:10.1107/S0907444905034293 (2006).

109 Guibe, F. Allylic protecting groups and their use in a complex environment - Part II: Allylic protecting groups and their removal through catalytic palladium pi-allyl methodology. *Tetrahedron* **54**, 2967-3042, doi:Doi 10.1016/S0040-4020(97)10383-0 (1998).

110 Trost, B. M. & VanVranken, D. L. Asymmetric transition metal-catalyzed allylic alkylations. *Chemical Reviews* **96**, 395-422 (1996).

111 Roos, E. C. *et al.* Palladium-Catalyzed Transprotection of Allyloxycarbonyl-Protected Amines - Efficient One-Pot Formation of Amides and Dipeptides. *Journal of Organic Chemistry* **60**, 1733-1740 (1995).

112 Santra, M., Ko, S. K., Shin, I. & Ahn, K. H. Fluorescent detection of palladium species with an O-propargylated fluorescein. *Chemical communications* **46**, 3964-3966, doi:10.1039/c001922d (2010).

113 Coleman, R. S. & Shah, J. A. Chemoselective cleavage of benzyl ethers, esters, and carbamates in the presence of other easily reducible groups. *Synthesis-Stuttgart*, 1399-1400 (1999).

114 Ramesh, R., Bhat, R. G. & Chandrasekaran, S. Highly Selective Deblocking of Propargyl Carbonates in the Presence of Propargyl Carbamates with Tetrathiomolybdate. *J. Org. Chem* **70**, 837-840 (2005).

115 Bielski, R. & Witczak, Z. Strategies for Coupling Molecular Units if Subsequent Decoupling Is Required. *Chem Rev* **113**, 2205-2243, doi:Doi 10.1021/Cr200338q (2013).

116 Papageorgiou, E. A., Gaunt, M. J., Yu, J. & Spencer, J. B. Selective Hydrogenolysis of Novel Benzyl Carbamate Protecting Groups. *Organic Letters* **2**, 1049-1051 (2000).

117 Liu, B. *et al.* A new ratiometric ESIPT sensor for detection of palladium species in aqueous solution. *Chemical communications* **48**, 2867-2869, doi:10.1039/c2cc17677g (2012).

118 Kuo, L. J. & Yang, L. γ-H2AX – A Novel Biomarker for DNA Double-strand Breaks. *In Vivo* **22**, 305-310 (2008).

119 Wallace, K. N. & Pack, M. Unique and conserved aspects of gut development in zebrafish. *Developmental Biology* **255**, 12-29, doi:10.1016/s0012-1606(02)00034-9 (2003).

120 Ng, A. N. *et al.* Formation of the digestive system in zebrafish: III. Intestinal epithelium morphogenesis. *Developmental Biology* **286**, 114-135, doi:10.1016/j.ydbio.2005.07.013 (2005).

121 Weissman, S. A. & Zewge, D. Recent advances in ether dealkylation. *Tetrahedron* **61**, 7833-7863, doi:10.1016/j.tet.2005.05.041 (2005).

122 Song, F., Garner, A.L., Koide, K. A Highly Sensitive Fluorescent Sensor for Palladium Based on the Allylic Oxidative Insertion Mechanism. *J. AM. CHEM. SOC.* **129**, 12354-12355 (2007).

123 Longley, D. B., Harkin, D. P. & Johnston, P. G. 5-fluorouracil: mechanisms of action and clinical strategies. *Nature reviews. Cancer* **3**, 330-338, doi:10.1038/nrc1074 (2003).

124 Kirk, K. L. Fluorination in Medicinal Chemistry: Methods, Strategies and Recent Developments *Organic Process Research & Development* **12**, 305-321 (2008).

125 Santi, D. V., McHenry, C. S. & Sommer, H. Mechanism of Interaction of Thymidylate Synthetase with 5-Fluorodeoxyuridylate. *Biochemistry* **13**, 471-481 (1974).

126 Kanamaru, R., Kakut, H., Sato, T., Ishioka, C. & Wakui, A. The Inhibitory Effects of 5-fluorouracil on the Metabolism of Preribosomal and ribosomal RNA in L-1210 cells in vitro. *Cancer Chemother Pharmacol* **17**, 43-46 (1986).
127 Santi, D. V. & Hardy, W. L. Catalytic Mechanism and Inhibition of tRNA (Uracil-5-)methyltransferase: Evidence of Covalent Catalysis. *Biochemistry* **26**, 8599-8606 (1987).
128 Doong, S.-L. & Dolnick, B. J. 5-Fluorouracil Substitution Alters Pre-mRNA Splicing in Vitro. *J. Biol. Chem.* **263**, 4467-4473 (1987).
129 Dobritzsch, D., Ricagno, S., Schneider, G., Schnackerz, K. D. & Lindqvist, Y. Crystal structure of the productive ternary complex of dihydropyrimidine dehydrogenase with NADPH and 5-iodouracil. Implications for mechanism of inhibition and electron transfer. *The Journal of Biological Chemistry* **277**, 13155-13166, doi:10.1074/jbc.M111877200 (2002).
130 Jang, Y. H., Sowers, L. C., Cagin, T. & Goddard III, W. A. First Principles Calculation of p*K*a Values of 5-Substituted Uracils. *J. Phys. Chem. A.* **105**, 274-280 (2001).
131 Kaleta, C., Figueiredo, L.F., Werner, S., Guthke, R., Ristow, M., Schuster, S.,. In Silico Evidence for Gluconeogenesis from Fatty Acids in Humans. *PLoS Computational Biology* **7**, 1-10, doi:10.1371/journal.pcbi.1002116.g001 (2011).
132 Spurrier, B., Ramalingam, S. & Nishizuka, S. Reverse-phase protein lysate microarrays for cell signaling analysis. *Nat Protoc* **3**, 1796-1808, doi:10.1038/nprot.2008.179 (2008).
133 O'Mahony, F. C. *et al.* The use of reverse phase protein arrays (RPPA) to explore protein expression variation within individual renal cell cancers. *J Vis Exp*, doi:10.3791/50221 (2013).
134 Levine, A. J. & Oren, M. The first 30 years of p53: growing ever more complex. *Nat Rev Cancer* **9**, 749-758, doi:10.1038/nrc2723 (2009).
135 Meek, D. W. Tumour suppression by p53: a role for the DNA damage response? *Nat Rev Cancer* **9**, 714-723, doi:10.1038/nrc2716 (2009).
136 De Angelis, P. M., Svendsrud, D. H., Kravik, K. L. & Stokke, T. Cellular response to 5-fluorouracil (5-FU) in 5-FU-resistant colon cancer cell lines during treatment and recovery. *Mol Cancer* **5**, 20, doi:10.1186/1476-4598-5-20 (2006).
137 Zhou, H. L., Li, X. M., Meinkoth, J. & Pittman, R. N. Akt regulates cell survival and apoptosis at a postmitochondrial level. *J Cell Biol* **151**, 483-494, doi:DOI 10.1083/jcb.151.3.483 (2000).
138 Ben-Sahra, I. *et al.* Sestrin2 integrates Akt and mTOR signaling to protect cells against energetic stress-induced death. *Cell Death Differ* **20**, 611-619, doi:Doi 10.1038/Cdd.2012.157 (2013).
139 Tannock, I. F. & Rotin, D. Acid Ph in Tumors and Its Potential for Therapeutic Exploitation. *Cancer Research* **49**, 4373-4384 (1989).
140 Xu, L., Fukumura, D. & Jain, R. K. Acidic extracellular pH induces vascular endothelial growth factor (VEGF) in human glioblastoma cells via ERK1/2 MAPK signaling pathway. Mechanism of low pH-induced VEGF (vol 277, pg 11368, 2002). *Journal of Biological Chemistry* **277**, 19242-19242 (2002).
141 Wikehooley, J. L., Haveman, J. & Reinhold, H. S. The Relevance of Tumor Ph to the Treatment of Malignant Disease. *Radiotherapy and Oncology* **2**, 343-366, doi:Doi 10.1016/S0167-8140(84)80077-8 (1984).
142 Creedon, H. *et al.* Exploring mechanisms of acquired resistance to human epidermal growth factor receptor 2 targeted therapies in breast cancer. *Biochem. Soc. Trans.* **(in press)** (2014).

143 van Laar, J. A. M., Rustum, Y. M., Ackland, S. P., van Groeningen, C. J. & Peters, G. J. Comparison of 5-fluoro-2 '-deoxyuridine with 5-fluorouracil and their role in the treatment of colorectal cancer. *Eur J Cancer* **34**, 296-306, doi:Doi 10.1016/S0959-8049(97)00366-3 (1998).
144 Tsume, Y. *et al.* Enhanced absorption and growth inhibition with amino acid monoester prodrugs of floxuridine by targeting hPEPT1 transporters. *Molecules* **13**, 1441-1454 (2008).
145 Galmarini, C. M., Mackey, J. R. & Dumontet, C. Nucleoside analogues and nucleobases in cancer treatment. *Lancet Oncol* **3**, 415-424 (2002).
146 Power, D. G. & Kemeny, N. E. The role of floxuridine in metastatic liver disease. *Mol Cancer Ther* **8**, 1015-1025, doi:10.1158/1535-7163.MCT-08-0709 (2009).
147 Willmore, E. & Durkacz, B. W. Cytotoxic mechanisms of 5-fluoropyrimidines. Relationships with poly(ADP-ribose) polymerase activity, DNA strand breakage and incorporation into nucleic acids. *Biochem Pharmacol* **46**, 205-211 (1993).
148 Yin, M. B. & Rustum, Y. M. Comparative DNA strand breakage induced by FUra and FdUrd in human ileocecal adenocarcinoma (HCT-8) cells: relevance to cell growth inhibition. *Cancer Commun* **3**, 45-51 (1991).
149 Ensminger, W. D. *et al.* A clinical-pharmacological evaluation of hepatic arterial infusions of 5-fluoro-2'-deoxyuridine and 5-fluorouracil. *Cancer Research* **38**, 3784-3792 (1978).
150 Creaven, P. J. *et al.* Phase I and pharmacokinetic evaluation of floxuridine/leucovorin given on the Roswell Park weekly regimen. *Cancer chemotherapy and pharmacology* **34**, 261-265 (1994).
151 von Roemeling, R. & Hrushesky, W. J. Determination of the therapeutic index of floxuridine by its circadian infusion pattern. *J Natl Cancer Inst* **82**, 386-393 (1990).
152 Tobias, S. C. & Borch, R. F. Synthesis and biological studies of novel nucleoside phosphoramidate prodrugs. *J Med Chem* **44**, 4475-4480 (2001).
153 Tanabe, K. *et al.* One-electron reduction characteristics of N(3)-substituted 5-fluorodeoxyuridines synthesized as radiation-activated prodrugs. *Bioorg Med Chem* **11**, 4551-4556 (2003).
154 Tanabe, K., Makimura, Y., Tachi, Y., Imagawa-Sato, A. & Nishimoto, S. Hypoxia-selective activation of 5-fluorodeoxyuridine prodrug possessing indolequinone structure: radiolytic reduction and cytotoxicity characteristics. *Bioorg Med Chem Lett* **15**, 2321-2324, doi:10.1016/j.bmcl.2005.03.013 (2005).
155 Tanabe, K., Ishizaki, J., Ando, Y., Ito, T. & Nishimoto, S. Reductive activation of 5-fluorodeoxyuridine prodrug possessing azide methyl group by hypoxic X-irradiation. *Bioorg Med Chem Lett* **22**, 1682-1685, doi:10.1016/j.bmcl.2011.12.106 (2012).
156 Tanabe, K., Sugiura, M., Ito, T. & Nishimoto, S. Synthesis and one-electron reduction characteristics of radiation-activated prodrugs possessing two 5-fluorodeoxyuridine units. *Bioorg Med Chem* **20**, 5164-5168, doi:10.1016/j.bmc.2012.07.008 (2012).
157 Wilson, W. R. & Hay, M. P. Targeting hypoxia in cancer therapy. *Nat Rev Cancer* **11**, 393-410, doi:10.1038/nrc3064 (2011).
158 Brown, J. M. & Wilson, W. R. Exploiting tumour hypoxia in cancer treatment. *Nat Rev Cancer* **4**, 437-447, doi:10.1038/nrc1367 (2004).
159 Nordsmark, M., Overgaard, M. & Overgaard, J. Pretreatment oxygenation predicts radiation response in advanced squamous cell carcinoma of the head and neck. *Radiother Oncol* **41**, 31-39 (1996).
160 Gabbert, H., Wagner, R. & Hohn, P. The relation between tumor cell proliferation and vascularization in differentiated and undifferentiated colon carcinomas in the rat. *Virchows Arch B Cell Pathol Incl Mol Pathol* **41**, 119-131 (1982).

161 Comerford, K. M. *et al.* Hypoxia-inducible factor-1-dependent regulation of the multidrug resistance (MDR1) gene. *Cancer Research* **62**, 3387-3394 (2002).
162 Zeman, E. M., Brown, J. M., Lemmon, M. J., Hirst, V. K. & Lee, W. W. SR-4233: a new bioreductive agent with high selective toxicity for hypoxic mammalian cells. *Int J Radiat Oncol Biol Phys* **12**, 1239-1242 (1986).
163 Patterson, L. H. Bioreductively activated antitumor N-oxides: the case of AQ4N, a unique approach to hypoxia-activated cancer chemotherapy. *Drug Metab Rev* **34**, 581-592, doi:10.1081/DMR-120005659 (2002).
164 Zhang, X., Lin, Y. & Gillies, R. J. Tumor pH and its measurement. *J Nucl Med* **51**, 1167-1170, doi:10.2967/jnumed.109.068981 (2010).
165 Malhotra, V. & Perry, M. C. Classical chemotherapy: mechanisms, toxicities and the therapeutic window. *Cancer biology & therapy* **2**, S2-4 (2003).
166 Raschi, E. *et al.* Anticancer drugs and cardiotoxicity: Insights and perspectives in the era of targeted therapy. *Pharmacology & therapeutics* **125**, 196-218, doi:10.1016/j.pharmthera.2009.10.002 (2010).
167 Sawyers, C. L. The cancer biomarker problem. *Nature* **452**, 548-552, doi:10.1038/nature06913 (2008).
168 Hopkins, A. L. Network pharmacology: the next paradigm in drug discovery. *Nature chemical biology* **4**, 682-690, doi:10.1038/nchembio.118 (2008).
169 Wataha, J. C., Hanks, C. T. & Craig, R. G. The in vitro effects of metal cations on eukaryotic cell metabolism. *J Biomed Mater Res* **25**, 1133-1149, doi:10.1002/jbm.820250907 (1991).
170 Wataha, J. C., Hanks, C. T. & Sun, Z. In vitro reaction of macrophages to metal ions from dental biomaterials. *Dent Mater* **11**, 239-245, doi:10.1016/0109-5641(95)80056-5 (1995).
171 Li, H., Fan, J. & Peng, X. Colourimetric and fluorescent probes for the optical detection of palladium ions. *Chem Soc Rev* **42**, 7943-7962, doi:10.1039/c3cs60123d (2013).
172 Sanchez, M. I., Penas, C., Vazquez, M. E. & Mascarenas, J. L. Metal-catalyzed uncaging of DNA-binding agents in living cells. *Chemical Science* **2014**, 1901-1907 (2014).
173 Wang, Z. *et al.* Fluorescent artificial enzyme-linked immunoassay system based on Pd/C nanocatalyst and fluorescent chemodosimeter. *Anal Chem* **85**, 11602-11609, doi:10.1021/ac403001y (2013).
174 Sasmal, P. K., Carregal-Romero, S., Parak, W. J. & Meggers, E. Light-Triggered Ruthenium-Catalyzed Allylcarbamate Cleavage in Biological Environments. *Organometallics* **31**, 5968-5970, doi:Doi 10.1021/Om3001668 (2012).
175 Wang, J. Y., Song, F. L., Wang, J. Y. & Peng, X. J. A near-infrared and ratiometric fluorescent chemosensor for palladium. *Analyst* **138**, 3667-3672, doi:Doi 10.1039/C3an00616f (2013).
176 Diasio, R. B. & Harris, B. E. Clinical pharmacology of 5-fluorouracil. *Clin Pharmacokinet* **16**, 215-237, doi:10.2165/00003088-198916040-00002 (1989).
177 Birnie, G. D., Kroeger, H. & Heidelberger, C. Studies of Fluorinated Pyrimidines. Xviii. The Degradation of 5-Fluoro-2'-Deoxyuridine and Related Compounds by Nucleoside Phosphorylase. *Biochemistry* **2**, 566-572 (1963).
178 Zawilska, J. B., Wojcieszak, J. & Olejniczak, A. B. Prodrugs: a challenge for the drug development. *Pharmacol Rep* **65**, 1-14 (2013).

APPENDIX

nature COMMUNICATIONS

ARTICLE

Received 13 Jul 2013 | Accepted 17 Jan 2014 | Published 13 Feb 2014

DOI: 10.1038/ncomms4277 OPEN

Extracellular palladium-catalysed dealkylation of 5-fluoro-1-propargyl-uracil as a bioorthogonally activated prodrug approach

Jason T. Weiss[1], John C. Dawson[1], Kenneth G. Macleod[1], Witold Rybski[1,2], Craig Fraser[1], Carmen Torres-Sánchez[3], E. Elizabeth Patton[1,2], Mark Bradley[4], Neil O. Carragher[1] & Asier Unciti-Broceta[1]

A bioorthogonal organometallic reaction is a biocompatible transformation undergone by a synthetic material exclusively through the mediation of a non-biotic metal source; a selective process used to label biomolecules and activate probes in biological environs. Here we report the *in vitro* bioorthogonal generation of 5-fluorouracil from a biologically inert precursor by heterogeneous Pd^0 catalysis. Although independently harmless, combined treatment of 5-fluoro-1-propargyl-uracil and Pd^0-functionalized resins exhibits comparable antiproliferative properties to the unmodified drug in colorectal and pancreatic cancer cells. Live-cell imaging and immunoassay studies demonstrate that the cytotoxic activity of the prodrug/Pd^0-resin combination is due to the *in situ* generation of 5-fluorouracil. Pd^0-resins can be carefully implanted in the yolk sac of zebrafish embryos and display excellent biocompatibility and local catalytic activity. The *in vitro* efficacy shown by this masking/activation strategy underlines its potential to develop a bioorthogonally activated prodrug approach and supports further *in vivo* investigations.

[1] Edinburgh Cancer Research UK Centre, MRC Institute of Genetics and Molecular Medicine, University of Edinburgh, Crewe Road South, Edinburgh EH4 2XR, UK. [2] MRC Human Genetics Unit, MRC Institute of Genetics and Molecular Medicine, University of Edinburgh, Crewe Road South, Edinburgh EH4 2XR, UK. [3] Wolfson School of Mechanical and Manufacturing Engineering, Loughborough University, Loughborough LE11 3TU, UK. [4] School of Chemistry, University of Edinburgh, West Mains Road, Edinburgh EH9 3JJ, UK. Correspondence and requests for materials should be addressed to M.B. (email: Mark.Bradley@ed.ac.uk) or to A.U.-B. (email: Asier.Unciti-Broceta@igmm.ed.ac.uk).

© 2014 Macmillan Publishers Limited. All rights reserved.

Bertozzi's landmark works in the early 2000s (refs 1,2) demonstrated that artificial chemistry and biological chemistry can take place within the same physical space, yet do not interfere with each other. Through the development of labelling strategies based on the chemospecific conjugation of two biologically-inert reactive partners, this revolutionary chemical paradigm—so-called bioorthogonal chemistry—has enabled the non-intrusive real-time study of a wide range of biomolecules in their native environs[3,4]. Because of the exclusive nature of the bioorthogonal concept, the range of chemical reactions that meets its requirements has been limited in practice to the Staudinger ligation[1] and cycloadditions between spring-loaded reactive partners (metal-free click chemistry[2–4]). Nevertheless, the bioorthogonal concept may integrate additional bio-independent chemical processes that are promoted by abiotic activators such as biocompatible electromagnetic radiations[5–7] and non-biological transition metals[8,9].

Although the application of transition metals in medicine have been investigated for many centuries, its use to mediate chemoselective transformations in cells—for example, bioorthogonal organometallic (BOOM) reactions[8]—is a recent addition to the chemical biology field[8–14]. In 2006, Streu and Meggers[10] described the first application of a ruthenium catalyst to carry out Alloc deprotection of a caged fluorophore inside human cells. The aim to minimize the inherent toxicity of the catalyst motivated the Bradley group to investigate heterogeneous catalysis to mediate palladium chemistry inside cells. Pd^0-functionalized microspheres operated as a dual catalytic/cell delivery system able to enter cells *in vitro* and catalyse allylcarbamate cleavage and Suzuki-Miyaura cross-coupling in the cytoplasm without cytotoxicity[9,11]. Notable examples of palladium-based applications in cell culture includes copper-free Sonogashira coupling of an alkyne-encoded cytoplasmic ubiquitin protein[12], extracellular Suzuki reaction to label *Escherichia coli* cell surface components[13] and the detection of intracellular CO based on the reactivity of a cyclopalladated probe towards carbonylation[14].

Owing to its biological inertness, metallic Pd^0 shows the safest toxicity profile among all palladium species[15] and is frequently used in metal alloys for dental restoration[16]. Based on the unique catalytic properties and biocompatibility of this metal, we hypothesized that extracellular heterogeneous catalysis mediated by a palladium-functionalized implant could enable the chemospecific conversion of a systemically administered prodrug into its active form in a spatially controlled manner. As opposed to biolabile prodrugs, whose activation process relies on metabolic pathways[17], an efficient palladium-activated prodrug therapy would be entirely dependent on the distinct catalytic properties of this transition metal and therefore the prodrug would remain intact in the absence of a palladium source. By intratumoural implantation of a metal-functionalized device, palladium-labile prodrugs would be exclusively activated within the cancerous tissue. Locoregional generation of cytotoxic agents would enable increasing dosing while reducing adverse side effects in distant tissues and organs, an optimal strategy to treat advanced tumours that cannot be resected by surgery. Notably, this spatially targeted approach would serve to expand the therapeutic window and scope of potent cytotoxic drugs such as 5-fluorouracil (5FU), which has a long history in oncology practice but a clinical activity limited by its safety profile[18].

5FU is converted intracellularly into cytotoxic nucleotidic metabolites via functionalization on its *N*1 position. Its active metabolites either inhibit directly thymidylate synthase or become incorporated into RNA and DNA molecules to disrupt normal cell functions (Fig. 1)[19]. Based on this mode of action, modification of the *N*1 position of 5FU with biochemically stable groups would hinder its intracellular activation and result in a significant loss of cytotoxic activity. Here we report the introduction of allyl, propargyl and benzyl moieties at the *N*1 position of 5FU as a means to minimize prodrug's susceptibility to cleavage by hydrolytic enzymes, while, at the same time, rendering them potentially sensitive to palladium catalysis. These alkyl functional groups have been widely used in organic

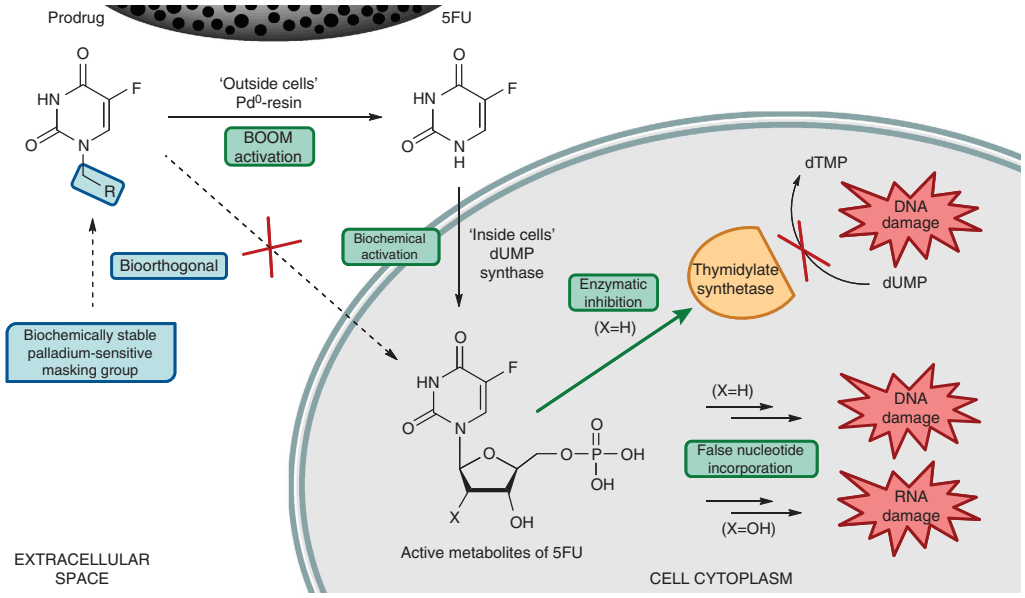

Figure 1 | Bioorthogonally activated prodrug strategy and toxigenic mode of action. Chemical masking of the *N*1 position of 5-fluorouracil (5FU) with a biochemically inert palladium-sensitive group would impede 5FU intracellular activation and, consequently, prevent its pharmacological activity. Such a prodrug will be selectively converted into 5FU by the catalysis of Pd^0, for instance, in the affected area, organ or tissue where a Pd^0-functionalized device has been surgically implanted, thus inducing a local treatment of the disease and reducing side effects of drug in distant tissues and organs. dTMP, thymidine monophosphate; dUMP, deoxyuridine monophosphate.

© 2014 Macmillan Publishers Limited. All rights reserved.

synthesis as OH protection strategies[20] and, importantly, recent studies have shown the sensitivity of allyl and propargyl phenolic ethers to oxidative cleavage by palladium species in biocompatible conditions[21–23]. Although palladium-mediated *N*-dealkylations typically require temperatures incompatible with cell survival (>80 °C)[24–26], we hypothesized that the particular features of the 5FU heterocyclic system (relatively low pK_a values because of the charge delocalization of 5FU aromatic conjugate bases[27], Supplementary Fig. 1a) could promote its properties as a leaving group relative to more basic amino groups.

To activate prodrugs in the extracellular space, we investigate the application of a robust heterogeneous catalytic system based on Pd^0-functionalized polyethylene glycol (PEG)-polystyrene resins[28] (Pd^0-resins) that are larger than human cells (150 μm in diameter). As previously reported[9,11], Pd^0 nanoparticles display high catalytic activity, can be readily generated and trapped in an amino-functionalized polymer matrix, and are safe for biological applications. Our results show that alkylation of the *N*1 position of 5FU suppresses the drug's cytotoxic properties and exhibits full stability in cell culture. Remarkably, the propargyl derivative (5-fluoro-1-propargyl-uracil (Pro-5FU)) displays high sensitivity to Pd^0-mediated heterogeneous catalysis, thus allowing the bioorthogonal generation of 5FU under biocompatible conditions (37 °C, isotonic media and physiologic pH). Although independently harmless, combined treatment of Pro-5FU and Pd^0-resins exhibits equivalent antiproliferative properties to unmodified 5FU in colorectal and pancreatic cancer cells, underlining the *in vitro* efficacy of this unprecedented masking/activation strategy.

Results

Preparation of Pd^0-resins and 5FU prodrugs. Pd^0-resins (Fig. 2a,b) were prepared from NovaSyn TG amino resin HL using the procedure developed in the Bradley group[28] with minor modifications. Transmission electron microscope images showed dark nanoparticles (5 nm) regularly distributed across the resins (Fig. 2b), whereas the powder X-ray diffraction spectra presented the distinctive pattern of the face-centred cubic lattice of Pd^0 (Supplementary Fig. 1b). Pd^0-resins were visibly differentiated from non-functionalized resins (naked resins) because of the dark colour of the former (Supplementary Fig. 1c). Palladium content was determined to be 2.83% (w/w) by inductively coupled plasma-optical emission spectrometry.

1-Allyl-5FU (All-5FU), Pro-5FU and 1-benzyl-5FU (Bn-5FU; Fig. 2c) were synthesized in a single step by reaction of 5FU with the corresponding alkyl bromide in the presence of 1,8-diazabicyclo[5.4.0]undec-7-ene. *N*-propargyl-2-pyridone (**1a**) and *N*-propargyl-4-pyridone (**1b**) were synthesized following the same procedure (Supplementary Methods).

Cell-free Pd^0-mediated prodrug-into-drug conversion. To recreate a biocompatible scenario, reactions were carried out at 37 °C in an isotonic solution with a physiologic pH. Prodrugs (100 μM) and Pd^0-resins (1 mg ml^{-1}, [Pd^0] = 266 μM) were dispersed in PBS, incubated for 6–48 h and analysed by high-performance liquid chromatography (HPLC). Figure 2d shows Pro-5FU completely disappeared from the crude mixture after 24 h, with 5FU being the major reaction product. In accordance with previous observations[26], mass spectrometry analysis of the reaction crude indicated the formation of nontoxic 1-hydroxyacetone—a natural lipid metabolite also known as acetol[29]—as a byproduct from the oxidative cleavage of the propargyl group (Supplementary Fig. 2a,b). In contrast, conversion analysis of All-5FU and Bn-5FU did not show substantial levels of 5FU after 48 h (Supplementary Fig. 3a).

N-Depropargylation of Pro-5FU using sub-stoichiometric amounts of Pd^0 confirmed the catalytic nature of the reaction, albeit 72 h were required to achieve completion (Supplementary Fig. 3b). To determine whether Pro-5FU dealkylation is mediated by heterogeneous catalysis, Pd^0-resins were incubated in PBS at 37 °C for 24 h, micro-filtered to eliminate solid contents and Pro-5FU added to the solid-free solution for additional 24 h incubation. HPLC analysis detected unreacted Pro-5FU as major mixture component and relatively small quantities of 5FU (Supplementary Fig. 3c), indicating that Pd^0 is in part released from the resins into the solution, although this amount contributes

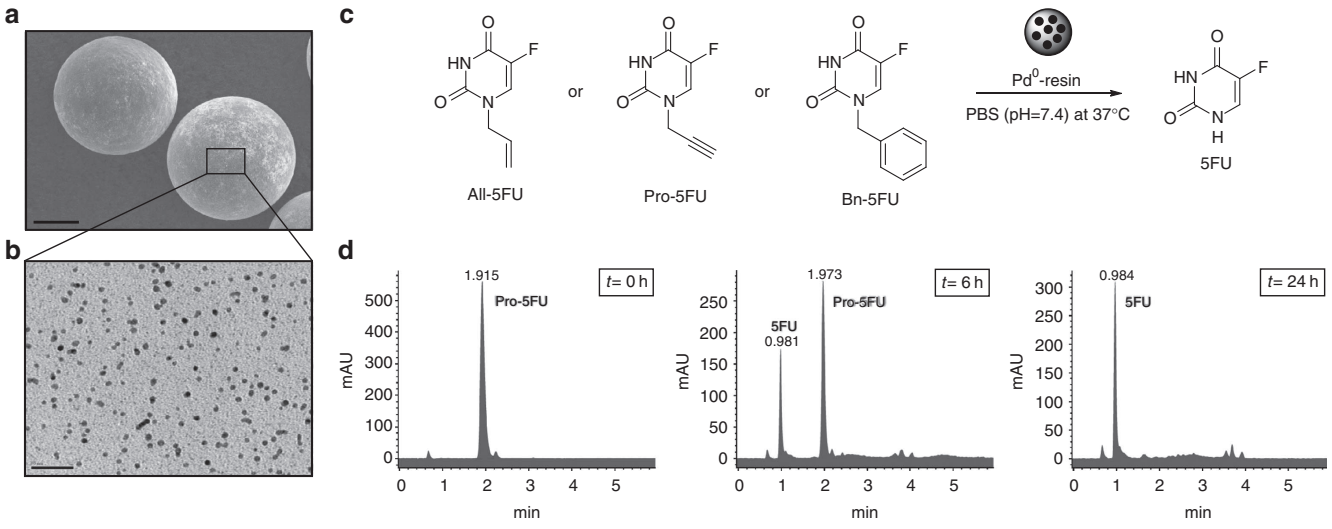

Figure 2 | Pd^0-mediated prodrug-into-drug conversion assays in biocompatible environment. (**a**) Scanning electron microscope image of Pd^0-resins at approximately 200 magnification. Scale bar, 50 μm. (**b**) Transmission electron microscope image of a Pd^0-resin cross-section at approximately 190,000 magnification. Scale bar, 50 nm. (**c**) Pd^0-mediated dealkylation of 5-fluorouracil (5FU) prodrugs under biocompatible conditions (37 °C, isotonic media and physiologic pH). (**d**) Representative HPLC traces of Pd^0-mediated conversion of Pro-5FU into 5FU. Reaction crudes were analysed using an ultraviolet detector (280 nm) at $t = 0$ h, $t = 6$ h and $t = 24$ h. Conversion studies were performed in triplicate. All-5FU, 1-allyl-5FU; Bn-5FU, 1-benzyl-5FU; Pro-5FU, 5-fluoro-1-propargyl-uracil.

© 2014 Macmillan Publishers Limited. All rights reserved.

minimally to the reaction catalysis. Treatment of two additional *N*-propargylated heterocycles, *N*-propargyl-2-pyridone (**1a**) and *N*-propargyl-4-pyridone (**1b**), under the same conditions afforded the dealkylated derivatives in 24 h (Supplementary Fig. 3d).

Pro-5FU bioorthogonality. Based on the primary malignancies against which 5FU is currently prescribed[18,19], colorectal HCT116 and pancreatic BxPC-3 cancer cell lines were chosen as models for antiproliferative and mechanism-of-action studies. To evaluate the efficacy of the masking strategy in suppressing 5FU cytotoxic properties, dose response studies were carried out with unmodified drug and Pro-5FU (0.01 μM to 1 mM). Cell viability was determined at day 5 using PrestoBlue reagent and analysed by spectrofluorometry to calculate EC_{50} (5FU) values of 2 and 0.14 μM for HCT116 and BxPC-3 cells, respectively (Supplementary Fig. 4a,b). Notably, Pro-5FU displayed no cytotoxicity at any concentration used (EC_{50} [Pro-5FU]/EC_{50} [5FU] > 500), proving the effectiveness of the deactivation strategy. To test whether Pro-5FU could be biotransformed into 5FU in cells with higher metabolic capacity, cell viability assays were carried out in liver HepG2 cells[30]. As shown in Supplementary Fig. 4c, although 5FU was significantly cytotoxic at low micromolar concentration (EC_{50} = 1.4 μM), Pro-5FU did not exhibit a toxic effect (EC_{50} > 1 mM), illustrating the high biochemical stability of the propargyl group to enzymatic cleavage.

Because of the close structural similarities between Pro-5FU and 5FU, it was considered that the prodrug could function as a competitive inhibitor of the enzymatic routes followed by 5FU to generate its cytotoxic metabolites. This potential drawback of the prodrug strategy was ruled out by incubating 5FU with increasing concentrations of Pro-5FU up to a prodrug/drug ratio of 100:1, which exhibited no antagonistic effect (Supplementary Fig. 5a,b). In addition, dose response studies of 1-hydroxyacetone (main reaction byproduct) with HCT116 and BxPC-3 cancer cell lines showed no effect in cell viability (Supplementary Fig. 5c,d).

Antiproliferative effect of Pro-5FU/Pd^0-resin combination. After assessing the catalyst concentration range tolerated by cells and optimal for catalysis (Supplementary Fig. 6), 1 mg ml^{-1} (for HCT116) and 0.66 mg ml^{-1} (for BxPC-3) of Pd^0-resins were used for the biological assays. Preliminary cell screening of palladium-mediated generation of 5FU from the three prodrugs confirmed that Pro-5FU/Pd^0-resin combination was effective in producing a strong toxigenic effect (Supplementary Fig. 7a,b). Hence, a range of concentrations of Pro-5FU and Pd^0-resins was incubated independently (negative controls) and in combination (BOOM conversion assay) to study cell proliferation in comparison to unmodified 5FU (positive control). As observed in Fig. 3a,b, the toxigenic effect generated by the prodrug/catalyst combination was comparable to 5FU cytotoxicity, exhibiting similar EC_{50} values (Supplementary Fig. 7c,d). Independently incubated, neither the prodrug nor the palladium source exhibited antiproliferative activity.

Cytotoxic mode of action of Pro-5FU/Pd^0-resin combination. To study the phenotypic effect of the prodrug/catalyst system compared with 5FU, cell proliferation was monitored in real-time using an IncuCyte ZOOM microscope, which allows quantification of cell confluence as a function of time by image-based analysis. As shown in Fig. 3c,d, negative controls exhibited a standard growth curve, whereas the proliferation of cells treated with 5FU rapidly decreased after a few hours. Growth curves of HCT116 cells incubated with the Pd^0-resin/Pro-5FU combination showed two distinct phases: a regular increment for 24 h followed by a drastic fall to reach cytotoxic levels comparable to 5FU at day 5. In the case of BxPC-3 cells, population curves of cells incubated with either 5FU or the Pd^0-resin/Pro-5FU combination showed similar bell-shaped growth curves. As observed in Fig. 3e,f and Supplementary Movies 1 and 2, treatment-induced changes in cell morphology indicate analogous antiproliferative/cell death induction between 5FU and the prodrug/catalyst system.

To study these phenotypic responses at the molecular level, total expression and post-translational modifications of cancer relevant pathways were quantified using Zeptosens Reverse Phase Protein Microarray analysis[31]. Supplementary Fig. 8a shows that total and phosphorylated p53 (Ser15) were significantly upregulated in HCT116 cells at 24 h following exposure to Pro-5FU/Pd^0-resin combination, which correlates with the response observed under 5FU treatment and the DNA damage response mechanism expected from this drug[32]. In contrast, no induction was observed in cells treated with either Pro-5FU or Pd^0-resin on their own. These observations were corroborated by western blotting (Supplementary Fig. 9).

Pd^0-Resin biocompatibility and catalytic activity in zebrafish. The biocompatibility of the palladium-functionalized device *in vivo* was investigated by carefully introducing a single Pd^0-resin in the yolk sac of zebrafish embryos 24 h after fertilization and monitoring their early development by phase contrast microscopy. As shown in Fig. 4a, zebrafish embryos containing a Pd^0-resin (indicated with a red arrow) developed normally into the larval stage with no signs of toxicity or alteration of phenotype.

To study the catalytic functionality of the Pd^0-resins in the zebrafish yolk, palladium-sensitive pro-fluorophore **3** (Fig. 4b) was prepared and incubated with zebrafish embryos containing either a non-functionalized resin (naked resin) or a Pd^0-resin for 24 h. *N*,*N*′-bis(propargyloxycarbonyl)-protected rhodamine 110 (**3**) was synthesized from rhodamine 110 chloride by reaction with propargyl chloroformate and triethylamine in dry dimethylformamide (DMF). The enhanced lipophilic properties of non-fluorescent probe **3** facilitated its diffusion across biological barriers. On the contrary, highly fluorescent rhodamine 110 generated upon propargylcarbamate cleavage was trapped in the physiological compartment where it was produced because of its high hydrophilicity, thus enabling the imaging of localized palladium-mediated catalysis[8,10,11]. As shown in Fig. 4c, a strong fluorescent signal was clearly observed from the area surrounding the Pd^0-resin in the yolk sac (lower panel), confirming that the palladium-functionalized device is catalytically active *in vivo*. Concurrently, a strong fluorescent signal was also observed from the gastrointestinal system[33,34] in fish incubated with pro-fluorophore **3** regardless of the presence or absence of Pd^0-resin (Fig. 4c, pointed with white arrow heads, and Supplementary Fig. 10), suggesting that the *N*-propargyloxycarbonyl (*N*-Poc) group is biochemically cleaved by digestive enzymes. Although compound **3** exhibited high sensitivity to palladium catalysis, it also displayed low chemical stability in the digestive system, indicating that *N*-Poc masked prodrugs could not be used via oral administration in a bioorthogonal strategy.

Discussion

For more than a decade[1–3], the concept of bioorthogonal chemistry (understood as performing chemical reactions by artificial biologically inert means under biocompatible conditions) has inspired the search for novel biocompatible organic reactions and found a niche application as a labelling strategy to study biomolecules in their native state[1–5,35]. Indeed, bioorthogonal reactions have become particularly useful to study biological small molecules and macromolecules that cannot be

© 2014 Macmillan Publishers Limited. All rights reserved.

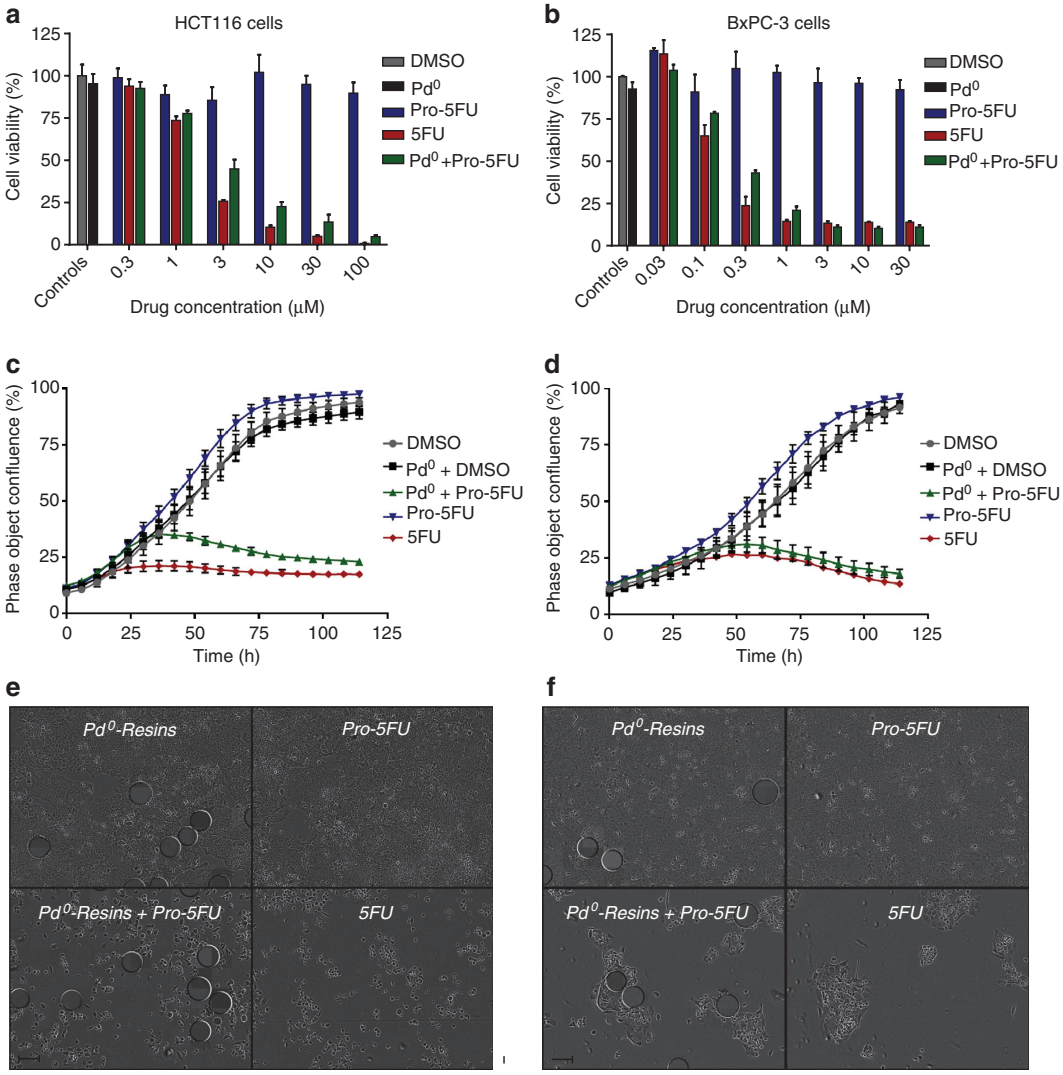

Figure 3 | Bioorthogonal generation of 5FU in cancer cell culture. Experiments: 0.1% (v/v) dimethylsulphoxide (DMSO, untreated cell control; in grey), Pd^0-resins (negative control; in black); 0.01–100 μM of 5-fluoro-1-propargyl-uracil (Pro-5FU; negative controls; in blue); 0.01–100 μM of 5FU (positive controls; in red) and Pd^0-resins + Pro-5FU (bioorthogonal organometallic conversion assay; in green). HCT116 and BxPC-3 cell studies are shown at the left and right side of the figure, respectively. Error bars represent ± standard deviation from $n = 3$. (**a**,**b**) Dose response study of cell viability after 5 days of treatment. (**c**,**d**) Real-time cell confluence study. Cell population was monitored for 5 days (120 h) using an IncuCyte ZOOM system in an incubator (5% CO_2, 37 °C). Drug/prodrug concentrations: 100 μM, for HCT116 cells, and 30 μM, for BxPC-3 cells. (**e**,**f**) Phase-contrast images of cells after 4 days of treatment (96 h). Scale bar, 150 μm. Pd^0-resins are identified as spheres of 150 μm (average diameter).

monitored by genetically encoded reporters or antibodies (for example, lipids, glycans, and so on) both in cells and *in vivo*[4,35]. Although metal-free bioorthogonal reactions are considered optimal for living systems because of their biocompatibility, significant progress has been made in recent years in the development of cell-tolerated BOOM reactions[8–14,35,36], opening up new avenues for the exploitation of the bioorthogonal paradigm. However, the potential of such selective processes in medicine is yet to be determined. Within an inclusive notion of bioorthogonality[5], the clinical potential of bioorthogonal processes has only been explored to date with the photoinduced generation of cytotoxic reactive oxygen species through the use of a harmless visible light source and a non-toxic photosensitizer, which has become a valuable therapeutic option for local treatment of disease (so-called photodynamic therapy[37]).

In this line of reasoning, here we report a novel palladium-mediated *N*-dealkylation that takes place under biocompatible conditions and its application beyond the current scope of BOOM reactions: a highly efficient masking method that achieves complete elimination of 5FU cytotoxic activity, while enabling the bioorthogonal restoration of the drug's pharmacological properties by heterogeneous palladium chemistry in cell culture.

In accordance with 5FU mode of action (Fig. 1), modification of its *N*1 position with each of the three alkyl groups investigated (allyl, propargyl and benzyl; Fig. 2c) generates harmless prodrugs (Supplementary Fig. 7a,b), which demonstrates the low susceptibility of alkyl groups to cleavage by hydrolytic enzymes. However, under biocompatible conditions, only the propargyl group displays high sensitivity to Pd^0-resins, thereby allowing the palladium-catalysed N-dealkylation of Pro-5FU at 37°C in PBS (isotonic, aqueous solution buffered at pH = 7.4) within 24 h. Although the high stability of the benzyl moiety was anticipated because of the lack of an additional hydrogen source[20], the drastic difference in Pd^0 sensitivity between Pro-5FU and All-5FU suggests that electronic and/or conformational aspects are critical

© 2014 Macmillan Publishers Limited. All rights reserved.

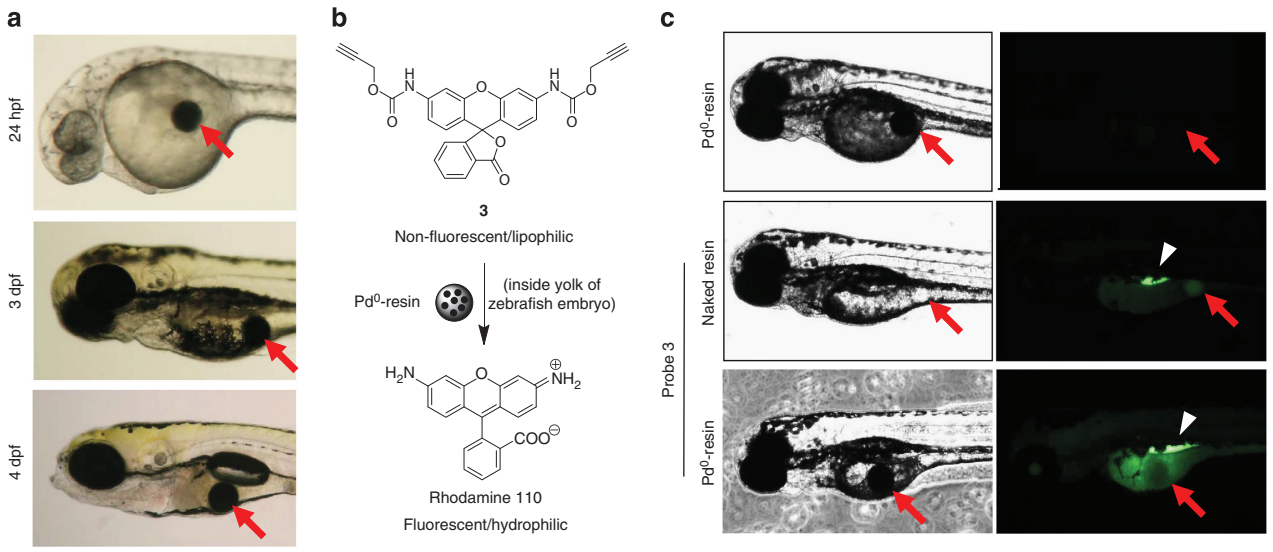

Figure 4 | Biocompatibility and catalytic activity of Pd^0-resins in zebrafish embryos. (**a**) Images of a zebrafish embryo containing a Pd^0-resin (red arrow) in the yolk sac at different stages of development. Twenty-four hours after fertilization (24 h.p.f.), a Pd^0-resin was implanted in each embryo yolk ($n=5$), incubated at 28 °C and fish monitored for 4 days. Fish were imaged at 24 h.p.f., 3 days post fertilization (3 d.p.f.) and 4 d.p.f. (**b**) Palladium-mediated conversion of non-fluorescent lipophilic compound **3** into highly fluorescent hydrophilic rhodamine 110. (**c**) *In vivo* carbamate cleavage of compound **3**. One day after implantation, zebrafish embryos ($n=5$) containing a Pd^0-resin (black colour) or a naked resin (white colour) in the yolk sac were incubated with compound **3** (5 μM) for 24 h at 31 °C. Subsequently, fish were imaged using confocal microscopy (Ex/Em: 488/521 nm). Pd^0-resins and naked resin are indicated with red arrows. Fluorescently labelled gastrointestinal tract is indicated with a white arrow head.

for efficient metal coordination and cleavage (Supplementary Fig. 2a). To briefly examine the potential scope of the *N*-depropargylation process, *N*-propargyl-2-pyridone (**1a**) and *N*-propargyl-4-pyridone (**1b**) were synthesized and treated under the same conditions as Pro-5FU (Supplementary Fig. 3d). Dealkylated products were obtained within 24 h, indicating that this environmentally friendly methodology could be translated to other heterocyclic systems with lactam/lactim tautomery. Because of its implications for the bioorthogonal use of this novel masking/activation strategy, it is important to highlight that the palladium-mediated oxidative cleavage of the *N*-propargyl group in aqueous media results in the formation of non-toxic 1-hydroxyacetone[26] (Supplementary Fig. 2b). The generation of this natural compound[29] would minimize any local off-target effects caused by side products originated from the activation process itself.

Our results show that, at the concentrations tested, neither the prodrug nor the palladium source exhibits antiproliferative activity in any of the cancer cell lines (Fig. 3), thus validating the *in vitro* bioorthogonality of the materials. In contrast, the combined use of Pro-5FU and Pd^0-resins led to a toxigenic effect comparable to 5FU antiproliferative activity, which demonstrates the *in situ* generation of 5FU. A variance in cytotoxicity was observed at several doses (Fig. 3a,b), which may be due to the time lag required for the BOOM reaction to take place and produce cytotoxic levels of drug. This difference was not significant in BxPC-3 cells at Pro-5FU doses higher than 1 μM (Fig. 3b), indicating that cytotoxic levels for this sensitive cell line are rapidly generated.

Monitoring of HCT116 cell proliferation by time-lapse imaging allowed visualizing the slower antiproliferative effect led by the Pro-5FU/Pd^0-resins combination (BOOM conversion assay) in comparison to unmodified 5FU (Fig. 3c). This result is in accordance with the time delay required to generate cytotoxic levels of drug for this cell line. Owing to the higher sensitivity of BxPC-3 cells to 5FU, both drug and the prodrug/catalyst combination experiments showed comparable bell-shaped population curves (Fig. 3d). In agreement with these observations, our immunoassay studies shows an analogous cell death induction mechanism between 5FU and the prodrug/catalyst system, corroborating that the cytotoxic activity generated by the prodrug/Pd^0-resin combination is due to the BOOM synthesis of 5FU in cell culture.

In conclusion, the development of a biochemically resistant palladium-labile 5FU precursor and an extracellular Pd^0-functionalized device enabled the *in vitro* bioorthogonal transformation of a biologically inert substance into a cytotoxic agent. Although this novel prodrug strategy is yet to be tested in disease models *in vivo*, the robustness of the masking strategy, the biocompatibility of the dealkylation conditions and the innocuous reaction byproduct (natural product 1-hydroxyacetone[26,29]) underline the therapeutic potential of this novel masking/activation approach. Finally, the biocompatibility and local catalytic activity exhibited by the Pd^0-resin implanted within the zebrafish yolk supports the development of more comprehensive *in vivo* pharmacodynamics, pharmacokinetics and toxicity investigations in order to study the applicability and potential benefits of implementing a bioorthogonally activated prodrug approach.

Methods

General methods. Chemicals and solvents were purchased from Fisher Scientific, Sigma-Aldrich or VWR International Ltd. Nuclear magnetic resonance (NMR) spectra were recorded at ambient temperature on a 500-MHz Bruker Avance III spectrometer (Bruker). Chemical shifts are reported in parts per million (p.p.m.) relative to the solvent peak. Rf values were determined on Merck TLC Silica gel 60 F254 plates (Merck) under a 254-nm ultraviolet source. Purification of compounds was carried out via manual flash column chromatography using commercially available silica gel (220–440 mesh, Sigma-Aldrich). Cell lines were grown in culture media supplemented with serum (10% fetal bovine serum) and L-glutamine (2 mM) and incubated in a Heracell 240i tissue culture incubator at 37 °C and 5% CO_2. Human colorectal carcinoma HCT116 cells (a kind gift from Dr Van Schaeybroeck) were cultured in Dulbecco's Modified Eagle Media (DMEM). Human pancreas adenocarcinoma BxPC-3 cells (a kind gift from Dr Mark Duxbury) were cultured in Roswell Park Memorial Institute media. Human hepatocyte carcinoma HepG2 cells were obtained from Sigma-Aldrich and cultured in DMEM.

© 2014 Macmillan Publishers Limited. All rights reserved.

Synthesis and characterization of Pd^0-resins. NovaSyn TG amino resin HL (1,000 mg, 0.39 mmol NH_2 per g) and palladium acetate (263 mg, 1.17 mmol) were added into a 25 ml Biotage microwave vial (Biotage) with toluene (10 ml) and heated to 80 °C under stirring for 10 min. The mixture was then stirred at room temperature for 2 h and the resins subsequently filtered and washed with dichloromethane (5 × 20 ml) and methanol (5 × 20 ml). Resins were dispersed in 10% hydrazine monohydrate in methanol (10 ml) and stirred at room temperature for 25 min. The resins were then filtered and washed with methanol (5 × 20 ml) and dichloromethane (5 × 20 ml). Resins were added to a solution of Fmoc-Glu(OH)-OH (216 mg, 0.59 mmol), Oxyma (166 mg, 1.17 mmol), *N*,*N*′-diisopropylcarbodiimide (DIC) (148 mg, 1.17 mmol) and DCM/DMF (2:1, 9 ml) and stirred for 2 h at room temperature. The resins were filtered and washed with dichloromethane (5 × 20 ml), methanol (5 × 20 ml) and H_2O (5 × 20 ml) and dried in an oven at 40 °C for 3 days. Complete coupling was verified by the ninhydrin test after the last methanol wash. Scanning electron microscope/transmission electron microscope images and Pd^0 quantification (by inductively coupled plasma-optical emission spectrometry) were carried out as previously described[8]. Resins were characterized using X-ray difractometry (Bruker D2 PHASER with LYNXEYE detector (Bruker), Cu radiation source at 30 kV, 10 mA and a Ni filtre) before and after Pd^0-functionalization. Without any extra preparation or post-processing, samples were mounted on a 1 inch diameter standard holder. The phase constituents were identified as per Supplementary Fig. 1c.

Synthesis and characterization of 5FU prodrugs. 5FU (200 mg, 1.54 mmol) and 1,8-diazabicyclo[5.4.0]undec-7-ene (269 µl, 1.80 mmol) were dissolved in dry DMF (2 ml) under N_2 atmosphere and cooled to 4 °C. Either allyl, propargyl or benzyl bromide (1.54 mmol) were dissolved in dry DMF (0.5 ml). The solution was added dropwise to the mixture and the resulting mixture stirred at room temperature overnight. Solvents were then removed under reduced pressure and the crude purified via flash chromatography (3% MeOH in DCM).

1-Allyl-5FU (All-5FU): colourless solid, 80 mg (31% yield); Rf = 0.5 (6% MeOH in DCM); ^{1}H NMR (500 MHz, dimethylsulphoxide (DMSO)-d_6) δ = 11.80 (br s, 1H, N*H*), 8.01 (d, *J*(HH) = 6.7 Hz, 1H, Ar*H*), 5.88 (ddt, *J*(HH) = 17.0, *J*(HH) = 10.5 Hz, *J*(HH) = 5.5 Hz, 1H, N–CH_2–C*H*), 5.19 (m, 2H, CH_2–CH = CH_2), 4.24 (d, *J*(HH) = 5.3 Hz, 2H, N–CH_2–CH); ^{13}C NMR (126 MHz, DMSO) δ = 157.45 (d, *J*(CF) = 25.5 Hz, C), 149.46 (C), 139.68 (d, *J*(CF) = 229.5 Hz, C), 132.63 (CH), 129.79 (d, *J*(CF) = 33.0 Hz, CH), 117.64 (CH_2), 49.34 (CH_2); high-resolution mass spectrometry (HRMS) fast atom bombardment (FAB) (*m*/*z*): $[M]^+$ calcd for $C_7H_7O_2N_2F$, 170.0486; found, 170.0489.

Pro-5FU: colourless solid, 104 mg (40% yield); Rf = 0.35 (6% MeOH in DCM); ^{1}H NMR (500 MHz, DMSO-d_6) δ = 11.91 (br s, 1H, N*H*), 8.13 (d, *J*(HH) = 5.0 Hz, 1H, Ar*H*), 4.46 (d, *J*(HH) = 2.5 Hz, 2H, N–CH_2–C), 3.44 (t, *J*(HH) = 2.5 Hz, 1H, C≡C*H*); ^{13}C NMR (126 MHz, DMSO) δ = 157.35 (d, *J*(CF) = 26.0 Hz, C), 149.11 (C), 139.80 (d, *J*(CF) = 230.5 Hz, C), 128.95 (d, *J*(CF) = 34.0 Hz, CH), 78.40 (C), 76.15 (CH), 37.00 (CH_2); HRMS (FAB) (*m*/*z*): $[M]^+$ calcd for $C_7H_5O_2N_2F$, 168.0332; found, 168.0330.

1-Benzyl-5FU (Bn-5FU): pale yellow solid, 133 mg (38% yield); Rf = 0.44 (6% MeOH in DCM); ^{1}H NMR (500 MHz, DMSO-d_6) δ = 11.86 (br s, 1H, N*H*), 8.22 (d, *J*(HH) = 6.7 Hz, 1H, Ar*H*), 7.39–7.28 (m, 5H, Ar*H*), 4.83 (s, 2H, N–CH_2–Ph); ^{13}C NMR (126 MHz, DMSO-d_6) δ = 157.42 (d, *J*(CF) = 25.5 Hz, C), 149.68 (C), 139.62 (d, *J*(CF) = 228.0 Hz, C), 136.52 (C), 130.08 (d, *J*(CF) = 33.5 Hz, CH), 128.67 (CH), 127.75 (CH), 127.49 (CH), 50.63 (CH_2); HRMS (FAB) (*m*/*z*): $[M]^+$ calcd for $C_{11}H_9O_2N_2F$, 220.0643; found, 220.0643.

Synthesis and characterization of probe 3. Rhodamine 110 chloride (250 mg, 0.68 mmol) was dissolved in dry DMF (4 ml) under nitrogen atmosphere. Separately, propargyl chloroformate (273 µl, 2.80 mmol) and triethylamine (488 µl, 3.50 mmol) were added dropwise to the mixture. The reaction mixture was stirred at room temperature for 48 h, solvents removed *in vacuo* and the resulting crude re-suspended in 25% isopropanol in DCM (20 ml) and washed with H_2O. The aqueous layer was then washed five times with 25% isopropanol in DCM (20 ml). The combined organic layers were dried over anhydrous $MgSO_4$, the solids filtered off and concentrated *in vacuo*. Crude was purified via flash chromatography (hexane/ethyl acetate 2:1) and yielded bis-*N*,*N*′-propargyloxycarbonyl-rhodamine 110 (**3**) as a white solid (67 mg, 20%). Rf = 0.13 (hexane/ethyl acetate 2:1); ^{1}H NMR (500 MHz, CD_3OD) δ = 8.02 (d, *J*(HH) = 7.5 Hz, 1H, Ar*H*), 7.77 (td, *J*(HH) = 7.5 Hz, 1.1, 1H, Ar*H*), 7.71 (td, *J*(HH) = 7.5 Hz, 0.9, 1H, Ar*H*), 7.61 (d, *J*(HH) = 2.0 Hz, 2H, Ar*H*), 7.21 (d, *J*(HH) = 7.6, 1H, Ar*H*), 7.08 (dd, *J*(HH) = 8.5 Hz, 2.2, 2H, Ar*H*), 6.68 (d, *J*(HH) = 8.5 Hz, 2H, Ar*H*), 4.78 (d, *J*(HH) = 2.4 Hz, 4H, CH_2–C≡CH), 2.94 (t, *J*(HH) = 2.4 Hz, 2H, C≡C*H*); ^{13}C NMR (126 MHz, MeOD) δ = 171.35 (C), 154.59 (C), 154.43 (C), 153.18 (C), 142.65 (C), 136.74 (CH), 131.27 (CH), 129.47 (CH), 127.76 (C), 125.89 (CH), 125.19 (CH), 115.60 (CH), 114.42 (C), 107.04 (CH), 84.48 (C), 79.08 (C), 76.22 (C), 53.40 (CH_2); mass spectrometry (electrospray ionization) (*m*/*z*): 495.2 $[M + H]^+$.

Pd^0-mediated prodrug dealkylation in biocompatible environ. All-5FU, Pro-5FU and Bn-5FU (100 µM) were dissolved in PBS (1 ml) with 1 mg of Pd^0-resins and shaken at 1,400 r.p.m. and 37 °C in a Thermomixer. Reaction crudes were monitored at 0, 6, 24 and 48 h by analytical HPLC (Agilent) using the ultraviolet detector at 280 nm to avoid the detection of PBS salts. Eluent A: water and formic acid (0.1%); eluent B: acetonitrile, formic acid (0.1%); A/B = 95:5 to 5:95 in 3 min, isocratic 1 min, 5:95 to 95:5 in 1 min, isocratic 1 min. Catalytic conversion assay: Pro-5FU in 0.1% (v/v) DMSO was dissolved in PBS (1 ml) with Pd^0-resins (1 mg ml^{-1}, $[Pd^0] \sim 266$ µM) to reach a final Pro-5FU concentration 300 µM and incubated for 24, 48, 72 h at 37 °C. Pro-5FU presence was monitored by HPLC. For the heterogeneous catalysis assay, Pd^0-resins (2 mg) were dispersed into a PBS solution (2 ml) and incubated for 24 h at 37 °C. The mixture was filtrated using a Millipore microfiltre (0.22 µm, Millipore) and, subsequently, Pro-5FU added to the mixture (final concentration = 100 µM). The reaction mixture was incubated for additional 24 h and analysed by HPLC (ultraviolet detector at 280 nm).

Cell viability studies of 5FU versus Pro-5FU. Cells were seeded in a 96-well plate format at the appropriate cell concentration (3,000 cells per well for HCT116 and BxPC-3 cells, and 4,000 cells per well for HepG2 cells) and incubated for 48 h before treatment. Each well was then replaced with fresh media containing 5FU (0.01 µM to 1 mM) with DMSO (0.1% v/v); or Pro-5FU (0.01 µM to 1 mM) with DMSO (0.1% v/v) and incubated for 5 days. Untreated cells were incubated with DMSO (0.1% v/v). PrestoBlue cell viability reagent (10% v/v) was added to each well and the plate incubated for 45 min. Fluorescence emission was detected using a PerkinElmer EnVision 2101 multilabel reader (Perkin Elmer; excitation filtre at 540 nm and emissions filtre at 590 nm). All conditions were normalized to the untreated cells (100%) and curves fitted using GraphPad Prism using a sigmoidal variable slope curve.

Pd^0-mediated dealkylation of Pro-5FU in cell culture. HCT116 and BxPC-3 cells were seeded in a 96-well plate format with a density of 3,000 cells per well and incubated for 48 h before treatment. Each well was then replaced with fresh media containing: Pd^0-resins (0.67 or 1 mg ml^{-1} for BxPC-3 or HCT116, respectively) with DMSO (0.1% v/v); Pro-5FU (0.01–100 µM) with DMSO (0.1%, v/v); 5FU (0.01 µM to 1 mM) with DMSO (0.1%, v/v) or combination of Pd^0-resin + Pro-5FU (0.01–100 µM) with DMSO (0.1%, v/v). Untreated cells were incubated with DMSO (0.1% v/v). For the cell viability assay, cells were incubated with drugs for 5 days. PrestoBlue cell viability reagent (10% v/v) was added to each well and the plate incubated for 45 min. Fluorescence emission was detected and results normalized as described above. For the time lapse imaging study, cell growth studies were carried out at a single dose of 5FU or Pro-5FU (100 µM for HCT116 and 30 µM for BxPC-3). Each well was imaged every 2 h over 5 days under standard incubation conditions using an IncuCyte ZOOM microscope (placed inside the incubator). Imaged-based analysis of cell confluence and Supplementary Movies 1 and 2 were carried out using the IncuCyte software.

Reverse phase protein array analysis. Cells were plated in a 6-well plate at a density of 480,000 cells per well and incubated for 48 h. Before adding the prodrug to the HCT116 cells, Pro-5FU (100 µM) and Pd^0-resins (1 mg ml^{-1}) were incubated in media at 37 °C for 24 h to overcome the time delay required to convert Pro-5FU into 5FU, which was seen to have a relevant effect in this cell type. This pre-incubation procedure was not carried out for the study with BxPC-3 cells (30 µM). Pd^0 resin/Pro-5FU combination and the controls (as before, untreated cells; Pd^0-resins; Pro-5FU and 5FU) were incubated with each cell line for 6 and 24 h. Afterwards, the cells were washed with PBS (2 × 3 ml) and lysed with Zeptosens CLB1 lysis buffer (90 µl, Zeptosens). Samples were analysed by Zeptosens RPPA (Zeptosens) as previously described[31] using the following specific conditions. Tumour cell lysates were normalized to a uniform protein concentration with spotting buffer CSBL1 (Zeptosens-Bayer) before preparing a final fourfold concentration series of 0.2, 0.15, 0.1 and 0.05 mg ml^{-1}. The diluted concentration series of each sample was printed onto Zeptosens protein microarray chips (ZeptoChip, Zeptosens-Bayer) under environmentally controlled conditions (constant 50% humidity and 14 °C temperature) using a non-contact printer (Nanoplotter 2.1e, GeSiM). A single 400 Pico litre droplet of each lysate concentration was deposited onto the Zeptosens chip (thus representing four spots per each biological replicate). A reference grid of Alexa Fluor-647 conjugate BSA consisting of 4 column × 22 rows was spotted onto each sub-array. Each sample concentration series were spotted in between reference columns. After array printing, the arrays were blocked with an aerosol of BSA solution using a custom designed nebulizer device (ZeptoFOG, Zeptosen-Bayer) for 1 h. The protein array chips were subsequently washed in double-distilled H_2O and dried before performing a dual antibody immunoassay comprising of a 24-h incubation of primary antibody (the library of primary antibodies used is in Supplementary Table 1 and were purchased from Cell Signaling Technologies) followed by 2.5 h incubation with secondary Alexa Fluor-conjugated antibody detection reagent (anti-rabbit A647 Fab; Invitrogen). Following secondary antibody incubation and a final wash step in BSA solution, the immunostained arrays were imaged using the ZeptoREADER instrument (Zeptosens-Bayer). For each sub-array, five separate images were acquired using different exposure times ranging from 0.5 to 10 s. Microarray images representing the longest exposure without saturation of fluorescent signal detection were automatically selected for analysis using the ZeptoView 3.1 software (Zeptosens-Bayer). A weighted linear fit through the

© 2014 Macmillan Publishers Limited. All rights reserved.

fourfold concentration series was used to calculate relative fluorescence intensity (RFI) value for each sample replicate. Local normalization of sample signal to the reference BSA grid was used to compensate for any intra- or inter-array/chip variation. Local normalized RFI values were used for all subsequent analysis. Abundance levels of total p53 protein, phosphorylated p53 (Serine 15) and phosphorylated Akt (Ser 473) were plotted as RFI data calculated by the ZeptoView 3.1 software.

Western blot analysis. Cell lysates for HCT116 and BxPC-3 cells were prepared as described above for Zeptosens analysis. Protein samples (35 μg) and SeeBlue Plus2 Pre-Stained Standard (7.5 μg) were separated by SDS-PAGE (Bio-Rad, 4–15% gels) and transferred to PVDF membranes (GE). Western blotting was performed using rabbit monoclonal antibodies against human p53 and Phospho-p53 (Ser 15) (1:1,000 for each one, Cell Signaling Technologies, cat. no. 9282 and 9284, respectively) at 4 °C overnight. This was followed by 1 h incubation at room temperature with secondary horseradish peroxidase (HRP)-linked antibody (1:10,000, anti-rabbit IgG, Sigma). The loading control, actin, was detected using a mouse monoclonal antibody (1:40,000, Calbiochem, cat. no. CP01) followed by a secondary HRP-linked antibody treatment (1:40,000, anti-mouse IgM, Calbiochem). HRP was detected by addition of POD ECL (Roche) and bands visualized using a ChemiDoc MP Imager (Bio-Rad).

Zebrafish studies. For the biocompatability assay, wild-type zebrafish embryos were collected from AB-TPL breeding pairs and reared at 28 °C in E3 embryo medium. Twenty-four hours post fertilization, embryos were treated with tricaine (anesthetic) and pierced in the yolk with a fine needle. Either a naked resin or a Pd^0-resin was then rapidly inserted into the yolk opening to minimize loss of yolk. Embryos that lost significant yolk in the procedure were removed from the experiment. Embryos were then gently transferred to fresh E3 medium ($n = 5$), returned to 28 °C and monitored over 3 days by microscopy. For the catalytic activity assay, either a naked resin or a Pd^0-resin was implanted in 24 h.p.f. zebrafish embryos ($n = 5$) following the above procedure and gently transferred to fresh E3 medium. Embryos were incubated for 24 h at 28 °C to ensure the yolk wound was closed. Embryos that lost significant yolk in the procedure were removed from the experiment. Compound **3** was added to the embryo medium (final concentration 5 μM) and fish incubated for additional 24 h at 31 °C to increment the probe activation rate. Fish were imaged using fluorescent microscopy (Olympus Scan-R, Olympus). It is important to note that the zebrafish embryos looked older than developmental 3 d.p.f., probably due to the increased incubation temperature (31°C). Experiments were repeated three times. Zebrafish husbandry and experiments were performed under Home Office License in compliance with the Animals (Scientific Procedures) Act 1986, and approved by the University of Edinburgh Ethics Committee.

References

1. Saxon, E. & Bertozzi, C. R. Cell Surface Engineering by a Modified Staudinger Reaction. *Science* **287,** 2007–2010 (2000).
2. Agard, N. J., Prescher, J. & Bertozzi, C. R. A strain-promoted [3 + 2] azide – alkyne cycloaddition for covalent modification of biomolecules in living systems. *J. Am. Chem. Soc.* **126,** 15046–15047 (2004).
3. Sletten, E. M. & Bertozzi, C. R. From mechanism to mouse: a tale of two bioorthogonal reactions. *Acc. Chem. Res.* **44,** 666–676 (2011).
4. Bertozzi, C. R. A decade of bioorthogonal chemistry. *Acc. Chem. Res.* **44,** 651–653 (2011).
5. Lim, R. K. & Lin, Q. Photoinducible bioorthogonal chemistry: a spatiotemporally controllable tool to visualize and perturb proteins in live cells. *Acc. Chem. Res.* **44,** 828–839 (2011).
6. Klán, P. *et al.* Photoremovable protecting groups in chemistry and biology: reaction mechanisms and efficacy. *Chem. Rev.* **113,** 119–191 (2013).
7. Sánchez, M. I. *et al. In vivo* light-driven DNA binding and cellular uptake of nucleic acid stains. *ACS Chem. Biol.* **7,** 1276–1280 (2012).
8. Unciti-Broceta, A., Johansson, E. M. V., Yusop, R. M., Sánchez-Martín, R. M. & Bradley, M. Synthesis of polystyrene microspheres and functionalization with Pd(0) nanoparticles to perform bioorthogonal organometallic chemistry in living cells. *Nat. Protoc.* **7,** 1207–1218 (2012).
9. Sasmal, P. K., Streu, C. N. & Meggers, E. Metal complex catalysis in living biological systems. *Chem. Commun.* **49,** 1581–1587 (2013).
10. Streu, C. & Meggers, E. Ruthenium-induced allylcarbamate cleavage in living cells. *Angew. Chem. Int. Ed.* **45,** 5645–5648 (2006).
11. Yusop, R. M., Unciti-Broceta, A., Johansson, E. M. V., Sánchez-Martín, R. M. & Bradley, M. Palladium-mediated intracellular chemistry. *Nat. Chem.* **3,** 239–243 (2011).
12. Li, N., Lim, R. K., Edwardraja, S. & Lin, Q. Copper-free Sonogashira cross-coupling for functionalization of alkyne-encoded proteins in aqueous medium and in bacterial cells. *J. Am. Chem. Soc* **133,** 15316–15319 (2011).
13. Spicer, C. D., Triemer, T. & Davis, B. G. Palladium-mediated cell surface labeling. *J. Am. Chem. Soc.* **134,** 800–803 (2012).
14. Michel, B. W., Lippert, A. R. & Chang, C. J. A reaction-based fluorescent probe for selective imaging of carbon monoxide in living cells using a palladium-mediated carbonylation. *J. Am. Chem. Soc.* **134,** 15668–15671 (2012).
15. Environmental Health Criteria 226: Palladium. World Health Organization, Geneva, http://whqlibdoc.who.int/ehc/WHO_EHC_226.pdf (2002).
16. Rushforth, R. Palladium in restorative dentistry: superior physical properties make palladium an ideal dental metal. *Platinum Metals Rev.* **48,** 30–31 (2004).
17. Rautio, J. *et al.* Prodrugs: design and clinical applications. *Nat. Rev. Drug Discov* **7,** 255–270 (2008).
18. Saif, M. W., Choma, A., Salamone, S. J. & Chu, E. Pharmacokinetically guided dose adjustment of 5-fluorouracil: a rational approach to improving therapeutic outcomes. *J. Natl Cancer Inst.* **101,** 1543–1552 (2009).
19. Longley, D. B., Harkin, D. P. & Johnston, P. G. 5-Fluorouracil: mechanisms of action and clinical strategies. *Nat. Rev. Cancer* **3,** 330–338 (2003).
20. Weissman, S. A. & Zewge, D. Recent advances in ether dealkylation. *Tetrahedron* **61,** 7833–7863 (2005).
21. Song, F., Garner, A. L. & Koide, K. A highly sensitive fluorescent sensor for palladium based on the allylic oxidative insertion mechanism. *J. Am. Chem. Soc.* **129,** 12354–12355 (2007).
22. Santra, M., Ko, S.-K., Shin, I. & Ahnz, K. H. Fluorescent detection of palladium species with an O-propargylated fluorescein. *Chem. Commun.* **46,** 3964–3966 (2010).
23. Liu, B. *et al.* A new ratiometric ESIPT sensor for detection of palladium species in aqueous solution. *Chem. Commun.* **48,** 2867–2869 (2012).
24. Pal, M., Parasuraman, K. & Yeleswarapu, K. R. Palladium-catalyzed cleavage of O/N-propargyl protecting groups in aqueous media under a copper-free condition. *Org. Lett.* **5,** 348–352 (2003).
25. Escoubet, S., Gastaldi, S. & Bertrand, M. Methods for the cleavage of allylic and propargylic C–N bonds in amines and amides – selected alternative applications of the 1,3-hydrogen shift. *Eur. J. Org. Chem.* **2005,** 3855–3873 (2005).
26. Rambabua, D., Bhavani, S., Swamy, N. K. & Rao, M. V. B. Pd/C mediated depropargylation of propargyl ethers/amines in water. *Tetrahedron Lett.* **54,** 1169–1173 (2013).
27. Jang, Y. H., Sowers, L. C., Cagin, T. & Goddard III, W. A. First principles calculation pka values for 5-substituted uracils. *J. Phys. Chem. A* **105,** 274–280 (2001).
28. Cho, J. K. *et al.* Captured and cross-linked palladium nanoparticles. *J. Am. Chem. Soc.* **128,** 6276–6277 (2006).
29. Kaleta, C. *et al. In silico* evidence for gluconeogenesis from fatty acids in humans. *PLoS Comput. Biol.* **7,** e1002116 (2011).
30. Gerets, H. H. *et al.* Selection of cytotoxicity markers for the screening of new chemical entities in a pharmaceutical context: a preliminary study using a multiplexing approach. *Toxicol. In Vitro* **2,** 319–332 (2009).
31. van Oostrum, J. *et al.* Tracing pathway activities with kinase inhibitors and reverse phase protein arrays. *Proteomics Clin. Appl.* **3,** 412–422 (2009).
32. De Angelis, P. M., Svendsrud, D. H., Kravik, K. L. & Stokk, T. Cellular response to 5-fluorouracil (5-FU) in 5-FU-resistant colon cancer cell lines during treatment and recovery. *Mol. Cancer* **5,** 20 (2006).
33. Wallace, K. N. & Pack, M. Unique and conserved aspects of gut development in zebrafish. *Dev. Biol.* **255,** 12–29 (2003).
34. Ng, A. N. *et al.* Formation of the digestive system in zebrafish: III. Intestinal epithelium morphogenesis. *Dev. Biol.* **286,** 114–135 (2005).
35. Lin, Q. & Ramil, C. P. Bioorthogonal chemistry: strategies and recent developments. *Chem. Comm.* **49,** 11007–11022 (2013).
36. Uttamapinant, C. *et al.* Fast, cell-compatible click chemistry with copper-chelating azides for biomolecular labeling. *Angew. Chemie Int. Ed.* **51,** 5852–5856 (2012).
37. Castano, A. P., Mroz, P. & Hamblin, M. R. Photodynamic therapy and anti-tumour immunity. *Nat. Rev. Cancer* **6,** 535–545 (2006).

Acknowledgements

J.T.W. thanks the College of Medicine and Veterinary Medicine and the University of Edinburgh for a Darwin International Scholarship and an Edinburgh Global Research Scholarship. N.O.C. and A.U.-B. thank RCUK and IGMM, respectively, for an Academic Fellowship. We are grateful to the Edinburgh Cancer Research UK Centre for funding this research through the CRUK Development Fund. E.E.P., C.F. and W.R. are funded by the MRC. We thank Marcel Dreger and Dr Zhiqiang Zeng for assistance with developing the zebrafish assays and imaging, and Professor Joan Heath for advice in assigning the location of compound **3** bioactivation.

Author contributions

J.T.W. prepared and characterized the materials, planned and performed the experiments, analysed the data and prepared figures and experimental section; J.C.D. supervised the cell viability assays, the Incucyte and western blot experiments; E.E.P. planned,

© 2014 Macmillan Publishers Limited. All rights reserved.

performed and analysed the zebrafish assays; K.G.M. performed the Zeptosens analysis; W.R. performed the surgical insertion of resins in zebrafish embryos; C.F. prepared materials and contributed to the zebrafish studies; C.T.-S. characterized the Pd^0-resins by powder XRD; M.B. conceived the original concept of using palladium to synthesize probes and drugs in living systems; N.O.C. supervised the biological assays, designed and analysed the Zeptosens, Incucyte and western blot assays, and contributed to the paper preparation; A.U.-B. designed the prodrug approach and the materials, planned and supervised the research, analysed the data and wrote the paper.

Additional information

Supplementary Information accompanies this paper at http://www.nature.com/naturecommunications

Competing financial interests: The authors declare that a patent (application number GB1311107.5) is pending on Pro-5FU and its method of activation for medical use.

Reprints and permission information is available online at http://npg.nature.com/reprintsandpermissions/

How to cite this article: Weiss, J. T. *et al.* Extracellular palladium-catalysed dealkylation of 5-fluoro-1-propargyl-uracil as a bioorthogonally activated prodrug approach. *Nat. Commun.* 5:3277 doi: 10.1038/ncomms4277 (2014).

This work is licensed under a Creative Commons Attribution-NonCommercial-ShareAlike 3.0 Unported License. To view a copy of this license, visit http://creativecommons.org/licenses/by-nc-sa/3.0/

© 2014 Macmillan Publishers Limited. All rights reserved.

NEWS AND VIEWS NEWS AND VIEWS NEWS AND VIEWS

Extracellular Palladium-Catalyzed Dealkylation of 5-Fluoro-1-propargyl-uracil as a Bioorthogonally Activated Prodrug Approach

Nat. Commun. **2014**, *5*, 3277

Chemotherapy is most effective at killing cells that divide rapidly, which is one of the principal features of cancer cells. However, non-cancerous cells are also heavily affected by the chemotherapeutic treatment. As a result, antineoplastic drugs are limited by lack of selectivity. To mitigate unwanted side effects, many efforts have been made on the design of cancer-specific strategies such as prodrugs, which are inactive precursors of cytotoxic agents that are *biochemically* converted into their active forms in a specific biological setting. As an unprecedented prodrug approach, the Edinburgh Cancer Discovery Unit (University of Edinburgh, Scotland, UK) is investigating the application of solid metals as implantable activating devices to modulate the cytotoxic activity of antineoplastic drugs in a spatially controlled manner.

The novel approach, so-called bioorthogonally activated chemotherapy, is based on the use of palladium, a benign metal able to catalyze various chemical reactions in biocompatible environments (*Nat. Chem.* **2011**, *3*, 239; *Synform* **2011**, *06*, A48; *Nat. Protocols* **2012**, *7*, 1207; *Chem. Soc. Rev.* **2013**, *42*, 7943). "While soluble palladium species such as Pd^{2+} complexes exhibit inherent cytotoxic properties, metallic palladium (Pd^0) is biocompatible (e.g., it is employed in dental restoration) and we have now shown that it is catalytically active both in vitro (cell culture) and in vivo (zebrafish)," said Dr. Unciti-Broceta, who led the research program that resulted in this *Nat. Commun*. article.

As opposed to classical prodrugs, whose activation process relies on metabolic pathways, an efficient palladium-activated prodrug therapy ought to be entirely dependent on the presence of this metal and the prodrug should remain intact in distant tissues and organs. "The principal challenges to overcome were to make the prodrug metabolically stable (= bioorthogonal) while at the same time sensitive to palladium catalysis," confirmed Dr. Unciti-Broceta. 5-Fluorouracil (5FU), a potent antimetabolite drug, whose clinical use has been limited by a narrow therapeutic index, was used to develop such a prodrug. According to the authors, 5FU was modified at its *N*1 position (i) because of its relatively low pK_a value due to the heterocycle's lactam/lactim tautomery, which was expected to promote its properties as a leaving group, and (ii) due to its relevance in the drug's mode of action (see Figure, A). "We hypothesized that the alkylation of the *N*1 position of 5FU would both suppress the drug's cytotoxic properties and make the resulting prodrug become resistant to enzymatic cleavage," said Dr. Unciti-Broceta.

"We have found that inactive prodrugs can be generated by masking the *N*1 position of 5FU with allyl, propargyl and benzyl groups. Our results show, however, that only the propargyl derivative displays high sensitivity to palladium in biocompatible conditions and enables the bioorthogonal generation of 5FU by heterogeneous palladium catalysis in cancer cell culture (see Figure, B)," said Jason Weiss, currently a final-year PhD student in the Unciti-Broceta group. The authors noted that the oxidative cleavage of the propargyl group generates 1-hydroxyacetone, a harmless natural compound, as reaction byproduct, making the reaction optimal to activate any kind of prodrug in vivo (not only cytotoxic ones).

"This is the first example showing that the pharmacological activity of a clinically approved antineoplastic drug can be locally activated by means of an internal self-renewable control element rather than an external radiation source (such as in photodynamic therapy)," said Dr. Neil Carragher, a group leader of the Edinburgh Cancer Research UK Centre and expert in phenotypic screening. According to Dr. Carragher, this novel approach would allow for a reduction in adverse side effects of current chemotherapeutic regimes. The proposed strategy would be optimal to treat advanced cancers that cannot be resected by surgery, since it would allow local treatment with increased dosing. Once the tumor has shrunk to a resectable size, the surgeon could remove the tumor along with the palladium implants. Dr. Unciti-Broceta concluded: "The next steps of the project are to validate this approach in a mouse cancer model and to expand the chemistry to other pharmaceuticals."

SYNFORM, 2014/07
Published online: 16.06.2014, **DOI**: 10.1055/s-0033-1340189

2014 © THIEME STUTTGART · NEW YORK

Downloaded by: Edinburgh University. Copyrighted material.

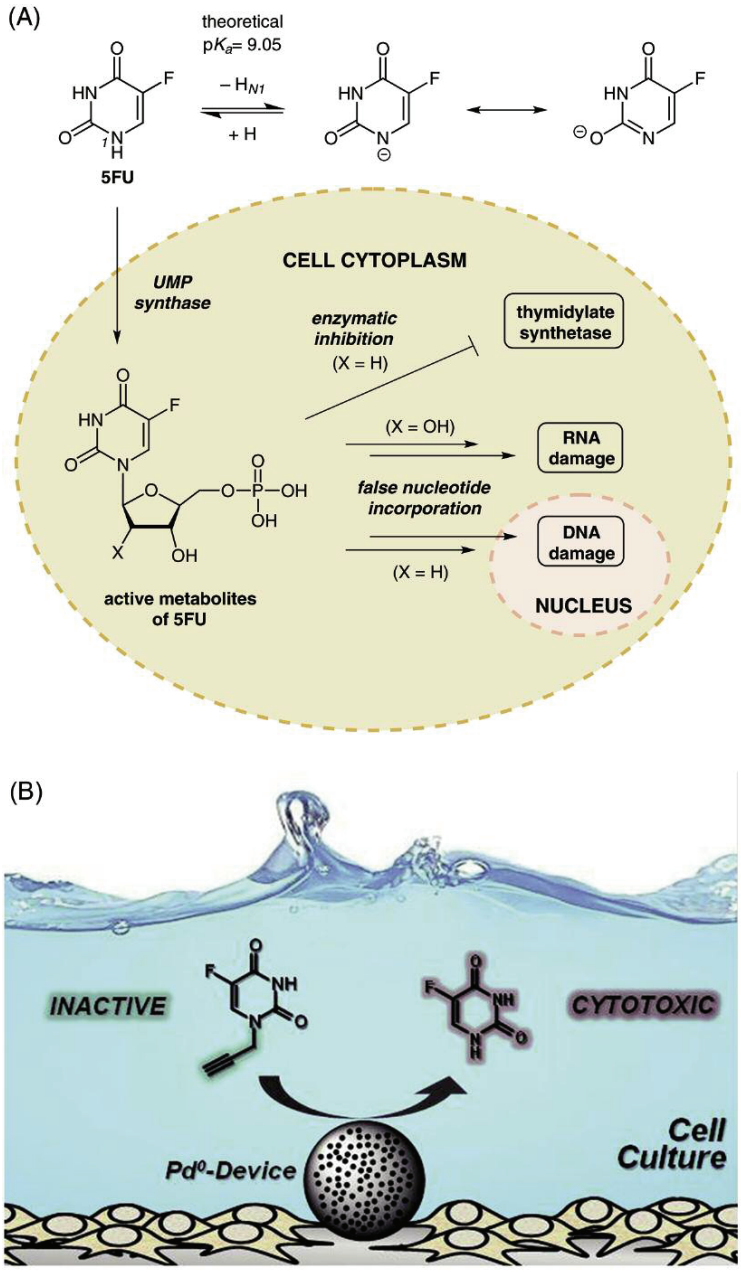

Figure *(A) 5FU and its conjugate bases (top) and intracellular biofunctionalization of 5FU to generate cytotoxic metabolites (bottom). (B) In situ transformation of an inert drug precursor into a bioactive material (5FU) by the mediation of an extracellular biocompatible catalyst in cell culture.*

Matteo Zanda

SYNFORM, 2014/07
Published online: 16.06.2014, **DOI**: 10.1055/s-0033-1340189

2014 © THIEME STUTTGART · NEW YORK

Downloaded by: Edinburgh University. Copyrighted material.

About the authors



From left to right: Dr. A. Unciti-Broceta, J. Weiss, Dr. N. Carragher (other authors: J. Dawson, K. Macleod, C. Fraser, L. Patton, M. Bradley)

Jason Weiss was born in Ottawa (Canada) in 1985. He completed his Honors Bachelor of Science degree in Biotechnology at Carleton University (Ottawa). Afterwards, he worked for Nordion in the radiopharmaceutical production division as a drug production technician synthesizing medical isotopes. After two years, he went back to school to the University of Edinburgh (UK) where he obtained his MSc in Biomedical Sciences. He is currently pursuing his PhD in Molecular Medicine (Edinburgh Cancer Research UK Centre, University of Edinburgh) under the supervision of Asier Unciti-Broceta working on the development of antineoplastic prodrugs sensitive to palladium as a novel spatially controlled anticancer chemotherapy.

Neil Carragher was born in Uphall, Scotland (UK) in 1970. He studied 'Cell and Immunobiology' at the University of Aberdeen (UK) prior to accepting a position at the Yamanouchi Research Institute, Oxford (UK) where he obtained his PhD in 1996. He held consecutive postdoctoral positions within the Department of Pathology, University of Washington, Seattle (USA) and at the Beatson Institute for Cancer Research, Glasgow (UK). In 2004 Neil returned to the pharmaceutical industry as Principal Scientist with the Advanced Science and Technology Laboratory at AstraZeneca where he pioneered early multiparametric high-content phenotypic screening approaches. In 2010 he returned to academia and took up the post of Principal Investigator at the University of Edinburgh where he leads a research group and is currently co-director of the Edinburgh Cancer Discovery Unit. Current research interests include advancing high-content analysis, phenotypic screening, reverse-phase protein array technology and cancer drug discovery.

Asier Unciti-Broceta was born in La Linea (Spain) in 1976. After studying 'Pharmaceutical Sciences' at the University of Granada (Spain), he completed his PhD in Medicinal Chemistry under the supervision of Professor A. Espinosa and sponsored by the Ramón Areces Foundation in 2004. He then moved to the University of Edinburgh (UK) to join the group of Professor M. Bradley (School of Chemistry) as a postdoctoral fellow. Following a Scottish Enterprise Proof of Concept Award in 2008, which resulted in the foundation of the spin-out company Deliverics Ltd, in 2010 he became the first chemistry group leader of the Edinburgh Cancer Research UK Centre (MRC Institute of Genetics and Molecular Medicine, University of Edinburgh). His research interests lie on the interface of medicinal chemistry and chemical biology, with particular emphasis on the design and development of innovative anticancer prodrugs and kinase inhibitors. Among his awards, highlights include being the recipient of the Nexxus Young Life Scientist Award of 2010 and the RSC Young Industrialist Award of 2012. In 2013 he was appointed co-director of the Edinburgh Cancer Discovery Unit and member of the RSE Young Academy of Scotland.

Downloaded by: Edinburgh University. Copyrighted material.

SYNFORM, 2014/07
Published online: 16.06.2014, **DOI**: 10.1055/s-0033-1340189

2014 © THIEME STUTTGART · NEW YORK

Journal of Medicinal Chemistry

ACS Editors' Choice

Article

pubs.acs.org/jmc

Terms of Use

Development and Bioorthogonal Activation of Palladium-Labile Prodrugs of Gemcitabine

Jason T. Weiss,[†] John C. Dawson,[†] Craig Fraser,[†] Witold Rybski,[†,‡] Carmen Torres-Sánchez,[§] Mark Bradley,[∥] E. Elizabeth Patton,[†,‡] Neil O. Carragher,[†] and Asier Unciti-Broceta*[,†]

[†]Edinburgh Cancer Research UK Centre, and [‡]MRC Human Genetics Unit, MRC Institute of Genetics and Molecular Medicine, University of Edinburgh, Crewe Road South, Edinburgh EH4 2XR, U.K.

[§]Wolfson School of Mechanical and Manufacturing Engineering, Loughborough University, Loughborough LE11 3TU, U.K.

[∥]School of Chemistry, University of Edinburgh, West Mains Road, Edinburgh EH9 3JJ, U.K.

Supporting Information

ABSTRACT: Bioorthogonal chemistry has become one of the main driving forces in current chemical biology, inspiring the search for novel biocompatible chemospecific reactions for the past decade. Alongside the well-established labeling strategies that originated the bioorthogonal paradigm, we have recently proposed the use of heterogeneous palladium chemistry and bioorthogonal Pd^0-labile prodrugs to develop spatially targeted therapies. Herein, we report the generation of biologically inert precursors of cytotoxic gemcitabine by introducing Pd^0-cleavable groups in positions that are mechanistically relevant for gemcitabine's pharmacological activity. Cell viability studies in pancreatic cancer cells showed that carbamate functionalization of the 4-amino group of gemcitabine significantly reduced (>23-fold) the prodrugs' cytotoxicity. The *N*-propargyloxycarbonyl (*N*-Poc) promoiety displayed the highest sensitivity to heterogeneous palladium catalysis under biocompatible conditions, with a reaction half-life of less than 6 h. Zebrafish studies with allyl, propargyl, and benzyl carbamate-protected rhodamines confirmed *N*-Poc as the most suitable masking group for implementing *in vivo* bioorthogonal organometallic chemistry.

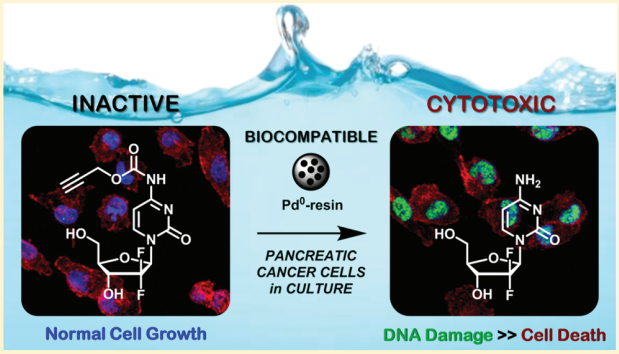

INTRODUCTION

Bioorthogonal chemistry is an emerging field of research that focuses on the development and application of selective chemical reactions susceptible to occurring in a biological environment without interfering with the normal function of its components.[1,2] These reactions are used as labeling methods to study cell constituents in their native state, including proteins and biomolecules that cannot be monitored by genetically encoded reporters (e.g., glycans, lipids, DNA, etc.).[1−4] Looking beyond the well-established labeling strategies that originated the bioorthogonal field, the induction of local chemotherapy by biologically inert means could allow for the reduction of adverse pharmacological effects in distant organs and tissues. This therapeutic paradigm has so far reached the clinic with the so-called photodynamic therapy, a method based on the local generation of cytotoxic reactive oxygen species by spatially controlled excitation (and subsequent energy transfer to the molecular oxygen present in the tissue) of a nontoxic systemically administered photosensitizer with a benign light source.[5] Following the same principle of bioorthogonality, novel strategies are being currently investigated by several groups to enable local conversion of chemically masked prodrugs into cytotoxic small molecules using either harmless electromagnetic radiations[6,7] or biocompatible heterogeneous catalysts.[8]

Technically speaking, for a bioorthogonal reaction to be optimal to living systems, the corresponding nonbiotic reactive partners need to display (i) high chemical stability to enzymatic processing and (ii) selective reciprocal reactivity in biocompatible conditions (water, pH 7.4, isotonicity, and 37 °C). Importantly, the reactants and the resulting product/s should be nontoxic, unless this is the intended outcome of the process. The Staudinger ligation and the copper-free azide alkyne cycloaddition, originally developed by the Bertozzi group,[9−11] are representative examples of such chemistry. In addition to catalyst-free ligations, the use of transition metals to functionalize biomolecules or activate fluorogenic probes in living cells has recently emerged as a new alternative in the field.[8,12,13] These biocompatible processes, also known as bioorthogonal organometallic (BOOM) reactions,[14] are mediated by nonbiotic transition metals such as copper(I),[15] ruthenium(II),[16−18] or palladium species[8,14,18−23] and have expanded

Received: April 3, 2014
Published: May 27, 2014

 © 2014 American Chemical Society dx.doi.org/10.1021/jm500531z | *J. Med. Chem.* 2014, 57, 5395−5404

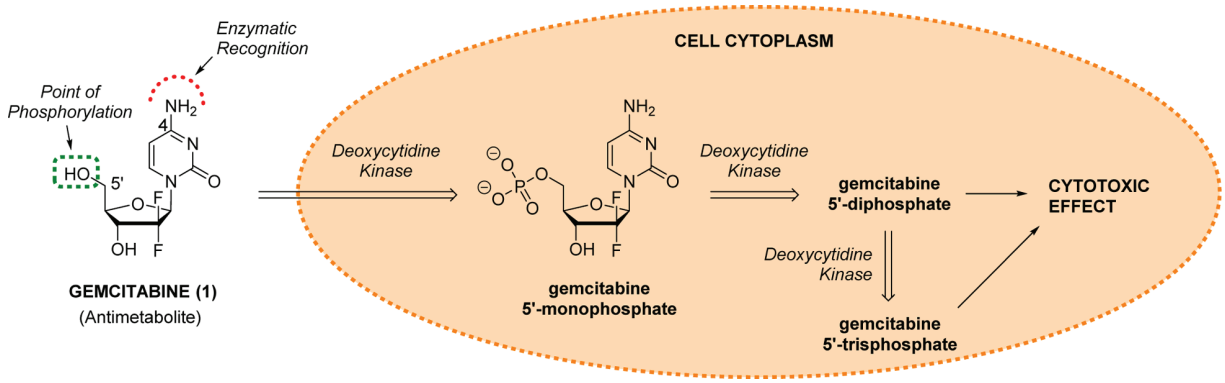

Figure 1. Gemcitabine and its cytotoxic mode of action. Following cell entry, gemcitabine is successively phosphorylated by deoxycytidine kinase at its 5′-OH position to generate cytotoxic metabolites.

Scheme 1. Synthesis of Gemcitabine Prodrugs[a]

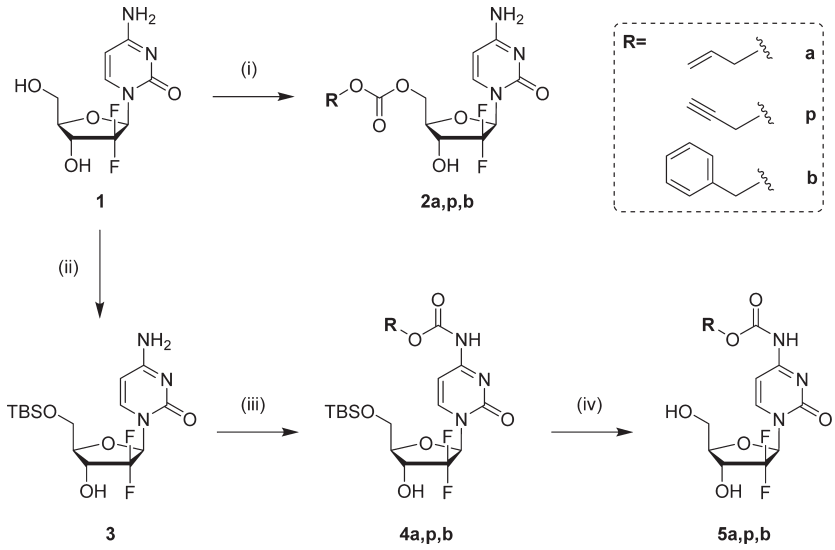

[a]Reagents and conditions: (i) DBU (2.5 equiv), DMF, addition of alkylchloroformate (1.5 equiv) at 4 °C, then r.t. overnight (47−53%); (ii) TBS-Cl (1.1 equiv), imidazole (3.5 equiv), DMF, r.t., 2.5 h (88%); (iii) pyridine (3.2 equiv), DMF or THF, addition of alkylchloroformate (1.5 equiv) at 4 °C, then r.t. overnight 12−48h (42−69%); (iv) TBAF (2.5 equiv), THF, r.t., overnight (62−92%).

the diversity of chemical groups and transformations suitable for use *bioorthogonally* in cell culture.

Aiming to modulate drug activity by an internal self-renewable control element rather than an external radiation source (e.g., light in photopharmacology[7]), we have recently proposed the development of nonbiological transition metals into biocompatible catalytic devices to allow the activation of systemically administered prodrugs at the location determined by the device.[8] This bioorthogonally activated chemotherapeutic strategy would be optimal to implement focalized treatment of unresectable primary or metastatic tumors and could also find application in the treatment of other disorders such as local infections, Parkinson's disease, cardiovascular disorders, etc. In the seminal investigation of such an approach,[8] we reported the development of a selective metallo-substrate (5-fluoro-1-propargyluracil) and a solid-phase palladium catalyst (Pd^0-resins) as a highly efficient bioorthogonal prodrug/activator system. On the basis of their complementary chemical roles, cytotoxic 5-fluorouracil was efficiently generated via extracellular BOOM catalysis in cell culture.[8] Importantly, when each of these reagents was cultured separately, neither of them exhibited cytotoxicity, demonstrating the feasibility of the method.

To explore this paradigm further, herein we report a comprehensive study on the development and evaluation of novel Pd^0-labile prodrugs of gemcitabine (deoxycytidine analogue clinically used to treat several types of cancers[24]) using two masking strategies: (i) carbonate formation at the 5′-OH group of the sugar moiety and (ii) carbamate masking of the 4-NH_2 group of the cytosine base (Figure 1).

RESULTS AND DISCUSSION

Design and Synthesis of Pd^0-Labile Gemcitabine Prodrugs. Gemcitabine (marketed as Gemzar by Eli Lilly and Co.) is an antimetabolite antineoplastic agent widely employed, in combination or alone, to treat several difficult-to-cure cancerous processes (e.g., nonsmall-cell lung carcinoma, metastatic breast cancer, and ovarian cancer),[24] including being a first-line therapy in the treatment of pancreatic cancer.[25] It displays a narrow therapeutic index, with its most severe side effects being myelosuppression, pulmonary toxicity, and renal failure.[24] Gemcitabine is intracellularly converted by deoxy-

dx.doi.org/10.1021/jm500531z | J. Med. Chem. 2014, 57, 5395−5404

cytidine kinase into its therapeutically active metabolites, the 5′-diphosphate and 5′-triphosphate derivatives (Figure 1). Gemcitabine 5′-diphosphate inhibits ribonucleotide reductase, a strictly conserved enzyme among all living organisms responsible for regulating the total rate of DNA synthesis, while the triphosphorylated derivative can become incorporated into the DNA, thereby inhibiting nuclear replication.[26]

On the basis of gemcitabine's mode of action, masking the 5′-OH group of its sugar moiety would chemically block the generation of its cytotoxic metabolites (Figure 1). In a different manner but similarly relevant, modification of the 4-amino group of the cytosine base would result in a reduction of the enzyme−substrate recognition. The absence of a free NH_2 group in that position would hinder the formation of essential hydrogen bonding interactions with the amino acid Asp133 located within the activation site of the enzyme, thus reducing the efficacy of the phosphorylation process.[27] Furthermore, the main detoxification route of gemcitabine is via hydrolytic deamination of the 4-NH_2 group. This is mediated in the liver by cytidine deaminase, which irreversibly converts gemcitabine into its inactive metabolite difluoro-deoxyuridine.[28] Consequently, masking the 4-NH_2 group would result in a doubly beneficial effect to the bioorthogonal strategy: it would reduce the cytotoxic properties of the resulting prodrug and protect the circulating drug precursor from premature liver deactivation before reaching the target tissue.

Allyl and propargyloxycarbonyl groups (Alloc and Poc, respectively) have been widely employed as OH and NH_2 protection strategies[29−32] and have shown sensitivity to palladium catalysis in biocompatible conditions.[8,14,19] Therefore, both groups were chosen to derivatize gemcitabine **1** into palladium-labile prodrugs. Because of the requirement of an additional hydrogen source to undergo palladium-mediated cleavage, the carboxybenzyl group (Cbz) was used to generate control prodrugs resistant to oxidative catalysis.[29,33] Prodrugs were synthesized using a semisynthetic strategy by functionalization of gemcitabine, **1** (Scheme 1). Treatment of **1** with allyl, propargyl, or benzyl chloroformate in the presence of DBU formed the corresponding carbonate prodrugs **2a,p,b** in moderate yields. To synthesize the 4-carbamate derivatives, the primary alcohol in position 5′ was first silylated using TBS-Cl and imidazole, followed by treatment with the corresponding alkyl chloroformates. TBAF-mediated deprotection yielded the final carbamate prodrugs **5a,p,b** in moderate to good yields.

Bioorthogonality Study: Carbonate vs Carbamate Gemcitabine Prodrugs. Although, in principle, the masking of either the 5′-OH or the 4-NH_2 group of gemcitabine could both have a significant impact on the drug's antiproliferative properties, the limiting factor in the development of any bioorthogonally activated prodrug approach is the stability of the protecting group to enzymatic metabolism. To determine the robustness of each deactivation strategy in cell culture, dose−response studies with gemcitabine (**1**) and prodrugs **2a,p,b** and **5a,p,b** were carried out in two human cancer cell lines. Pancreas adenocarcinoma BxPC-3 and Mia PaCa-2 cells were chosen as cell models due to the clinical relevance of gemcitabine as a first-line drug in pancreatic cancer therapy.[24,25] As shown in Figure 2, carbamate-protected prodrugs **5a,p,b** showed significant reduction of cytotoxicity relative to that of gemcitabine (EC_{50} (**5a,p,b**)/EC_{50} (**1**) > 23) in both cell lines, verifying the efficacy of the deactivation strategy. On the contrary, prodrugs **2a,p,b** displayed cytotoxicity similar to that of gemcitabine (**1**), suggesting that these prodrugs are rapidly

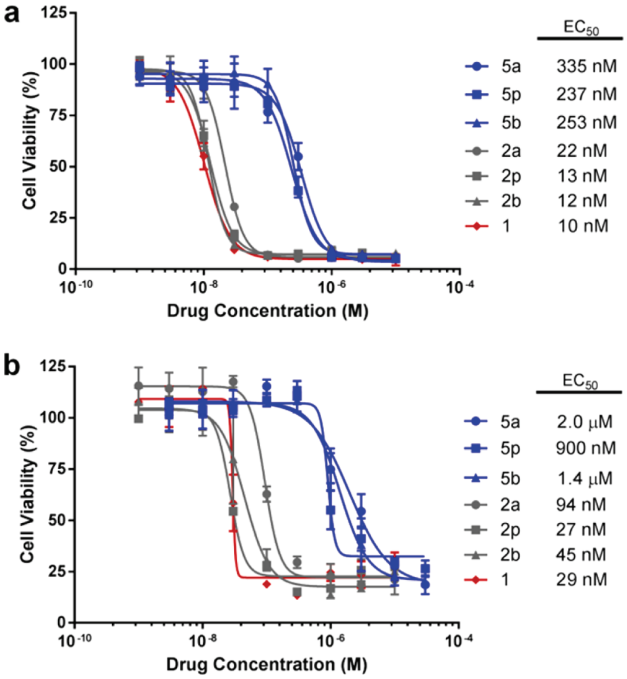

Figure 2. Study of the prodrugs' bioorthogonality. Semilog dose−response curves and calculated EC_{50} values of prodrugs **2a,p,b** (in gray) and **5a,p,b** (in blue) in comparison to those of unmodified gemcitabine (**1**, in red) in (a) BxPC-3 and (b) Mia PaCa-2 cells. Cell viability was measured at day 4 using PrestoBlue reagent. Error bars: ± SD from $n = 3$.

bioactivated inside cells. These results are in accordance with the weaker nature of the carbonate bond[32] and strongly indicate that carbonate-based masking strategies are not suitable for bioorthogonal applications. Consequently, only carbamate prodrugs **5a,p,b** were moved forward in this study.

Pd^0-Mediated Conversion of Prodrugs 5a,p,b into Gemcitabine. Polystyrene-supported reagents have been employed for a wide range of cell-based applications and have shown excellent biocompatibility both *in vitro* and *in vivo*.[8,34−36] As catalytically active Pd^0 nanoparticles can be readily generated and trapped in an amino-functionalized polystyrene matrix,[8,14] Pd^0-functionalized resins (150 μm in average diameter, Figure 3a) were prepared from NovaSyn TG amino resin HL following the procedure previously reported[8] and used as the heterogeneous palladium source (4.4% w/w in Pd). To test the susceptibility of the different carbamates to Pd^0-mediated catalysis in a biocompatible environment, compounds **5a,p,b** (100 μM) and Pd^0-resins (1 mg/mL, $[Pd^0]$ = 400 μM) were dispersed in PBS (300 mOsm/kg, pH 7.4) and incubated at 37 °C for 24 h (Figure 3b). Reactions were analyzed by HPLC at different time points (0, 6, and 24 h), with prodrugs **5a,p,b** being retained for 2.56, 2.45, and 2.96 min, respectively, and the gemcitabine peak appearing at 0.93 min (Figure 3c−f). Treatment of Cbz-protected compound **5b** with the palladium source produced negligible levels of gemcitabine (**1**) after 24 h (Figure 3f), which corresponds with the need for an additional hydrogen source to achieve reductive cleavage of Cbz groups.[29,33] On the contrary, incubation of compounds **5a** and **5p** with Pd^0-resins led to the generation of significant levels of gemcitabine (**1**) in less than 24 h (Figure 3d,e). Interestingly, deprotection of **5p** proceeded in a faster and cleaner manner, with a reaction half-

dx.doi.org/10.1021/jm500531z | J. Med. Chem. 2014, 57, 5395−5404

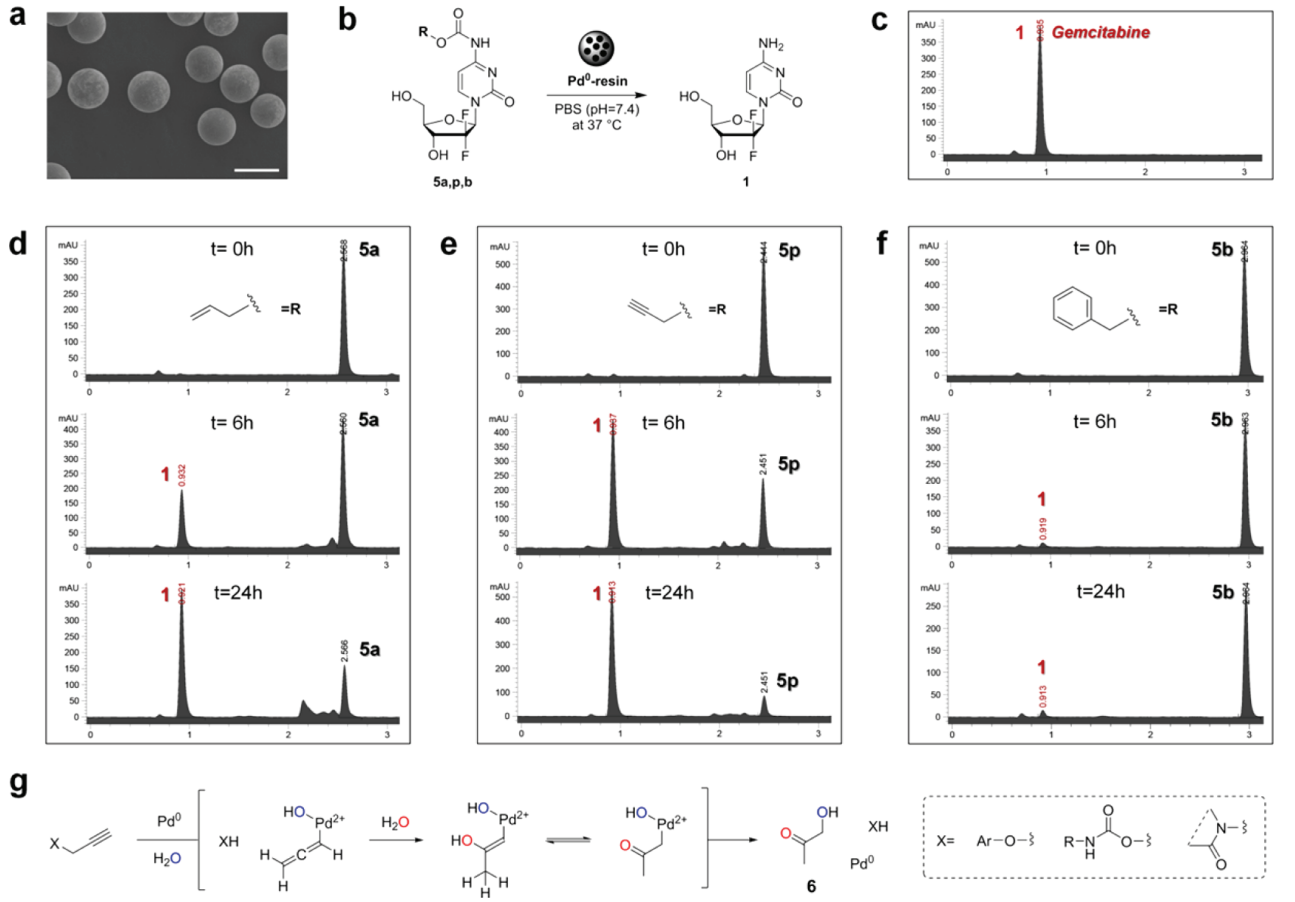

Figure 3. Palladium-mediated conversion assay in cell-free biocompatible conditions. (a) SEM image of Pd^0-resins. Scale bar = 150 μm. (b) Pd^0-mediated carbamate cleavage of compounds **5a,p,b**. (c) HPLC chromatogram of unmodified gemcitabine (**1**). (d–f) HPLC chromatograms (UV detector 280 nm) of 100 μM PBS solutions of compounds **5a** (left panel), **5p** (central panel), and **5b** (right panel) treated with Pd^0-resins at 37 °C for 0 h (top), 6 h (central), and 24 h (bottom). (g) Proposed mechanism for the Pd^0-catalyzed cleavage of *O*/*N*-propargyl groups in water.

life of <6 h (Figure 3e). These results are in accordance with previous observations[8,37,38] that have reported the efficient cleavage of various propargylated compounds by palladium species in biocompatible conditions. A potential mechanism for this process and for the reported formation of nontoxic 1-hydroxyacetone[8,39] (**6**) as a reaction byproduct is proposed in Figure 3g.

Pd^0-Mediated Prodrug Activation in Cell Culture. Bioorthogonal *in situ* generation of gemcitabine (**1**) from the carbamate prodrugs was first investigated in standard cell culture conditions with BxPC-3 cells using Pd^0-resins as the extracellular activating device. Prodrugs **5a,p,b** and Pd^0-resins were incubated independently (negative controls) or in combination (BOOM activation assay) and unmodified gemcitabine (**1**) used as the positive control. While neither the prodrugs nor the Pd^0-resins exhibited cytotoxicity, a combination of **5a** and **5p** with Pd^0-resins displayed a strong toxigenic effect (Figure 4), confirming the *in situ* bioorthogonal synthesis of cytotoxic gemcitabine (**1**). In the context of the present study, "toxigenic effect" describes the gemcitabine levels generated by each prodrug/Pd^0-resin combination in cell culture which in turn result in a cytotoxic phenotype. This effect is indirectly quantified by determining the antiproliferative activity caused by each prodrug/Pd^0-resin combination, which is directly proportional to the concentration of cytotoxic drug generated, and qualitatively proved by the verification of its mode of action. Consistent with the anticipated resistance of the *N*-Cbz functional group to palladium-mediated oxidative cleavage, cells treated with prodrug **5b** and Pd^0-resins did not produce any negative effect on cell viability.

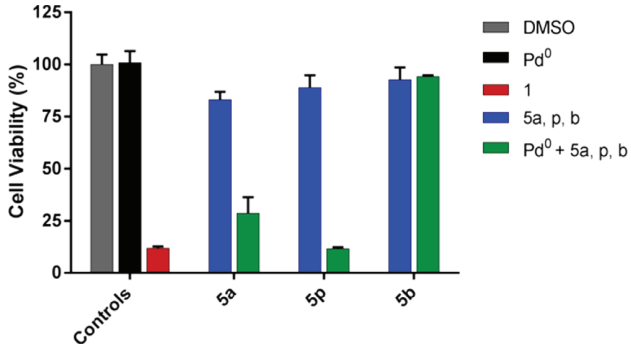

Figure 4. Palladium-mediated conversion of prodrugs **5a,p,b** into gemcitabine (**1**) in pancreatic cancer BxPC-3 cells. Experiments: 0.1% (v/v) DMSO (untreated cell control, in gray); 0.67 mg/mL of Pd^0-resins (negative control, in black); gemcitabine (100 nM, positive control, in red); prodrug **5a,p,b** (100 nM, negative control, in blue); and 0.67 mg/mL of Pd^0-resins + prodrug **5a,p,b** (100 nM, BOOM activation, in green). Cell viability was measured at day 5 using PrestoBlue reagent. Error bars: ± SD from n = 3.

dx.doi.org/10.1021/jm500531z | *J. Med. Chem.* 2014, 57, 5395–5404

Dose−response studies were subsequently carried out to compare the treatment of **5a** and **5p**/Pd^0-resin combinations at different concentrations in two cell lines: BxPC-3 and Mia PaCa-2 cells. As shown in Figure 5a,b, reduction of cell viability

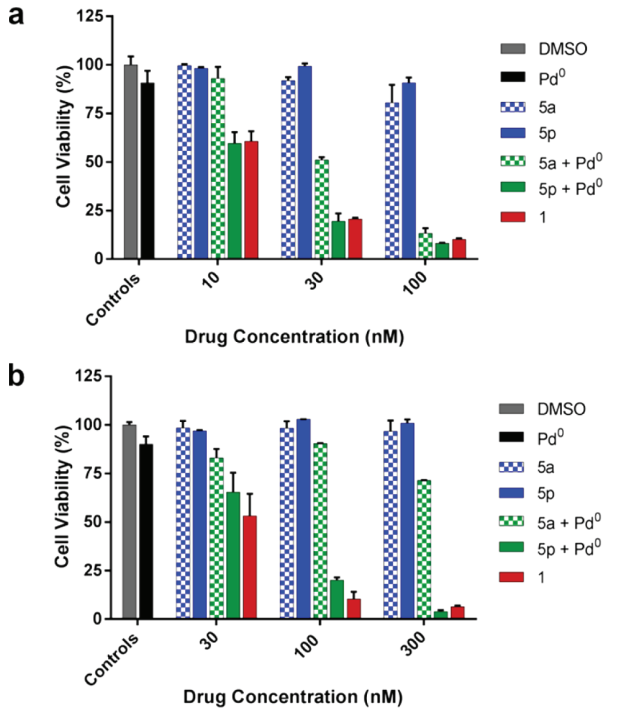

Figure 5. Bioorthogonally activated toxigenic effect in cancer cell culture: (a) BxPC-3 and (b) Mia PaCa-2 cells. Dose−response study: 0.1% (v/v) DMSO (untreated cell control, in gray); 0.67 mg/mL Pd^0-resins (negative control, in black); gemcitabine (positive control, in red); prodrug **5a,p** (negative control, in blue); and 0.67 mg/mL of Pd^0-resins + prodrug **5a,p** (BOOM activation, in green). Cell viability was measured at day 5 using PrestoBlue reagent. Error bars: ± SD from $n = 3$.

was observed with compounds **5a** and **5p** only when incubated with Pd^0-resins. Analysis of the toxigenic effect displayed by each prodrug/catalyst combination clearly ranked the *N*-Poc-protected prodrug **5p** as the most effective gemcitabine-generating precursor in the presence of Pd^0-resins, exhibiting analogous cytotoxic activity to that of the unmodified drug. Importantly, neither the palladium source nor the prodrugs exhibited antiproliferative activity when separately incubated at any of the concentrations tested, thus supporting the bioorthogonality of the strategy. It is important to note that the combination of *N*-Alloc-protected prodrug **5a** and Pd^0-resins resulted in significantly higher toxigenic effect against BxPC-3 cells than that in Mia PaCa-2 cells. Since both cell lines display similar sensitivity to unmodified gemcitabine, these results show that the palladium-mediated cleavage of the *N*-Alloc group of prodrug **5a** is significantly affected by either the cell type or the culture conditions (BxPC-3 cells are grown in RPMI, while Mia PaCa-2 cells are cultured in DMEM medium). On the contrary, the combined treatment of **5p** and Pd^0-resins displayed comparable toxigenic effects in both cell lines, indicating that the biological environment has little or no influence on the *N*-Poc deprotection process, as would be expected from a truly bioorthogonal reaction.

Real-time monitoring of BxPC-3 cell proliferation using an IncuCyte ZOOM microscope was performed to compare the effect of each prodrug/catalyst combination upon the kinetics of tumor cell growth. Time-lapse imaging of the negative controls **5a** and **5p** showed a standard growth curve up to 100% cell confluence level by day 4−5 (light and dark blue curves, respectively; Figure 6), while gemcitabine treatment efficiently

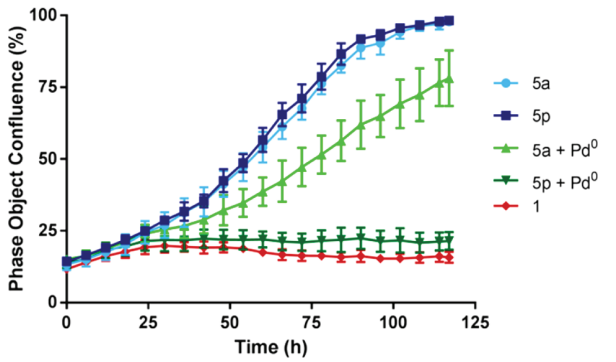

Figure 6. Real-time cell confluence study in pancreatic cancer BxPC-3 cells. The cell population was monitored for 120 h using an IncuCyte ZOOM system in an incubator (5% CO_2 and 37 °C). Drug/prodrug concentration: 30 nM. Error bars: ± SD from $n = 3$.

suppressed cell proliferation within 24 h. In accordance with the cell viability studies, the toxigenic effect mediated by either prodrug **5a** or **5p** incubated with Pd^0-resins (light and dark green curves, respectively; Figure 6) were patently different (see Supporting Information for a motion picture of the IncuCyte experiment). The prodrug **5p**/catalyst combination inhibited cell proliferation with the same efficacy and kinetic response as unmodified gemcitabine (**1**), proving that cytotoxic levels of the drug were rapidly generated. Although treatment with the **5a**/catalyst combination markedly delayed BxPC-3 cell growth relative to the negative controls, its antiproliferative effect was significantly inferior to either the **5p**/Pd^0-resins combination or unmodified gemcitabine (**1**), indicating quantitatively lower levels of active drug being generated.

Study of Cytotoxic Mode of Action. Double-stranded breaks caused by DNA damage induce phosphorylation of the variant histone of the H2A protein family, γ-H2AX. Phosphorylated γ-H2AX is responsible for recruiting and localizing the DNA repair mechanism.[40] Gemcitabine damages DNA through partial DNA chain termination and by stalling of replication forks.[41] In order to analyze the toxigenic effect caused by the prodrug/catalyst combination at the molecular level, immunofluorescence studies were carried out to probe for phosphorylated γ-H2AX as a marker of DNA damage in Mia PaCa-2 cells (Figure 7). While the negative controls (Pd^0-resins or prodrug **5p** separately incubated; Figure 7a,b) did not show the presence of phosphorylated γ-H2AX in the cell nuclei, cells treated with either gemcitabine (Figure 7c) or the Pd^0-resins + **5p** combination (Figure 7d) expressed significant levels of phospho-γ-H2AX. This study further illustrates that the cytotoxic activity generated from the prodrug/catalyst combination and unmodified gemcitabine is equivalent.

Pd^0-Mediated Probe Activation in Zebrafish. We have recently shown that catalytically functional Pd^0-resins can be implanted in the yolk sac of zebrafish embryos without inducing toxicity or affecting the embryo development.[8] To compare the *in vivo* bioorthogonality and palladium sensitivity

dx.doi.org/10.1021/jm500531z | J. Med. Chem. 2014, 57, 5395−5404

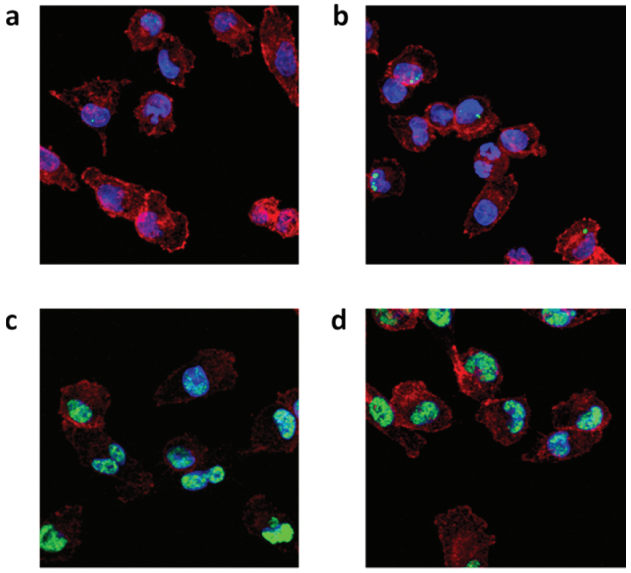

Figure 7. DNA damage study. Merge fluorescent images of Mia PaCa-2 cells 24 h after treatment with (a) 0.67 mg/mL Pd^0-resins (negative control); (b) prodrug **5p** (300 nM, negative control); (c) gemcitabine (300 nM, positive control); and 0.67 mg/mL of Pd^0-resins + prodrug **5p** (300 nM, BOOM activation assay). Fluorescent labels: Hoechst 33342 for cell nuclei (blue), Alexa Fluor 594 phalloidin for F-actin (red), and anti-phospho-histone γ-H2AX + Alexa Fluor 488 secondary antibody for phosphorylated γ-H2AX (green).

of each of the carbamate protecting groups under study, *N*,*N*′-bis(alkyloxycarbonyl) rhodamine derivatives **8a,p,b** were prepared and used as off-on fluorescent probes (Figure 8a). Compounds **8a,p,b** were synthesized from rhodamine 110, **7**, by reaction with the corresponding alkylchloroformate and a base (triethylamine or pyridine) in dry DMF. The resulting nonfluorescent rhodamine precursors were incubated with 2-dpf zebrafish embryos containing either a nonfunctionalized resin (nonactive resin) or a Pd^0-resin (active) in the yolk sac for 24 h and subsequently analyzed by fluorescence microscopy. Zebrafish embryos treated with Alloc-protected compound **8a** showed high levels of fluorescence emission regardless of the presence or absence of palladium, particularly from the yolk sac and the digestive system (Figure 8b,c, top panel). Because of the high levels of biochemically generated fluorescence background, local palladium-mediated activation of **8a** within the zebrafish yolk was not detectable, an indication of the low bioorthogonality of the *N*-Alloc group in zebrafish. On the contrary, compounds **8p** and **8b** showed improved biochemical stability, with the fluorescent background signal mostly being observed from the digestive system, which is in accordance with our previous observations.[8] As expected, Cbz-protected compound **8b** did not exhibit sensitivity to palladium catalysis (Figure 8b,c, lower panel), while local palladium-mediated generation of rhodamine 110 was clearly observed from **8p** in the zebrafish yolk sac containing a Pd^0-resin (Figure 8b,c, middle panel). As shown in Figure 8d, image analysis demonstrated up to a 4-fold increase in fluorescence intensity within close vicinity of the Pd^0-resin (blue line). On the contrary, apart from the autofluorescence intensity typically observed from the nonfunctionalized resin, this inactive resin did not lead to an increment of fluorescence levels in the area surrounding it (red line). This study suggests that, from the carbamate groups herein studied, only the *N*-Poc masking strategy would allow generating locally increased concentrations of a functionally active small molecule by palladium heterogeneous catalysis *in vivo*.

CONCLUSIONS

The chemical protection of gemcitabine's 4-amino group as a carbamate led to a significant reduction of the drug's cytotoxic activity. Among the carbamate derivatives investigated, the *N*-Poc group exhibited the highest sensitivity to palladium-mediated cleavage at 37 °C in both buffered solution and cell culture. This is noteworthy since, to date, our group[14,19] and others[12,13,16−18,42−44] have favored the use of *N*-Alloc groups over *N*-Poc to implement coupling and decoupling strategies[45] for BOOM studies. Cell viability, time-lapse microscopy, and DNA damage assays confirmed the bioorthogonal generation of cytotoxic gemcitabine from the combined treatment of extracellular Pd^0-resins and the *N*-Poc-protected precursor in pancreatic cancer cell culture. Unlike the *N*-Alloc- and *N*-Cbz-protected derivatives, the bis-*N*,*N*′-Poc-rhodamine 110[8] became locally activated by a Pd^0-resin implanted in the yolk sac of zebrafish embryos, further reinforcing its nomination as the carbamate group of choice for developing bioorthogonal studies based on heterogeneous palladium catalysis. Parallel independent studies from Chen et al. (intracellular protein activation by palladium-mediated homogeneous catalysis), published just before the submission of this article,[46] reported analogous findings with the *N*-Poc group. Finally, the simplicity of the masking strategy together with the biocompatibility and efficacy of the palladium-mediated deprotection process underlines the potential of this method to modulate the pharmacodynamics and pharmacokinetics of amino-containing drugs.

EXPERIMENTAL PROCEDURES

Synthetic Procedures. *General Methods.* Chemicals and solvents were purchased from Fisher Scientific, Sigma-Aldrich, or VWR International Ltd. Gemcitabine HCl was purchased from Shandong Boyuan Pharmaceutical Co. Ltd. NMR spectra were recorded at ambient temperature on a 500 MHz Bruker Avance III spectrometer. Chemical shifts are reported in parts per million (ppm) relative to the solvent peak. R_f values were determined on Merck TLC Silica gel 60 F254 plates under a 254 nm UV source. Purification was carried out by flash column chromatography using commercially available silica gel (220−440 mesh, Sigma-Aldrich). All compounds used in the biological experiments were >95% pure, as measured by HPLC using an evaporative light scattering detector. Method: eluent A, water and formic acid (0.1%); eluent B, acetonitrile and formic acid (0.1%); A/B = 95:5 to 5:95 in 3 min, isocratic 1 min, 5:95 to 95:5 in 1 min, and isocratic 1 min.

Synthesis of Pd^0-Resins. Pd^0-functionalized resins were prepared from NovaSyn TG amino resin HL (0.39 mmol NH_2/g) as previously described.[8]

*Synthesis of Carbonate-Protected Derivatives **2a,p,b**.* Gemcitabine HCl (150 mg, 0.5 mmol) was dissolved in dry DMF (3 mL) with DBU (194 μL, 1.30 mmol) under N_2 atmosphere. The mixture was then cooled to 4 °C in an ice bath. Allyl, propargyl, or benzyl chloroformate (0.75 mmol) was added dropwise to the mixture. The mixture was stirred overnight and allowed to warm up to room temperature (r.t.). The solvents were then removed *in vacuo*, the crude redissolved with 25% isopropanol (IPA) in $CHCl_3$ (20 mL), and washed with H_2O (20 mL). The aqueous layer was washed with 25% IPA in $CHCl_3$ (3 × 20 mL) and the combined organic layers dried over $MgSO_4$, filtered, and concentrated *in vacuo*.

*4-Amino-1-(2-deoxy-2,2-difluoro-5-O-[allyloxycarbon-yl]-β-D-erythro-pentofuranosyl)pyrimidin-2(1H)-one] (**2a**).* The crude was purified by column chromatography using 8% MeOH in DCM (R_f

dx.doi.org/10.1021/jm500531z | J. Med. Chem. 2014, 57, 5395−5404

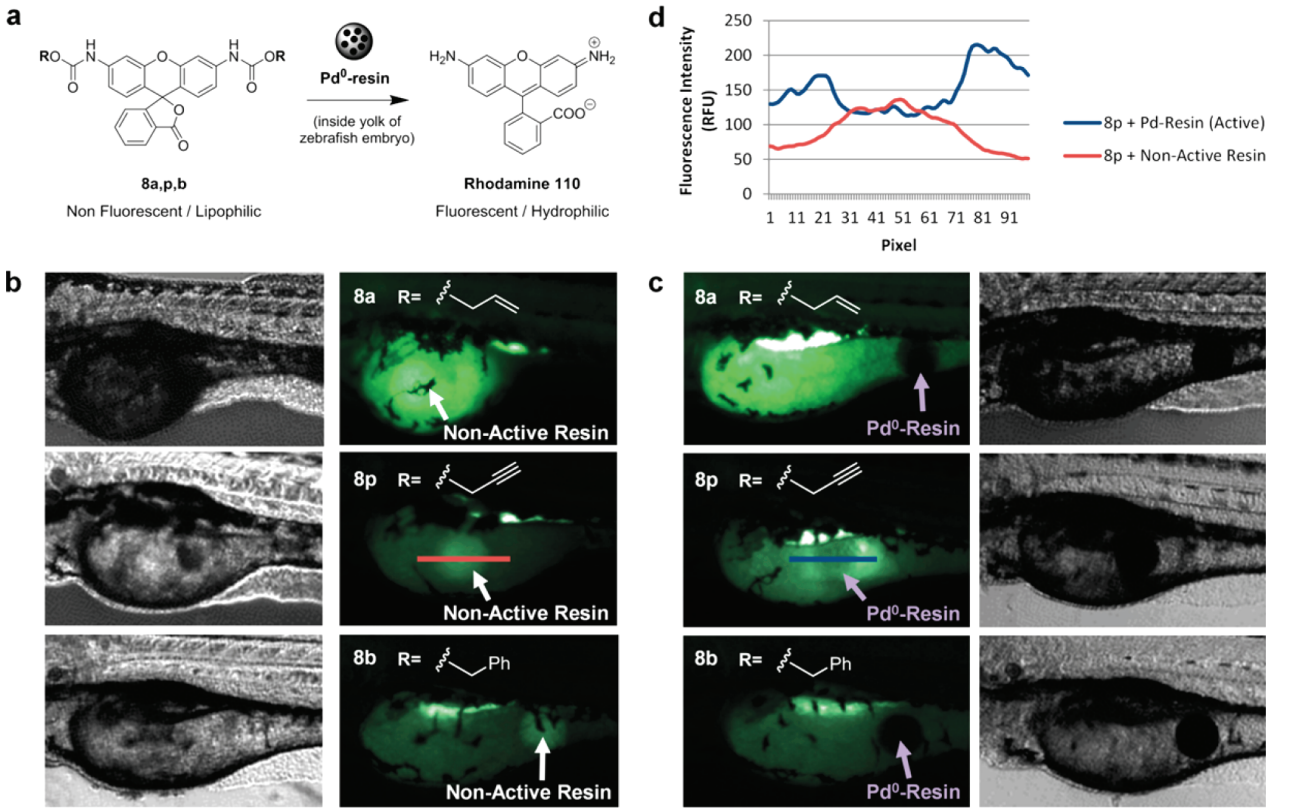

Figure 8. Pd^0-mediated carbamate cleavage of rhodamine precursors in zebrafish. (a) BOOM conversion of nonfluorescent lipophilic compounds **8a,p,b** into highly fluorescent hydrophilic rhodamine 110. (b) 3-dpf zebrafish embryos (n = 5) containing a nonfunctionalized resin (indicated with white arrows) after incubation with 5 μM of compounds **8a** (top), **8p** (middle), and **8b** (bottom) for 24 h at 31 °C. (c) 3-dpf zebrafish embryos (n = 5) containing a Pd^0-resin (indicated with purple arrows) after incubation with 5 μM of compounds **8a** (top), **8p** (middle), and **8b** (bottom) for 24 h at 31 °C. Fish were imaged by phase contrast and fluorescent microscopy (ex., 470/40; em., 525/50). (d) Analysis of fluorescence intensity/pixel across a horizontal line of approximately 300 μm drawn in the yolk sac of the zebrafish embryos and encompassing both the resin and the area surrounding it. Note: the red and blue lines represent the areas of fluorescence intensity profile measured over the inactive resin (b, middle right panel) and the Pd^0-resin (c, middle left panel), respectively.

0.29, 10% MeOH in DCM), which yielded a light green solid (90 mg, 52% yield). ^{1}H NMR (500 MHz, DMSO) δ 7.50 (d, J = 7.5, 1H), 7.42 (d, J = 5.7, 2H), 6.44 (d, J = 6.3, 1H), 6.17 (s, 1H), 5.99−5.89 (m, 1H), 5.79 (d, J = 7.5, 1H), 5.38−5.23 (m, 2H), 4.63 (dt, J = 5.5, 1.3, 2H), 4.47−4.37 (m, 2H), 4.18 (s, 1H), 4.07−4.00 (m, 1H). ^{13}C NMR (126 MHz, DMSO) δ 165.63 (C), 154.48 (C), 154.07 (C), 141.16 (CH), 132.02 (CH), 122.60 (t, J_{C-F} = 264.6, C), 118.56 (CH_2), 94.87 (CH), 83.89 (CH), 77.22 (CH), 70.09 (t, J_{C-F} = 25.2, CH), 68.16 (CH_2), 66.31 (CH_2). LRMS (ESI) m/z 346.0 $[M - H]^-$. HRMS (FAB) m/z $[M - H]^-$ calcd for $C_{13}H_{14}O_6N_3F_2$, 346.0856; found, 346.0859.

*4-Amino-1-(2-deoxy-2,2-difluoro-5-O-[propargyloxy-carbonyl]-β-D-erythro-pentofuranosyl)pyrimidin-2(1H)-one] (**2p**).* The crude was purified by column chromatography using 8% MeOH in DCM (R_f 0.23, 10% MeOH in DCM), which yielded a pale yellow solid (81 mg, 47%). ^{1}H NMR (500 MHz, DMSO) δ 7.65 (d, J = 7.5, 1H), 7.44 (d, J = 13.0, 2H), 6.24 (t, J = 5.0, 1H), 5.81 (d, J = 7.5, 1H), 5.28−5.26 (m, 2H), 4.88 (s, 2H), 4.22−4.16 (m, 1H), 3.79−3.62 (m, 3H). ^{13}C NMR (126 MHz, DMSO) δ 165.71 (C), 154.41 (C), 152.63 (C), 141.43 (CH), 121.48 (t, J_{C-F} = 262.1, C), 94.83 (CH), 83.76 (CH), 79.16 (CH), 78.11 (CH), 77.25 (C), 73.39 (t, J_{C-F} = 26.5, CH), 59.18 (CH_2), 56.37 (CH_2). LRMS (ESI) m/z 379.9 $[M + Cl]^-$. HRMS (FAB) m/z $[M - H]^-$ calcd for $C_{13}H_{12}O_6N_3F_2$, 344.0700; found, 344.0728.

*4-Amino-1-(2-deoxy-2,2-difluoro-5-O-[benzyloxy-carbonyl]-β-D-erythro-pentofuranosyl)pyrimidin-2(1H)-one] (**2b**).* The crude was purified by column chromatography using 6% MeOH in DCM (R_f 0.05, 4% MeOH in DCM), which yielded a white solid (70 mg, 53% yield). ^{1}H NMR (500 MHz, DMSO) δ 7.49 (d, J = 7.5, 1H), 7.44−7.33 (m, 7H), 6.44 (d, J = 6.2, 1H), 6.17 (s, 1H), 5.76 (d, J = 7.5, 1H), 5.17 (s, 2H), 4.52−4.35 (m, 2H), 4.18 (s, 1H), 4.03 (t, J = 6.1, 1H). ^{13}C NMR (126 MHz, DMSO) δ 165.60 (C), 154.45 (C), 154.20 (C), 141.15 (CH), 135.04 (C), 128.50 $(CH)_2$, 128.42 (CH), 128.17 $(CH)_2$, 122.57 (t, J_{C-F} = 258.3, C), 94.83 (CH), 83.86 (CH), 77.18 (CH), 70.10 (t, J_{C-F} = 23.4, CH), 69.22 (CH_2), 66.39 (CH_2). LRMS (ESI) m/z 398.0 $[M + H]^+$. HRMS (FAB) m/z $[M - H]^-$ calcd for $C_{17}H_{16}O_6N_3F_2$, 396.1013; found, 396.1016.

*Synthesis of Carbamate-Protected Derivatives **5a,p,b**. Synthesis of Silylated Derivative **3**.* Gemcitabine HCl (500 mg, 1.67 mmol) was dissolved in dry DMF (5 mL) with imidazole (398 mg, 5.85 mmol) and TBS-Cl (301 mg, 2.0 mmol) stirred at r.t. overnight. The mixture was then concentrated *in vacuo*, redissolved in EtOAc (50 mL), and washed with H_2O (50 mL). The aqueous layer was washed twice with EtOAc and, subsequently, the organic layers combined, washed with brine (150 mL), and dried over $MgSO_4$. The crude was purified by column chromatography (eluent 8% MeOH in DCM) to yield intermediate **3** as a white solid 552 mg (88%). ^{1}H NMR (500 MHz, DMSO) δ 7.63 (d, J = 7.5, 1H), 7.38 (s, 2H), 6.31 (d, J = 5.1, 1H), 6.14 (t, J = 7.7, 1H), 5.76 (d, J = 7.5, 1H), 4.19−4.06 (m, 1H), 3.95 (d, J = 11.8, 1H), 3.90−3.77 (m, 2H), 0.90 (s, 9H), 0.09 (d, J = 2.1, 6H). ^{13}C NMR (126 MHz, DMSO) δ 165.58 (C), 154.56 (C), 139.91 (CH), 122.95 (t, J_{C-F} = 258.3, C), 94.51 (CH), 83.45 (t, J_{C-F} = 31.5, CH), 79.76 (CH), 68.23 (t, J_{C-F} = 22.7, CH), 60.72 (CH_2), 25.71 (CH_3), 17.99 (C), −5.52$(CH_3)_3$, −5.63 $(CH_3)_2$. MS (ESI) m/z 378.0 $[M + H]^+$.

dx.doi.org/10.1021/jm500531z | J. Med. Chem. 2014, 57, 5395−5404

Synthesis of Intermediate ***4a***. Compound **3** (100 mg, 0.27 mmol) was dissolved in dry THF (2.5 mL) with pyridine (61 μL, 0.75 mmol) and the mixture cooled to 4 °C in an ice bath. Allyl chloroformate (55 μL, 0.52 mmol) was added dropwise to the mixture and stirred for 1 h. The solvent was removed *in vacuo* and purified via flash chromatography (eluent: 3% MeOH in DCM) to yield compound **4a** as a white solid.

*4-(Allyloxycarbonylamino)-1-(2-deoxy-2,2-difluoro-5-O-[tert-butyl(dimethyl)silyl]-β-D-erythro-pentofuranosyl)pyrimidin-2(1H)-one] (**4a**)*. Eighty-three milligrams, 69% yield (R_f 0.53, 10% MeOH in DCM). ^{1}H NMR (500 MHz, MeOD) δ 8.29 (d, *J* = 7.7, 1H), 7.32 (d, *J* = 7.6, 1H), 6.25 (t, *J* = 6.7, 1H), 6.04−5.94 (m, 1H), 5.39 (dq, *J* = 17.2, 1.5, 1H), 5.27 (dq, *J* = 10.5, 2.6, 1.3, 1H), 4.70 (dt, *J* = 5.6, 1.4, 2H), 4.33−4.24 (m, *J* = 12.5, 8.8, 1H), 4.10 (d, *J* = 12.0, 1H), 4.03−3.89 (m, 2H), 0.97 (s, 9H), 0.17 (s, 6H). ^{13}C NMR (126 MHz, MeOD) δ 165.38 (C), 157.33 (C), 154.35 (C), 144.81 (CH), 133.24 (CH), 123.87 (t, J_{C-F} = 259.7, C), 118.88 (CH_2), 96.95 (CH), 86.22 (t, J_{C-F} = 32.8, CH), 82.46 (CH), 69.56 (t, J_{C-F} = 23.9, CH), 67.56 (CH_2), 61.68 (CH_2), 26.37 (CH_3)$_3$, 19.26 (C), −5.35 (CH_3), −5.45 (CH_3). MS (ESI) *m*/*z* 462.0 [M + H]$^+$.

Synthesis of Intermediates ***4p,b***. Compound **3** (100 mg, 0.27 mmol) was dissolved in dry DMF (2.5 mL) with pyridine (61 μL, 0.75 mmol) and the mixture cooled to 4 °C in an ice bath. Propargyl (63 μL, 0.65 mmol) or benzyl chloroformate (56 μL, 0.39 mmol) was added dropwise to the mixture. The mixture was stirred at r.t. overnight (for **4b**) or for 48 h (for **4p**). The solvents were removed and the mixture redissolved with EtOAc (30 mL) and washed with H_2O (30 mL). The aqueous layer was washed twice more with EtOAc (30 mL each) and the combined organic layers dried over $MgSO_4$, solids filtered off, and concentrated *in vacuo*. The crude was purified via flash chromatography (eluent: 3% MeOH in DCM) to yield compounds **4p,b** as white solids.

*4-(Propargyloxycarbonylamino)-1-(2-deoxy-2,2-difluoro-5-O-[tert-butyl(dimethyl)silyl]-β-D-erythro-pentofuranosyl)pyrimidin-2(1H)-one] (**4p**)*. Fifty-three milligrams, 44% yield. (R_f 0.6, 10% MeOH in DCM) ^{1}H NMR (500 MHz, MeOD) δ 8.30 (d, *J* = 7.6, 1H), 7.29 (d, *J* = 7.6, 1H), 6.25 (t, *J* = 6.7, 1H), 4.84 (d, *J* = 2.5, 2H), 4.33−4.24 (m, 1H), 4.10 (d, *J* = 12.0, 1H), 4.03−3.90 (m, 2H), 2.99 (t, *J* = 2.3, 1H), 0.98 (s, 9H), 0.17 (s, 6H). ^{13}C NMR (126 MHz, MeOD) δ 165.28 (C), 157.29 (C), 154.57 (C), 144.97 (CH), 123.88 (t, J_{C-F} = 259.6, C), 96.93 (CH), 86.15 (t, J_{C-F} = 32.8, CH), 82.49 (CH), 77.70 (C), 76.92 (CH), 69.57 (t, J_{C-F} = 22.7, CH), 61.69 (CH_2), 54.34 (CH_2), 26.36 (CH_3)$_3$, 19.26 (C), −5.36 (CH_3), −5.46 (CH_3). MS (ESI) *m*/*z* 460.2 [M + H]$^+$.

*4-(Benzyloxycarbonylamino)-1-(2-deoxy-2,2-difluoro-5-O-[tert-butyl(dimethyl)silyl]-β-D-erythro-pentofuranosyl)pyrimidin-2(1H)-one] (**4b**)*. Fifty-six milligrams, 42% yield (R_f 0.5, 10% MeOH in DCM) which. ^{1}H NMR (500 MHz, CDCl3) δ 8.11 (d, *J* = 7.5, 1H), 7.40−7.32 (m, 5H), 7.25−7.20 (m, 1H), 6.40−6.32 (m, 1H), 5.22 (s, 2H), 4.41−4.31 (m, 1H), 4.09−3.85 (m, 3H), 0.93 (s, 9H), 0.12 (s, 6H). ^{13}C NMR (126 MHz, DMSO) δ 162.90 (C), 154.93 (C), 152.35 (C), 144.42 (CH), 135.02 (C), 128.85 ($CH)_2$, 128.43 ($CH)_2$, 122.32 (t, J_{C-F} = 258.3, C), 95.54 (CH), 84.56 (t, J_{C-F} = 32.8, CH), 81.62 (CH), 69.31 (t, J_{C-F} = 26.5, CH), 68.22 (CH_2), 60.69 (CH_2), 25.97 (CH_3)$_3$, 18.5 (C), −5.32 (CH_3), −5.41 (CH_3). MS (ESI) *m*/*z* 534.1 [M + Na]$^+$.

Synthesis of Carbamate-Protected Derivatives ***5a,p,b***. Compounds **4a,p,b** (48 mg, 0.1 mmol, 31 mg, 0.07 mmol, 73 mg, 0.14 mmol respectively) and TBAF solution (1.5 equiv for **4a,b** and 2.5 equiv for **4p**) were dissolved in anhydrous THF (3 mL) and stirred at room temperature for 3 h (for **5b**) or overnight (for **5a,p**). The resulting mixture was concentrated *in vacuo* and purified via flash chromatography (eluent: 6% MeOH in DCM) to yield compounds **5a,p,b** as white solids.

*4-(Allyloxycarbonylamino)-1-(2-deoxy-2,2-difluoro-β-D-erythro-pentofuranosyl)pyrimidin-2(1H)-one [**5a**]*. Thirty-two milligrams (92% yield). R_f 0.27 (10% MeOH in DCM). ^{1}H NMR (500 MHz, DMSO) δ 10.96 (s, 1H), 8.23 (d, *J* = 7.6, 1H), 7.10 (d, *J* = 7.6, 1H), 6.31 (d, *J* = 6.5, 1H), 6.16 (t, *J* = 7.5, 1H), 6.00−5.89 (m, 1H), 5.42−5.21 (m, 3H), 4.64 (d, *J* = 5.3, 2H), 4.24−4.13 (m, 1H), 3.88 (dt, *J* = 8.5, 3.1, 1H), 3.84−3.61 (m, 2H). ^{13}C NMR (126 MHz, DMSO) δ 163.40 (C), 153.99 (C), 152.82 (C), 144.45 (CH), 132.39 (CH), 122.94 (t, J_{C-F} = 258.3, C), 118.04 (CH_2), 94.82 (CH), 84.07 (t, J_{C-F} = 32.8, CH), 80.98 (CH), 68.37 (t, J_{C-F} = 22.7, CH), 65.64 (CH_2), 58.79 (CH_2). LRMS (ESI) *m*/*z* 346.0 [M − H]$^-$. HRMS (FAB) *m*/*z* [M − H]$^-$ calcd for $C_{13}H_{14}O_6N_3F_2$, 346.0856; found, 346.0853.

*4-(Propargyloxycarbonylamino)-1-(2-deoxy-2,2-difluoro-β-D-erythro-pentofuranosyl)pyrimidin-2(1H)-one (**5p**)*. Fifteen milligrams (62% yield). R_f 0.41 (10% MeOH in DCM). ^{1}H NMR (500 MHz, DMSO) δ 11.06 (s, 1H), 8.25 (d, *J* = 7.6, 1H), 7.08 (d, *J* = 7.6, 1H), 6.30 (d, *J* = 6.5, 1H), 6.16 (t, *J* = 7.4, 1H), 5.29 (t, *J* = 5.4, 1H), 4.80 (d, *J* = 2.3, 2H), 4.25−4.13 (m, 1H), 3.89 (dt, *J* = 8.5, 3.1, 1H), 3.84−3.63 (m, 2H), 3.62 (t, *J* = 2.3, 1H). ^{13}C NMR (126 MHz, DMSO) δ 163.26 (C), 153.93 (C), 152.37 (C), 144.61 (CH), 122.92 (C), 94.80 (CH), 84.09 (CH), 81.01 (CH), 78.21 (CH), 78.18 (C) 68.37 (CH), 58.78 (CH_2), 53.01 (CH_2). LRMS (ESI) *m*/*z* 344.0 [M − H]$^-$. HRMS (FAB) *m*/*z* [M − H]$^-$ calcd for $C_{13}H_{12}O_6N_3F_2$, 344.0700; found, 344.0719.

*4-(Benzyloxycarbonylamino)-1-(2-deoxy-2,2-difluoro-β-D-erythro-pentofuranosyl)pyrimidin-2(1H)-one (**5b**)*. Fifty-one milligrams, 92% yield. R_f 0.42 (10% MeOH in DCM). ^{1}H NMR (500 MHz, DMSO) δ 10.98 (s, 1H), 8.23 (d, *J* = 7.6, 1H), 7.45−7.32 (m, 5H), 7.11 (d, *J* = 7.6, 1H), 6.31 (d, *J* = 6.5, 1H), 6.16 (t, *J* = 7.4, 1H), 5.29 (t, *J* = 5.5, 1H), 5.20 (s, 2H), 4.25−4.13 (m, 1H), 3.88 (dt, *J* = 8.5, 3.1, 1H), 3.84−3.62 (m, 2H). ^{13}C NMR (126 MHz, DMSO) δ 163.38 (C), 153.99 (C), 153.00 (C), 144.46 (CH), 135.81 (C), 128.48 ($CH)_2$, 128.19 (CH), 127.96 ($CH)_2$, 122.93 (t, J_{C-F} = 259.6, C), 94.86 (CH), 84.08 (t, J_{C-F} = 30.2, CH), 80.98 (CH), 68.37 (t, J_{C-F} = 22.7, CH), 66.67 (CH_2), 58.78 (CH_2). LRMS (ESI) *m*/*z* 396.1 [M − H]$^-$. HRMS (FAB) *m*/*z* [M − H]$^-$ calcd for $C_{17}H_{16}O_6N_3F_2$, 396.1013; found, 396.1016.

Synthesis of Nonfluorescent Probes ***8a,p***. Probes **8a**[14] and **8p**[8] were prepared from rhodamine 110 chloride, **7**, as previously described.[14,8]

Synthesis of Nonfluorescent Probe ***8b***. Under a nitrogen atmosphere, rhodamine 110 chloride (150 mg, 0.41 mmol) was dissolved in dry DMF (4 mL). Separately, benzyl chloroformate (350 μL, 2.45 mmol) and pyridine (298 μL, 3.69 mmol) were dissolved in DMF (1 mL) and added dropwise to the mixture. The reaction mixture was stirred at r.t. for 48 h, solvents removed *in vacuo*, and the resulting crude resuspended in 25% isopropanol in $CHCl_3$ (30 mL) and washed with H_2O. The aqueous layer was then washed 5 times with 25% isopropanol in $CHCl_3$ (30 mL). The combined organic layers were dried over anhydrous $MgSO_4$ and the solids filtered off and concentrated *in vacuo*. The crude was purified via flash chromatography (hexane/ethyl acetate 2:1) to yield bis-*N*,*N*′-benzyloxycarbonyl-rhodamine 110 (**8b**) as a white solid (31 mg, 13%). R_f 0.23 (hexane/ethyl acetate 2:1); ^{1}H NMR (500 MHz, DMSO) δ 10.12 (s, 2H), 8.01 (d, *J* = 7.6, 1H), 7.78 (t, *J* = 7.1, 1H), 7.72 (t, *J* = 7.3, 1H), 7.58 (d, *J* = 1.7, 2H), 7.45−7.33 (m, 10H), 7.27 (d, *J* = 7.6, 1H), 7.20−7.12 (m, 2H), 6.70 (d, *J* = 8.7, 2H), 5.18 (s, 4H). ^{13}C NMR (126 MHz, DMSO) δ 168.66 (C), 153.25 $(C)_2$, 152.51 $(C)_2$, 150.94 (C), 141.43 $(C)_2$, 136.31 $(C)_2$, 135.71 (CH), 130.21 (CH), 128.53 (CH)2, 128.47 (CH)4 128.19 $(CH)_4$, 128.14 (CH)2 125.71 (C), 124.77 (CH), 123.95 (CH), 114.46 $(CH)_2$, 112.48 $(C)_2$, 105.10 $(CH)_2$, 81.94 (C), 66.07 $(CH_2)_2$. MS (ESI) *m*/*z* 597.2 [M − H]$^-$.

Biological Studies. *General Methods*. Cell lines were grown in culture media supplemented with serum (10% FBS) and L-glutamine (2 mM) and incubated in a tissue culture incubator at 37 °C and 5% CO_2. Human pancreas adenocarcinoma BxPC-3 cells (a kind gift from Dr. Mark Duxbury) were cultured in Roswell Park Memorial Institute (RPMI) media. Human pancreatic carcinoma Mia PaCa-2 cells (a kind gift from Dr. Simon Wilkinson) were cultured in Dulbecco's modified Eagle's media (DMEM).

Cell Viability Studies. Cells were seeded in a 96 well plate format at the appropriate cell concentration (2,500 cells/well for BxPC-3 cells and 1,000 cells/well for MiaPaCa-2 cells) and incubated for 48 h before treatment. Each well was then replaced with fresh media containing compound **1** or **2a,p,b**/**5a,p,b** and incubated for 4 days. Untreated cells were incubated with DMSO (0.1% v/v). PrestoBlue

cell viability reagent (10% v/v) was added to each well and the plate incubated for 1 h. Fluorescence emission was detected using a PerkinElmer Victor^2 multilabel reader (excitation filter at 540 nm and emissions filter at 590 nm). All conditions were normalized to the untreated cells (100%) and curves fitted using GraphPad Prism using a sigmoidal variable slope curve.

*Pd^0-Mediated Deprotection of **5a,p,b** in Biocompatible Conditions.* Compounds **5a**, **5p**, and **5b** (100 μM) were dissolved in PBS (1 mL) with 1 mg of Pd^0-resins and shaken at 1400 rpm and 37 °C in a Thermomixer. Reaction crudes were monitored at 0, 6, 24, and 48 h by analytical HPLC (Agilent) using an UV detector at 280 nm to avoid the detection of PBS salts. Eluent A, water and formic acid (0.1%); eluent B, acetonitrile and formic acid (0.1%); A/B = 95:5 to 5:95 in 3 min, isocratic 1 min, 5:95 to 95:5 in 1 min, and isocratic 1 min.

Pd^0-Mediated Dealkylation of 5a,p,b in Cell Culture. BxPC-3 and MiaPaCa-2 cells were plated as described before. Each well was then replaced with fresh media containing Pd^0-resins (0.67 mg/mL) with DMSO (0.1% v/v); **5a,p,b** (3, 10, 30, 100, and 300 nM) with DMSO (0.1% v/v); gemcitabine (3, 10, 30, 100, and 300 nM) with DMSO (0.1% v/v); or a combination of 0.67 mg/mL of Pd^0-resins + **5a,p,b** (3, 10, 30, 100, and 300 nM) with DMSO (0.1% v/v). Untreated cells were incubated with DMSO (0.1% v/v).

Cell Viability Assay. Cells were incubated with drugs for 5 days. PrestoBlue cell viability reagent (10% v/v) was added to each well and the plate incubated for 60 min. Fluorescence emission was detected and results normalized as described above.

Time-Lapse Imaging Study. BxPC-3 cell growth studies were carried out at a single dose of gemcitabine (1) or **5a,p** (30 nM). Each well was imaged every 3 h over 5 d under standard incubation conditions using an IncuCyte ZOOM microscope (placed inside the incubator). Image-based analysis of cell confluence and Supporting Information movie 1 were produced using the IncuCyte software.

DNA Damage Study. Mia PaCa-2 cells were seeded in an 8-well chamber slide with a density of 2,000 cells/well and incubated for 48 h prior to treatment. Each well was then replaced with fresh media containing 0.1% DMSO (v/v) and the following treatments: Pd^0-resins (0.67 mg/mL); **5p** (300 nM); **1** (300 nM); or a combination of Pd^0-resin + **5p** (300 nM). The combination of **5p** and Pd^0 resins were incubated for 24 h at 37 °C prior to treatment with cells. Following 24 h of treatment, cells were fixed with paraformaldehyde (4%, 20 min) and permeabilized cells (Triton X-100, 0.1%) subsequently treated with rabbit monoclonal antibody against Phospho-Histone H2AX (Ser139) (1:400, Cell Signaling Technologies, cat. no. 9718) for 1 h at room temperature. This was followed by 1 h of incubation at room temperature with secondary Alexa Fluor 488 linked antibody (1:1000, goat antirabbit, IgG, Life Technologies), Hoechst 33342 (1:8000, Life Technologies), and Alexa Fluor 594 Phalloidin (1:500, Life Technologies). Cells seeded in the chamber slide were imaged using an Olympus FV1000 microscope and merged using the ImageJ software (National Institutes of Health).

Zebrafish Studies. Wild type zebrafish embryos were collected from AB-TPL breeding pairs and reared at 28 °C in E3 embryo medium. Twenty-four hours postfertilization, embryos were treated with the anesthetic tricaine and pierced in the yolk with a fine needle. Either nonfunctionalized resin or a Pd^0-resin was then rapidly inserted into the yolk. Embryos that lost significant yolk in the procedure were removed from the experiment. Embryos were then gently transferred to fresh E3 medium and returned to 28 °C to ensure the yolk wound was closed. The corresponding probe (**8a,p,b**) was added to the embryo medium (final concentration 5 μM) and fish incubated for additional 24 h at 31 °C. Fish were imaged using fluorescent microscopy (Olympus Scan-R). The fold change in fluorescence with the Pd^0 resin + **8p** in comparison to that with the inactive resin + **8p** were quantified using ImageJ software. A line was drawn horizontally over the yolk sac of the embryo encompassing both the resin beads and the area surrounding them (Figure 8b,c), and the pixel intensities along the lines were calculated (Figure 8d). Experiments were repeated at least twice with n = 4/per condition. Zebrafish husbandry and experiments were performed under Home Office License in compliance with the Animals (Scientific Procedures) Act 1986 and approved by the University of Edinburgh Ethics Committee.

■ ASSOCIATED CONTENT

Ⓢ Supporting Information

NMR spectra of compounds **2a,p,b**, **5a,p,b**, and **8a,p,b** and 5-day time-lapse motion picture of pancreatic BxPC-3 cell proliferation under treatment with 30 nM **5a**; Pd^0-resins + 30 nM **5a**; 30 nM of **5p**; and Pd^0-resins + 30 nM of **5p**. This material is available free of charge via the Internet at http://pubs.acs.org.

■ AUTHOR INFORMATION

Corresponding Author

*Phone: 00 44 1317773584. E-mail: Asier.Unciti-Broceta@igmm.ed.ac.uk.

Notes

The opinions expressed in this publication are those of the authors and do not necessarily represent those of MSD, nor its affiliates.

The authors declare no competing financial interest.

■ ACKNOWLEDGMENTS

J.T.W. is grateful to the College of Medicine and Veterinary Medicine and the University of Edinburgh for a Darwin International Scholarship and an Edinburgh Global Research Scholarship. N.O.C. and A.U.B. thank RCUK and IGMM, respectively, for an Academic Fellowship. W.R., C.F., and E.E.P. are funded by the MRC. We are grateful to the Edinburgh Cancer Research UK Centre for funding this research through the CRUK Development Fund. This work has been partly funded by a Heriot Watt University − IGMM pilot project and the MSD Scottish Life Sciences Fund. We also thank Dr. Mark Duxbury for his helpful comments regarding the clinical applications of the prodrug approach.

■ ABBREVIATIONS USED

BOOM, bioorthogonal organometallic; Alloc, allyloxycarbonyl; Poc, propargyloxycarbonyl; Cbz, carboxybenzyl; TBS-Cl, *tert*-butyldimethylsilyl chloride; TBAF, tetrabutylammonium fluoride; dpf, days postfertilization; TLC, thin layer chromatography; DBU, 1,8-diazabicycloundec-7-ene; DMF, dimethylformamide; DCM, dichloromethane; r.t., room temperature; CD_3OD, deuterated methanol; RPMI, Roswell Park Memorial Institute; DMEM, Dulbecco's modified Eagle's media; DMSO, dimethyl sulfoxide

■ REFERENCES

(1) Sletten, E. M.; Bertozzi, C. R. Bioorthogonal chemistry: fishing for selectivity in a sea of functionality. *Angew. Chem. Int. Ed.* **2009**, *48*, 6974−6998.

(2) Ramil, C. P.; Lin, Q. Bioorthogonal chemistry: strategies and recent developments. *Chem. Commun.* **2013**, *49*, 11007−11022.

(3) Bertozzi, C. R. A decade of bioorthogonal chemistry. *Acc. Chem. Res.* **2011**, *44*, 651−653 and articles within the "Bioorthogonal Chemistry in Biology" special issue.

(4) Lang, K.; Chin, J. W. Bioorthogonal reactions for labeling proteins. *ACS Chem. Biol.* **2014**, *9*, 16−20.

(5) Castano, A. P.; Mroz, P.; Hamblin, M. R. Photodynamic therapy and anti-tumour immunity. *Nat. Rev. Cancer* **2006**, *6*, 535−545.

(6) Lim, R. K.; Lin, Q. Photoinducible bioorthogonal chemistry: a spatiotemporally controllable tool to visualize and perturb proteins in live cells. *Acc. Chem. Res.* **2011**, *44*, 828−839.

(7) Velema, W. A.; Szymanski, W.; Feringa, B. L. Photopharmacology: beyond proof of principle. *J. Am. Chem. Soc.* **2014**, *136*, 2178−2191.
(8) Weiss, J. T.; Dawson, J. C.; Macleod, K. G.; Rybski, W.; Fraser, C.; Torres-Sánchez, C.; Patton, E. E.; Bradley, M.; Carragher, N. O.; Unciti-Broceta, A. Extracellular palladium-catalysed dealkylation of 5-fluoro-1-propargyl-uracil as a bioorthogonally activated prodrug approach. *Nat. Commun.* **2014**, *5*, 3277.
(9) Saxon, E.; Bertozzi, C. R. Cell surface engineering by a modified Staudinger reaction. *Science* **2000**, *287*, 2007−2010.
(10) Agard, N. J.; Prescher, J.; Bertozzi, C. R. A strain-promoted [3 + 2] azide-alkyne cycloaddition for covalent modification of biomolecules in living systems. *J. Am. Chem. Soc.* **2004**, *126*, 15046−15047.
(11) Sletten, E. M.; Bertozzi, C. R. From mechanism to mouse: a tale of two bioorthogonal reactions. *Acc. Chem. Res.* **2011**, *44*, 666−676.
(12) Li, H.; Fan, J.; Peng, X. Colourimetric and fluorescent probes for the optical detection of palladium ions. *Chem. Soc. Rev.* **2013**, *42*, 7943−7962.
(13) Sasmal, P. K.; Streu, C. N.; Meggers, E. Metal complex catalysis in living biological systems. *Chem. Commun.* **2013**, *49*, 1581−1587.
(14) Unciti-Broceta, A.; Johansson, E. M. V.; Yusop, R. M.; Sánchez-Martín, R. M.; Bradley, M. Synthesis of polystyrene microspheres and functionalization with Pd(0) nanoparticles to perform bioorthogonal organometallic chemistry in living cells. *Nat. Protoc.* **2012**, *7*, 1207−1218.
(15) Salic, A.; Mitchison, T. J. A chemical method for fast and sensitive detection of DNA synthesis in vivo. *Proc. Natl. Acad. Sci. U.S.A.* **2008**, *105*, 2415−2420.
(16) Streu, C.; Meggers, E. Ruthenium-induced allylcarbamate cleavage in living cells. *Angew. Chem. Int. Ed.* **2006**, *45*, 5645−5648.
(17) Mascareñas, J. L.; Sánchez, M. I.; Penas, C.; Vázquez, M. E. Metal-catalyzed uncaging of DNA-binding agents in living cells. *Chem. Sci.* **2014**, *5*, 1901−1907.
(18) Sasmal, P. K.; Streu, C. N.; Meggers, E. Metal complex catalysis in living biological systems. *Chem. Commun.* **2013**, *49*, 1581−1587.
(19) Yusop, R. M.; Unciti-Broceta, A.; Johansson, E. M. V.; Sánchez-Martín, R. M.; Bradley, M. Palladium-mediated intracellular chemistry. *Nat. Chem.* **2011**, *3*, 239−243.
(20) Li, N.; Lim, R. K.; Edwardraja, S.; Lin, Q. Copper-free Sonogashira cross-coupling for functionalization of alkyne-encoded proteins in aqueous medium and in bacterial cells. *J. Am. Chem. Soc.* **2011**, *133*, 15316−15319.
(21) Spicer, C. D.; Triemer, T.; Davis, B. G. Palladium-mediated cell-surface labelling. *J. Am. Chem. Soc.* **2012**, *134*, 800−803.
(22) Michel, B. W.; Lippert, A. R.; Chang, C. J. A reaction-based fluorescent probe for selective imaging of carbon monoxide in living cells using a palladium-mediated carbonylation. *J. Am. Chem. Soc.* **2012**, *134*, 15668−15671.
(23) Spicer, C. D.; Davis, B. G. Rewriting the bacterial glycocalyx via Suzuki-Miyaura cross-coupling. *Chem. Commun.* **2013**, *49*, 2747−2749.
(24) Eli Lilly and Company. Gemzar (Gemcitabine) Prescribing Information. http://pi.lilly.com/us/gemzar.pdf.
(25) Rahma, O. E.; Duffy, A.; Liewehr, D. J.; Steinberg, S. M.; Greten, T. F. Second-line treatment in advanced pancreatic cancer: a comprehensive analysis of published clinical trials. *Ann. Oncol.* **2013**, *24*, 1972−1979.
(26) Cerqueira, N. M. F. S. A.; Fernández, P. A.; Ramos, M. J. Understanding ribonucleotide reductase inactivation by gemcitabine. *Chem.—Eur. J.* **2007**, *13*, 8507−8515.
(27) Hazra, S.; Ort, S.; Konra, M.; Lavie, A. Structural and kinetic characterization of human deoxycytidine kinase variants able to phosphorylate 5-substituted deoxycytidine and thymidine analogues. *Biochemistry* **2010**, *49*, 6784−6790.
(28) Ciccolini, J.; Mercier, C.; Dahan, L.; André, N. Integrating pharmacogenetics into gemcitabine dosing-time for a change? *Nat. Rev. Clin. Oncol.* **2011**, *8*, 439−444.
(29) Kocienski, P. J. In *Protecting Groups*; Georg Thieme: Stuttgart, Germany, 1994; and references therein.
(30) Guibé, F. Allylic protecting groups and their use in a complex environment part II: Allylic protecting groups and their removal through catalytic palladium π-allyl methodology. *Tetrahedron* **1998**, *54*, 2967−3042.
(31) Jarowicki, K.; Kocienski, P. Protecting groups. *J. Chem. Soc., Perkin Trans. 1* **2001**, 2109−2135.
(32) Ramesh, R.; Bhat, R. G.; Chandrasekaran, S. Highly selective deblocking of propargyl carbonates in the presence of propargyl carbamates with tetrathiomolybdate. *J. Org. Chem.* **2005**, *70*, 837−840.
(33) Papageorgiou, E. A.; Gaunt, M. J.; Yu, J.-Q.; Spencer, J. B. Selective hydrogenolysis of novel benzyl carbamate protecting groups. *Org. Lett.* **2000**, *2*, 1049−1051.
(34) Sanchez-Martin, R. M.; Muzerelle, M.; Chitkul, N.; How, S. E.; Mittoo, S.; Bradley, M. Bead-based cellular analysis, sorting and multiplexing. *ChemBioChem* **2005**, *6*, 1341−1345.
(35) Unciti-Broceta, A.; Díaz-Mochón, J. J.; Sánchez-Martín, R. M.; Bradley, M. The use of solid supports to generate nucleic acid carriers. *Acc. Chem. Res.* **2011**, *45*, 1140−1152.
(36) Dhaliwal, K.; Alexander, L.; Escher, G.; Unciti-Broceta, A.; Jansen, M.; Mcdonald, N.; Cardenas-Maestre, J. M.; Sanchez-Martin, R.; Simpson, J.; Haslett, C.; Bradley, M. Multi-modal molecular imaging approaches to detect primary cells in preclinical models. *Faraday Discuss.* **2011**, *149*, 107−114.
(37) Santra, M.; Ko, S.-K.; Shin, I.; Ahnz, K. H. Fluorescent detection of palladium species with an O-propargylated fluorescein. *Chem. Commun.* **2010**, 3964−3966.
(38) Liu, B.; Wang, H.; Wang, T.; Bao, Y.; Du, F.; Tian, J.; Li, Q.; Bai, R. A new ratiometric ESIPT sensor for detection of palladium species in aqueous solution. *Chem. Commun.* **2012**, *48*, 2867−2869.
(39) Rambabua, D.; Bhavani, S.; Swamy, N. K.; Rao, M. V. B.; Pal, M. Pd/C-mediated depropargylation of propargyl ethers/amines in water. *Tetrahedron Lett.* **2013**, *54*, 1169−1173.
(40) Kuo, L. J.; Yang, L. γ-H2AX − A novel biomarker for DNA double-strand breaks. *In Vivo* **2008**, *22*, 305−310.
(41) Ewald, B.; Sampath, D.; Plunkett, W. H2AX phosphorylation marks gemcitabine-induced stalled replication forks and their collapse upon S-phase checkpoint abrogation. *Mol. Cancer Ther.* **2007**, *6*, 1239−1248.
(42) Wang, Z.; Zheng, S.; Cai, J.; Wang, P.; Feng, J.; Yang, X.; Zhang, L.; Ji, M.; Wu, F.; He, N.; Wan, N. Fluorescent artificial enzyme-linked immunoassay system based on Pd/C nanocatalyst and fluorescent chemodosimeter. *Anal. Chem.* **2013**, *85*, 11602−11609.
(43) Sasmal, P. K.; Carregal-Romero, S.; Parak, W. J.; Meggers, E. Light-triggered ruthenium-catalyzed allylcarbamate cleavage in biological environments. *Organometallics* **2012**, *31*, 5968−5970.
(44) Wang, J.; Song, F.; Wang, J.; Peng, X. A near-infrared and ratiometric fluorescent chemosensor for palladium. *Analyst* **2013**, *138*, 3667−3672.
(45) Bielski, R.; Witczak, Z. Strategies for coupling molecular units if subsequent decoupling is required. *Chem. Rev.* **2013**, *113*, 2205−2224.
(46) Li, J.; Yu, J.; Zhao, J.; Wang, J.; Zheng, S.; Lin, S.; Chen, L.; Yang, M.; Jia, S.; Zhang, X.; Chen, P. R. Palladium-triggered deprotection chemistry for protein activation in living cells. *Nat. Chem.* **2014**, *6*, 352−361.

frontiers in CHEMISTRY

ORIGINAL RESEARCH ARTICLE
published: 29 July 2014
doi: 10.3389/fchem.2014.00056

N-alkynyl derivatives of 5-fluorouracil: susceptibility to palladium-mediated dealkylation and toxigenicity in cancer cell culture

Jason T. Weiss[1], Craig Fraser[1], Belén Rubio-Ruiz[1], Samuel H. Myers[1], Richard Crispin[1,2], John C. Dawson[1], Valerie G. Brunton[1], E. Elizabeth Patton[1,2], Neil O. Carragher[1] and Asier Unciti-Broceta[1]*

[1] *Edinburgh Cancer Research UK Centre, MRC Institute of Genetics and Molecular Medicine, University of Edinburgh, Edinburgh, UK*
[2] *MRC Human Genetics Unit, MRC Institute of Genetics and Molecular Medicine, University of Edinburgh, Edinburgh, UK*

Edited by:
Laurent G. Désaubry, CNRS and University of Strasbourg, France

Reviewed by:
Luis Álvarez De Cienfuegos Rodríguez, University of Granada, Spain
Frédéric Bihel, CNRS - Université de Strasbourg, France

****Correspondence:***
Asier Unciti-Broceta, Edinburgh Cancer Research UK Centre, Crewe Road South, Edinburgh EH4 2XR, UK
e-mail: asier.unciti-broceta@igmm.ed.ac.uk

Palladium-activated prodrug therapy is an experimental therapeutic approach that relies on the unique chemical properties and biocompatibility of heterogeneous palladium catalysis to enable the spatially-controlled *in vivo* conversion of a biochemically-stable prodrug into its active form. This strategy, which would allow inducing local activation of systemically administered drug precursors by mediation of an implantable activating device made of Pd^0, has been proposed by our group as a way to reach therapeutic levels of the active drug in the affected tissue/organ while reducing its systemic toxicity. In the seminal study of such an approach, we reported that propargylation of the *N*1 position of 5-fluorouracil suppressed the drug's cytotoxic properties, showed high stability in cell culture and facilitated the bioorthogonal restoration of the drug's pharmacological activity in the presence of extracellular Pd^0-functionalized resins. To provide additional insight on the properties of this system, we have investigated different *N*1-alkynyl derivatives of 5-fluorouracil and shown that the presence of substituents near the triple bond influence negatively on its sensitivity to palladium catalysis under biocompatible conditions. Comparative studies of the *N*1- vs. the *N*3-propargyl derivatives of 5-fluorouracil revealed that masking each or both positions equally led to inactive derivatives (>200-fold reduction of cytotoxicity relative to the unmodified drug), whereas the depropargylation process occurred faster at the *N*1 position than at the *N*3, thus resulting in greater toxigenic properties in cancer cell culture.

Keywords: chemotherapeutics, palladium, prodrugs, bioorthogonal chemistry, 5-fluorouracil

INTRODUCTION

Based on the ability to interfere with and/or halt cell division at different stages, cytotoxic agents of various classes have been used as chemotherapeutic drugs in antineoplastic treatment regimens for over 70 years (Chabner and Roberts, 2005; DeVita and Chu, 2008). Although highly effective, the mode of action of these drugs also renders them particularly harmful to healthy tissues with a high rate of cell regeneration. As a result, the clinical dose of most cytotoxic drugs is limited by their lack of selectivity for cancer cells (Chabner and Roberts, 2005; DeVita and Chu, 2008). To reinvigorate the medical use of approved drugs without a satisfactory safety profile and promising drug candidates that failed in clinical trials due to pharmacokinetic issues, one of the main strategies followed by medicinal chemists is to transform chemotherapeutic agents into latent prodrugs that become active in specific organs or tissues by a biological / metabolic mediator (Huttunen et al., 2008; Rautio et al., 2008).

Many different classes of prodrugs have been developed to date (Huttunen et al., 2008; Rautio et al., 2008), resulting in clinically approved therapeutics (e.g., the dopamine precursor levodopa Jenner, 2008) and numerous prodrug candidates and advanced technologies currently in preclinical and clinical development (such as directed enzyme prodrug therapies, which are based on the metabolic activation of drug precursors through enzymes artificially introduced into the organism Xu and McLeod, 2001). While most popular prodrugs become active through a biochemical process, significant progress on the use of benign non-biological means to activate drug precursors (Castano et al., 2006; Versteegen et al., 2013; Clavel et al., 2014; Velema et al., 2014; Weiss et al., 2014a,b; Zanda, 2014) mandate the consideration of expanding the classical prodrug concept and the distinction between two fundamentally different classes of prodrugs: biolabile and bioorthogonal prodrugs. Since the term biolabile is used to define compounds prone to transformation by biological means, the first class would represent all drug precursors belonging to the classical definition of prodrug (Huttunen et al., 2008; Rautio et al., 2008). On the other hand, inspired by the concept of bioorthogonality developed by Bertozzi in the early 2000's (Saxon and Bertozzi, 2000; Agard et al., 2004; Sletten and Bertozzi, 2011), bioorthogonal prodrugs would

encompass physiologically-stable drug precursors subject to activation by non-native, non-biological, non-perturbing means, such as benign light sources (Castano et al., 2006; Velema et al., 2014), metal-free click chemistry (Versteegen et al., 2013), mild hyperthermia (Clavel et al., 2014) or bioorthogonal organometallic (BOOM) reactions (Weiss et al., 2014a,b; Zanda, 2014).

As a first-in-class prodrug approach, our group is investigating the application of metallic palladium as an activating device to modulate the cytotoxic activity of antineoplastic drugs in a bioorthogonal, spatially-controlled manner. The strategy is based on the unique catalytic properties and biocompatibility of heterogeneous Pd^0 both *in vitro* and *in vivo* (Yusop et al., 2011; Unciti-Broceta et al., 2012; Weiss et al., 2014a,b), which has enabled the *in situ* BOOM activation of precursors of 5-fluorouracil (5FU) and gemcitabine in cancer cell culture (Weiss et al., 2014a,b). The surgical insertion of benign palladium-functionalized implants in the disease area (e.g., advanced tumors) in combination with the general administration of palladium-labile prodrugs, could not only decrease systemic levels of the active drug (thereby reducing unwanted toxicity in healthy tissues and organs), but also enhance cancer treatment by generating greater drug levels localized at the disease site than could ever be safely reached by systemic chemotherapy.

A palladium-labile prodrug needs to be designed in such a manner that it only undergoes chemical activation by mediation of this metal. Consequently, the nature of the chemical group used to mask the drug together with the position to be functionalized, are essential features which will determine the overall success of the strategy. In practice, based on the drug's mode of action and the selective catalytic properties of Pd^0, masking strategies are designed to accomplish three goals: (i) eliminating drug's pharmacological properties; (ii) minimizing prodrugs' susceptibility to enzymatic cleavage; and (iii) rendering them "cleavable" by palladium catalysis.

Due to its long clinical history, its well-established mode of action and its narrow therapeutic index (Longley et al., 2003), cytotoxic 5FU was our first choice to explore this challenging strategy (Weiss et al., 2014a). 5FU is as an antimetabolite that undergoes intracellular metabolization on the NH group in position 1 to generate cytotoxic nucleotides (**Figure 1A**), which are the direct cause of 5FU pharmacological activity (Longley et al., 2003). Blocking the formation of active 5FU metabolites by functionalization of the *N*1 position was thus the rationale followed to chemically mask the cytotoxic properties of the drug. Moreover, due to 5FU's lactam/lactim tautomery (see **Figure 1B**), the *N*1 position of the ring possesses a pK_a value of ∼9 (Jang et al., 2001), an unusually low value for NH groups that prompted us to explore chemical groups uncharacteristic for NH protection chemistries. The use of allyl, propargyl and benzyl moieties [alkyl groups widely employed in protection strategies for phenolic OH ($pK_a \sim 9$) (Weiss et al., 2014a)] was investigated on the basis on their anticipated biochemical stability and their potential lability in the presence of palladium (Weiss et al., 2014a). As expected, inactive prodrugs were successfully obtained by alkylation with each of the three groups employed. Remarkably, only the propargyl derivative displayed high sensitivity to palladium in

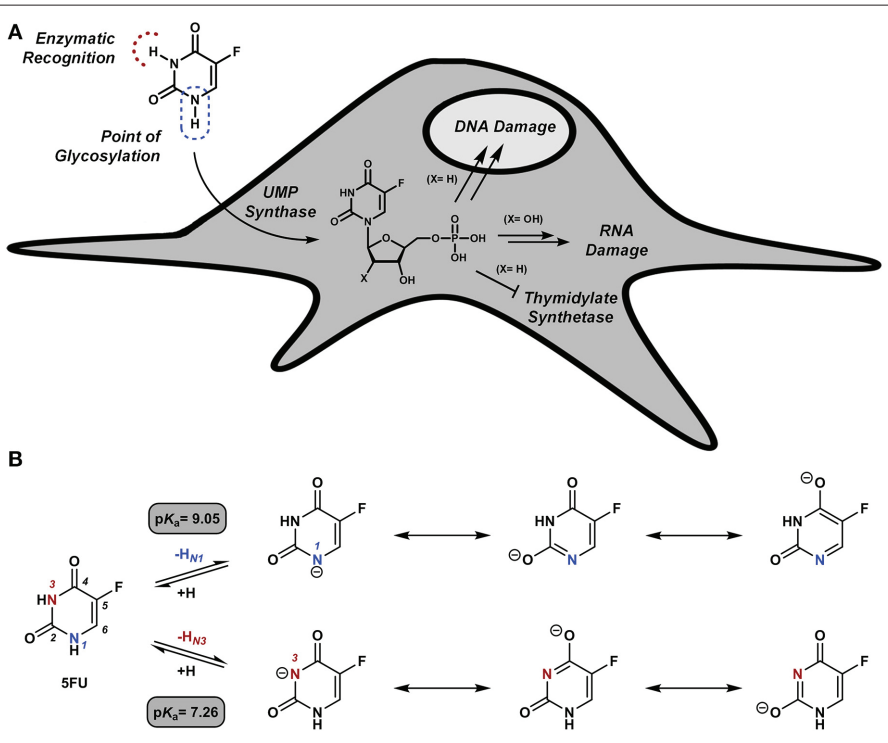

FIGURE 1 | (A) Intracellular bio-functionalization of 5FU to generate cytotoxic metabolites. **(B)** 5FU its conjugate bases and their theoretical pK_a values (Jang et al., 2001).

biocompatible conditions, allowing the chemical rescue of 5FU's pharmacological activity in cancer cell culture by the mediation of extracellular Pd^0-functionalized resins.

Herein we report a follow-on study to provide additional insights on the properties, scope and optimization of this novel prodrug system. A set of *N*1-alkynyl derivatives of 5FU have been developed and their sensitivity to palladium catalysis tested under biocompatible conditions. In addition, biological studies have been carried out to determine the difference in bioorthogonality and palladium sensitivity of the *N*1- vs. the *N*3-propargyl derivatives of 5FU.

MATERIALS AND METHODS

GENERAL METHODS

Chemicals and solvents were purchased from Fisher Scientific, Sigma-Aldrich or VWR International Ltd. NMR spectra were recorded at ambient temperature on a 500 MHz Bruker Avance III spectrometer. Chemical shifts are reported in parts per million (ppm) relative to the solvent peak. *Rf* values were determined on Merck TLC Silica gel 60 F254 plates under a 254 nm UV source. Purifications were carried out by flash column chromatography using commercially available silica gel (220–440 mesh, Sigma-Aldrich).

SYNTHESIS OF Pd^0-RESINS

Pd^0-functionalized resins were prepared from NovaSyn TG amino resin HL (0.39 mmol NH_2/g) as previously described (Weiss et al., 2014a).

SYNTHESIS OF 5-FLUORO-1-PROPARGYLURACIL (3a)

Compound **3a** was prepared from 5-fluorouracil, **1**, as previously described (Weiss et al., 2014a).

SYNTHESIS OF *N*1-FUNCTIONALIZED 5FU DERIVATIVES 3b-e

5FU (100 mg, 0.77 mmol) and DBU (115 µl, 0.77 mmol) were dissolved in acetonitrile (2 ml), and the mixture was cooled down to 4°C in an ice bath. The corresponding alkyl bromide (0.77 mmol) was added dropwise and the reaction mixture allowed to warm up to room temperature. The mixture was stirred overnight, the solvents removed *in vacuo* and the resulting crude purified via flash chromatography (eluent: 1.5% MeOH in DCM), to yield compounds **3b-e** as pure white solids.

1-(1-BUTYN-3-YL)-5-FLUOROURACIL (3b)

75 mg, 54% yield. $R_f = 0.55$ (10% MeOH in DCM). ^{1}H NMR (500 MHz, DMSO) δ 11.89 (s, 1H), 8.15 (*d*, *J* = 6.8, 1H), 5.40–5.30 (*m*, 1H), 3.61 (*d*, *J* = 2.4, 1H), 1.47 (*d*, *J* = 7.0, 3H). ^{13}C NMR (126 MHz, DMSO) δ 157.01 (*d*, *J* = 26.0, C), 148.69, 140.19 (*d*, *J* = 231.4, C), 125.97 (*d*, *J* = 33.8, CH), 81.34, 76.53 (CH), 42.92 (CH), 20.47 (CH_3). MS (ESI) m/z 181.0 [M-H]$^-$. HRMS (FAB) m/z calcd for $C_8H_6O_2N_2F_1$, 181.0412; found 181.0419.

1-(2-BUTYN-1-YL)-5-FLUOROURACIL (3c)

63 mg, 45% yield. $R_f = 0.53$ (10% MeOH in DCM). ^{1}H NMR (500 MHz, DMSO) δ 11.86 (*s*, 1H), 8.11 (*d*, *J* = 6.7, 1H), 4.41 (*q*, *J* = 2.3, 2H), 1.82 (*t*, *J* = 2.4, 3H). ^{13}C NMR (126 MHz, DMSO) δ 157.30 (*d*, *J* = 25.9, C), 149.04, 139.71 (*d*, *J* = 230.2, C), 128.93 (*d*, *J* = 33.8, CH), 81.61, 73.39, 37.30 (CH_2), 3.07 (CH_3). MS (ESI) m/z 181.0 [M-H]$^-$. HRMS (FAB) m/z calcd for $C_8H_6O_2N_2F_1$, 181.0412; found 181.0419.

1-(2-PENTYN-1-YL)-5-FLUOROURACIL (3d)

56 mg, 37% yield. $R_f = 0.53$ (10% MeOH in DCM). ^{1}H NMR (500 MHz, DMSO) δ 11.86 (s, 1H), 8.10 (*d*, *J* = 6.6, 1H), 4.43 (*t*, *J* = 2.2, 2H), 2.21 (*qt*, *J* = 7.5, 2.2, 2H), 1.06 (*t*, *J* = 7.5, 3H). ^{13}C NMR (126 MHz, DMSO) δ 157.31 (*d*, *J* = 25.9, C), 149.03, 139.71 (*d*, *J* = 230.2, C), 128.87 (*d*, *J* = 33.7, CH), 87.05, 73.53, 37.27 (CH_2), 13.45 (CH_3), 11.60 (CH_2). MS (ESI) m/z 195.0 [M-H]$^-$. HRMS (FAB) m/z calcd for $C_9H_8O_2N_2F_1$, 195.0573; found 195.0575.

1-(3-PHENYL-1-PROPARGYL)-5-FLUOROURACIL (3e)

66 mg, 35% yield. $R_f = 0.66$ (10% MeOH in DCM). ^{1}H NMR (500 MHz, DMSO) δ 11.92 (*s*, 1H), 8.22 (*d*, *J* = 6.6, 1H), 7.49–7.36 (*m*, 5H), 4.73 (*s*, 2H). ^{13}C NMR (126 MHz, DMSO) δ 157.35 (*d*, *J* = 25.9, C), 149.12, 139.83 (*d*, *J* = 230.4, C), 131.53 (CH), 129.01 (*d*, *J* = 34.0, CH), 129.04 (CH), 128.69 (CH), 121.60, 84.38, 83.79, 37.64 (CH_2). MS (ESI) m/z 243.0 [M-H]$^-$. HRMS (FAB) m/z calcd for $C_{13}H_8O_2N_2F_1$, 243.0575; found 243.0574.

SYNTHESIS OF 5-FLUORO-3-PROPARGYLURACIL (6)

N-^{t}Boc protection of N1 position

5FU (100 mg, 0.77 mmol) was dissolved in a 2:1 mixture of acetonitrile and DMF (3 ml). Boc_2O (252 mg, 1.16 mmol) and DMAP (19 mg, 0.15 mmol) were subsequently added to the mixture and stirred overnight at room temperature. The solvents removed *in vacuo* and the resulting crude purified via flash chromatography (eluent: hexane/ EtOAc 3:1), to yield compound **4** as a white solid (70 mg, 40%). ^{1}H NMR (500 MHz, DMSO) δ 10.60 (*s*, 1H), 7.64 (*d*, *J* = 4.7, 1H), 1.62 (*s*, 9H). ^{13}C NMR (126 MHz, DMSO) δ 159.21 (*d*, *J* = 24.4, C), 150.70, 139.59 (*d*, *J* = 224.8, C), 123.02 (*d*, *J* = 31.6, CH), 61.45, 29.35 (CH_3).

Propargylation of N3 position

*N*1-^{t}Boc-protected compound **4** (56 mg, 0.24 mmol), propargyl bromide (31 µl, 0.29 mmol) and DBU (55 µl, 0.36 mmol) were dissolved in dry DCM (2 ml), and the mixture stirred at room temperature for 4 h. The solvents were removed *in vacuo* and the reaction crude purified via flash chromatography (eluent: hexane / EtOAc 5:1), to yield compound **5** as an colorless oil (43 mg, 67%). ^{1}H NMR (500 MHz, $CDCl_3$) δ 7.40 (*d*, *J* = 4.6, 1H), 4.45 (*d*, *J* = 2, 2H), 2.49 (*t*, *J* = 2.6, 1H), 1.68 (*s*, 9H). ^{13}C NMR (126 MHz, $CDCl_3$) δ 159.08 (*d*, *J* = 24.3, C), 150.31, 140.51 (*d*, *J* = 233.9, C), 123.13 (*d*, *J* = 33.9, CH), 76.22, 75.88 (CH), 64.18, 38.01 (CH_2), 29.76 (CH_3).

N1-Boc deprotection

Compound **5** (28 mg, 0.1 mmol) and K_2CO_3 (7 mg, 0.05 mmol) were dissolved in MeOH (2 ml), and the mixture stirred at room temperature for 3 h. The solvents were removed *in vacuo* and the resulting crude purified via flash chromatography (eluent: 3% MeOH in DCM), to yield compounds **6** as a colorless solid (12 mg, 71%). ^{1}H NMR (500 MHz, MeOD) δ 7.61 (*d*, *J* = 5.2, 1H), 4.64 (*dd*, *J* = 2.5, 0.5, 2H), 2.57 (*t*, *J* = 2.5, 1H). ^{13}C NMR (126 MHz, MeOD) δ 158.82 (*d*, *J* = 25.8, C), 151.06, 141.35 (*d*,

$J = 229.9$, C), 125.88 (*d*, $J = 32.1$, CH), 78.65, 71.94 (CH), 31.06 (CH_2). MS (ESI) m/z 167.0 $[M\text{-}H]^-$. HRMS (FAB) m/z calcd for $C_7H_4O_2N_2F_1$, 167.0262; found 167.0252.

SYNTHESIS OF 1,3-DIPROPARGYL-5-FLUOROURACIL (7)

5FU (100 mg, 0.8 mmol) and DBU (345 µl, 2.3 mmol) were dissolved in dry DMF (2 ml) under a nitrogen atmosphere, and the mixture was cooled down to 4°C in an ice bath. Propargyl bromide (170 µl, 1.6 mmol) was added dropwise and the reaction mixture allowed to warm up to room temperature. The mixture was stirred overnight, the solvents removed *in vacuo* and the resulting crude purified via flash chromatography (eluent: 1.5% MeOH in DCM), to yield compounds **7** as a colorless solid (136 mg, 86%). ^{1}H NMR (500 MHz, $CDCl_3$) δ 7.60 (*d*, $J = 5.3$, 1H), 4.72 (*d*, $J = 2.4$, 2H), 4.61 (*d*, $J = 2.6$, 2H), 2.56 (*t*, $J = 2.6$, 1H), 2.20 (*t*, $J = 2.5$, 1H). ^{13}C NMR (126 MHz, $CDCl_3$) δ 156.19 (*d*, $J = 26.0$, C), 148.92, 140.26 (*d*, $J = 237.3$, C), 125.33 (*d*, $J = 33.7$, CH), 77.24, 76.74 (CH), 75.47, 71.51 (CH), 38.18 (CH_2), 31.27 (CH_2). MS (ESI) m/z 435.2 $[2M+Na]^+$. HRMS (FAB) m/z calcd for $C_{10}H_6O_2N_2F_1$, 205.0419; found 205.0414.

Pd^0-MEDIATED 5FU SYNTHESIS IN BIOCOMPATIBLE CONDITIONS

Prodrugs **3a-e**, **6** and **7** (100 µM in DMSO) were dissolved in PBS (1 mL) with 1 mg of Pd^0-resins and shaken at 1,200 rpm and 37°C in a Thermomixer. Reaction crudes were monitored at 0, 6, and 24 h by analytical HPLC (Agilent) using the UV detector at 280 nm to avoid the detection of PBS salts. Eluent A: water and formic acid (0.1%); eluent B: acetonitrile, formic acid (0.1%); $A/B = 95$: 5 to 5: 95 in 3 min, isocratic 1 min, 5: 95 to 95: 5 in 1 min, isocratic 1 min.

Study of the influence of pH in the conversion rate

The pH of the PBS buffer was adjusted with 1 N solutions of hydrochloric acid or sodium hydroxide using a pH meter (Mettler Toledo). Reactions and analyses were carried out at pH 6.5, 7.0, and 7.5 as described above.

CELL CULTURE

Cell lines were grown in culture media supplemented with serum (10% FBS) and L-glutamine (2 mM) and incubated in a tissue culture incubator at 37°C and 5% CO_2. Human pancreas adenocarcinoma BxPC-3 cells (a kind gift from Dr Mark Duxbury) were cultured in Roswell Park Memorial Institute (RPMI) media. Human breast adenocarcinoma MCF7 cells (purchased from ATCC), human ovarian carcinoma PE04 cells (a kind gift from Prof Charlie Gourley), human colorectal carcinoma HCT116 cells (a kind gift from Dr Van Schaeybroeck) and human breast cancer R-SKBR3a cells were all cultured in Dulbecco's Modified Eagle Media (DMEM).

CELL VIABILITY STUDIES

HCT116 cells were seeded in a 96 well plate format at 1000 cells/well and incubated for 48 h before treatment. Each well was then replaced with fresh media containing compound **1**, **3a**, **6,** or **7** and incubated for 5 days. Untreated cells were incubated with DMSO (0.1% v/v). PrestoBlue™ cell viability reagent (10% v/v) was added to each well and the plate incubated for 1 h. Fluorescence emission was detected using a PerkinElmer EnVision 2101 multilabel reader (Perkin Elmer; excitation filter at 540 nm and emissions filter at 590 nm). All conditions were normalized to the untreated cells (100%) and curves fitted using GraphPad Prism using a sigmoidal variable slope curve.

TIME-LAPSE PROLIFERATION STUDY OF DRUG vs. BOOM ACTIVATION ASSAYS OF COMPOUNDS 3a, 6, AND 7

HCT116 cells were plated as described before and each well was then replaced with fresh media containing: Pd^0-resins (0.67 mg/mL) with DMSO (0.1% v/v); **3a**, **7**, or **6** (100 µM) with DMSO (0.1% v/v); 5FU **1** (100 µM) with DMSO (0.1% v/v); or combination of 0.67 mg/mL of Pd^0-resins + **3a**, **7**, or **6** (100 µM) with DMSO (0.1% v/v). Untreated cells were incubated with DMSO (0.1% v/v). Each well was imaged every 3 h over 5 d under standard incubation conditions using an IncuCyte™ ZOOM microscope (placed inside the incubator). Imaged-based analysis of cell confluence was carried out using the IncuCyte™ software.

Pd^0-MEDIATED DEALKYLATION OF COMPOUNDS 3a AND 6 IN CELL CULTURE

HCT116 cells, were plated as described above. BxPC-3 were plated at 2500 cell / well, MCF7 cells were plated at 2000 cells/well, PE04 cells were plated at 1000 cells / well and R-SKBR3a cells were plated at 156 cells/well. Each well was then replaced with fresh media containing: Pd^0-resins (0.67 mg/mL) with DMSO (0.1% v/v); **3a**, or **6** (3, 10, 30, 100 µM) with DMSO (0.1% v/v); 5FU **1** (3, 10, 30, 100 µM) with DMSO (0.1% v/v); or combination of 0.67 mg/mL of Pd^0-resins + **3a** or **6** (3, 10, 30, 100 µM) with DMSO (0.1% v/v). Untreated cells were incubated with DMSO (0.1% v/v). Cells were incubated with drugs for 5 days. PrestoBlue™ cell viability reagent (10% v/v) was added to each well and the plates were incubated between 60 and 180 min depending on the cell line. Fluorescence emission was detected and results normalized as described above.

RESULTS AND DISCUSSION

Pd^0-FUNCTIONALIZED RESINS AS HETEROGENEOUS CATALYSTS FOR BOOM CHEMISTRY

Based on the potential toxicity of palladium as a contaminant in the food chain, most of the early examples of palladium substrates employed in chemical biology were colorimetric and fluorogenic probes used to detect palladium in biological samples (Li et al., 2013). Nevertheless, our group (Yusop et al., 2011; Unciti-Broceta et al., 2012; Weiss et al., 2014a,b; Zanda, 2014) and others (Li et al., 2011, 2014; Michel et al., 2012; Spicer et al., 2012; Spicer and Davis, 2013) have recently shown that the catalytic properties of palladium are biocompatible and its cytotoxicity controllable to a certain degree, thus allowing the development of various BOOM reactions in cell culture. While soluble palladium species can display significant cytotoxic properties (Environmental Health Criteria, 2002), metallic palladium is the safest form of this transition metal (Environmental Health Criteria, 2002; Rushforth, 2004). On this basis, we investigated the development of solid devices functionalized with palladium nanoparticles as a way to eliminate the free mobility of palladium and induce spatially-controlled chemical reactions.

To mediate BOOM heterocatalysis outside cells, we developed a functional device consisting of palladium nanoparticles entrapped in a biocompatible polymer matrix. These palladium-functionalized resins (Pd^0-resins) are larger than cells (150 μm in average diameter) and formed by a co-polymer matrix made of polyethylene glycol grafted onto polystyrene resin (Weiss et al., 2014a), two polymers that have been extensively employed in the manufacture of a variety of biomedical devices (Alcantar et al., 2000; Sanchez-Martin et al., 2005; Dhaliwal et al., 2011; Unciti-Broceta et al., 2011). As previously reported (Weiss et al., 2014a,b), we have demonstrated the high biocompatibility of these catalyst-entrapped polymeric structures both *in vitro* and *in vivo*. On this basis, Pd^0-resins (containing 4.4% *w*/*w* in Pd) were used as the extracellular activating device in the studies subsequently described.

DESIGN, SYNTHESIS AND Pd^0-LABILITY OF *N*1-ALKYNYL DERIVATIVES OF 5FU

The clinical application and effective therapeutic response to several chemotherapeutics with a cytotoxic mechanism-of-action, including 5FU, is severely limited by numerous dose-limiting toxicities in patients. As previously reported (Weiss et al., 2014a), functionalization of the *N*1 position of 5FU with a propargyl group resulted in a bioorthogonal prodrug (**3a**) prone to conversion into 5FU in the presence of Pd^0-resins both in PBS (biocompatible solution) and cell culture; a strategy that could allow for the reduction of systemic side effects of 5FU treatment. In order to investigate whether other alkynes could increase the rate of the dealkylation process, a set of *N*1-alkynyl derivatives of 5FU were synthesized following the procedure described in **Figure 2**. Subsequently, to study the susceptibility of derivatives **3b-e** to palladium catalysis, Pd^0-resins were used as the heterogeneous catalyst and palladium-labile 5-fluoro-1-propargyluracil (**3a**) as positive control (**Figure 3A**). Compounds **3a-e** (100 μM) and Pd^0-resins [1 mg/mL, (Pd^0) = 400 μM] were dispersed in PBS (isotonic buffered solution at pH =7.4), incubated at 37°C for 24 h and the reaction crudes analyzed by HPLC using a UV detector. While compound **3a** led to 100% conversion in less than 24 h, compounds **3b-e** generated considerably lower levels of 5FU, **1** (see small table in **Figure 3A**). The susceptibility to palladium of compounds **3c-e** (containing a methyl, ethyl and benzyl group at the terminal carbon of the triple bond, respectively) was inversely proportional to the size of the moiety, indicating that the lesser the accessibility to the triple bond, the slower the reaction occurs. 24 h reaction of compound **3b** with Pd^0-resins resulted in a 26% conversion into 5FU, a clear improvement over derivatives **3c-e** but significantly inferior to the reactivity of **3a** toward palladium. These results indicate that steric hindrance is a limiting factor in the reaction kinetics and, therefore, suggest that the non-substituted propargyl group is the optimal choice to generate palladium-labile bioorthogonal probes and prodrugs.

*N*1- vs. *N*3-PROPARGYL DERIVATIVES OF 5FU: SENSITIVITY TO Pd^0

Due to 5FU tautomerism, the NH groups at positions 1 and 3 possess relatively low pK_a values. Since, according to the literature (Jang et al., 2001), the *N*3 position has a lower pK_a value than the *N*1, we hypothesized that propargylation of the *N*3 position could in principle generate derivatives with improved sensitivity to palladium catalysis. Importantly, the absence of a free NH group in that position would impede the formation of hydrogen bonding interactions between the substrate and the active site of the enzyme (UMP synthase) (Wittmann et al., 2008), thus reducing the efficacy of the phosphorylation process and the generation of 5FU's cytotoxic nucleotides (**Figure 1A**). On this basis, bioorthogonal prodrugs could also be generated by chemical masking of that particular position. To investigate this, 5-fluoro-3-propargyluracil (**6**) and 1,3-dipropargyl-5-fluorouracil (**7**) were synthesized from 5FU (see **Figure 2**) and their susceptibility to palladium catalysis tested as described above (**Figures 3A,B**). Interestingly, palladium-mediated dealkylation of compound **6** underwent depropargylation at a slower rate than compound **3a,** with a conversion rate of approx. 85% after 24 h incubation. As observed in **Figure 3B** (right panel), 24 h reaction of bis-protected compound **7** with Pd^0-resins resulted in the generation of 5FU (26%) and derivative **6** (43%), thus confirming that dealkylation of the propargyl group proceeds faster at the *N*1 position than the *N*3 one. While the theoretical pK_a values of each group (Jang et al., 2001) would have predicted the opposite outcome, the *N*3 is flanked by two oxo groups and the *N*1 by only one, underlining again the relevance of steric and conformational effects on the depropargylation kinetics.

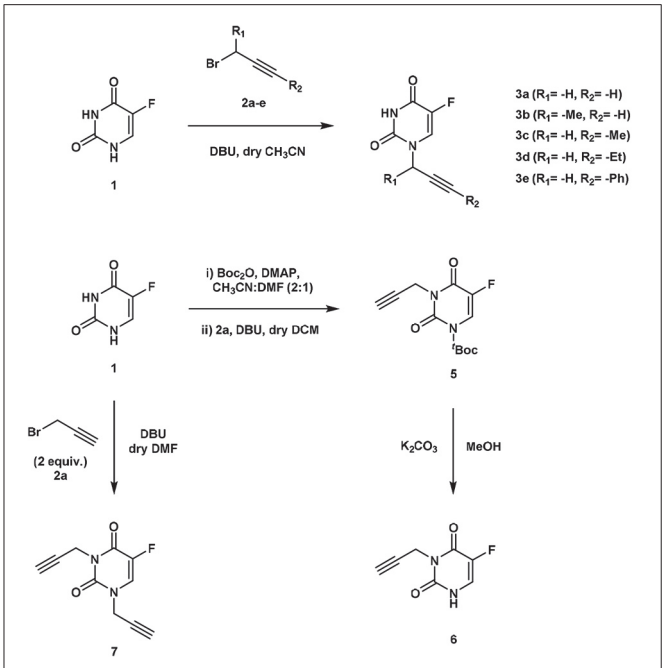

FIGURE 2 | Synthesis of compounds 3a-e (upper panel) and compounds 6, 7 (lower panel).

*N*1- vs. *N*3-PROPARGYL DERIVATIVES OF 5FU: INFLUENCE OF PH ON THE Pd^0-MEDIATED DEALKYLATION OF COMPOUNDS 3a AND 6

Due to hypoxia and glucose deprivation, solid tumors are estimated to have a pH in the order of 0.5 units lower than healthy tissues (Tannock and Rotin, 1989; Xu et al., 2002). Since the prodrug strategy proposed herein is expected to have application

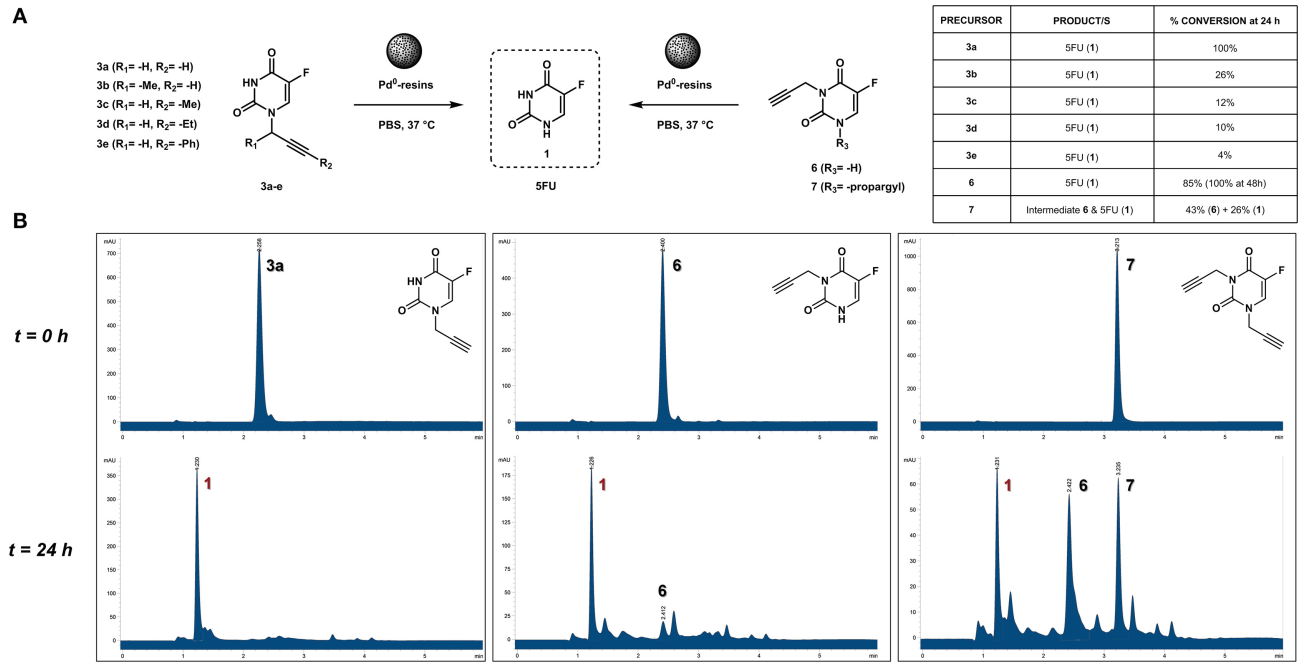

PRECURSOR	PRODUCT/S	% CONVERSION at 24 h
3a	5FU (1)	100%
3b	5FU (1)	26%
3c	5FU (1)	12%
3d	5FU (1)	10%
3e	5FU (1)	4%
6	5FU (1)	85% (100% at 48h)
7	Intermediate 6 & 5FU (1)	43% (6) + 26% (1)

FIGURE 3 | (A) Palladium-mediated dealkylation of compounds **3a-e**, **6**, and **7** and table containing conversion percentages (relative values calculated by chromatographic peak integration). Each of the drug precursors (100 μM) were incubated with 1 mg/mL of Pd^0-resins in PBS at 37°C for 24 h and the crude reaction analyzed by HPLC. **(B)** HPLC chromatograms (UV detector 280 nm) of 100 μM PBS solutions of compounds **3a** (left panel), **6** (central panel), and **7** (right panel) treated with Pd^0-resins at 37°C for 0 h (top) and 24 h (bottom).

Table 1 | Influence of pH in the palladium-mediated dealkylation of compounds 3a and 6.

Prodrug	$t = 6$ h			$t = 24$ h		
	pH = 6.5	pH = 7.0	pH = 7.5	pH = 6.5	pH = 7.0	pH = 7.5
3a	28.9%	33.7%	44.4%	100%	100%	100%
6	21.3%	33.4%	39.1%	75.6%	76.9%	80.6%

Conversion percentages were calculated by chromatographic peak integration.

against locally-advanced tumors, it was suggested to examine the effect of pH changes in the reaction conversion rate. Hence, palladium-mediated depropargylation of compounds **3a** and **6** was carried out as above described at various pH (6.5, 7.0, and 7.5), and reactions analyzed by HPLC at different timepoints (6 and 24 h). As shown in **Table 1**, the pH had a noticeable effect on the conversion rates, particularly after short incubation periods. While propargyl cleavage of compound **3a** was completed in less than 24 h at each of the pH's tested, the conversion rate after 6 h was higher at a slightly basic pH (7.5). The same trend was observed for compound **6**. Importantly, even though the reaction is enhanced at slightly basic pH, this study demonstrates that the *N*-depropargylation process is compatible with the range of pH expected to be found *in vivo*.

*N*1- vs. *N*3-PROPARGYL DERIVATIVES OF 5FU: STUDY OF BIOORTHOGONALITY

To evaluate whether the cytotoxic activity of the 5FU prodrugs were successfully masked, dose response viability studies were carried out with HCT116 colorectal cancer cells. Data analysis confirmed that, likewise for prodrug **3a**, compounds **6** and **7** did not display antiproliferative properties at any of the concentrations used (**Figure 4A**), thus confirming that propargylation of any NH group of 5FU result in the elimination of the drug's pharmacological properties.

*N*1- vs. *N*3-PROPARGYL DERIVATIVES OF 5FU: Pd^0-MEDIATED PRODRUG ACTIVATION IN CANCER CELL CULTURE

In situ generation of cytotoxic 5FU (**1**) from prodrugs **3a**, **6** and **7** was first investigated with HCT116 cells in standard cell culture conditions using Pd^0-resins as the extracellular activating device. Prodrugs (100 μM) and Pd^0-resins (0.67 mg/mL) were incubated independently (negative controls) or in combination (BOOM activation assay), and unmodified 5FU (**1**) used as the positive control. Because each prodrug/Pd^0-resin combination was expected to become phenotypically active at a different rate (see above studies), automated kinetic analysis of cell proliferation rate over time was used as a screening strategy to determine and rank the efficiency of distinct prodrug/Pd^0-resin combinations. To enable the temporal visualization and quantification of the experiment, cell growth was monitored for 5 days by time-lapse imaging using an IncuCyte ZOOM device (Weiss et al., 2014a,b). To obtain the maximal differentiation among the experiments, the cell seeding density was optimized to reach confluency at day 5. While neither the prodrugs nor the Pd^0-resins exhibited cytotoxicity, combinations of prodrugs with Pd^0-resins displayed significant toxigenic effect (**Figure 4B**), confirming that the three prodrugs were bioorthogonally converted– at least partly– into cytotoxic 5FU (**1**). The enhanced sensitivity

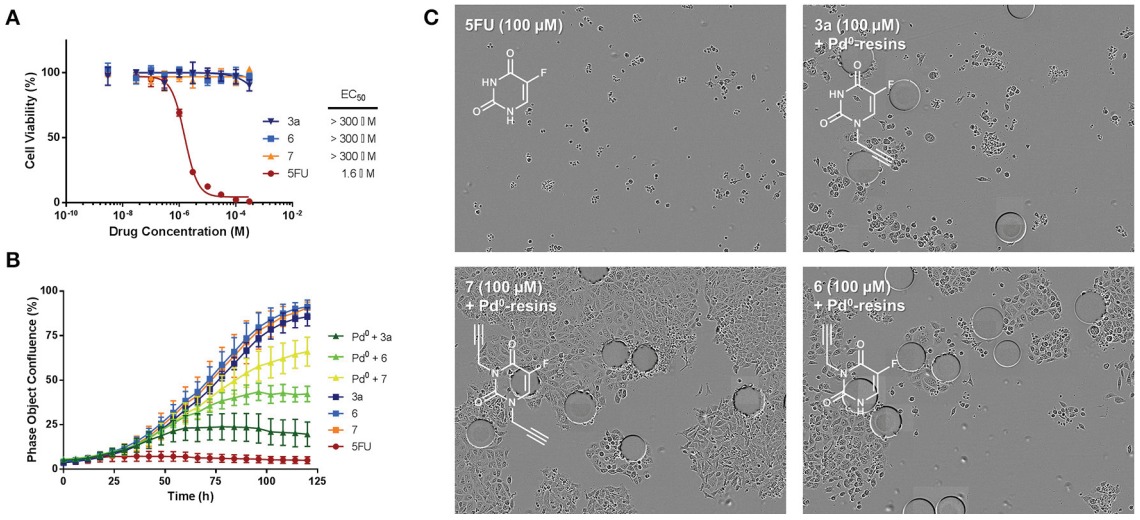

FIGURE 4 | (A) Study of prodrugs' bioorthogonality. Semi Log dose response curves and calculated EC_{50}values of prodrugs **3a**, **6**, and **7** in comparison to unmodified 5FU (**1**) in HCT116 cells. Cell viability was measured at day 5 using PrestoBlue™ reagent. Error bars: ± *SD* from $n = 3$. **(B)** Bioorthogonally-activated toxigenic effect in HCT116 cancer cell culture: Real-time cell confluence study. The cell population was monitored for 120 h using an IncuCyte ZOOM system in an incubator (5% CO2 and 37°C). Drug/prodrug concentration: 100 µM. Pd^0-resins concentration: 0.67 mg/mL. Error bars: ± *SD* from $n = 3$. **(C)** Phase-contrast images of cells after 5 days of treatment with: 100 µM of 5FU (top left); 0.67 mg/mL Pd^0-resins + 100 µM of **7** (bottom left); 0.67 mg/mL Pd^0-resins + 100 µM of **3a** (top right); 0.67 mg/mL Pd^0-resins + 100 µM of **6** (bottom right). Pd^0-resins are identified as spheres of 150 µm (average diameter).

of prodrug **3a** to BOOM heterocatalysis was evidenced by a significantly smaller bell-shaped curve than those caused by either prodrug **6** and **7** in the presence of the palladium source. As shown in **Figure 4C** (phase contrast images of cells after 5 days of treatment), the antiproliferative effect of prodrugs **6** and **7** incubated with Pd^0-resins was significantly lower than that of 5FU (**1**), whereas prodrug **3a** generated similar cytotoxic effect to the unmodified drug. In the presence of Pd^0-resins, only compounds **3a** and **6** induced less than 50% of cell viability at 100 µM.

On the basis of the toxigenicity demonstrated by prodrugs **3a** and **6** in combination with the heterogeneous palladium source, these prodrugs were selected for further exemplification of the strategy with a range of human cancer cell types, i.e., colorectal cancer HCT116 cells, pancreatic adenocarcinoma BxPC-3 cells, ovarian carcinoma PE04 cells and two types of breast cancer cell lines: ER-overexpressing MCF7 cells and R-SKBR3a cells, a derivative of HER2-overexpressing SKBR3 cells with induced resistance to AZD8931 (Creedon et al., in press). Once again, low cell seeding numbers were used to augment the effect of 5FU treatment and thus impose more discriminative conditions to the rate of drug generation. In accordance with previous observations, although both prodrugs **3a** and **6** showed high bioorthogonality in the absence of palladium at the range of concentrations used, prodrug **3a** proved again to possess enhanced susceptibility to palladium-mediated activation by displaying superior toxigenic effect in all the cell lines tested (**Figure 5**). Nevertheless, it is noteworthy that prodrug **3a**/and prodrug **6**/Pd^0-resins combinations induced similar cytotoxic phenotype in pancreatic cancer BxPC-3 cells (**Figure 5B**). This is considered to be due to the high sensitivity of this cell line to 5FU treatment, thus requiring the generation of relatively low levels of drug to induce a strong antiproliferative effect. On the contrary, in the presence of cancerous cells with higher resistance to 5FU such as HCT116, MCF7, and PE04, the difference in the activation rate (= toxigenicity Weiss et al., 2014b) between both prodrug/activator combinations was highly discriminative, thus evidencing the lower toxigenic effect enabled by the prodrug **6**/Pd^0-resins combination (**Figures 5A,C,E**). This study strongly indicates that the rate of activation is a key limiting factor for the translation of palladium-labile prodrugs into the clinic. To successfully achieve sustained and effective cytotoxic levels of drug and be able to control tumor growth, the kinetics of the activation process needs to superior to the rate of cancer cell proliferation.

CONCLUSIONS

In conclusion, a set of 2-alkyn-1-yl groups (containing a triple bond in position 2 relative to the point of connection to 5FU) were used to synthesize, test and rank palladium-labile prodrugs of 5FU. Even if the drug was generated from all the precursors via palladium-mediated cleavage under biocompatible conditions, the propargyl group demonstrated superior sensitivity to palladium catalysis. The present study suggests that reaction kinetics is strongly influenced by the accessibility of the catalyst to the triple bond.

We have demonstrated that the pharmacological activity of 5FU can be "switched off" by alkylation chemistry of not only the *N*1 position but also the *N*3 position of 5FU. We have also shown that palladium-mediated *N*-propargylation occurs faster at position *N*1 than at position *N*3, and that pH can influence the reaction conversion rate. Bioorthogonal restoration of the drug's cytotoxic properties with either *N*1 or *N*3-propargylated

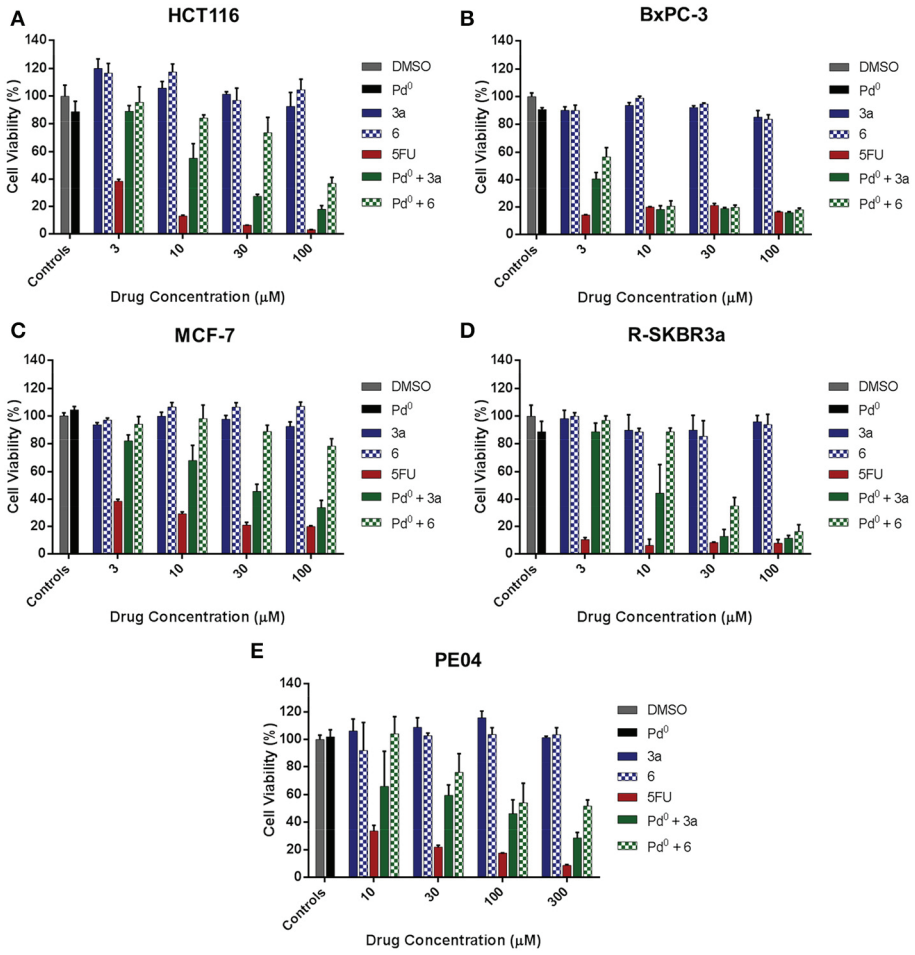

FIGURE 5 | Palladium-mediated conversion of prodrugs 3a and 6 into 5FU in cancer cell culture. (A) Colorectal cancer HCT116 cells; **(B)** Pancretic adenocarcinoma BxPC-3 cells; **(C)** Breast cancer MCF-7; **(D)** Breast cancer R-SKBR3a cells; **(E)** Ovarian carcinoma PE04 cells. Drug generation was indirectly measured by analysis of cell viability after 5 days of treatment using the PrestoBlue™ Reagent (Life Technologies). Treatments: untreated cell control (0.1% *v/v* DMSO in media, negative control); Pd^0-resins (0.67 mg/mL, negative control); 3–100 μM of **3a** or **6** (negative control); 3–100 μM of 5FU (positive control); and Pd^0-resin (0.67 mg/mL) + **3a** or **6** (BOOM reaction assay).

5FU by extracellular palladium chemistry in a range of cancer cells demonstrated that the rate of activation is an essential factor to rapidly achieve sustained and effective cytotoxic levels of drug. Overall, the studies reported herein indicate that the propargylation of 5FU's *N*1 position [masking strategy used by our group in the seminal work on palladium-activated prodrugs (Weiss et al., 2014a)] is yet the best approach available -in terms of bioorthogonality and palladium lability- to implement a BOOM-activated prodrug strategy with this particular chemotherapeutic drug.

ACKNOWLEDGMENTS

Jason T. Weiss is grateful to the College of Medicine and Veterinary Medicine and the University of Edinburgh for a Darwin International Scholarship and an Edinburgh Global Research Scholarship. Craig Fraser and E. Elizabeth Patton are funded by the MRC, and Richard Crispin by the IGMM Research Translation Fund. Belén Rubio-Ruiz is supported by a postdoctoral fellowship from the Alfonso Martín Escudero Foundation (Spain). Neil O. Carragher and Asier Unciti-Broceta thank RCUK and IGMM, respectively, for an Academic Fellowship. Samuel H. Myers, Valerie G. Brunton, and Asier Unciti-Broceta thank Scottish Power for funding. We are grateful to the Edinburgh Cancer Research UK Centre for funding this research through the CRUK Development Fund.

REFERENCES

Agard, N. J., Prescher, J., and Bertozzi, C. R. (2004). A strain-promoted [3 + 2] azide-alkyne cycloaddition for covalent modification of biomolecules in living systems. *J. Am. Chem. Soc.* 126, 15046–15047. doi: 10.1021/ja044996f

Alcantar, N. A., Aydil, E. S., and Israelachvili, J. N. (2000). Polyethylene glycol-coated biocompatible surfaces. *J. Biomed. Mater. Res.* 51, 343–351. doi: 10.1002/1097-4636

Castano, A. P., Mroz, P., and Hamblin, M. R. (2006). Photodynamic therapy and anti-tumour immunity. *Nat. Rev. Cancer* 6, 535–545. doi: 10.1038/nrc1894

Chabner, B. A., and Roberts, T. G. Jr. (2005). Chemotherapy and the war on cancer. *Nat. Rev. Cancer* 5, 65–72. doi: 10.1038/nrc1529

Clavel, C. M., Păunescu, E., Nowak-Sliwinska, P., and Dyson, P. J. (2014). Thermoresponsive organometallic arene ruthenium complexes for tumour targeting. *Chem. Sci.* 5, 1097–1101. doi: 10.1039/c3sc53185f

Creedon, H., Byron, A., Main, J., Hayward, L., Klinowska, T., and Brunton, V. G. (in press). Exploring mechanisms of acquired resistance to human epidermal growth factor receptor 2 targeted therapies in breast cancer. *Biochem. Soc. Trans.* doi: 10.1042/BST20140109

DeVita, V. T. Jr., and Chu, E. (2008). A History of Cancer Chemotherapy. *Cancer Res.* 68, 8643–8653. doi: 10.1158/0008-5472.CAN-07-6611

Dhaliwal, K., Alexander, L., Escher, G., Unciti-Broceta, A., Jansen, M., Mcdonald, N., et al. (2011). Multi-modal molecular imaging approaches to detect primary cells in preclinical models. *Faraday Discuss.* 149, 107–114. doi: 10.1039/c005410k

Environmental Health Criteria 226: Palladium. (2002). *World Health Organization*. Geneva. Available online at: http://whqlibdoc.who.int/ehc/WHO_EHC_226.pdf

Huttunen, K. M., Raunio, H., and Rautio, J. (2008). Prodrugs-from serendipity to rational design. *Pharmacol. Rev.* 63, 750–771. doi: 10.1124/pr.110.003459

Jang, Y. H., Sowers, L. C., Cagin, T., and Goddard, W. A. I. I. I. (2001). First principles calculation pka values for 5-substituted uracils. *J. Phys. Chem. A* 105, 274–280. doi: 10.1021/jp994432b

Jenner, P. (2008). Molecular mechanisms of L-DOPA-induced dyskinesia. *Nat. Rev. Neurosci.* 9, 665–677. doi: 10.1038/nrn2471

Li, H., Fan, J., and Peng, X. (2013). Colourimetric and fluorescent probes for the optical detection of palladium ions. *Chem. Soc. Rev.* 42, 7943–7962. doi: 10.1039/c3cs60123d

Li, J., Yu, J., Zhao, J., Wang, J., Zheng, S., Lin, S., et al. (2014). Palladium-triggered deprotection chemistry for protein activation in living cells. *Nat. Chem.* 6, 352–361. doi: 10.1038/nchem.1887

Li, N., Lim, R. K., Edwardraja, S., and Lin, Q. (2011). Copper-free Sonogashira cross-coupling for functionalization of alkyne-encoded proteins in aqueous medium and in bacterial cells. *J. Am. Chem. Soc.* 133, 15316–15319. doi: 10.1021/ja2066913

Longley, D. B., Harkin, D. P., and Johnston, P. G. (2003). 5-fluorouracil: mechanisms of action and clinical strategies. *Nat. Rev. Cancer* 3, 330–338. doi: 10.1038/nrc1074

Michel, B. W., Lippert, A. R., and Chang, C. J. (2012). A reaction-based fluorescent probe for selective imaging of carbon monoxide in living cells using a palladium-mediated carbonylation. *J. Am. Chem. Soc.* 134, 15668–15671. doi: 10.1021/ja307017b

Rautio, J., Kumpulainen, H., Heimbach, T., Oliyai, R., Oh, D., Järvinen, T., et al. (2008). Prodrugs: design and clinical applications. *Nat. Rev. Drug Discov.* 7, 255–270. doi: 10.1038/nrd2468

Rushforth, R. (2004). Palladium in restorative dentistry: superior physical properties make palladium an ideal dental metal. *Platinum Metals Rev.* 48, 30–31.

Sanchez-Martin, R. M., Muzerelle, M., Chitkul, N., How, S. E., Mittoo, S., and Bradley, M. (2005). Bead-based cellular analysis, sorting and multiplexing. *Chembiochem* 6, 1341–1345. doi: 10.1002/cbic.200500059

Saxon, E., and Bertozzi, C. R. (2000). Cell surface engineering by a modified Staudinger reaction. *Science* 287, 2007–2010. doi: 10.1126/science.287.5460.2007

Sletten, E. M., and Bertozzi, C. R. (2011). From mechanism to mouse: a tale of two bioorthogonal reactions. *Acc. Chem. Res.* 44, 666–676. doi: 10.1021/ar200148z

Spicer, C. D., and Davis, B. G. (2013). Rewriting the bacterial glycocalyx via Suzuki-Miyaura cross-coupling. *Chem. Commun.* 49, 2747–2749. doi: 10.1039/c3cc38824g

Spicer, C. D., Triemer, T., and Davis, B. G. (2012). Palladium-mediated cell-surface labelling. *J. Am. Chem. Soc.* 134, 800–803. doi: 10.1021/ja209352s

Tannock, I. F., and Rotin, D. (1989). Acid pH in tumors and its potential for therapeutic exploitation. *Cancer Res.* 49, 4373–4384.

Unciti-Broceta, A., Díaz-Mochón, J. J., Sánchez-Martín, R. M., and Bradley, M. (2011). The use of solid supports to generate nucleic acid carriers. *Acc. Chem. Res.* 45, 1140–1152. doi: 10.1021/ar200263c

Unciti-Broceta, A., Johansson, E. M. V., Yusop, R. M., Sánchez-Martín, R. M., and Bradley, M. (2012). Synthesis of polystyrene microspheres and functionalization with Pd(0) nanoparticles to perform bioorthogonal organometallic chemistry in living cells. *Nat. Protoc.* 7, 1207–1218. doi: 10.1038/nprot.2012.052

Velema, W. A., Szymanski, W., and Feringa, B. L. (2014). Photopharmacology: beyond proof of principle. *J. Am. Chem. Soc.* 136, 2178–2191. doi: 10.1021/ja413063e

Versteegen, R. M., Rossin, R., ten Hoeve, W., Janssen, H. M., and Robillard, M. S. (2013). Click to release: instantaneous doxorubicin elimination upon tetrazine ligation. *Angew. Chem. Int. Ed. Engl.* 52, 14112–14116. doi: 10.1002/anie.201305969

Weiss, J. T., Dawson, J. C., Fraser, C., Rybski, W., Torres-Sánchez, C., Bradley, M., et al. (2014b). Development and bioorthogonal activation of palladium-labile prodrugs of Gemcitabine. *J. Med. Chem.* 57, 5395–5404. doi: 10.1021/jm500531z

Weiss, J. T., Dawson, J. C., Macleod, K. G., Rybski, W., Fraser, C., Torres-Sánchez, C., et al. (2014a). Extracellular palladium-catalysed dealkylation of 5-fluoro-1-propargyl-uracil as a bioorthogonally activated prodrug approach. *Nat. Commun.* 5, 3277. doi: 10.1038/ncomms4277

Wittmann, J. G., Heinrich, D., Gasow, K., Frey, A., Diederichsen, U., and Rudolph, M. G. (2008). Structures of the human orotidine-5'-monophosphate decarboxylase support a covalent mechanism and provide a framework for drug design. *Structure* 16, 82–92. doi: 10.1016/j.str.2007.10.020

Xu, G., and McLeod, H. L. (2001). Strategies for enzyme/prodrug cancer therapy. *Clin. Cancer Res.* 7, 3314–3324.

Xu, L., Fukumura, D., and Jain, R. K. (2002). Acidic extracellular pH induces vascular endothelial growth factor (VEGF) in human glioblastoma cells via ERK1/2 MAPK signaling pathway: mechanism of low pH-induced VEGF. *J. Biol. Chem.* 277, 11368–11374. doi: 10.1074/jbc.M108347200

Yusop, R. M., Unciti-Broceta, A., Johansson, E. M. V., Sánchez-Martín, R. M., and Bradley, M. (2011). Palladium-mediated intracellular chemistry. *Nat. Chem.* 3, 239–243. doi: 10.1038/nchem.981

Zanda, M. (2014). Synstory on extracellular palladium-catalyzed dealkylation of 5-Fluoro-1-propargyl-uracil as a bioorthogonally activated prodrug approach. *Synfacts* 10, A90–A92. doi: 10.1055/s-0033-1340191

Conflict of Interest Statement: The authors declare that a patent is pending on the N-alkynyl derivatives of 5FU and its method of activation for medical use.

Received: 16 June 2014; accepted: 10 July 2014; published online: 29 July 2014.
*Citation: Weiss JT, Fraser C, Rubio-Ruiz B, Myers SH, Crispin R, Dawson JC, Brunton VG, Patton EE, Carragher NO and Unciti-Broceta A (2014) N-alkynyl derivatives of 5-fluorouracil: susceptibility to palladium-mediated dealkylation and toxigenicity in cancer cell culture. Front. Chem. **2**:56. doi: 10.3389/fchem.2014.00056*
This article was submitted to Medicinal and Pharmaceutical Chemistry, a section of the journal Frontiers in Chemistry.
Copyright © 2014 Weiss, Fraser, Rubio-Ruiz, Myers, Crispin, Dawson, Brunton, Patton, Carragher and Unciti-Broceta. This is an open-access article distributed under the terms of the Creative Commons Attribution License (CC BY). The use, distribution or reproduction in other forums is permitted, provided the original author(s) or licensor are credited and that the original publication in this journal is cited, in accordance with accepted academic practice. No use, distribution or reproduction is permitted which does not comply with these terms.

SCIENTIFIC REPORTS



OPEN

SUBJECT AREAS:
CHEMOTHERAPY
CHEMICAL TOOLS
DRUG DISCOVERY AND DEVELOPMENT

Received
2 December 2014

Accepted
26 February 2015

Published
19 March 2015

Correspondence and requests for materials should be addressed to A.U.-B. (Asier.Unciti-Broceta@igmm.ed.ac.uk)

Palladium-Mediated Dealkylation of *N*-Propargyl-Floxuridine as a Bioorthogonal Oxygen-Independent Prodrug Strategy

Jason T. Weiss, Neil O. Carragher & Asier Unciti-Broceta

Edinburgh Cancer Research UK Centre, MRC Institute of Genetics and Molecular Medicine, University of Edinburgh, Crewe Road South, Edinburgh EH4 2XR, UK.

Herein we report the development and biological screening of a bioorthogonal palladium-labile prodrug of the nucleoside analogue floxuridine, a potent antineoplastic drug used in the clinic to treat advanced cancers. *N*-propargylation of the N3 position of its uracil ring resulted in a vast reduction of its biological activity (~6,250-fold). Cytotoxic properties were bioorthogonally rescued in cancer cell culture by heterogeneous palladium chemistry both in normoxia and hypoxia. Within the same environment, the reported chemo-reversible prodrug exhibited up to 1,450-fold difference of cytotoxicity whether it was in the absence or presence of the extracellular palladium source, underlining the precise modulation of bioactivity enabled by this bioorthogonally-activated prodrug strategy.

Bioorthogonally-activated prodrug therapies are a heterogeneous group of experimentally and clinically-used therapeutic strategies that are founded on a common principle: the site-specific activation of pharmaceutical substances by the mediation of non-biological, non-perturbing physical or chemical stimuli. While the nature and properties of the triggering stimulus can be manifestly diverse and seemingly unrelated (e.g. benign electromagnetic radiations[1–4], metal-free click chemistry[5–7], mild hyperthermia[8,9], bioorthogonal organometallic (BOOM) reactions[10–13], etc.), all these strategies are intrinsically linked by the wide-ranging notion of bioorthogonality coined by Bertozzi a decade ago[14–16]. By virtue of the bioorthogonal action of an external or internal source, precursors of various therapeutic substances, such as reactive oxygen species (photodynamic therapy[1]), cytotoxic small molecules (activated by photolysis[2–4], or chemolysis[5–7,10–13]) or thermoresponsive drugs[8,9], can be selectively activated within an anatomical area of a patient (e.g. a tumour), thus reducing the systemic adverse effects of the therapy.

Contributing to the "explosive" emergence of palladium in chemical biology[17–25], we have recently reported a novel application of BOOM chemistry whereby polymer-entrapped palladium nanoparticles are deployed as extracellular heterogeneous catalysts in cancer cell culture to cleave protecting groups used to inactivate cytotoxic agents, thus restoring the drugs' pharmacological properties *in situ*[10–12]. Unlike other classes of locally-activated chemotherapies where the activating source generates a short-lived triggering stimulus, the catalytic nature of the reported BOOM reactions means that palladium-functionalized inserts could induce successive activating stimuli (catalytic cycles) in a continuous manner. Thereby, following the intratumoral implantation of a palladium-functionalized device (e.g. by minor surgery), cytotoxic drugs could be locally generated in the area surrounding the insert at levels sustained by the controlled flow (*via* dosing regulation) of a systemically-administered prodrug.

To develop this experimental approach into an effective therapeutic option, such novel class of drug precursors —i.e. palladium-labile prodrugs— have to be specifically designed to accomplish three goals: (i) eliminating their pharmacological properties; (ii) minimizing their susceptibility to enzymatic cleavage; and (iii) rendering them "cleavable" by palladium catalysis within physiological and pathophysiological environs. So far, only two prodrugs meeting such requirements have been described: 5-fluoro-1-propargyluracil (Pro-5FU, **1**)[10], which generates cytotoxic 5-fluorouracil (5FU) upon palladium-mediated *N*-dealkylation; and *N*-propargyloxycarbonyl (*N*-Poc) gemcitabine (**2**)[11] which undergoes rapid carbamate cleavage by Pd^0 catalysis (Fig. 1a). On the basis of its high sensitivity to palladium and remarkable bioorthogonality (>500-fold less cytotoxic than 5FU), Pro-5FU (**1**)

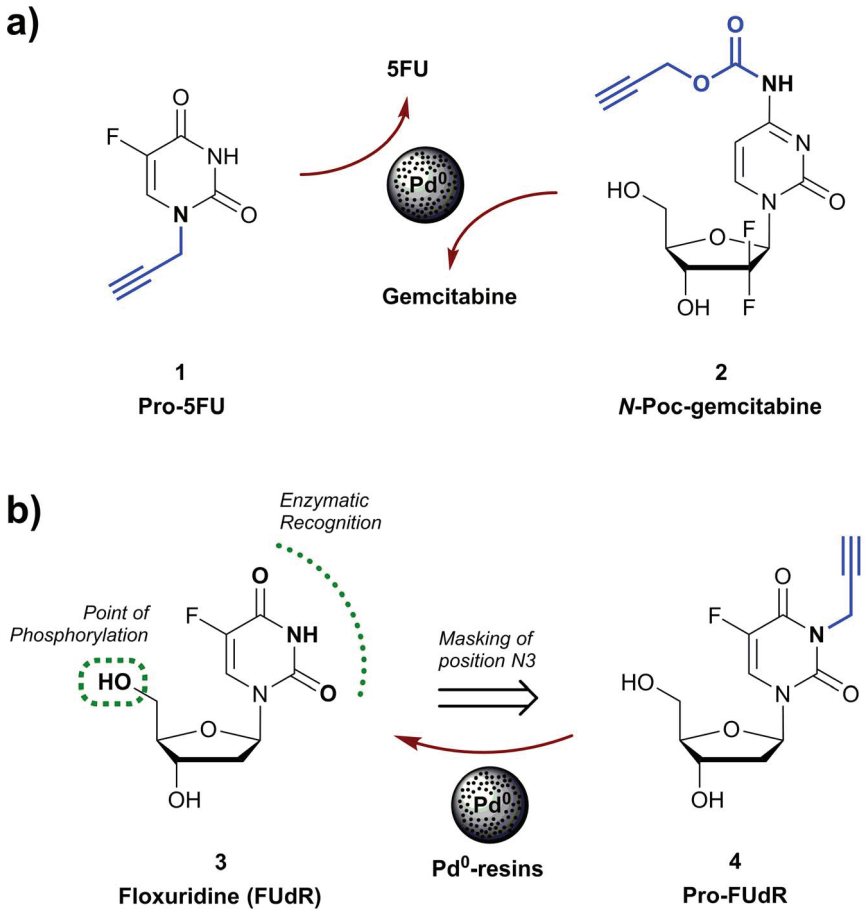

Figure 1 | (a) Palladium labile precursors of 5FU (**1**) and gemcitabine (**2**). (b) FUdR (**3**) and the proposed palladium-labile precursor Pro-FUdR (**4**).

ideally features the sought-after properties required to implement a palladium-activated prodrug approach. However, since 5FU is a cytotoxic nucleobase of relatively low antiproliferative potency[10,12], the levels of drug required to induce a strong phenotypic response could become a limiting factor for its clinical application. On the contrary, the BOOM activation of *N*-Poc-gemcitabine (**2**) results in the rapid and efficient generation of a potent anticancer drug ($EC_{50} < 100$ nM in tumoral cell lines)[11]. The caveat for this strategy is that, although it enables the reduction of the prodrug's bioactivity to levels that were satisfactory for cell culture studies (~25-fold decrease of cytotoxicity relative to the parental drug), the limitations in bioorthogonality of the *N*-Poc masking group were exposed *in vivo* in zebrafish embryos, where *N*-Poc-protected rhodamine showed low biochemical stability in the intestinal tract[11]. Hence, this masking strategy is likely to be suboptimal to satisfy the stability demands required for the translation of this chemistry into the clinic; particularly when the preferable route of administration is enteral.

Given the superior bioorthogonal properties of *N*-alkyl protecting groups and the efficacy of palladium to cleave propargyl groups at endocyclic nitrogen atoms with lactam/lactim tautomery[10,12], we were prompted to investigate whether this novel chemistry could be compatible with drugs of higher structural complexity such as nucleoside analogues, which are reported to be significantly more potent than cytotoxic nucleobases[26,27]. Based on its chemical structure (Fig. 1b), we reasoned that the clinically-used anticancer drug floxuridine (also known as FUdR, **3**) was optimal for developing, and further validating, a propargylation/depropargylation strategy (coupling & decoupling chemistry[28]).

Results and Discussion

FUdR is an antineoplastic antimetabolite that upon intracellular phosphorylation (on its 5′-OH) causes the inhibition of thymidylate synthetase, resulting in the disruption of DNA synthesis and cytotoxicity. It is the deoxynucleoside analogue of 5FU, possessing superior activity both in cancer cell lines and animal tumour model systems[29]. While 5FU is predominantly converted into its uridine analogue and incorporated into the RNA, the active forms of FUdR (phosphorylated derivatives) directly disrupt DNA replication, what is supposed to account for the comparative difference in cytotoxicity between the two antimetabolites[27,29]. FUdR is most commonly administered to patients with advanced colorectal, kidney and stomach cancer, including use as a specific treatment for patients to whom the primary colorectal tumour has metastasized to the liver, where it cannot be removed by surgery[30]. FUdR clinical trials for the treatment of other late-stage cancers, e.g. advanced pancreatic cancer[31], have also found improved survival rates as compared to other chemotherapeutic agents. Treatment with FUdR is however limited by several severe side effects including dose limiting toxicities upon diarrhoea and neutropenia[30,31]. Apart from systemic adverse effects, its therapeutic action is limited by a short half-life[30]. FUdR is systemically catabolized into 5FU[29,32], thus largely reducing the pharmacodynamic advantage of using FUdR over 5FU.

To overcome FUdR pharmacokinetics issues, a number of prodrugs have been reported in the literature during the last decade[33–39], among which include studies from Nishimoto, Tanabe and coworkers[36–39], who have intensively investigated the development of a varied range of *N*3-modified stimuli-sensitive FUdR prodrugs. These masking strategies significantly decrease the cytotoxic effect of the drug, thus potentially improving FUdR's therapeutic window, but at levels similar to those found by us when using the carbamate masking strategy[11]. In contrast, a recent study reported by our group have shown that alkylation of the *N*3 position of the related drug 5FU results in superior suppression of drug's antiproliferative properties

(>100-fold difference)[12]. Along with this fact, this hydrogen donor group is known to display a fundamental role in the substrate recognition of FUdR by both anabolic and catabolic enzymes[40]. Consequently, the propargylation of the *N*3 position of FUdR would not only suppress drug's pharmacological activity but should also protect it from its systemic metabolization into 5FU before reaching the target. Encouraged by this rationale and the unique chemistry of the *N*3 position (it possesses lactam/lactim tautomery), we decided to investigate the implementation of a bioorthogonal control of drug's pharmacodynamics via heterogeneous palladium chemistry. Pro-FUdR (**4**) was therefore synthesized following the 3 step procedure described in Fig. 2. In short, hydroxyl groups in the positions 3′ and 5′ of FUdR (**3**) were first protected using tert-butyldimethylsilyl chloride (TBS-Cl) and imidazole to yield bis-silylated derivative **5**. *N*-alkylation using propargyl bromide[41] in the presence of 1,8-diazabicycloundec-7-ene (DBU) and subsequent desilylation of (non-isolated) intermediate **6** with tetrabutylammonium fluoride (TBAF) in THF yielded Pro-FUdR (**4**) in good overall yield.

The efficacy and stability of the deactivation strategy was first tested in cell culture by performing dose response studies with FUdR and Pro-FUdR in two human cancer cell lines: colorectal cancer HCT116 cells and pancreas adenocarcinoma BxPC-3 cells. As shown in Fig. 3, the 3-propargyl derivative of FUdR displayed a vast reduction in its biological properties relative to the parental drug, with a difference in antiproliferative activity between the two of >6,000-fold (EC_{50} (Pro-FUdR)/EC_{50} (FUdR)). This dramatic decrease in cytotoxicity does not only underline the relevant role played by the *N*3 position in the drug's biological properties, but also the remarkable stability (=bioorthogonality) of the *N*-propargyl group to the cell metabolism.

Based on the validated biocompatibility of the components of the solid support[42,43] and its suitable size (spheres of 150 μm in diameter, much larger than human cells), Pd^0-resins consisting of palladium nanoparticles captured in PEG-grafted polystyrene particles (Supplemental Figure 1) were used to mediate the BOOM conversion of Pro-FUdR into FUdR. Since advanced solid tumors are estimated to have a slightly acidic pH (approx. 0.5–1.0 units below that of healthy tissues)[44–46], *N*-dealkylation of Pro-FUdR's was tested in PBS (isotonic buffered solution) at two different pH's (6.5 and 7.5) to assess the compatibility of the reaction in both slightly alkaline and acidic pH's typical from normal and cancer-like extracellular environs. Pd^0-resins (0.67 mg/ml) and Pro-FUdR (30 μM) were dispersed in the corresponding biocompatible solution and incubated at 37°C in a thermomixer. Reaction crudes were analyzed at 3 time points (4, 8 and 24 h) by HPLC using a UV detector. Chromatogram analysis showed that, while Pro-FUdR was fully stable in the absence of the triggering stimulus, it completely disappeared in the presence of Pd^0 at each of the pH's tested before 24 h incubation, generating FUdR as the main reaction product (see HPLC chromatograms in Supplemental Figure 2). The effect of the pH was noticeable in the shorter incubation periods (4 and 8 h), with slightly superior reaction kinetics being observed at pH = 7.5 (see Table 1). This experiment suggests that the palladium-mediated *N*-dealkylation of Pro-FUdR is compatible with the range of pH expected to be found in both early (normoxic) and late-stage (hypoxic) cancers.

The efficacy by which the floxuridine prodrug is reverted to its active form via heterogeneous palladium catalysis (=Pro-FUdR's toxigenicity[11]) was investigated in cancer cell culture. BxPC-3 and HCT116 cells were treated with Pd^0-resins (0.67 mg/ml) and Pro-FUdR (0.0003 to 30 μM) separately (negative controls) or in combination (BOOM activation assay), and unmodified FUdR (0.0003–30 μM) used as the positive control. As expected, cells independently treated with either Pro-FUdR or Pd^0-resins did not exhibit any reduction in cell viability (Fig. 4a, b). By contrast, the Pro-FUdR/Pd^0-resins combinations displayed a strong toxigenic effect, evidence of the *in situ* generation of FUdR. Under the action of the triggering stimulus (Pd^0-resins), Pro-FUdR exhibited an EC_{50} value of 0.319 μM in HCT116 cells (see Supplemental Figure 3). Considering that its EC_{50} without Pd^0-resins was 181.1 μM, Pro-FUdR displayed a difference in biological properties of >560-fold from being in the presence or the absence of palladium (EC_{50} (Pro-FUdR)/EC_{50} (Pro-FUdR + Pd^0)). In agreement with the lower levels of drug required to generate a cytotoxic phenotype in BxPC-3 cells, the EC_{50} value of the Pro-FUdR/Pd^0-resins combination was 0.016 μM (Supplemental Figure 2), thus showing an even higher

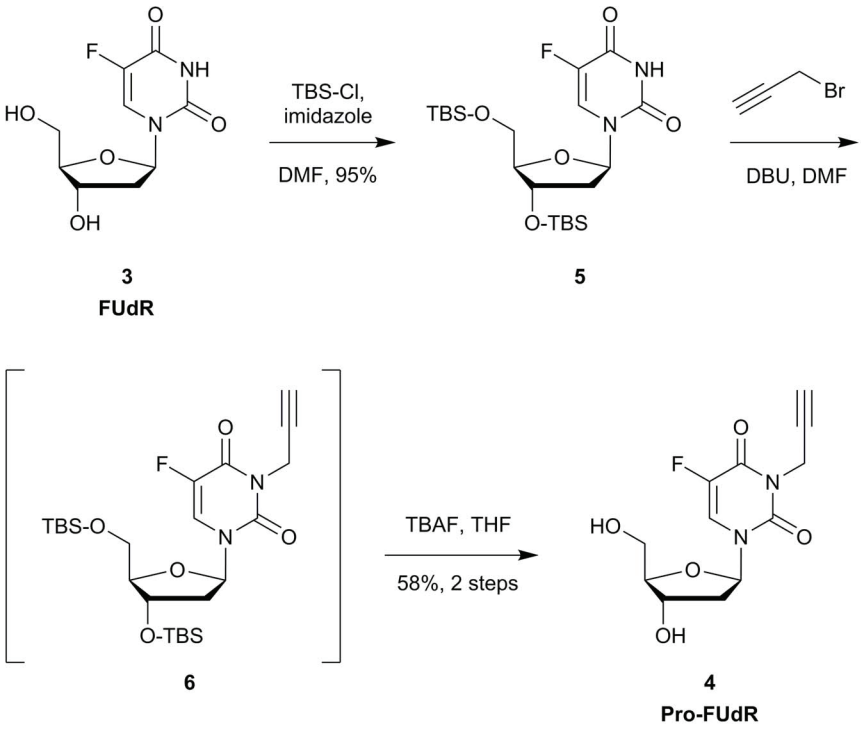

Figure 2 | Semisynthesis of 3-propargylfloxuridine, 4 (Pro-FUdR).

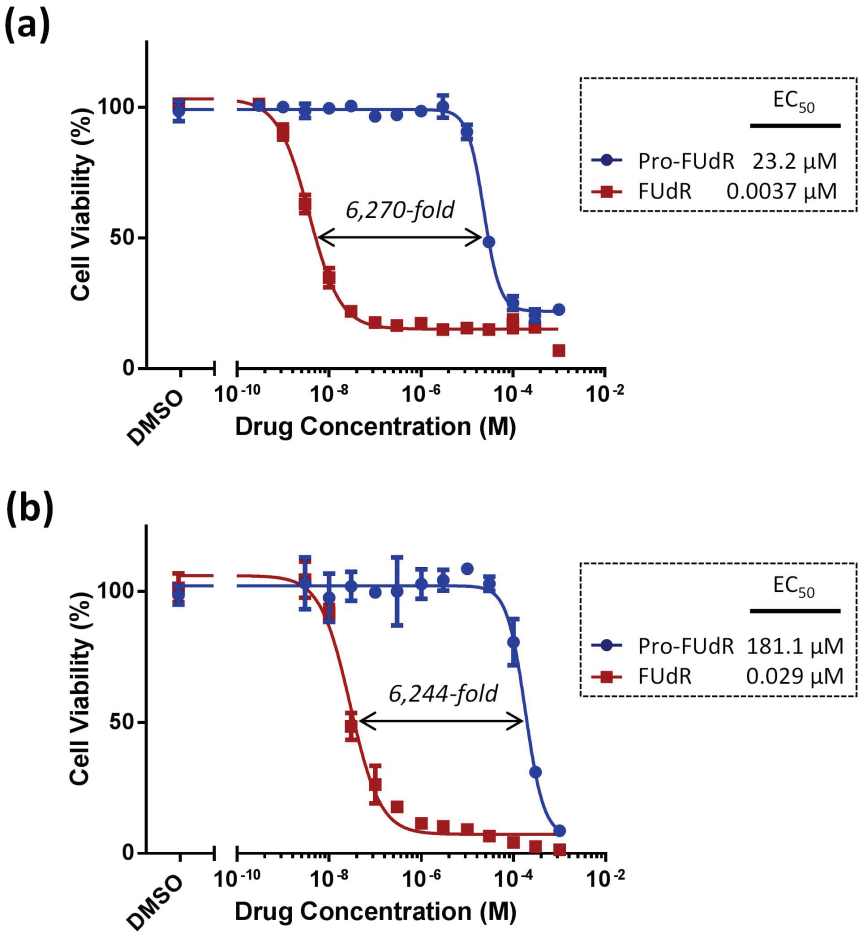

Figure 3 | Semi Log dose response curves and calculated EC50 values of Pro-FUdR (in blue) in comparison to unmodified FUdR (in red) in (a) BxPC-3 and (b) HCT116 cells. Cell viability was determined at day 5 using PrestoBlue™ reagent and a microplate reader. Error bars: ±SD from n = 3.

disparity between the inactive and reactivated drug (23.2 µM vs. 0.016 µM = 1,450-fold). To the best of our knowledge, Pro-FUdR exhibits one of the greatest therapeutic windows displayed *in vitro* by an antimetabolite prodrug, while having the smallest pro-moiety (38 atomic mass units) used to mask the activity of this family of drugs.

To evaluate whether the reaction kinetics between Pro-FUdR and Pd^0-resins could match the direct cytotoxic effect provided by treatment with unmodified FUdR, cell proliferation was monitored for five days by time-lapse imaging using an IncuCyte ZOOM device. As shown in Fig. 4c–f, cells incubated with either Pro-FUdR (in blue) or Pd^0-resins (in black) showed a growth curve equivalent to that of untreated cells (in grey). Conversely, combination of Pro-FUdR with Pd^0-resins displayed a cytotoxic effect (in green) identical to that of cells incubated with the parental drug (in red). Pro-FUdR's ability to generate an immediate phenotypic effect only when Pd^0-resins have been deployed in the culture media (see Supplemental Movies 1 and 2) demonstrates the efficacy of the deactivation strategy, the rapid reaction kinetics of the palladium-mediated *N*-depropargylation process and the high cytotoxic activity of the released drug (FUdR is 50 to 100-fold more potent than 5FU)[10].

Last, the compatibility of the Pro-FUdR's BOOM activation within oxygen deprived environs was investigated by performing the conversion assays with colorectal cancer HCT116 cells inside a hypoxic chamber ($[O_2]$ = 0.5%)[46]. As shown in Fig. 5, the toxigenic effect mediated by the Pro-FUdR/Pd^0-resins combination in HCT116 cells in hypoxia were found to be equivalent to that of the combination in normoxic conditions (Fig. 4b), indicating that the oxygen levels have minimal or no influence on the BOOM reaction (see EC_{50} calculations in Supplemental Figure 4). While this result was anticipated based upon the mechanistic understanding of the dealkylation process[11], it is nevertheless important because it suggests that the Pd^0-mediated prodrug activation would be compatible

Table 1 | Palladium-mediated conversion of Pro-FUdR into FUdR. Relative percentages as calculated by chromatogram peak integration

		REACTANTS			
		Pro-FUdR		Pro-FUdR + Pd^0	
	Time	pH = 6.5	pH = 7.5	pH = 6.5	pH = 7.5
PRODUCT (% of FUdR)	**at t = 4 h**	N/D	N/D	26.6%	37.3%
	at t = 8 h	N/D	N/D	49.0%	65.9%
	at t = 24 h	0%	0%	100%	100%

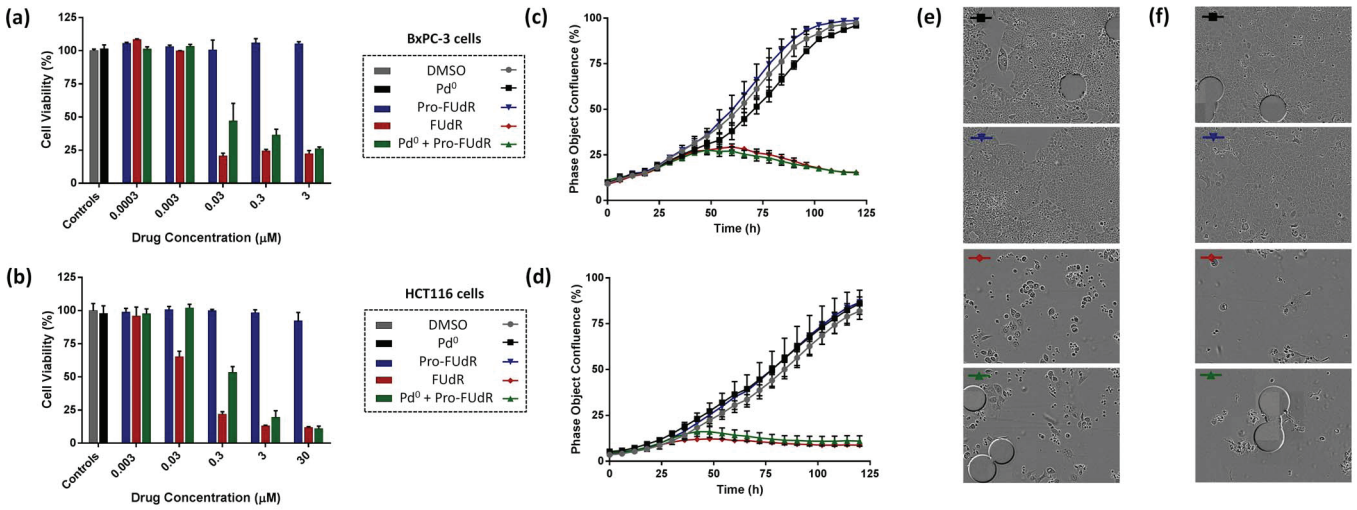

Figure 4 | Palladium-mediated activation of Pro-FUdR in cancer cell culture: (a, c, e) BxPC-3 and (b, d, f) HCT116 cells. (a, b) Log dose response study of Pro-FUdR toxigenicity. Treatments: untreated cells (negative control); Pd^0-resins (0.67 mg/mL, negative control); 0.0003–30 μM of Pro-FUdR (negative control); 0.0003–30 μM of FUdR (positive control); and Pd^0-resin (0.67 mg/mL) + 0.0003–30 μM of Pro-FUdR (BOOM activation assay). All experiments, including the untreated cells, contained 0.1% *v*/*v* of DMSO. Cell viability was determined at day 5 of treatment using the PrestoBlue™ reagent (Life Technologies). Error bars: ±SD from n = 3. (c, d) Time-lapse imaging of cell proliferation: study of BOOM activation kinetics. Cell growth was monitored for 120 h using an IncuCyte ZOOM system in an incubator (5% CO_2 and 37°C). [Drug/prodrug] = (c) 3 or (d) 10 μM. [Pd^0-resins] = 0.67 mg/mL. Error bars: ±SD from n = 3. (e, f) Phase-contrast images of HCT116 (e) and BxPC-3 cells (f) after 5 days of treatment. Experiments are indicated with colored bars (top left corner), corresponding to each specific treatment displayed in (c, d). Pd^0-resins are identified as grey spheres of approx. 150 μm in average diameter.

with the anticipated oxygen deprived environment found in late-stage tumours. From a chemical point of view, given that the reductive environment of the hypoxic chamber is expected to significantly favour the oxidation state zero of the metal, these results further support that the dealkylation process is mediated by Pd^0 in the liquid-solid interphase.

Conclusions

In conclusion, a propargylation/depropargylation strategy has been successfully implemented to develop a truly-bioorthogonal palladium-labile prodrug of a nucleoside analogue, the cytotoxic agent floxuridine (FUdR): a potent drug employed in the clinic to fight advanced solid tumours. Propargylation of the NH group of FUdR's pyrimidine ring yielded a biochemically stable derivative (Pro-FUdR) displaying a vast reduction in cytotoxic activity relative to the unmodified drug (~6,250-fold). Complete palladium-mediated dealkylation of Pro-FUdR was shown to occur in less than 24 h across a range of pH from slightly acidic to physiological, allowing for the induction of a strong and rapid toxigenic effect in cancer cell culture regardless of the oxygen levels. This is the first study to report that palladium depropargylation chemistry is compatible with the relatively low pH and oxygen levels typically found in advanced human cancers. Within the same cellular environment, chemoreversible Pro-FUdR enabled an exquisite pharmacodynamic control by displaying a difference in biological activity of up to 1,450-fold whether it was in the presence or absence of palladium. From a synthetic perspective, the efficacy of palladium in triggering the dealkylation of a compound with the structural complexity of Pro-FUdR significantly expands the scope and applicability of the *N*-depropargylation approach as a bioorthogonal reaction. The

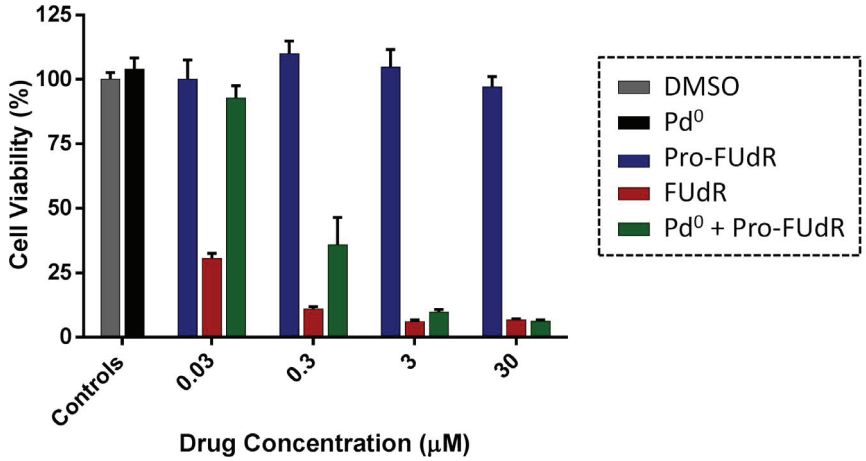

Figure 5 | Palladium-mediated activation of Pro-FUdR in HCT116 cells under hypoxic conditions. Treatments: untreated cells (negative control); Pd^0-resins (0.67 mg/mL, negative control); 0.03–30 μM of Pro-FUdR (negative control); 0.03–30 μM of FUdR (positive control); and Pd^0-resin (0.67 mg/mL) + 0.03–30 μM of Pro-FUdR (BOOM activation assay). Cell viability was determined at day 5 using the PrestoBlue™ reagent (Life Technologies) and a microplate reader. Error bars: ±SD from n = 3.

remarkable biological and chemical properties of Pro-FUdR supports further investigations in clinically-relevant animal models and underline the precise modulation of prodrug activation that can be enabled by biocompatible palladium catalysis.

Methods

General. Cell lines were grown in culture media supplemented with serum (10% FBS) and L-glutamine (2 mM) and incubated in a tissue culture incubator at 37°C and 5% CO2. Human pancreas adenocarcinoma BxPC-3 cells (a kind gift from Dr Mark Duxbury) were cultured in Roswell Park Memorial Institute (RPMI) media. Human colorectal carcinoma HCT116 cells (a kind gift from Dr Van Schaeybroeck) was cultured in Dulbecco's Modified Eagle Media (DMEM).

Cell viability studies. Cells were seeded in a 96 well plate format (at 1,000 cells/well for HCT116 and 2,500 cells/well for BxPC-3) and incubated for 48 h before treatment. Each well was then replaced with fresh media containing compound Pro-FUdR or FUdR and incubated for 5 days. Untreated cells were incubated with DMSO (0.1% *v/v*). Experiments were performed in triplicates. PrestoBlue™ cell viability reagent (10% *v/v*) was added to each well and the plate incubated for 1 h. Fluorescence emission was detected using a PerkinElmer EnVision 2101 multilabel reader (Perkin Elmer; excitation filter at 540 nm and emissions filter at 590 nm). All conditions were normalized to the untreated cells (100%) and curves fitted using GraphPad Prism using a sigmoidal variable slope curve.

Pd^0-mediated dealkylation of Pro-FUdR in cancer cell culture. HCT116 and BxPC-3 cells were plated as described above. Each well was then replaced with fresh media containing: Pd^0-resins (0.67 mg/mL); Pro-FUdR (0.3 nM to 30 μM); FUdR (0.3 nM to 30 μM); or combination of 0.67 mg/mL of Pd^0-resins + Pro-FUdR (0.3 nM to 30 μM). All experiments, including the untreated cells, contained 0.1% *v/v* of DMSO and were performed in triplicates. Cells were incubated with drugs for 5 days. PrestoBlue™ cell viability reagent (10% *v/v*) was added to each well and the plates were incubated for 1 h. Fluorescence emission was detected using a microplate reader and results normalized.

Time-lapse IncuCyte proliferation study. Cell seeding density was optimized to reach confluency at day 5. HCT116 and BxPC-3 cells were plated as described above and each well was then replaced with fresh media containing: Pd^0-resins (0.67 mg/mL); Pro-FUdR (3 μM for BxPC-3 and 10 μM for HCT116 cells); FUdR (3 or 10 μM); or combination of 0.67 mg/mL of Pd^0-resins + Pro-FUdR (3 or 10 μM). All experiments, including the untreated cells, contained 0.1% *v/v* of DMSO and were performed in triplicate. Each well was imaged every 3 h over 5 d under standard incubation conditions using an IncuCyte™ ZOOM microscope placed inside an incubator. Image-based analysis of cell confluence was carried out using the IncuCyte™ software.

Pd^0-mediated dealkylation of Pro-FUdR in hypoxic model of colorectal cancer. Before treatment, 1,000 cells/well of HCT116 cells were seeded and incubated for 48 h under normoxic conditions. Cells were then treated as described above and immediately placed in a hypoxia chamber H35 Hypoxystation (Don Whitley, Yorks), which was flushed by a gas mixture calibrated to 0.5% O2 concentration. Cell viability experiments were performed and analysed at day 5 of treatment as described before.

1. Castano, A. P., Mroz, P. & Hamblin, M. R. Photodynamic therapy and anti-tumour immunity. *Nat. Rev. Cancer* **6**, 535–545 (2006).
2. Bio, M. *et al.* Site-specific and far-red light-activatable prodrug of combretastain A-4 using photo-unclick chemistry. *J. Med. Chem.* **56**, 3936–3942 (2013).
3. Tietze, L. F., Müller, M., Duefert, S.-C., Schmuck, K. & Schuberth, I. Photoactivatable prodrugs of highly potent duocarmycin analogues for a selective cancer therapy. *Chem. Eur J.* **19**, 1726–1731 (2013).
4. Velema, W. A., Szymanski, W. & Feringa, B. L. Photopharmacology: beyond proof of principle. *J. Am. Chem. Soc.* **136**, 2178–2191 (2014).
5. Van Brakel, R., Vulders, R. C. M., Bokdam, R. J., Grüll, H. & Robillard, M. S. A doxorubicin prodrug activated by the staudinger reaction. *Bioconjugate Chem.* **19**, 714–718 (2008).
6. Versteegen, R. M., Rossin, R., ten Hoeve, W., Janssen, H. M. & Robillard, M. S. Click to Release: Instantaneous Doxorubicin Elimination upon Tetrazine Ligation. *Angew. Chem. Int. Ed. Engl.* **52**, 14112–14116 (2013).
7. S. Murray, B. S., Crot, S., Siankevich, S. & Dyson, P. J. Potential of Cycloaddition Reactions To Generate Cytotoxic Metal Drugs In Vitro. *Inorg. Chem.* **53**, 9315–9321 (2014).
8. Clavel, C. M. *et al.* Thermoresponsive Chlorambucil Derivatives for Tumour Targeting. *Angew. Chem., Int. Ed.* **50**, 7124–7127 (2011).
9. Clavel, C. M., Păunescu, E., Nowak-Sliwinska, P. & Dyson, P. J. Thermoresponsive organometallic arene ruthenium complexes for tumour targeting. *Chem. Sci.* **5**, 1097–1101 (2014).
10. Weiss, J. T. *et al.* Extracellular palladium-catalysed dealkylation of 5-fluoro-1-propargyl-uracil as a bioorthogonally activated prodrug approach. *Nat. Commun.* **5**, 3277 (2014).
11. Weiss, J. T. *et al.* Development and Bioorthogonal Activation of Palladium-Labile Prodrugs of Gemcitabine. *J. Med. Chem.* **57**, 5395–5404 (2014).
12. Weiss, J. T. *et al. N*-alkynyl derivatives of 5-fluorouracil: susceptibility to palladium-mediated dealkylation and toxigenicity in cancer cell culture. *Front. Chem.* **2**, 56 (2014).
13. Völker, T., Dempwolff, F., Graumann, P. L. & Meggers, E. Progress towards Bioorthogonal Catalysis with Organometallic Compounds. *Angew. Chem.* **53**, 10536–10540 (2014).
14. Saxon, E. & Bertozzi, C. R. Cell surface engineering by a modified Staudinger reaction. *Science* **287**, 2007–2010 (2000).
15. Agard, N. J., Prescher, J. & Bertozzi, C. R. A strain-promoted [3 + 2] azide-alkyne cycloaddition for covalent modification of biomolecules in living systems. *J. Am. Chem. Soc.* **126**, 15046–15047 (2004).
16. Sletten, E. M. & Bertozzi, C. R. Bioorthogonal chemistry: fishing for selectivity in a sea of functionality. *Angew. Chem.* **48**, 6974–6998 (2009).
17. Yusop, R. M., Unciti-Broceta, A., Johansson, E. M. V., Sánchez-Martín, R. M. & Bradley, M. Palladium-mediated intracellular chemistry. *Nat. Chem.* **3**, 239–243 (2011).
18. Unciti-Broceta, A., Johansson, E. M. V., Yusop, R. M., Sánchez-Martín, R. M. & Bradley, M. Synthesis of polystyrene microspheres and functionalization with Pd(0) nanoparticles to perform bioorthogonal organometallic chemistry in living cells. *Nat. Protoc.* **7**, 1207–1218 (2012).
19. Li, N., Lim, R. K., Edwardraja, S. & Lin, Q. Copper-free Sonogashira cross-coupling for functionalization of alkyne-encoded proteins in aqueous medium and in bacterial cells. *J. Am. Chem. Soc.* **133**, 15316–15319 (2011).
20. Spicer, C. D., Triemer, T. & Davis, B. G. Palladium-mediated cell-surface labelling. *J. Am. Chem. Soc.* **134**, 800–803 (2012).
21. Michel, B. W., Lippert, A. R. & Chang, C. J. A reaction-based fluorescent probe for selective imaging of carbon monoxide in living cells using a palladium-mediated carbonylation. *J. Am. Chem. Soc.* **134**, 15668–15671 (2012).
22. Spicer, C. D. & Davis, B. G. Rewriting the bacterial glycocalyx via Suzuki-Miyaura cross-coupling. *Chem. Commun.* **49**, 2747–2749 (2013).
23. Li, J. *et al.* Ligand-free palladium-mediated site-specific protein labeling inside gram-negative bacterial pathogens. *J. Am. Chem. Soc.* **135**, 7330–7338 (2013).
24. Li, J. *et al.* Palladium-triggered deprotection chemistry for protein activation in living cells. *Nat. Chem.* **6**, 352–361 (2014).
25. Li, N., Ramil, C. P., Lim, R. K. V. & Lin, Q. A Genetically Encoded Alkyne Directs Palladium-Mediated Protein Labeling on Live Mammalian Cell Surface. *ACS Chem. Biol.* DOI:10.1021/cb500649q.
26. Galmarini, C. M., Mackey, J. R. & Dumontet, C. Nucleoside analogues and nucleobases in cancer treatment. *Lancet Oncol.* **3**, 415–424 (2002).
27. Galmarini, C. M., Popowycz, F. & Joseph, B. Cytotoxic nucleoside analogues: different strategies to improve their clinical efficacy. *Curr. Med. Chem.* **15**, 1072–1082 (2008).
28. Bielski, R. & Witczak, Z. Strategies for coupling molecular units if subsequent decoupling is required. *Chem. Rev.* **113**, 2205–2224 (2013).
29. van Laar, J. A., Rustum, Y. M., Ackland, S. P., van Groeningen, C. J. & Peters, G. J. Comparison of 5-fluoro-2′-deoxyuridine with 5-fluorouracil and their role in the treatment of colorectal cancer. *Eur. J. Cancer* **34**, 296–306 (1998).
30. Power, D. G. & Kemeny, N. E. The role of floxuridine in metastatic liver disease. *Mol. Cancer Ther.* **8**, 1015–1025 (2009).
31. Ardalan, B. & Lima, M. J. A phase II trial of FUdR in patients with advanced pancreatic cancer. *Cancer Res. Clin. Oncol.* **130**, 561–566 (2004).
32. Peters, G. J., Laurensse, E., Leyva, A., Lankelma, J. & Pinedo, H. M. Sensitivity of human, murine, and rat cells to 5-fluorouracil and 5′-deoxy-5-fluorouridine in relation to drug-metabolizing enzymes. *Cancer Res.* **46**, 20–28 (1986).
33. Tsume, Y. *et al.* Enhanced absorption and growth inhibition with amino acid monoester prodrugs of floxuridine by targeting hPEPT1 transporters. *Molecules* **13**, 1441–1454 (2008).
34. Lorey, M., Meiera, C., De Clercq, E. & Balzarini, J. CycloSaligenyl-5-fluoro-2′ deoxyuridine monophosphate (cycloSal-FdUMP)-a new prodrug approach for FdUMP. *Nucleosides Nucleotides* **16**, 789–792 (1997).
35. Tobias, S. C. & Borch, R. F. Synthesis and biological studies of novel nucleoside phosphoramidate prodrugs. *J. Med. Chem.* **44**, 4475–4480 (2001).
36. Tanabe, K. *et al.* One-electron reduction characteristics of N(3)-substituted 5-fluorodeoxyuridines synthesized as radiation-activated prodrugs. *Bioorg. Med. Chem.* **11**, 4551–4556 (2003).
37. Tanabe, K., Makimura, Y., Tachi, Y., Imagawa-Sato, A. & Nishimoto, S. Hypoxia-selective activation of 5-fluorodeoxyuridine prodrug possessing indolequinone structure: radiolytic reduction and cytotoxicity characteristics. *Bioorg. Med. Chem. Lett.* **15**, 2321–2324 (2005).
38. Tanabe, K., Ishizaki, J., Ando, Y., Ito, T. & Nishimoto, S. Reductive activation of 5-fluorodeoxyuridine prodrug possessing azide methyl group by hypoxic X-irradiation. *Bioorg. Med. Chem. Lett.* **22**, 1682–1685 (2012).
39. Tanabe, K., Sugiura, M., Ito, T. & Nishimoto, S. Synthesis and one-electron reduction characteristics of radiation-activated prodrugs possessing two 5-fluorodeoxyuridine units. *Bioorg. Med. Chem.* **20**, 5164–5168 (2012).
40. Wittmann, J. G. *et al.* Structures of the human orotidine-5′-monophosphate decarboxylase support a covalent mechanism and provide a framework for drug design. *Structure* **16**, 82–92 (2008).

41. Sirivolu, V. R., Chittepu, P. & Seela, F. DNA with branched internal side chains: synthesis of 5-tripropargylamine-dU and conjugation by an azide-alkyne double click reaction. *Chembiochem* **9**, 2305–2316 (2008).
42. Alcantar, N. A., Aydil, E. S. & Israelachvili, J. N. Polyethylene glycol-coated biocompatible surfaces. *J. Biomed. Mater. Res.* **51**, 343–351 (2000).
43. Unciti-Broceta, A., Díaz-Mochón, J. J., Sánchez-Martín, R. M. & Bradley, M. The use of solid supports to generate nucleic acid carriers. *Acc. Chem. Res.* **45**, 1140–1152 (2011).
44. Tannock, I. F. & Rotin, D. Acid pH in tumors and its potential for therapeutic exploitation. *Cancer Res.* **49**, 4373–4384 (1989).
45. Zhang, X., Lin, Y. & Gillies, R. J. Tumor pH and its measurement. *J. Nucl. Med.* **51**, 1167–1170 (2010).
46. Ward, C. *et al*. New strategies for targeting the hypoxic tumour microenvironment in breast cancer. *Cancer Treat. Rev.* **39**, 171 (2013).

Acknowledgments

We are grateful to the Edinburgh Cancer Research UK Centre for funding this research through the CRUK Development Fund. JTW is grateful to the College of Medicine and Veterinary Medicine and the University of Edinburgh for a Darwin International Scholarship and an Edinburgh Global Research Scholarship. NOC and AUB thank RCUK and IGMM, respectively, for an Academic Fellowship. We thank Carol Ward for her guidance on cell culture in hypoxia.

Author contributions

J.T.W. prepared and characterized the materials, performed the experiments, analysed the data and wrote the methods section; N.O.C. supervised the biological assays and revised the manuscript; A.U.-B. designed the prodrug approach and the materials, planned and supervised the research, analysed the data and wrote the paper.

Additional information

Supplementary information accompanies this paper at http://www.nature.com/scientificreports

Competing financial interests: The authors declare that a patent (application number PCT/GB2014/051894) is pending on Pro-FUdR and its method of activation for medical use.

How to cite this article: Weiss, J.T., Carragher, N.O. & Unciti-Broceta, A. Palladium-Mediated Dealkylation of *N*-Propargyl-Floxuridine as a Bioorthogonal Oxygen-Independent Prodrug Strategy. *Sci. Rep.* **5**, 9329; DOI:10.1038/srep09329 (2015).

This work is licensed under a Creative Commons Attribution 4.0 International License. The images or other third party material in this article are included in the article's Creative Commons license, unless indicated otherwise in the credit line; if the material is not included under the Creative Commons license, users will need to obtain permission from the license holder in order to reproduce the material. To view a copy of this license, visit http://creativecommons.org/licenses/by/4.0/

(12) INTERNATIONAL APPLICATION PUBLISHED UNDER THE PATENT COOPERATION TREATY (PCT)

(19) World Intellectual Property Organization
International Bureau

(43) International Publication Date
24 December 2014 (24.12.2014)

WIPO | PCT

(10) International Publication Number
WO 2014/202994 A1

(51) International Patent Classification:
C07D 239/54 (2006.01) *A61P 25/08* (2006.01)
A61K 31/513 (2006.01) *A61P 35/00* (2006.01)
A61P 9/00 (2006.01)

(21) International Application Number:
PCT/GB2014/051894

(22) International Filing Date:
19 June 2014 (19.06.2014)

(25) Filing Language: English

(26) Publication Language: English

(30) Priority Data:
1311107.5 21 June 2013 (21.06.2013) GB

(71) Applicant: **THE UNIVERSITY COURT OF THE UNIVERSITY OF EDINBURGH** [GB/GB]; Old College South Bridge, Edinburgh EH8 9YL (GB).

(72) Inventors: **USIER-BROSCETA, Asier**; c/o The University Court of the University of Edinburgh, Old College South Bridge, Edinburgh EH8 9YL (GB). **WEISS, Jason**; c/o The University Court of the University of Edinburgh, Old College South Bridge, Edinburgh EH8 9YL (GB).

(74) Agents: **CLEGG, Richard** et al.; Mewburn Ellis LLP, 33 Gutter Lane, London, Greater London EC2V 8AS (GB).

(81) Designated States *(unless otherwise indicated, for every kind of national protection available)*: AE, AG, AL, AM, AO, AT, AU, AZ, BA, BB, BG, BH, BN, BR, BW, BY, BZ, CA, CH, CL, CN, CO, CR, CU, CZ, DE, DK, DM, DO, DZ, EC, EE, EG, ES, FI, GB, GD, GE, GH, GM, GT, HN, HR, HU, ID, IL, IN, IR, IS, JP, KE, KG, KN, KP, KR, KZ, LA, LC, LK, LR, LS, LT, LU, LY, MA, MD, ME, MG, MK, MN, MW, MX, MY, MZ, NA, NG, NI, NO, NZ, OM, PA, PE, PG, PH, PL, PT, QA, RO, RS, RU, RW, SA, SC, SD, SE, SG, SK, SL, SM, ST, SV, SY, TH, TJ, TM, TN, TR, TT, TZ, UA, UG, US, UZ, VC, VN, ZA, ZM, ZW.

(84) Designated States *(unless otherwise indicated, for every kind of regional protection available)*: ARIPO (BW, GH, GM, KE, LR, LS, MW, MZ, NA, RW, SD, SL, SZ, TZ, UG, ZM, ZW), Eurasian (AM, AZ, BY, KG, KZ, RU, TJ, TM), European (AL, AT, BE, BG, CH, CY, CZ, DE, DK, EE, ES, FI, FR, GB, GR, HR, HU, IE, IS, IT, LT, LU, LV, MC, MK, MT, NL, NO, PL, PT, RO, RS, SE, SI, SK, SM, TR), OAPI (BF, BJ, CF, CG, CI, CM, GA, GN, GQ, GW, KM, ML, MR, NE, SN, TD, TG).

Declarations under Rule 4.17:

— *as to the identity of the inventor (Rule 4.17(i))*

— *as to applicant's entitlement to apply for and be granted a patent (Rule 4.17(ii))*

[Continued on next page]

(54) Title: BIOORTHOGONAL METHODS AND COMPOUNDS

FIGURE 5

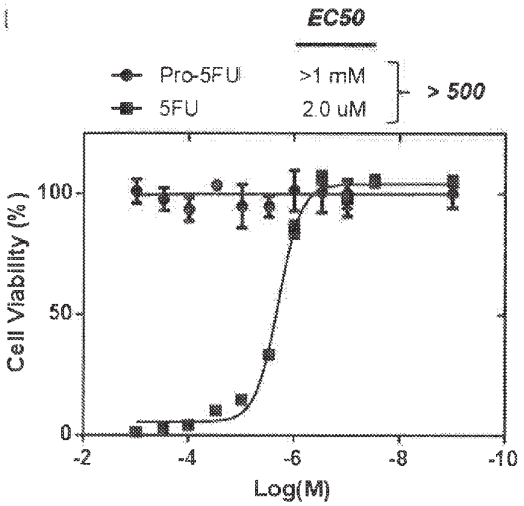

A

(57) Abstract: The invention provides a new bioorthogonal deprotection method for preparing heterocyclic compounds by bond cleavage using palladium. The methods have general application in the field of biological synthetic chemistry. Compounds, such as prodrugs, which are useful in such methods are also provided.

WO 2014/202994 A1